Cardiff
Catalysis Institute

Sefydliad Catalysis
Caerdydd

Intensification of Biomass Upgrading Processes Catalysed by Heterogeneous Catalysts

Thesis submitted in accordance with the requirements of
Cardiff University for the degree of doctor in philosophy by

Massimiliano Caiti

Cardiff Catalysis Institute
School of Chemistry
Cardiff University
2021

Abstract

Developing efficient catalytic processes to upgrade biomass is critical to steer chemical production from fossil feedstock and towards renewable carbon sources. Although some promising heterogeneous catalysed reactions for biomass valorisation have been developed in laboratory research, intensification studies aimed at maximising their efficiency and scalability are much less common. Therefore, the real potential of these technologies to be industrialised is currently unknown. For this reason, during my PhD I intended to intensify appealing biomass upgrading reactions, hitherto explored only on small-scale batch systems, with aim of better evaluating their industrial implementation.

Specifically, in Chapter 3, the development of a continuous process to decompose formic acid into hydrogen by means of palladium nanoparticles was attempted. Detailed catalyst deactivation studies allowed the conceptualisation of a more efficient continuous system, which achieved enhanced continuous performances.

In the fourth chapter, a liquid-phase continuous process to dehydrate sorbitol to isosorbide was explored. The employment of a liquid-phase and the use of methanol as reaction solvent permitted unprecedented catalyst stability and isosorbide productivity to be achieved.

In light of the process improvements achieved in Chapter 4, the employment of methanol as reaction solvent was studied also for the continuous dehydration of fructose to furanic compounds, which is described in Chapter 5. The use of methanol allowed the reaction to tolerate additions of water to the reaction environment without compromising furanics stability, as has been reported when other solvents are employed. The possibility of conducting fructose dehydration in presence of small water amounts allowed new cutting-edge solutions for furanics production to be proposed, such as the integration of fructose dehydration with glucose isomerisation.

The intensification studies performed within this thesis demonstrate that there are still margins to improve biomass upgrading technologies, which must be pursued to make possible the replacement of fossil feedstock with renewable sources in chemical production.

Acknowledgment

First and foremost, I am sincerely grateful to Dr. Ceri Hammond and Cardiff University for giving me the opportunity of undertaking this fructuous professional journey. This experience improved me as a researcher and as a person, honing my ability of approaching challenges in an analytical and resolutive way.
I would like to thank Dr. Hammond also for the stimulating scientific arguments and motivating guidance he always provided during my PhD, and to taught me that scientific data might reveal further different insights if only plotted in different ways! Thus, that also in scientific disciplines things must be viewed from various perspectives to achieve comprehensive knowledges.

I would like to acknowledge also Imperial College London for offering me the unique opportunity to spend the final part of my PhD in its facilities as visiting student.
Especially I am grateful to the College for supporting me since April 2020 and for supporting in full the work described in Chapter 5, which was developed in its facilities starting from January 2021.

A big thank goes also to all the members (present and past) of the Ceri Hammond's group, who have always provided a cheerful, collaborative and supporting working environment.

I would like to extend my gratitude also to all friends and peoples who shared this journey across UK with me and to whom I created warm and truthful relationships, making these four years even more rewarding.

Special acknowledgements are for my family and loved ones, who always encouraged me in pursuing my personal ambitions despite the sacrifices they are exposed to. Thank you for making me feel your warm and support even from oversea, without that this achievement would have not been possible.

Table of contents

List of Abbreviations and Acronyms

Activation energy: E_a

Atomic emission spectroscopy: AES

Barrett–Joyner–Halenda: BJH

Brunauer–Emmett–Teller: BET

Continuous stirred tank reactor: CSTR

Dimethyl sulfoxide: DMSO

Dimethyl formamide: DMF

Density functional theory: DFT

Diffuse reflectance infra-red Fourier transform: DRIFT

2,5-dimethylfuran: DMF

Evaporative light-scattering detector: ELSD

Extended X-ray absorption fine structure: EXAFS

Flame ionization detector: FID

Fluid catalytic cracking: FFC

Fourier transform infra-red: FT-IR

2,5-furandicarboxylic acid: FDCA

Gas chromatography: GC

High performance liquid chromatography: HPLC

5-hydroxymethylfufural: HMF

Inductively coupled plasma: ICP

Infra-red: IR

Liquid hourly space velocity: LHSV

Levulinic acid: LEVA

Magic angle spinning nuclear magnetic resonance: MAS-NMR

Mass spectroscopy: MS

Meerwein–Ponndorf–Verley: MPV

Metal organic framework: MOF

Methyl fructoside: Met-Fru

Methyl isobutyl ketone: MIBK

Methyl lactate: ML

1-methyl-2-pyrrolidone: NMP

Methyl vinyl glycolate: MVG

5-methoxymethyl furfural: MMF

Monte Carlo: MC

Nuclear magnetic resonance: NMR

5% Palladium on active carbon catalyst: Pd/C

Phosphate tin oxide: SnPO

Plug flow reactor: PFR

Poly-(butylene succinate): PBS

Polyethylene: PE

Poly-(ethylene-co-isosorbide) terephthalate: PEIT

Polyethylene 2,5-furandicarboxylate: PEF

Poly-(isosorbide carbonate): PIC

Polyethylene terephthalate: PET

Polylactate: PLA

Polyvinylchloride: PVC

Proton exchange membranes: PEM

Refractive index: RI

Refractive index detector: RID

Research & Development: R&D

Scanning transmission electron microscopy: STEM

Silicoaluminophosphate: SAPO

Sulphated copper oxide: CuSO

Temperature programmed desorption / reduction / oxidation: TPDRO

Tetraethylammonium hydroxide: TEAOH

Tetraethyl orthosilicate: TEOS

Thermogravimetric analysis: TGA

Transmission electron microscopy: TEM

Tungstophosphoric acid: PW

Turnover frequency: TOF

Turnover number: TON

Ultraviolet-visible: UV-VIS

γ-valerolactone: GVL

X: conversion

X-ray absorption near edge structure: XANES

X-ray diffraction: XRD

X-ray photoelectron spectroscopy: XPS

Y: Yield

Chapter 1 - Introduction

1.1 Present day fossil fuel economy

Today, the world's primary source of energy which sustains human activities, such as the production of goods and the transport sector, resides in fossil feedstocks. Fossil resources comprise all those carbon-based materials like crude oil, natural gas and coal, that have formed over millions of years by anaerobic decomposition of ancient dead organisms.[1-3] In particular, oil constitutes the largest share (33%) of the global energy demand, followed by coal (27%) and natural gas (24%).[4] However, these resources can be employed in two distinct ways. Firstly, they can be utilised as energy sources through their combustion for industrial power generation, heat supply or transportation. Alternatively, they can be processed and exploited as carbon sources in the production of chemical commodities such as transportation fuels, solvents and polymers.

In 2019, liquid fossil fuels demand exceeded 100 million barrels per day for the first time in human history, and their consumption is projected to increase greatly due to the global economic progress and continued population growth.[4, 5] In particular, the transport sector accounts for some 60% of this increasing fossil fuels demand, and in the emerging economies of India and China is predicted to grow again by at least 3% per year.[6] However, the production of chemical commodities also depends strongly on these carbon reserves. In fact, the majority of chemical goods are currently produced from oil refinery and almost 4% of oil is worldwide used for chemicals and plastics production.[7]

Although fossil fuels have played a crucial role in the 20th century industrial and technological revolution, increasing environmental and political concerns arise from their utilisation and provision. In fact, although fossil feedstocks are a natural source of energy and matter, they are considered non-renewable materials due to the millions-of-year timescales required for their formation. As such, there is only a limited quantity of these resources available, and many studies estimates their full depletion in 50-100 years.[5] In fact, in the past decades and still today, societal dependence on these limited fossil feedstock, connected to their diminishing supply, has caused political concern and conflict. Moreover, reduction of fossil fuel utilisation is crucial to reduce greenhouse gasses (GHG) emission in order to limit global warming and to keep global temperature increases below 1.5°C compared to pre-industrial times.[134] In this context, material and energy balance models have shown that a reduction of GHG emission by 88% to 94% can be achieved by the chemical industry if fossil fuels[135, 136] are replaced by biomass as starting materials.

Therefore, a renewable alternative solution needs to be found for the sustainability of future human activities. Moreover, there are clear scientific evidences which denounce the exploitation of fossil fuels as detrimental for earth environment and human health. In

fact, combustions of fossil feedstocks emit dangerous amounts of greenhouse gasses, such as carbon dioxide, methane and nitrous oxides, which, in addition to be toxic, largely contribute to the global worming effect. Furthermore, fossil reserves extraction involves extensive land-use and deforestation which accelerate the detrimental effect of climate change.[8]

For these reasons, scientific society has begun to recognize the opportunities offered by a future sustainable economy based on renewable sources, and has been starting to finance R&D activities for the implementation of such a sustainable society. For energy and heat supply, several alternative renewable sources have already been found to be suitable, based on the exploitation of wind, sun, water or geothermal heat. However, given that organic chemicals are evidently dependent on the use of carbon-based resources, for the production of chemicals and transportation fuels, biomass (i.e. annually renewable organic material) represents one of the only sustainable sources of carbon.

1.2 Biomass, a renewable source of carbon atoms

Commonly with the term biomass the scientific community refers to non-fossilized and biodegradable organic material originating from plants, animals, and microorganisms derived from biological sources.[9, 10] Vegetable biomass, or lignocellulose, is grown by plant kingdom organisms as a support structure of their cell wall. These structures are formed through carbon dioxide reduction, a process known as chlorophyllin photosynthesis. Accordingly, biomass represents a renewable resource of carbon atoms, potentially exploitable for chemical purposes.

Nowadays the worldwide biomass production is estimated to be 170 billion of tons per year, which can be divided in 75% of carbohydrates, 20% of lignin and 5% of oil, fats and proteins.[11, 12] This huge amount of carbon supply is considered to be sufficient to cover the overall production of chemical commodities, and in this way, has the potential to replace fossil feedstocks in the production of chemical goods.[13] However, nowadays, the 62% of the vegetable origin fraction of the entire biomass matter is destined to human feeding.[14] Therefore, ethical concerns arise among scientific and political communities regarding utilising biomass for energetic and chemical purposes instead of as a food supply. For this reason, researchers are currently focusing to valorise biomass feedstocks that today are not exploited for human feeding, for example those fractions that constitute wastes or residues. In fact, tons of biomass wastes are produced worldwide by the agricultural and forestry sector each day. For example, the food industry produces 120 megatons of rice husk and 220 megatons of bagasse per year, the main fractions of which are discarded in landfills or used as heat source.[15] Solid municipal residues are another potential waste stream that could be converted to chemicals, as a large proportion of them is made up of paper and organics.[16] Hence, in addition to its renewability, the sustainability

features in exploiting biomass as carbon feedstock for chemical purposes also reside in valorising residue materials that today constitute a cost for our society. Accordingly, in the last decades, several studies have been conducted to develop technologies aimed to convert biomass waste streams in useful chemical products and energy, in order to diminish fossil resource exploitation and make more sustainable the whole industrial sector on which our modern society is based on.[17]

Currently, there are different ways in which vegetable biomass is transformed into useful chemicals. For example, a way to process biomass is its conversion using biological catalysts. In this regards, enzymes are microbiological catalysts able to perform specific reactions with high selectivity. For example, one of the most world exploited biochemical process is the fermentation of sugar to obtain bio-ethanol.[20] Another way to valorise biomass into useful goods is via thermochemical processes in which biomass is treated at elevated temperature in order to obtain pyrolytic oil and syngas for energy and chemical purposes.[18, 19] Thermochemical processes might also be assisted by the presence of a wide range of catalysts which allow to obtain more selective chemical products such as solvents, fuels and platform molecules used in the production of other chemical commodities. For example, transesterification processes exploit different kind of catalysts to convert exhausted vegetable oils into a useful product such as biodiesel, a mixture of methyl and ethyl esters of fatty acids.[21]

The most abundant and cheapest fraction of terrestrial biomass, mostly discarded today as agricultural waste, is the inedible part of plant cell walls, called lignocellulose.[22, 23] Due to these sustainable features, lignocellulose is considered by the scientific community to be the most promising biomass feedstock employable as carbon source for fossil fuel replacement. Lignocellulose is a complex material, mainly constituted by three different polymers: cellulose, hemicellulose and lignin. Depending on the type and source of the biomass, the quantities of these constituents may vary, yielding in highly diversified feedstocks. For instance, hardwood have greater amounts of cellulose, whereas wheat straws and leaves contain more hemicellulose.[24] The diversity of the three components arises from the different building block molecules they are composed of.[25] For example, cellulose is a crystalline homopolymer formed by anhydroglucose units, assembled together by 1,4-β-glycosidic bonds, (Figure 1). It constitutes the 35% to 50% of the lignocellulose composition, representing the most abundant fraction of the vegetable biomass.[26]

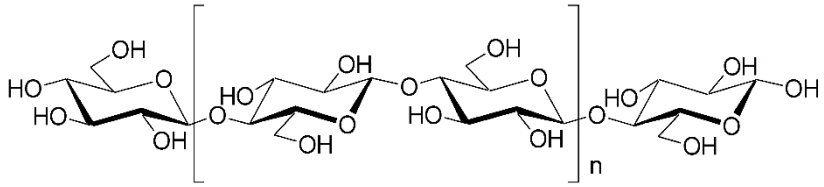

Figure 1 Cellulose is a polymer constituted by anhydrous glucose units.

In contrast, hemicellulose is a copolymer made of both hexose and pentose monosaccharide such as glucose, mannose, xylose, and galactose, (Figure 2). Due to its more heterogeneous composition than cellulose, it shows an amorphous morphology and a lower polymerization degree. Accordingly, it represents the softer components of the lignocellulosic matrix. It constitutes about the 25% of the biomass material and its composition varies on the considered kind of substrate.[27] For instance, in hardwood and grasses the major sugar compound in hemicellulose is xylose, whereas in softwood the most common monomer is mannose. Hence, in the same manner as cellulose, it could be exploited as a bio-source of sugar starting materials for further added value chemical products.[28]

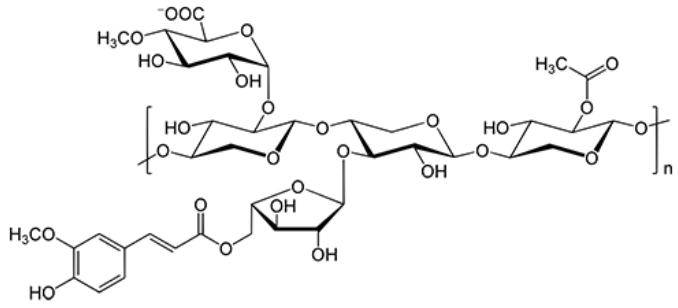

Figure 2 Hemicellulose polymer chain. It is clear the more heterogeneous composition than cellulose.

On the other hand, lignin is the most complex polymer of lignocellulose and it is formed mainly of phenolic monomers, (Figure 3).[28] However, the main bottleneck with respect to upgrading of lignin is to break down the bonds between the monomers to obtain aromatic ring molecules, which can be then utilised for further chemical derivatisation. In fact, one of the major challenges of valorising lignocellulose is that must be depolymerized in its smaller and simpler constituents, that can be then utilised as platform molecules to produce further chemical derivates. Cellulose and hemicellulose are generally hydrolysed, employing strong mineral acids, such as sulfuric or hydrochloric, in order to obtain their relative saccharides monomers.[29] Whereas, to deconstruct lignin, harsher chemical and physical processes are required, which often are performed simultaneously with biomass fractionation. Biomass fractionation is that process used to separate lignocellulose in its three components: cellulose,

hemicellulose and lignin. Many fractionation approaches have been developed to date, ranging from traditional paper making to more sophisticated and environmentally friendly innovations. Each of these methods results in a specific lignin product, which can be isolated in the form of a solid residue, a lignin precipitate, or even directly as a depolymerised product mixture. For example, alkaline fractionation methods promote lignin solubilisation and are therefore widely employed in pulping industry. Kraft pulping, which use NaOH and Na_2S, is the main pulping process, producing over 90% of all chemical pulps. Alkali fractionation methods can be also coupled with fiber explosion/expansion in which wet biomass is reacted with ammonia under elevated pressure resulting in partial solubilisation of the lignin polymer. Subsequently, ammonia is evaporated by a rapid and explosive pressure release, which opens up the biomass structure and redistributes lignin and hemicellulose in the pre-treated solid. Alternatively, organosolv processes are another type of pulping processes in which an organic solvent, often used in combination with mineral acids and/or water, is employed to solubilise lignin and hemicellulose. Ionic liquid can also be utilised in the so-called ionosolv processes to selectively dissolve cellulose, hemicellulose or lignin and thus fractionating biomass.[23, 30, 137, 138]

Depending on the lignocellulosic fraction processed different platform molecules can be obtained and, hence, the type of chemistry which derives.

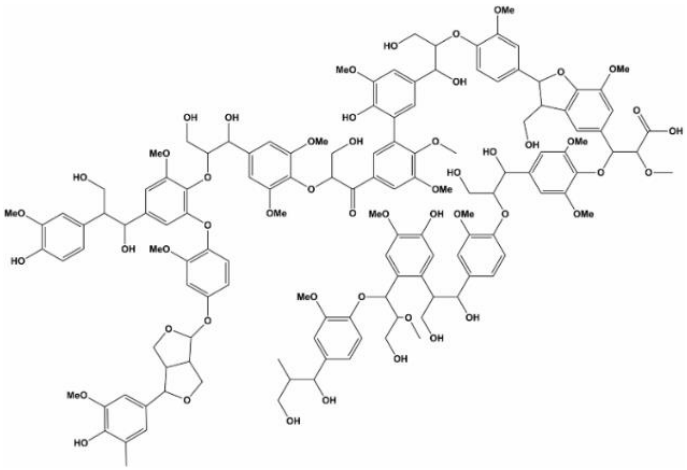

Figure 3 Example of a fragment of the complex lignin chemical composition. The major constituents of lignin are phenolic monomers.

Cellulose can be depolymerised into its only constituent monomer, glucose, which thus constitutes the most widespread and cheapest monosaccharide available in nature.[31] For this reason, in the last decades, many studies have been focused to exploit glucose as carbon source in the production of chemical commodities. As consequence, today glucose is an established platform molecule among bio-industries. Indeed, a large branch of valuable products can be obtained from glucose (Scheme 1), ranging from biofuels to monomers, or bulk commodities such as bio-solvents.[32]

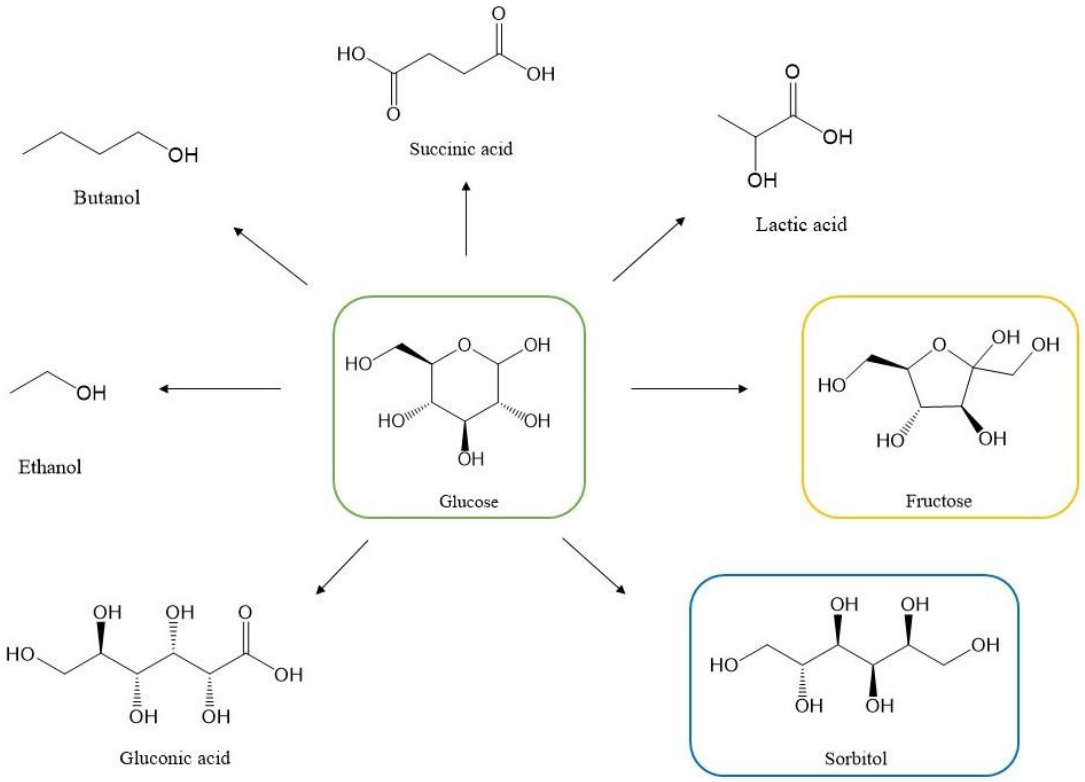

Scheme 1 Schematic representation of valuable building block obtainable from conversion of glucose.

For example, glucose constitutes the main substrate to produce bio-ethanol via fermentation, a renewable product that, thanks to its high research octane number, can be employed as fuel for petrol engines.[33] Moreover, bio-ethanol can be dehydrated to ethylene and used as monomer for the production of polyethylene (PE), one of the most exploited polymeric compounds in the world. Alternatively, bio-based ethylene can be transformed into vinylchloride, employed in the manufacturing of polyvinylchloride (PVC).[34] Therefore, ethanol obtained from renewable feedstocks, such as glucose, is receiving increasing industrial interest as suitable platform molecule to replace fossil derived compounds. As a demonstration of its potential, current bio-ethanol demand reaches values up to 10^{11} L per year.[35] Butanol can also be obtained from glucose fermentation, and is a compound that has found application in the production of solvents, acrylates, plasticisers, perfumes and jet fuel.[33] It is reported that butanol obtained from renewable resources, in addition of having less

environmental impact, is 30-60% less expensive than that obtained from petroleum.[33] Furthermore, glucose can be transformed into lactic and succinic acid, two promising molecules that can be used in the manufacturing of bio-plastics such as polylactate (PLA) and poly-(butylene succinate) (PBS), respectively.[36, 37] Additionally, glucose can be oxidised to gluconic acid, an intermediate product widely used by pharmaceutical for drugs synthesis. For instance, quinone gluconate is an efficient medicine to treat tropical malaria.[33] However, the largest industrial biocatalytic process on earth is represented by glucose isomerisation to fructose, with a production volume on the order of 10^7 tons per year.[38, 39] Indeed, fructose is utilised worldwide as a sweetener by alimentary industries, but it can also be converted into a variety of commercially relevant chemicals such as, furanics, levulinates and unsaturated hydroxyesters.[40, 41] Although the enzymatic conversion of glucose into fructose offers single pass yields up to 42%, it possess several disadvantages that limit the applicability of the process towards bulk chemical manufacture.[42, 43] Indeed, enzymes require strict reaction conditions to operate such as a restricted range of temperature, pH and feed purity that make economically competitive process intensification in the context of bulk manufacture difficult.[44, 45] In this regard, alternative catalytic processes able to isomerise glucose to fructose, such as heterogenous catalytic processes, might constitute a key step to open new chemical pathways from glucose, thus broadening the window of competitive building blocks obtainable from renewable feedstock. For example, the dehydration of fructose leads to 5-hydroxymethylfurfural (HMF) (Scheme 2), a versatile furanic compound which can be further converted in a wide range of commodity chemicals and products.[46]

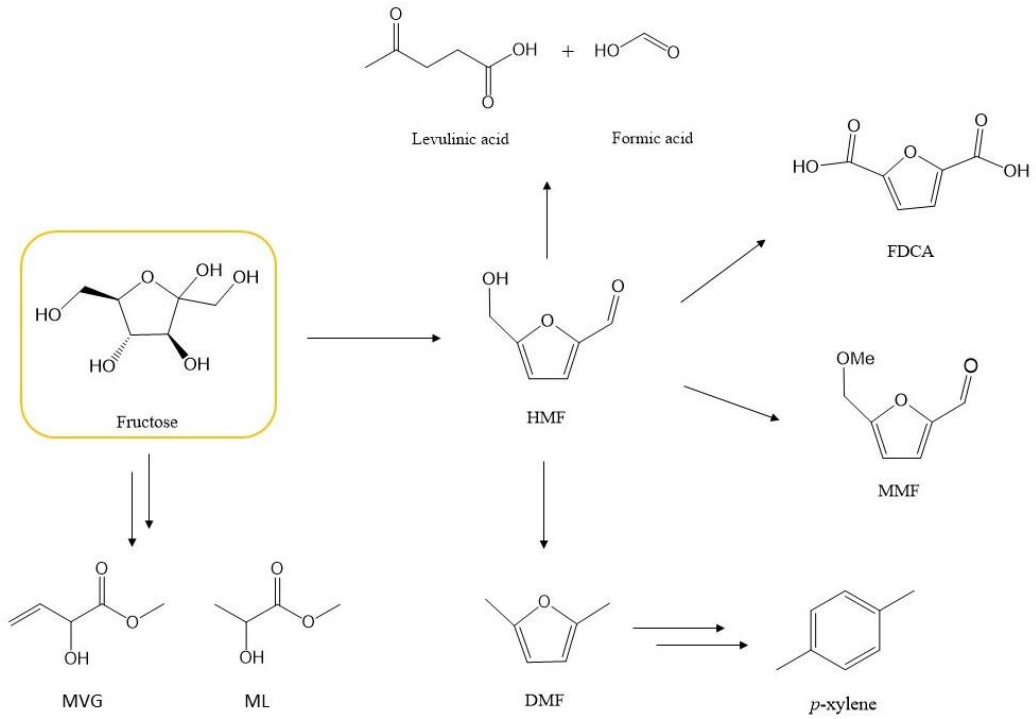

Scheme 2 Schematic representation of valuable building block obtainable from conversion of fructose and HMF.

For instance, the hydrogenation product of HMF, 2,5-dimethylfuran (DMF), is considered a promising biofuel. If HMF is oxidised, 2,5-furandicarboxylic acid (FDCA) is obtained, and it represents a suitable bio-monomer for food packaging materials.[47] Indeed, due to its similar molecular structure, FDCA may substitute terephthalic acid, the primary monomer of polyethylene terephtalate (PET), which is the most widely produced monomer in the bulk chemistry industry.[48, 49] It has been reported that the production of PEF can reduce the non-renewable energy use approximately 40% to 50% while greenhouse gas emissions can be reduced approximately 45% to 55%, compared to PET for the system cradle to grave.[133] Furthermore, PEF polymers have superior gas barrier and mechanical properties compared to PET polymers.[50] *p*-xylene, which is the fossil precursor of terephthalic acid, also represents one of the largest fundamental feedstock in petroleum chemistry, reporting a demand of approximately 3 x10^7 t per year.[33] Laboratory researchers have demonstrated that *p*-xylene can be produced from HMF, via DMF, thus offering also the opportunity to synthesise a renewable based PET.[33] Furthermore, etherification of HMF with short carbon chain alcohol such as methanol, yields in useful compounds (e.g. 5-methoxymethyl furfural (MMF)) employable as fuels or fuel additives.[51] In addition, ring-opening of HMF under acid condition leads to a 1:1 molar mixture of formic and levulinic acid.[32] Formic acid is recently explored as hydrogen storage molecule, since it can be catalytically decomposed into hydrogen, employed to produce electric energy by means of fuel-cells.[52] Levulinic acid is a low-molecular weight carboxylic acid having a ketone and carbonyl group. Levulinic acid occupies a broad area of research since its derivates can be used as bio-solvents, agrochemicals, herbicides and starting materials for the preparation of a variety of industrial and pharmaceutical compounds.[53-55] Additionally, retro-aldol cleavage of monosaccharides yields α-hydroxy esters, such as methyl vinyl glycolate (MVG) and methyl lactate (ML), from which essential monomers for the production of biodegradable polymers can be obtained.[32, 56]

Another interesting platform molecule obtained from glucose is sorbitol (Scheme 1), a sugar alcohol which its derivates found application in many industrial sectors, either to produce major commodities, like synthetic resins, or in the production of fine chemicals, such as vitamin C.[57] The hydrogeneration of glucose to sorbitol is an established technology since 1942, when Raney Nickel was used as a suspended catalyst in batch reactors. Then continuous processes have been developed for glucose hydrogenation such as fixed bed and trickled bed reactors achieving sorbitol yields up to 98.6%. Moreover, during the last decades, Raney Nickel catalyst has been deeply improved with the incorporation of several metals such as molybdenum, chromium and aluminium to increase the catalyst lifetime.[58] Recently, also ruthenium nanoparticles supported on active carbon have been proposed as an attractive catalyst for glucose hydrogenation and platinum-based catalysts have been investigated for the direct conversion of raw biomass into sorbitol.[33]

As consequence, the hydrogenation of glucose to sorbitol is currently an optimised technology with an estimated 2020 annual production of up to 2.3 millions tons.[59] Accordingly, sorbitol has been rated one of top-ten platform molecules derived from biomass.[60]

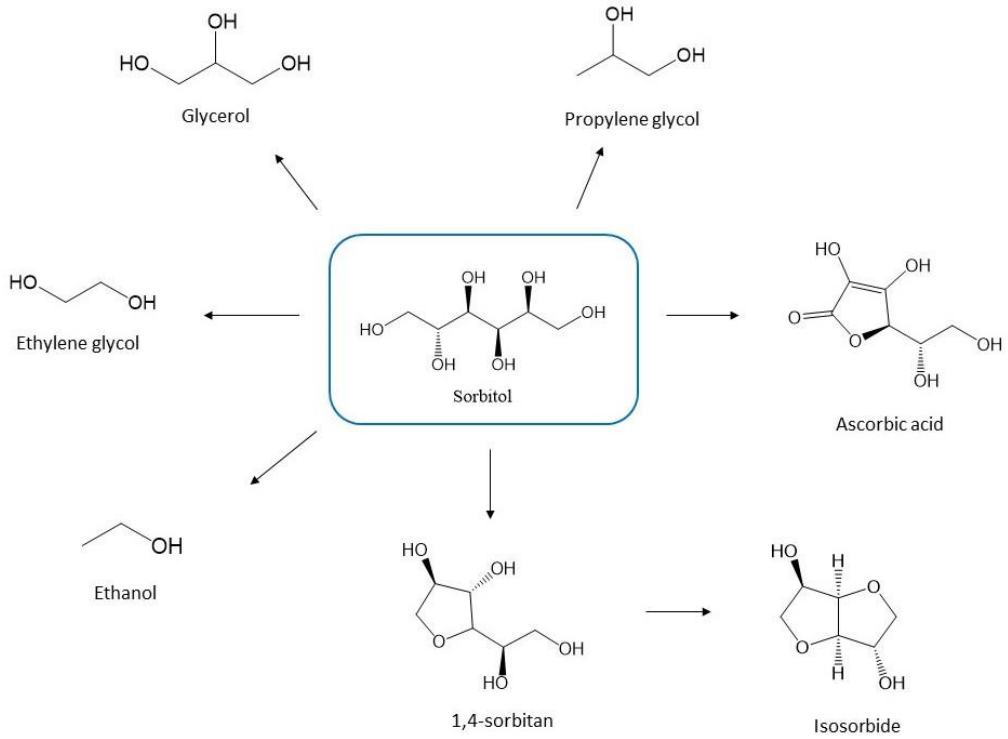

Scheme 3 Schematic representation of valuable building block obtainable from sorbitol conversion.

In fact, sorbitol can be, for example, dehydrated into 1,4-sorbitan (Scheme 3), a compound which its esters are used as emulsifiers for foods, pharmaceuticals and cosmetics, with low environmental impact.[33] Moreover, 1,4-sorbitan can be further dehydrated into isosorbide (scheme 3), an interesting molecule able to replace many commercial product that are today are generated from fossil resources. For example, isosorbide is a promising monomer for enhanced performance polymers such as poly-(ethylene-co-isosorbide)terephthalate (PEIT), which exhibits higher thermal stability than PET.[33] Poly(isosorbide carbonate) (PIC) is another isosorbide based polymer which can replace polycarbonate derived from bisphenol A, a compound classified as carcinogenic.[61] Moreover, isosorbide derivates are extensively used in medicine to treat cardiovascular diseases, tumours and glaucoma.[33] For instance, mono and dinitrate derivates of isosorbide are employed in the treatment of angina pectoris.[62] Furthermore, hydrogenolysis of sorbitol yields important chemical derivates such as glycerol, ethylene and propylene glycol, used in the production of a large-scale commodity chemical.[32, 63]

However, although some of these technologies for biomass upgrading are already established, the potential to improve such branch of chemistry is still wide. In fact, the majority of the systems currently employed to valorise biomass are bio-chemical

processes, which are normally very energy demanding. Furthermore, as already introduced, the rigid conditions that have to be satisfied for the enzyme to operate do not allow high productivities to be achieved, nor do they provide much operational flexibility.[44, 45, 64] In addition, the incompatibility of enzymes with many organic solvents or reactants prevents the development of multistep reactions, resulting in a limitation of the type of products obtainable and making the diversification of the chemistry difficult.[65, 66] For these reasons, the scientific community is still exploring solutions to valorise biomass alternative to the fermentation pathway. In this regard, heterogeneous catalysis offers a good alternative for this kind of chemistry. Indeed, heterogeneous catalysts allow to operate in a broader range of reaction condition compared to enzymes, including temperature, pressure and pH. Furthermore, they are compatible with the majority of organic solvents, allowing to develop more efficient downstream processes, such as the recovery of final products. For these advantages, heterogenous catalysts have been widely utilised during the last century by petrol industries to upgrade crude oil streams into platform molecules.[67] Processing biomass derivate molecules with catalytic materials similar to the ones employed for crude oil valorisation, such as heterogeneous catalysts, represent a huge opportunity for an engineering standpoint, since the existing technologies and industrial practices utilised in petroleum refinery may potentially be extended also for biomass feedstocks. Moreover, in this way, the same industrial concept and design may potentially be preserved since both conversions require the degradation and transformation of complex starting materials towards useful components. However, it is important to stress that the type of chemistry required to process biomass-derived substrates differs totally to the one of fossil origin. In fact, biomass-derived molecules, compared to crude oil, present a high content of oxygenated functional groups, such as alcohol, carbonyl and carboxylic acid, in contrast to fossil fuels where hydrocarbons are the main constituent. Therefore, the chemistry and engineering solutions involved in processing this new class of molecules has to be revised. For example, the presence of oxygenated functional groups makes biomass feedstocks less volatile, and more susceptible to thermal degradation. Accordingly, gas-phase systems utilised to upgrade crude oil are hardly suitable to process biomass platform molecules, which instead, would be more prone to be converted in condensed phases, such as the aqueous phase.[68] The conduction of chemical reactions in different media implies substantial differences in the catalytic mechanism and, hence, to the reaction kinetics and potentially, catalyst stability. Therefore, the whole catalytic process must be re-developed, in order to achieve those operational conditions that maximize the catalyst productivity. For example, zeolites, which are a range of heterogenous catalyst widely employed for the valorisation of crude oil, show remarkably stability features in gas-phase reactions. However, when zeolites are employed in aqueous media, the solvent might hydrolyse the catalyst or its support, inducing

irreversible deactivation phenomena, hence nullifying their activity.[69] In addition to the thermal instability, the broader variety of chemical functional groups present in biomass starting materials, leads to a larger number of possible secondary reactions. Hence, when biomass substrates are processed, the evaluation of the whole range of reactions pathway becomes a key factor to obtain high process productivities. In fact, the presence of multiple by-products, in addition to a decreased selectivity, might also compromise the catalytic material itself. For example, it is reported that at high reaction temperatures, biomass substrates are more likely to be transformed into carbonaceous substances that, depositing on the catalyst surface, inhibit its activity.[70]

Therefore, investigating the behaviour of heterogeneous catalysts during the processing of biomass-derived substrates becomes of crucial importance to evaluate the real potential of these materials to valorise lignocellulose. In addition, studying these systems from an applied perspective offers the opportunity to conduct optimisation studies, which allow more efficient processes to be designed, thus increasing the competitiveness of using biomass feedstocks instead of fossil sources.

1.3 Heterogeneous Catalysis

Catalysts, by definition, are compounds able to accelerate the rate of a chemical reaction without modifying the energy states of reactants and products. They act through two different mechanism: providing an alternative pathway which leads from the reactant to the products, or stabilization of the reaction transition state. In both cases, the activation energy (E_a), or rather the energy barrier of the chemical reaction is reduced, thus allowing an increment of the reaction rate. In fact, according to the Arrhenius equation (Equation 1), the kinetic rate of a reaction (k) is correlated to its activation energy.

Equation 1, **Arrhenius equation** $$k = Ae^{\frac{-E_a}{RT}}$$

Where:
k = rate constant
A = pre-exponential factor
R = universal gas constant
T = temperature
Ea = activation energy

Therefore, in the presence of the catalyst the energy barrier of the reaction is reduced: $E_{a\ with\ cat} < E_{a\ without\ cat}$. As consequence the kinetic rate of the reaction in presence of the catalyst is lower compared to the reaction performed in absence of the catalyst.

Equation 1.A $$k_{with\ cat} = Ae^{\frac{-E_{a\ with\ cat}}{RT}}$$

Equation 1.B $$k_{without\ cat} = Ae^{\frac{-E_{a\ without\ cat}}{RT}}$$

However, the intrinsic energy of reactants and products is not affected by the presence of a catalyst, and consequently the Gibbs Free Energy change (ΔG) of the reaction remains unvaried, (Figure 4). For this reason, use of a catalyst only affects the kinetics aspect of the chemical reaction and not its thermodynamic equilibrium, which define the final composition of reactants and products. Furthermore, since the catalyst only assist the chemical transformation but does not stoichiometrically take part to the reaction, it is not consumed by the chemical process and is then able to perform multiples reaction cycles.

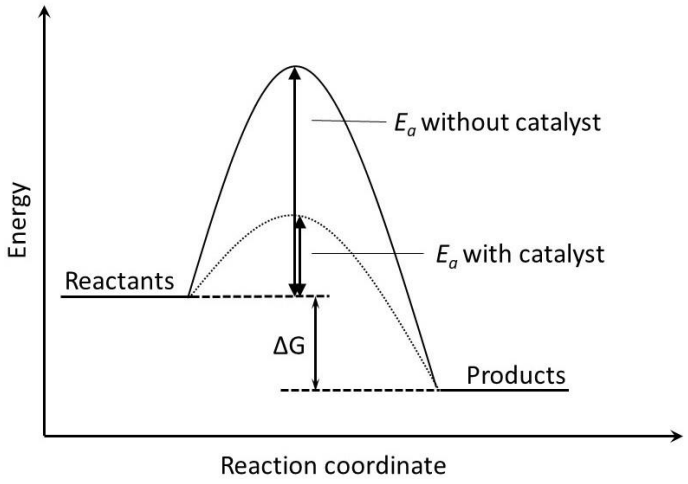

Figure 4 Energetic diagram of a chemical reaction performed in presence or absence of a catalytic material. It can be noted that the presence of the catalyst only decreases the activation energy of the reaction without affecting the energy sate of reactants and products. As consequence, the energy Gibbs gradient between products and reactants is not modified by the presence of the catalyst, hence the thermodynamic equilibrium of the process remains unvaried

Although chemical reactions could always be theoretically performed, both in presence and absence of a catalyst, for certain processes the presence of a catalytic material is mandatory to obtain the target product in a reasonable period of time. Moreover, the decreasing of the activation energy, induced by the catalyst, does not only enhance the reaction rate but also permits the reaction to be conducted at milder conditions, for example at lower temperatures and pressures. In fact, the collision theory states that in order for a chemical reaction to occur, reactant particles must collide with enough kinetic energy to overcome the activation energy barrier. By Boltzman distribution law, the number of molecules having a certain kinetics energy to overcome a set activation energy is function of temperature *i.e.* the higher the temperature, the higher the number of molecules having a kinetics energy which allow the chemical reaction to take place. Therefore, in presence of a catalyst the reaction activation energy is reduced and thus,

the temperature at which reactant particles have enough kinetic energy to overcome the activation energy is lower compared to the reaction performed in absence of the catalyst. In this way, the introduction of catalytic species allows to save energy and to conduct chemical processes in much efficient apparatuses. In some cases, catalytic materials also help to prevent the formation of side and consecutive products, therefore facilitating downstream operations such as products recovery and purification, which often represent one of the biggest costs in chemical productions. For these reasons, catalysts represent a massive opportunity to improve the efficiency of chemical processes both in term of economy and sustainability. Accordingly, in the last century, the study and development of catalytic materials has been strongly intensified to improve both the economic and environmental benefit of the chemical industry. It has been reported that more than 60% of the 63 major products and 90% of the 34 chemical process innovations from 1930 to 1980 have involved catalysis, which illustrates the critical contribution of these active materials in the historical industrial development.[71]

Furthermore, catalytic processes are nowadays considered one of the most attractive ways to satisfy the strict requirements imposed by the Green Chemistry legislations. Indeed, at present, because of environmental issues, catalysis appears to be even more important than before, and constitutes one of the major sources of improvements in our society. As a demonstration, more than 90% of the installed chemical processes since 1980 involve the utilisation of catalytic materials in at least one of their steps, bringing the 2013 catalyst world market turnover up to 17.5 billion dollars per year, with an expected annual increasing of 4-5%.[72]

Catalysts can be classified as heterogeneous or homogeneous, depending on whether a catalyst exists in the same phase as the substrate. Homogeneous catalysis covers the field of soluble catalysts, which are therefore dispersed in the reaction solution. As a result, they intimately interact with the reaction substrate, providing great activity and selectivity. Conversely, heterogeneous catalysts are present in a different phase to that of the reaction solution, then are typically used as solids. Heterogenous catalysis offer a wide range of advantages compared to the homogeneous one, especially concerning industrial applications. One of the major benefits about heterogeneous catalysts is their facile separation from the reaction mixture that permits, at the end of the chemical process, to reuse these active materials for other reaction cycles. For example, in heterogeneous catalysed systems, thanks to the different phase of the catalyst to the reaction solution, product separation can typically be performed through simple operations, such as filtration or pressure decrease. As already anticipated, the easier product recovery constitutes a massive economic advantage since, in the majority of chemical processes, downstream operations represent one of the most energy-intensive steps.[73] Furthermore, the solid features of heterogeneous catalysts also assure a lower dispersion of the active sites

among the reaction species, thus reducing eventual product contaminations. In addition, the physical separation of the catalyst and the reaction mixture, integrated with the ability to perform multiple-reaction cycles, make heterogeneous catalysts the optimal solution to develop continuous processes, which today are considered the most attractive systems for industrial scale production. Additionally, heterogeneous catalysts are typically more tolerant to extreme operational conditions than their homogeneous analogues, allowing to conduct reactions in a broader range of conditions. Another major benefit of heterogeneous catalysts is their intrinsic safety due to their solid physical state. In fact, solids exhibit lower concentration if compared to the hazardous liquid acids usually employed in homogeneous catalysis, and they do not release toxic vapours. This, together with safety and environmental importance, is an enormous advantage also during all the side operations concerning industrial productions, such as storing, shipping and handling of chemical compounds. For these reasons, heterogeneous catalysis represents a massive opportunity to improve the economic and sustainability potential of chemical industry. In fact, much interest is recently addressed to them also as active materials to process biomass feedstocks, in order to develop much more competitive sustainable systems to the fossil-based ones.

The variety of heterogeneous catalysts employed by the chemical sector is enormous. In fact, depending to the reaction undergoing study there are many families of solid materials which exhibit active features such as metals, oxides, sulphides, carbons, silicates etc.. In addition, liquid or in solution active species can be immobilised on solid inert supports in order to generate heterogeneous catalysts, thus further enlarging the array of solid compounds able to assist chemical reactions. It is also possible to combine multiple active species on a single support in order to develop catalysts capable of promoting different kind of reactions and thus, enabling the so-called cascade reaction chemistry. In fact, one of the most attractive features of heterogeneous catalysis resides in the possibility to design ad hoc materials to promote specific reactions and, at the same time, tolerate particular operational conditions, such as extreme pH, high temperatures and pressures or strong mechanical strains. Accordingly, during the last decades, the major improvements achieved in heterogenous catalysis were made thanks to those materials which composition can be specifically tuned and modified to increase the efficiency of chemical reactions and thus to optimise industrial processes. In this regard, zeolites and supported metal catalysts offer versatile structures that can be tailored and highly functionalised to assist specific target reactions. As consequence, these materials are nowadays the most studied and employed heterogeneous catalysts for industrial application. For the same reasons, these classes of catalysts, are extensively explored by the scientific community as optimal structures to process biomass-derived molecules.

1.3.1 Zeolites

Zeolites are highly porous, crystalline, aluminosilicates that have played a major role in petrochemistry and organic synthesis during the twentieth century. They consist of TO_4 tetrahedra arrangements (T is usually Si^{4+} and Al^{3+} tetrahedrally coordinated atoms), assembled together through corner-sharing oxygen atoms to form sodalite cages, which repeat to create an infinite three-dimensional lattice. Typically, the crystalline lattice of zeolites is characterised by 1D or 3D system of channels whose diameters are within 2 nm, thus conferring to these materials high porosity features. The highly porous structure of these aluminosilicates ensures an extremely wide surface area, which can be exploited for catalytic purposes. At present, more than 300 different types of zeolite frameworks are known, with only a few (BEA, FAU, MFI, MOR, SAPO-34) having important industrial catalytic applications. For example, Figure 5 presents some of the most common zeolite structures employed today in catalytic processes.

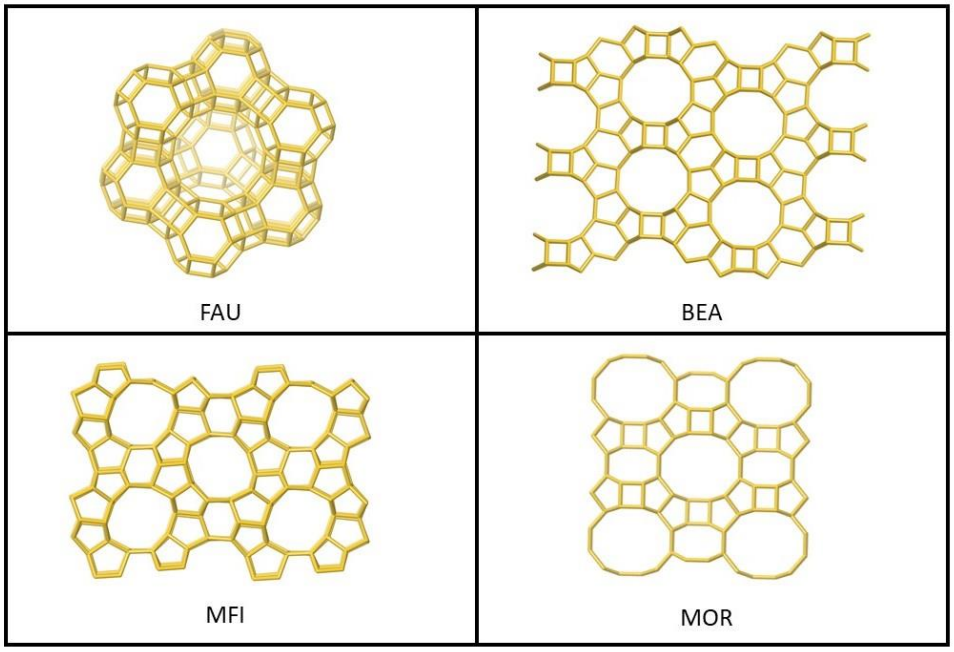

Figure 5 Representation of some of the most common zeolite structures. Only the silicon atoms are displayed. From top left to bottom right: Faujasite (FAU), ZSM-5 (MFI), Beta (BEA), Mordenite (MOR).

The presence of aluminium atoms tetrahedrally coordinated among the silicate framework induces a negative charge that is typically balanced by cations and more often by protons, (Figure 6). In this latter case, zeolites can act as Brønsted acids since they provide exchangeable mobile protons. In light of this, the capacity of these materials to catalyse the wide array of reactions assisted by acid species, such as isomerization,[74] dehydration,[75] hydrolysis and cracking of hydrocarbons, is evident.[76] Since the number of protons is generally proportional to the number of aluminium atoms, the acidity of the

zeolites can be tailored by varying the Si/Al ratio of the lattice. Notably, the higher is the ratio, the lower is the amount of aluminium atoms, thereby the acid site density of the material results to be decreased.

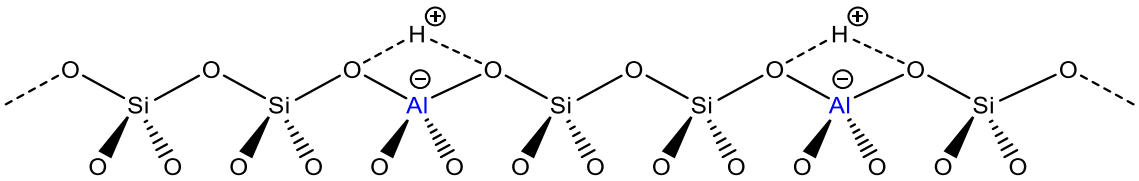

Figure 6 Schematic representation of the tetrahedral units of SiO_4 and AlO_4. In proximity of the aluminium atoms is present a proton in order to preserve the electroneutrality of the structure.

The catalytic features of zeolites can be further modified, either during the synthesis or through post-synthetic treatments, by replacing aluminium atoms with different metals, known as heteroatoms, such as Ti, Sn, Hf, Zr (Figure 7). These heteroatoms typically confer to zeolites unique features of Lewis acidity, opening a new field of chemical reactivity suitable for biomass-derived substrates.

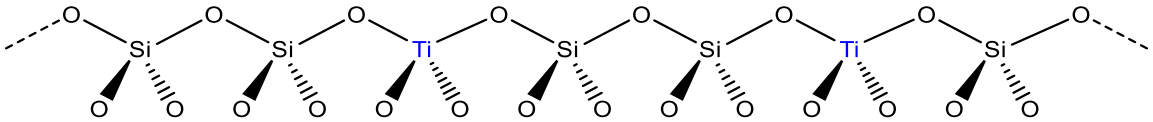

Figure 7 Schematic representation of the tetrahedral units of SiO_4 and TiO_4 in the Ti hetero-substituted zeolites. Opposite to conventional zeolite, no cations are needed in the structure in order to preserve the electroneutrality.

By definition, a Lewis acid, is a species which has an empty orbital and thus can accommodate lone pairs of electrons from a donor, which is then addressed as Lewis base. Therefore, the large presence of electron-rich substituents (like carbonyl and alcohol groups) in biomolecules, makes them available to react with the Lewis active sites of hetero-substituted zeolites.

Interestingly, the reactivity of a particular zeolite does not uniquely depend on its elemental composition, but also its framework structure plays a crucial role. In fact, the molecular size of the channel networks confers to zeolites the fascinating property of *shape selectivity*.[77] According to the zeolite catalytic mechanism, a substrate must diffuse through the cavities and channels of the aluminosilicate framework in order to react with the active sites. Hence, molecules which do not have suitable dimension to diffuse through the lattice are prevented from reaching and/or reacting with the active site. In fact, there are several types of shape selectivity, depending on whether it is the substrates, the transition state and/or the product(s) which are discriminated in terms of diffusion (For further discussion on Diffusion limitation see section 1.4.4).

Substrate selectivity occurs when the reacting solution is composed by a variety of molecules and the only ones with the suitable shape can access to the zeolites cavities an react. An example is the dehydration of an alcohol mixture composed by n-butanol and iso-butanol. The process assisted over narrow-pore zeolites permits only n-butanol to be dehydrated, since its linear geometry permits it access to the catalytic framework, whereas iso-butanol is excluded and thus not converted due to its branched nature.[71]
Transition-state selectivity is maybe the more fascinating of the three mechanisms, in which transition-states with too large steric hinderance are prevented to form inside the zeolite cavities. In this manner, some reaction pathways are preferred than others and it is possible to obtain products composition distribution different from the one favoured by thermodynamic. Furthermore, in this way is discouraged the formation of too big molecules which can easily deactivated the catalyst, such as the polymerization of the substrate.
Product selectivity results in the enhanced formation of the products which has the most suitable shape to diffuse out from the zeolite cavities. Others by- or co-products which do not show the right dimensions experience restricted diffusion from the pores, and continuously react until they reach the right configuration to escape. This is well demonstrated in the industrial alkylation of toluene with methanol over H-MFI. Inside the zeolite channel, the diffusion of the *para*-isomer is favoured than the *orto*- and *meta*-adducts. Hence, once *p*-xylene is formed rapidly diffuse out from the zeolite framework, whereas *o*- and *m*-xylene, which show a less linear geometry, remains for longer time inside the catalyst where are further isomerized into the para configuration. In this manner, enhanced *p*-xylene yield can be obtained than would be predicted by standard thermodynamic arguments.[71]
Therefore, the geometry and tortuosity of the zeolite channel-cavity system can potentially be designed in order to match the size and configuration of reacting substrates, intermediates and products to maximize the production of the industrial target molecule. Accordingly, over the decades have been screened and synthesised a large number of zeolites with different composition and configuration with the purpose of intensify chemical industrial productions. In fact, precisely because of the possibility to widely tune the chemical and physical properties of these materials, zeolites have been one of the most successful catalysts employed over the last century by the chemical industry to upgrade crude oil. For the same versatile properties, zeolites may also represent the best potential catalysts to selectively convert biomass-derived compounds into chemical platform molecules. However, as previously illustrated, the different chemical nature of renewable feedstocks to the one of fossil resources implies to ascertain, through kinetic and stability studies, the suitability of these catalytic materials for the new proposed chemical approach.

1.3.2 Supported metal catalysts

As is well-known, most of the chemical reactions exploited in industrial processes such as (de) hydrogenation, oxidation, hydrodesulfurization and polymerization, amongst others, are catalysed by metal elements or by their oxidised phases.

Heterogeneous catalytic reactions usually occur on the surface of the catalyst, hence the utilization of bulk metal or metal oxide as such might result an inefficient way for catalytic purposes. Indeed, due to the non-porous nature of metallic species, only the few atoms situated on the external surface area are available to interact with the substrate, whereas the atoms inside the structure are typically inactive.

Accordingly, metal catalysts have been widely investigated during the decades in order to increase their efficiency. In this regard one of the most successful development is the employment of inert supports on which particles of catalytic metals are dispersed, thus extremely enhancing the metal active surface area. Thanks to this solution, minimum quantities of precious metals are required to obtain efficient catalytic materials, thus dramatically reducing the cost of the catalyst. Furthermore, it has been discovered that the active features of metal-based catalysts not only depend to the chemical nature of the species and to the surface area, but also to the crystallographic conformation of the metal particles. Indeed, depending to the type of the metal crystal lattice, different crystallographic planes are exposed, which in turn show different activity properties. For example, cubic Pd only display (100) plane atoms on the surface, while Pd octahedra only present (111) plane atoms and cubo-octahedra have a mixture of both.[78] Thereby, depending to the lattice structure, more metal atoms may be present in specific position known as low-coordination sites, such as edges, corner and step of the lattice itself, that result particularly active and selective for specific reactions, (Figure 8). In this case, one can talk about a *shape effect* of the metal particles, but also *size effects* can also play an interesting role. Indeed, crystals smaller than 3 nm in size start to lose their bulk properties, since higher number of low-coordinated atoms are present, thus modifying the electronic properties of the material and conferring particularly active or selective feature to the catalyst. In this case we talk about nanoparticles-based catalyst, which activity strictly depend to the particles size.[78, 79] For example in the dehydrocyclization of n-heptane over Pt catalysts, a large increase in activity was observed with decreasing particle size from 4 to 1.5 nm.[80]

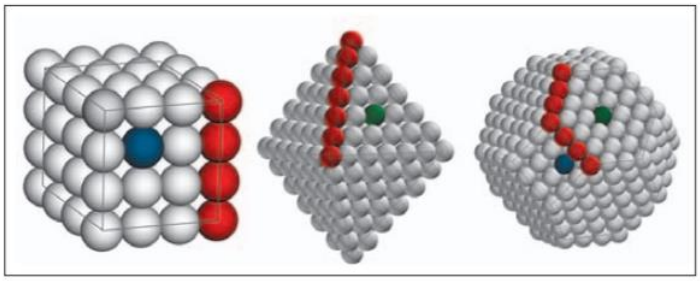

Figure 8 Three common shapes of Pd nanocrystal. From left to right: cubic, octahedral and cubo-octahedra. Each crystal lattice exposes different crystallographic planes: in blue $Pd_{(100)}$ and green $Pd_{(111)}$. In red are showed edge and vertex Pd atoms.[131]

In addition to the enhanced efficiency, supporting materials confer to the catalyst higher thermal and mechanical stability. Furthermore, supports might induce shape selectivity properties and if they own acid or basic features can benefit to the reaction collaborating with the metal active sites. Depending to the active metal species to incorporate and to the condition required by the assisted chemical reaction can be selected different types of catalytic support. For example, common support materials consist of refractory oxides such as SiO_2, Al_2O_3, or TiO_2. These materials exhibit high specific surface areas, high porosities, high thermal and mechanical stability and may be manufactured in a variety of pore sizes. Furthermore, they are mostly chemically inert. Moreover, a wide range of supports, in addition to those involving the oxides of transition or non-transition metals, have been investigated and shown to have the potential to augment the catalytic potential of platinum and other catalytically active metals returning the so-called Strong Metal-Support Interaction (SMSI) effect.[139] Carbon is also widely used as support, while zeolites are often applied in many oil-refining and petrochemical applications. Recently, an increased attention is addressed also to metal organic frameworks (MOFs) for their application as catalytic support.

The possibility of combing different metal elements with different supports allow to design catalysts with optimal properties to assist specific target reactions. Furthermore, the active properties of supported metal catalysts can be tuned utilising different metal deposition techniques or via post-deposition treatments. Thereby, the large array of possibilities to synthetise different active materials, makes metal supported catalysts, together with zeolites, the most exploited and studied heterogeneous catalyst for industrial applications.[81, 82]

1.3.3 Catalysts lifetime: a keystone feature for industrial scale applications

In chemicals production, the cost of the catalytic element often represents a large capital investment which must be break even as soon as possible over the process lifetime. Thereby, if the same catalyst amount can be utilized for multiple reaction cycles, the

economic potential of the chemical process increases greatly. Moreover, the replacement of the exhausted catalyst with the fresh material implies production interruption and reactor shutdowns that greatly affect the economic potential of the whole process. At present, the economic cost related to the catalyst replacement and process shutdown total up to billions of dollars per year.[83] In addition to the economic standpoint, an extended lifetime of the catalyst implies enhanced benefits for the process sustainability, since fewer industrial wastes are produced, energy consumptions are reduced, and lower CO_2 quantities are emitted. Therefore, a keystone feature for a promising industrial catalyst, in addition to high levels of activity and target product selectivity is its long-term stability. Unfortunately, the catalyst stability during long-term reaction can be jeopardized by several phenomena which, individually or synergistically, change its chemical or structural properties, thus inducing its deactivation. The time scale of catalyst deactivation various tremendously depending on the chemical reaction and the catalytic material employed, having a profound consequence on the design of the chemical plant. For example, in fluid catalytic cracking (FCC) the aluminosilicate catalyst deactivates in seconds of reaction time, and thereby the whole process is fluidized in order to quickly recirculate the catalyst from the reactor into the regeneration unit. Conversely there are catalysts whose lifetime is measured in year timescales, hence the process design is simpler, such as the fixed bed reactor employed in the steam reforming.[84] Thereby the catalyst deactivation is an essential topic that must be known and considered since the first steps of conception and design of an industrial plant.

The importance of the catalyst deactivation is so relevant for industrial application that has been widely investigated for oil and petrochemical processes and extensively discussed in numerous reviews and books.[84] However, in the development of competitive processes for bioresource valorisation, the challenges encountered by catalyst in long-term operation for biomass conversion is often overlooked, especially among the academic literature and has not yet received significant attention.

Hence, in this work, particular attention is addressed to the catalyst stability and to the procedures which allow to mitigate catalyst deactivation during biomass valorisation reactions.

Here are briefly discussed the main chemical and structural changes which might meet the catalyst during the reaction, thus inhibiting its activity, with the methodology employed to identify them. The main events which may affect the catalyst stability can be summarized as: catalyst fouling, catalyst poisoning and active site reorganisation. These kind of deactivation phenomena can be mainly classified as reversible or irreversible, hence also the study of the catalyst regeneration represent an essential tool to identify the deactivation process.[85]

1.3.3.1 Catalyst Fouling

Fouling is considered the deposition of heavy insoluble materials on the catalyst surface which prevent the interaction of the substrate molecules with the catalytic active sites, thus impeding the chemical reaction, (Figure 9). In its advanced staged, it may also result in plugging of the reactors voids, causing dramatical pressure increases especially if the reaction is performed in tubular reactors, thereby representing a serious peril for the whole process.

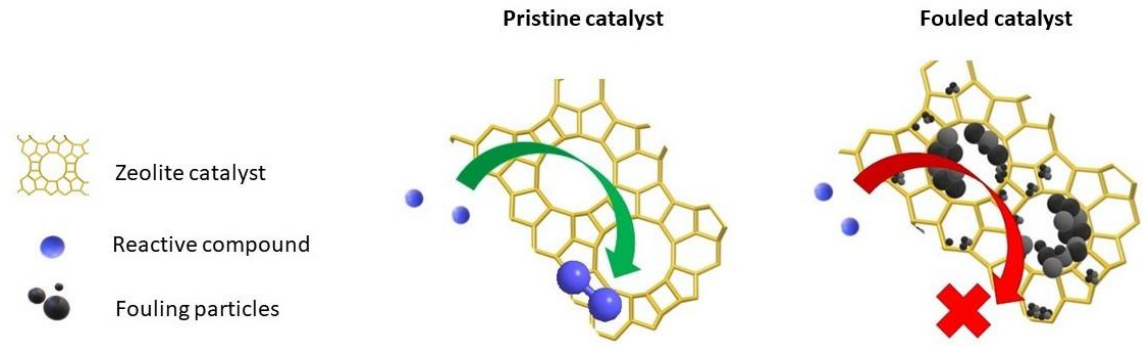

Figure 9 Graphic representation of pore fouling caused by carbonaceous deposition. On the left, the pores of the zeolite catalyst are available to promote the reaction. On the right, carbonaceous residues impede the reactive compound from accessing the zeolites pores and thus prohibit reaction.

These unwanted insoluble materials are either present in the feedstock, or may be formed in situ by decomposition of the substrate or even the products themselves.[86, 87] For this reason, deactivation by fouling is common among those reactions that process easily degradable bio-based feedstock. For example, catalyst deactivation by fouling is reported for the upgrading of bio-oil, as reviewed by Elliott *et al*.,[88] or in the processing of sugars,[89, 90] sugar derivates,[91-93] and crude glycerol.[94] Sometimes fouling is even due the to the precipitation of too heavy compounds that are processed as feedstock or which are formed in situ due to dramatically changes of some reaction conditions such as temperature or pH.

However, for biomass stream processes the most common formation of fouling is by thermal degradation, thereby, the insoluble particles are represented by carbonaceous residues, generally categorised as “coke”. The precise nature of these carbonaceous residue varies widely, and intimately depends on the nature of the reaction undergoing study, the chosen reaction conditions, the identity of the catalytic material, together with the nature of the feed solution.[95] Typically, these coke particles can lead to deactivation of a catalytic process through several types of mechanisms, including poisoning of the active site, physical plugging of the reactor channels, or more commonly blocking the

access of reactants to the active sites, either by encapsulation of the active site or pore blocking.

To understand if the deactivation of a catalyst is due to fouling, a set of characterization techniques can be used to investigate the catalyst properties at the end of the reaction. For example, porosimetry analysis can be conducted on fresh and on the used catalyst to evaluated if the catalytic material has lost surface area during the reaction. Indeed, especially for highly porous materials such as zeolites, if some insoluble compounds are formed inside their framework, catalyst surface area can decrease enormously. Moreover, with the porosimetry technique it is possible to evaluate the micro and mesopores volume and thus, understand which structural portion of the catalyst is most affected by such deactivation. Of course, double check analysis must be performed on the used catalyst to ascertain that the loss of porosity is due to the presence of some insoluble particles stuck in its frameworks and not to the collapse of the catalyst structure. Additionally, spectroscopic techniques, like Raman, UV-VIS or FT-IR may be employed to analyse the catalyst surface to verify the presence of unusual substances.

Furthermore, given that fouling relates to the formation of carbonaceous residue trapped within the bulk, or on the surface of the heterogeneous catalyst, thermogravimetric methods (e.g. TGA), represent another simple form of identification, by causing the combustion of any retained carbonaceous residue, and determine their quantity as a function of combustion temperature.

To restore the catalytic performances lost by fouling, an established procedure of catalyst regeneration, is the calcination treatment of the deactivated catalyst, in which the coke particles are burn and thus removed.

1.3.3.2 Catalyst Poisoning

Poisoning deactivation occurs when particular components of the reaction system result to be strong adsorbed on the heterogeneous catalyst, limiting its ability to convert further reactant molecules, (Figure 10). Mechanism by which a poison may affect catalytic activity can vary depending on the poison and catalyst nature. To begin with, a strongly adsorbed atom on the catalyst surface can physically blocks the substrate adsorption on the active site or its diffusion inside the catalyst framework, thus impeding the occurring of the reaction. Second, the presence of external chemical species on the catalyst surface can modify the electronic features of the nearer neighbour metal atoms, hence inducing different catalytic activity and selectivity features. A third effect may be the restructuring of the surface by the strongly adsorbed poison, possibly causing dramatic changes in catalytic properties, especially for reactions sensitive to surface structure.

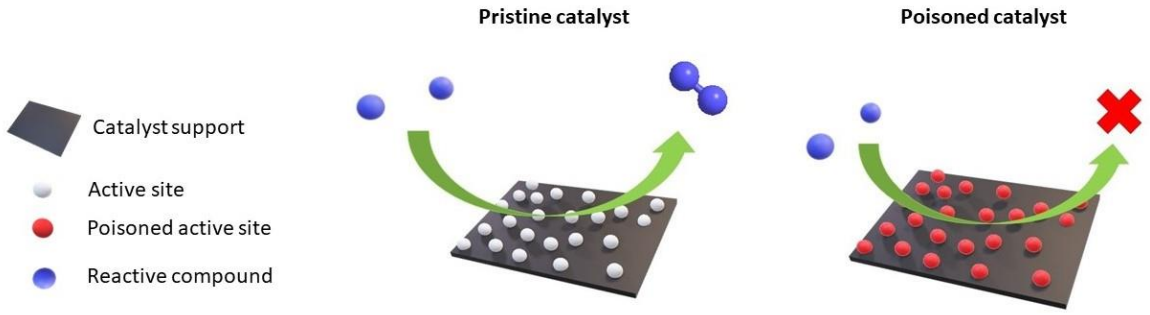

Figure 10 Schematic representation of poisoning. On the left it is shown the pristine catalyst able to convert the reactive substrate. After poisoning (on the right), the active sites are unable to assist the chemical reaction anymore.

Such poisons may be external, for example impurities present in the feed, or may be generated in situ during the catalytic reaction, such as by- and co-products. Biomass processing are particularly prone to suffer this type of deactivation since their upstream starting materials, such as agricultural residues or grasses, have a very broad heterogeneous compositions which also depend to the annual period and geographical area of their harvesting. Indeed, in lignocellulosic materials, several inorganic elements are often present, which can act as poison for metal-based catalysts. For example, depending on the origin of the bio-feedstock, nitrogen can account to up to 1 wt.% of the biomass, whereas sulphur to 0.2 wt.%, both known as strong poisons for metal-based catalysts. Among hard wood, grasses and starch, can also be present ppm traces of calcium, potassium, magnesium and sodium which instead could remove Brønsted acid sites, through ion- exchange on acid catalysts.[73, 96, 97] Furthermore, biomass streams are often highly functionalized, thereby their conversion may generate an extremely broad array of by- and co- products, increasing the chance of in situ poisoning. For example, Arena reported the deactivation of Ru-based catalyst due to gluconic acid, a co-product in the hydrogenation of glucose to sorbitol.[98] Hammond *et al*. identified that the major reason behind catalyst deactivation during the aerobic oxidation of benzyl alcohol, over supported iridium oxide nanoparticles, was the in-situ formation of trace amounts of benzoic acid.[99] Moreover, if the biomass-derivate used as feedstock is previously treated with a biological process, such as enzymatic fermentation, high amount of biogenic impurities which might act as poison tent to be present.[100] It is well-known that in chemical processes, the solvent media could deeply affect the outcome of the reaction, together with the (by-) products distribution. In some cases, it is reported that the solvent might even act as a proper poison for the catalyst. For example, water particularly inhibits Lewis acid materials through hydrolysis.[101] It is found that the intrinsic activity of Sn-β for the MPV transfer hydrogenation of cyclohexanone in 2-butanol decreased by more than 80%

following the addition of only 4 wt.% water to the feed.[102] Furthermore, its ability to catalyse the isomerisation of glucose to fructose decreases by two orders of magnitude when water is employed as reaction solvent instead of methanol.[103] Sometimes poison impurities may also derive from the apparatus in which the chemical process is conducted. For example, Lange and co-workers attributed the deactivation of $PtRe/ZrO_2$ catalyst for the hydrogenation of levulinic acid to γ-valerolactone, to some metal contaminants coming from the steel reactor.[104]

As described above, the origin of poison deactivation can be very diverse, and also the mechanism with which it affects the catalyst can depend on the reaction undergoing study, the exact nature of the contaminants, the reaction conditions, and the active site speciation of the heterogeneous catalyst. However, it generally occurs through the strong irreversible, chemisorption of the poison to the active sites, thus inhibiting their catalytic performances. Therefore, poisoning deactivation not only reduce the catalyst lifetime but might also result in abrupt decreases in reaction rates. For this reason, intrinsic kinetic experiments represent a powerful tool to investigate the propensity for a reaction species to act as poison. In particular, comparison of the rate of reaction in the absence and presence of various contaminants can readily reveal how the rate of the catalytic reaction is affected by the presence of particular (by-) products or impurities. Through this manner, Hammond and co-workers investigated how various by-products impacted the rate of Baeyer-Villiger oxidation over Sn-β. In this case, the product 6-hydroxyhexanoic acid and the co-product water, were found to decrease the initial rate of activity by up to 50%, demonstrating their strong ability to act as poison.[105,106]

Extraction studies are also useful methods of identifying poisoning. Indeed, treatment of the post reaction catalyst in various solvents, followed by $^{1}H/^{13}C$ (or related) NMR, and chromatographic analysis of the supernatant solution, allows to identify the presence of certain retained species.[107]

1.3.3.3 Active site reorganization

During the chemical reaction. the catalyst may undergo several chemical or physical processes that induce the reorganization of the active sites leading to a change of their catalytic properties. Such processes may include agglomerating of the active sites, causing lower active surface area, i.e. sintering; or chemical changing of the catalytic sites which lead to inactive or unselective species. Sometimes even more catastrophic events may occur such as the physical collapse of the catalyst structure, or the leaching of the active sites from the heterogeneous texture. As it can be expected most of these kind of deactivation processes are much more irreversible than fouling or poisoning, hence the evaluation of catalyst regeneration is a first important step to identify them.

Active sites *sintering* is a common deactivation process among the metal-based catalysts.[108-110] In this process, metal active particles agglomerate forming bigger metal clusters with lower active surface area or even losing their peculiar properties such in the case of nanomaterials, often due to harsh reaction conditions like temperature or pH, (Figure 11).[111, 112]

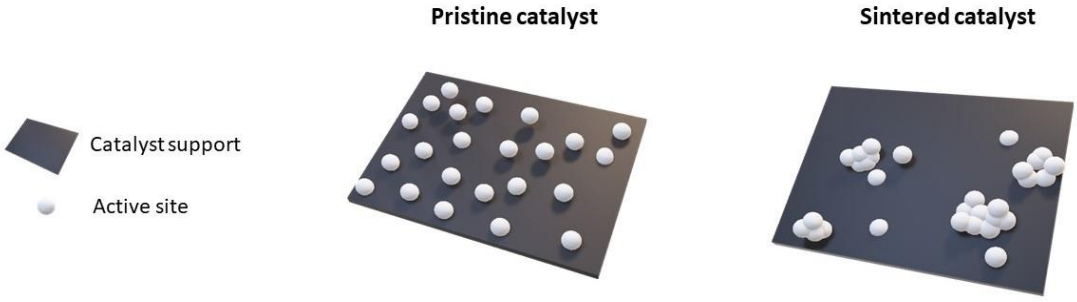

Figure 11 Schematic representation of catalyst sintering.

The particles can grow into larger ones through several mechanisms: particles might move and coalesce, or atoms move from one particle to another, either by volatilisation or by surface migration. However, sintering resembles crystallisation: larger particles grow at the expense of smaller ones since larger crystallites are more stable than the smaller ones. As reported by Bartholomew, the sintering of nanoparticles is strongly temperature dependent, but also the presence of a solvent can markedly affects their stability.[85, 113] Thus the choice of using a liquid-phase or a gas-phase reactor with this kind of catalyst must be thoroughly pondered. Moreover, the sintering of metal nanoparticles depends also on the choice of the support, the initial particle size, the composition of the metal nanoparticle and to the deposition method. In addition, special stabilisers can be added during the synthesis of the catalyst to enhance the nanoparticles stability.[114-116] Due to the nature of sintering process a variety of methods including, TEM, STEM microscopy, or XRD can be used on the pre- and post- reaction catalyst to identify the phenomenon.[117, 118]

Another type of physical reorganization, common for hetero-substituted zeolites catalysts, is the migration of the heteroatom from an active in-framework position to an inactive extra-framework position. Sometimes the migrating metal species eventually become extra-framework bulk oxides, that do not have any catalytic activity. To probe this particular site reorganization a combination of characterization techniques such as MAS-NMR and X-ray absorption spectroscopy (XANES, EXAFS) can be used on zeolite materials.[119]

Frequently, also chemical transformations may occur to catalytic active sites. For example, in metal-based catalysts the metal phase can be oxidized or reduced in-situ by

reactants, reaction condition, or even by reaction products into inactive species. In this case, techniques such as TPDRO, XRD and XPS can provide useful information.

As previously anticipated more extreme reorganizations can irreversibly damaging the catalyst structure, thereby, its performances.

Leaching can fully nullify catalyst activity since consists in the solubilization of the active sites in the reaction medium, (Figure 12).

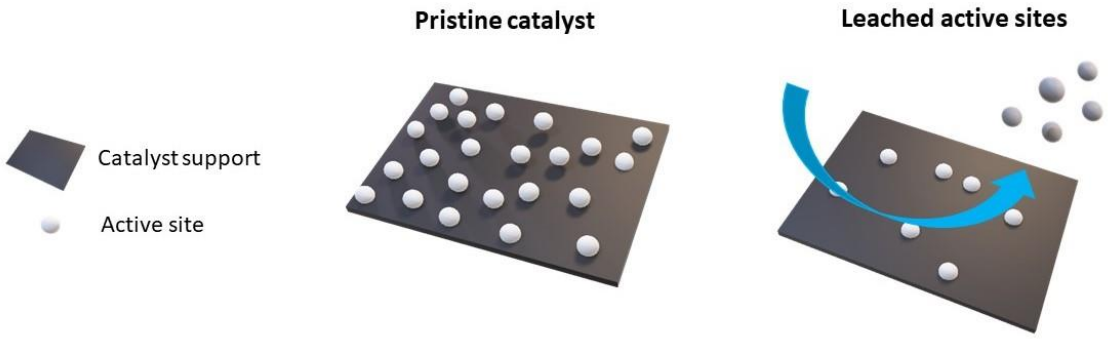

Figure 12 Schematic representation of active sites leaching.

Usually the phenomenon is due to the poor stability of the active particles on the catalyst support or to inappropriate reaction conditions. For example, a too acidic or basic environment can dissolve some components of the catalytic material. Sometimes even impurities present in the feedstock can favour the lixiviation of the metal active site. For instance, dry biomass contains about 1.5% of inorganic salts such as NaCl and it is reported that the dissolution rate of metal oxides could be dramatically enhanced by cations in solution.[120] The detrimental effect of the leaching is not only the loss of the catalytic performances, but metal atoms dissolved in the reaction medium may exhibit high reactivity thus favouring the formation of unwanted by-products, modifying the whole process selectivity.

Furthermore, the lixiviated species are potential toxic compounds which the presence in the reaction downstream might strongly damage the environmental feasibility of the process. Thereby, to recover the leached elements and to decontaminate the reaction effluent, intensive downstream separation units may be implemented, dramatically raising the fixed and operational costs of the whole plant. As consequence, the loss of expensive catalytic elements coupled with the requirement for special downstream unit operations, make leaching one of the most detrimental phenomena for the economic and environmental potential of chemical processes. One of the simpler methods to detect leaching is the elemental analysis of the reaction effluent with ICP-MS or AES technique. Otherwise, elemental analysis can be conducted on the residual digestion solution of the pre- and post-reaction catalyst. Accordingly, both fresh and used catalyst can be digested in aqua regia or HF and then, the elemental quantity present in the resultant solutions can

be compared. It should be noted that if leaching occurs in batch system, it is possible to not detect the loss of the catalytic activity. Indeed, even if few traces of the metal sites are dissolved in the solution medium, these leached species might be responsible for high level of reaction conversion through homogeneous catalytic mechanisms.[121-123] Obviously, this do not solve disadvantages due to leaching phenomena since all the downstream issues, as the product purification, persist. Contrarily, in continuous processes the leached species are continually washed away from the solid, thus it is far easier to detect the deactivation.[124]

Finally, catalyst deactivation can also be due to the structural collapse of the catalytic material. Usually this phenomenon takes place via hydrothermal dissolution or mechanical deconstruction of the catalyst texture, (Figure 13).

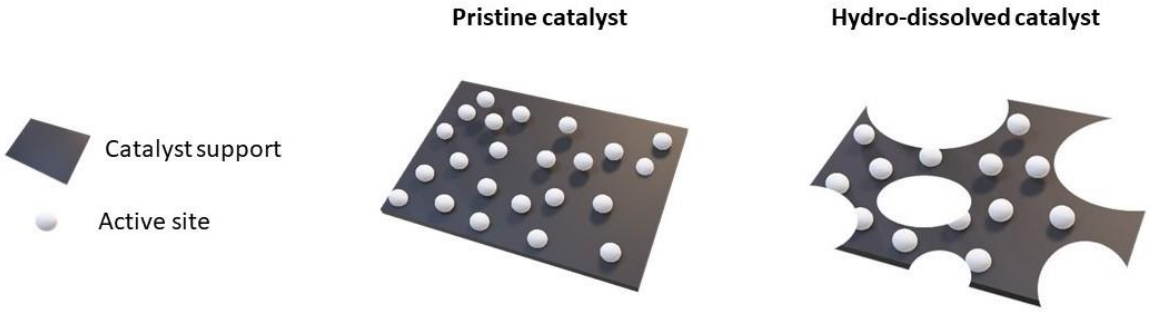

Figure 13 Schematic representation of catalyst hydrothermal dissolution.

Hydrothermal dissolution of the catalyst is due to its interaction with the reaction solvent. For aluminosilicate materials such dissolution may relate to the loss of the crystalline structure and hence, to total reorganisation of the active sites. For other heterogeneous catalysts, such dissolution may be related to the formation of new phases of a metal-metal oxide, or restructuring of the active sites such as sintering, upon treatment in the hot liquid medium. For crystalline materials, hydrothermal dissolution of the catalyst is best identified through powder XRD (pXRD) analysis prior to, and following, the chemical reaction. For example, Padovan *et al.* employed pXRD to demonstrate that amorphization of Sn-β occurs during the aqueous phase isomerisation of glucose to fructose at 110°C.[119] However, for highly porous material the measurement of the micropores volume, by means of porosimetry analysis, must also be performed to ascertain partial structural collapse. Indeed, Van der Vyver only detected partial degradation of Sn-β by performing detailed micropore volume measurements. Although such volumes decreased by ± 20%, strongly indicating at least some structural degradation, no evident changes to the crystalline structure could be detected by pXRD.[125]

The major mitigation strategy to avoid hydrothermal dissolution is the selection of the optimal reaction solvent, both in terms of activity and stability. For example, Sn-β reported

extensive and irreversible deactivation due to amorphization when employed in aqueous phase for the isomerisation of glucose to fructose.[119] In contrast, performing the reaction in methanol leads to a lower amorphization of the catalytic material during the reaction.
Mechanical failure of catalysts is observed in several different forms, including crushing of granular pellet, attrition and erosion, which result in the size reduction or breakup of the catalyst granules, thereby modifying the catalyst structure and causing reactor plugging. These mechanical fractures can result from a combination of several effects such as, continuous attritions and shear forces applied to the solid material inside the reactors system, or to thermal stresses. Thereby, even the mechanical and thermal stability of the material support may play a key role in the long-term performances of the catalyst.

1.4 Process intensification

Process intensification stands for an integrated approach for process and product innovation in chemical research and development, and chemical engineering in order to sustain profitability.[132] In chemical production, it consists in the development and design of the most appropriate operational methods, techniques and materials that improve the chemical plant efficiency by decreasing equipment size/production capacity ratio, energy consumption and waste generation, thus resulting in cheaper, safer and more sustainable processes. Usually, intensification of heterogeneously catalysed processes starts by investigating in lab-scale apparatuses those chemical and engineering conditions that allow the catalysts to express its maximum productivity. In fact, the good efficiency of a catalyst is not due only to its intrinsic activity and selectivity features but depends also on a series of other parameters such as catalyst stability, heat and mass transfer phenomena that can be evaluated and optimised also in small-scale systems such as lab reactors.
Due to the massive economic and environmental benefits that intensification studies return, they have been extensively performed over the last century on crude oil upgrading processes, thus yielding extremely efficient technologies. Conversely, intensification studies of the recently explored biomass-upgrading reactions are less common, thus leaving a lack of knowledge of the real potential of these technologies. For that reason, it is crucial to conduct optimisation studies also for new biomass valorisation reactions to better evaluate their competitiveness with the petrochemical based ones.
Therefore, in this paragraph are illustrated the main procedure and experimental methodologies that are employed in the experimental chapters of this thesis (Chapter 3, 4 and 5) to optimise heterogeneously catalysed reaction for biomass valorisation.

1.4.1 Catalyst parameters

In order to evaluate the potential of a catalytic material to assist a desired reaction, several performance indicators that express different catalyst ability are used. The main performance indicator on which a catalyst might be evaluated is the catalyst activity that, in turn, can be expressed in many different ways. For example, substrate conversion (Equation 2) indicates the amount of substrate converted by the catalyst under a defined set of reaction condition. Although conversion is a useful parameters to follow the reaction course, it does not consider the concentration of the active species on the catalyst, neither the time employed to convert a specific amount of substrate, hence is not indicative of the intrinsic activity of the catalyst. In this regard, to determine the intrinsic activity of a reaction is necessary to follow the conversion evolution, and hence the concentration of the chemical species involved in the reaction, over the reaction time. In this way is possible to obtain a rate of the variation of the concentration of the chemical species involved in the reaction and thus determine the catalyst activity. Catalyst activity can be also displayed by the turnover frequency, TOF (Equation 3) which give insight on the intrinsic potential of the active material. Also in this case, in order to determine the intrinsic activity of the reaction, is necessary to calculate the number of moles converted over the moles of active sites as function of reaction time.

Equation 2

$$Conversion\ (\%) = X_{(t)} = \frac{([R]_0 - [R]_t)}{[R]_0} \times 100$$

Equation 3

$$TOF = moles_{(converted)}\ moles^{-1}_{(active\ site)}\ time^{-1}$$

Another performance indicator pivotal for a promising active material is its capacity to specifically promote the desired reaction among the broad range of parallel and consecutive reactions that might occur in a chemical process. The ability of the catalyst to produce the target product, discriminating the generation of unwanted compounds, is named selectivity (Equation 4). The catalyst selectivity is a key feature for an active material to be implemented in industrial processes since downstream operation, like product separation and purification, normally represent one of the most cost-demanding steps. Therefore, the employment of high selective catalyst is often researched to increase the economic potential of the whole chemical process.

Equation 4

$$Selectivity\ (\%) = S_{(A)} = \frac{[P]_A}{\sum[P]_{(total)}} \times 100$$

Catalysts that demonstrate high activity and selectivity normally generate promising amount of the target product, which its value can be used to evaluate the catalyst potential for a more industrial perspective. In this regard, catalyst productivity considers the amount of target product yielded per mass of catalyst per unit time and may take in account also other process specification, such as the amount of catalyst employed (Equation 5) or the catalyst volume, thus returning the space-time yield, (Equation 6).

Equation 5 $$Catalyst\ productivity = \ grams_{(product)}\ grams^{-1}_{(catalyst)}\ time^{-1}$$

Equation 6 $$Space\ time\ yield = \ grams_{(product)}\ cm^{-3}_{(reactor\ volume)}\ time^{-1}$$

However, as previously illustrated, long-term stability is one of the main features, together with activity and selectivity, that makes a catalytic material attractive for industrial application. Indeed, during the chemical reaction the catalyst might undergo to several deactivation phenomena that jeopardise its performance, thus dramatically decreasing the process productivity. For this reason, to properly estimate the economic potential of any catalytic process it is of crucial importance to assess the catalyst stability. Catalyst stability is defined as the ability of the catalyst to perform catalytic cycles for an extended period of time whilst retaining its initial performance, or rather, without losing its activity or selectivity features during the reaction course. As consequence, the stability of a heterogeneous catalyst can be evaluated by the total number of turnovers (Equation 7) that a certain amount of active material can perform prior to losing its performances.

Equation 7 $$TON = moles_{(converted)}\ moles^{-1}_{(active\ site)}$$

However, TON does not consider the production of the target product, which is the primary purpose of every chemical process. Therefore, to properly compare different catalytic processes is useful to calculate the quantity of product obtained during the lifecycle of a certain amount of catalyst, hence using the total catalyst production, (Equation 8).

Equation 8 $$Total\ catalyst\ production = \ grams_{(product)}\ grams^{-1}_{(catalyst)}$$

Despite the stability of the catalyst being a critical aspect for the success of any catalytic process, deactivation of heterogeneous catalysts in biomass processing systems is a topic often overlooked both by academic and industrial institutions. Therefore, the potential to increase the performances of catalytic processes for biomass valorisation is still wide. In this regard, catalyst stability studies in which catalyst lifetimes are determined

and deactivation causes are investigated, represent powerful tools to dramatically increase the prospective of developing a sustainable chemistry based on renewable starting materials.

1.4.2 Experimental methods in catalysis kinetics

In order to determine reliable performance indicators, including catalyst stability, it is of crucial importance conducting a large number of accurate kinetic experiments. Depending on the information that needed to be acquired, the utilisation of discontinuous (batch) reactors or continuous flow reactors is more appropriate. In fact, batch experiments are typically performed at the preliminary stage of a kinetic study since provide useful information on the reaction itself. For example, batch time online experiments are employed to follow the reaction evolution over time by monitoring substrate conversion, products yield and selectivity and, hence, to determine reaction kinetics rate. In this way it is also possible to ascertain the nature of eventual by-products, deducing if are generated by parallel or consecutive reactions and, thus, understand the whole range of reaction pathways that characterise the chemical process. Batch systems, in regard of catalyst stability, are also sometimes employed to identify particular deactivation phenomena. For example, one of the most used technique to reveal active sites leaching is the hot filtration experiment performed in batch reactors. In this two-step experiment, a catalytic reaction is first performed at normal condition to determine the reaction evolution along the time online.[140] Subsequently, a second amount of fresh catalyst is screened for catalytic activity. In this second test, however, the catalyst is filtered out of the reaction solution after a given period of time and the remaining solution is placed back in the reactor without the solid catalyst. At this point, if the reaction continues to proceed even in the absence of the solid catalyst, it is clear that the active phase has leached in the solution and is acting as a homogeneous catalyst. In contrast, if after the removal of the solid catalyst the reaction terminates, active sites are not dissolved in the solvent media, (Figure 15).

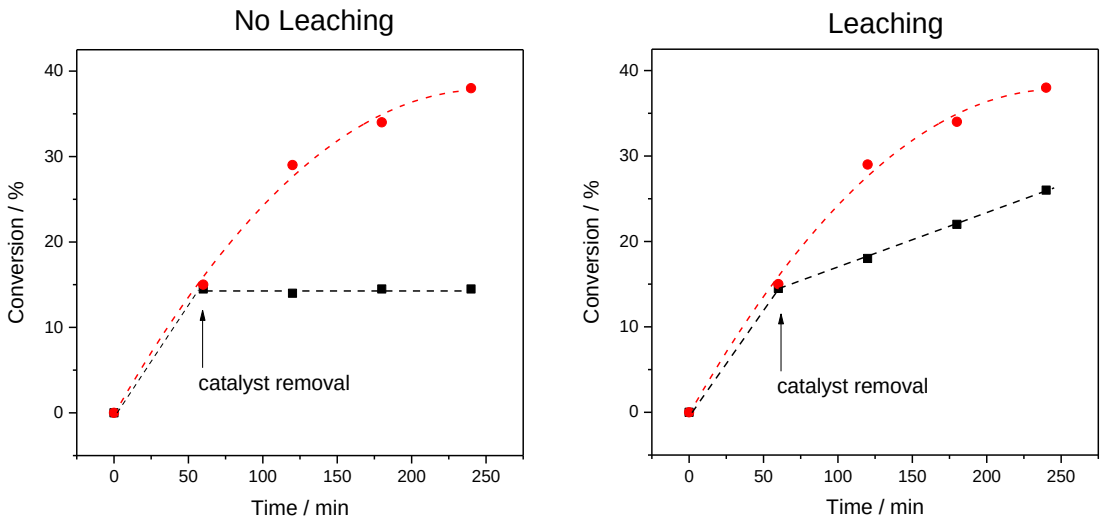

Figure 15 Example of hot filtration experiment during batch operation. The red line represents the conversion vs. time profile of the reaction performed with the solid catalyst in the mixture. The black line represents the kinetic profile after the hot filtration (removal of catalyst). On the left it can be seen that no conversion is observed after the removal of catalyst, suggesting that the reaction is purely heterogeneous catalysed. On the right the catalyst leached some of the active phase in the solution, some extent of conversion is detected during time, meaning that homogeneous catalysis is performed by the leached species.

Although discontinuous systems offer the opportunity to give insight in some important catalytic information, they do not represent the most appropriate solution to evaluate the catalysts stability. Indeed, in these types of apparatus reactants concentration decreases along the reaction time, due to their transformation in the products, which progressively accumulate inside the reaction vessels increasing their concertation. In this way, the steady state of the system is not verified and reaction rates decrease during the system operating. For this reason, in discontinuous processes, catalyst stability can be only determined by comparing reaction rates of subsequently reaction cycles, by means of the so-called reusability tests. In these experimental procedures the catalyst is separated from the solution media after the first reaction cycle, then tested in a second cycle with equal experimental conditions. By comparison of the kinetic rates of the two reaction cycles it can be evaluated if the catalyst has loss some activity performances.

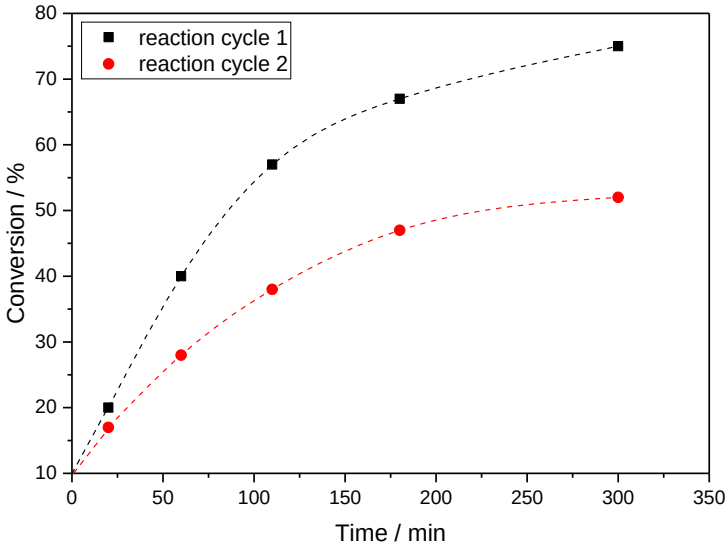

Figure 16 Example of reusability test performed in batch reactor to assess catalyst stability. The black line represents reaction time profile of the first reaction cycle. At the end of the first reaction cycle the used heterogeneous catalyst is separated from the reaction mixture and then dried to obtain the catalyst material in similar condition to the fresh one. The used catalyst is then re-tested for a second reaction cycle with fresh substrate feed, thus resulting the red line profile. Since the final conversion of the second cycle is lower to the first one, is evident that during the reaction occurring the catalyst undergoes to some deactivation phenomena which inhibit its activity during the second reaction cycle.

For instance, in the reusability test of Figure 16, the reaction rate of the second cycle is lower than the first one, implying that during the first reaction the catalyst has undergone to some phenomena that inhibits its activity. This implies that, in discontinuous systems, catalyst stability can only be assessed by means of multiple kinetics experiments, which can affect the accuracy of the data acquired. Indeed, the separation of the catalyst from the reaction solution and the subsequent treatments required to obtain the catalyst in a comparable state to the pristine one (i.e. drying), as required by reusability tests, can induce some physical changes that compromise the catalyst activity, falsifying the reaction rate of the second cycle. This might induce in over/underestimations of the deactivation effect on the catalyst performances. For example, the reaction might induce the formation of detrimental species that adsorbed on the surface of the catalyst inhibit its activity. If these adsorbates are released during the drying procedure between the two reaction cycles, their detrimental effect can not be observed, hence impeding to detect the deactivation phenomenon during the reaction. Moreover, promising catalysts which show promising long-term performances, would require higher number of reusability tests to determine their stability, increasing the uncertainty of the data acquired. In addition, batch reactions are typically conducted at low substrate / active site molar ratio than to the one utilised in industrial application. In this way, at the low substrate turnover in which the

stability tests are performed in batch reactors the deactivation phenomena might yet not arise, which instead promptly occur at the higher substate turnover of industrial processes.

In contrast, lab scale continuous flow systems mimic more faithfully the real industrial scale scenario in which catalysts are employed. Furthermore, these apparatus operate by definition under steady-state regime, implying that the proceeding of the reaction is not time depended such as in batch reactors. In this condition, if no deactivation processes occur, the substrate conversion monitored against the time on stream should not vary with time, providing constant reaction rates, (catalyst A, Figure 17). Conversely, if the catalyst undergoes to some deactivation phenomena, a decreasing of conversion is promptly observed, (catalyst B, Figure 17).

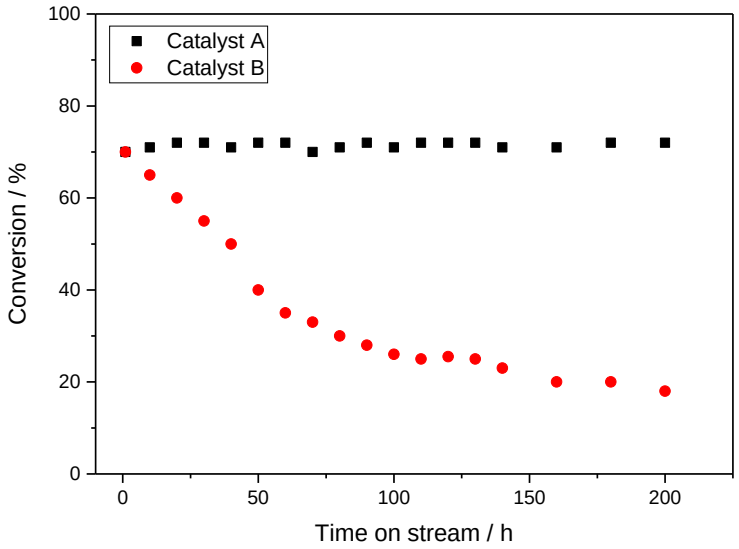

Figure 17 Time on stream profile of a continuous flow reaction. The black squares represent conversion points obtained using a catalyst that does not undergo deactivation phenomena. In this condition the conversion provided by the catalyst is constant along the whole time on stream of the continuous reaction. On the contrast, red circles represent a time on stream reaction profile of a continuous reaction assisted by a catalyst that suffer deactivation along the reaction. In this last case the conversion provided by the catalyst decreases along the time on stream due to the occurring of some deactivation phenomena that inhibit the catalyst activity.

In this way, continuous flow systems offer the possibility to detect deactivation phenomena simply by monitoring the catalyst performance as function of the time on stream of the reaction. Therefore, the catalyst stability can be observed in one single experiment, returning much more reliable data.

However, the first step to comprehend a phenomenon is the ability to measure and quantify it. Therefore, in order to understand how intensively a catalyst deactivates in continuous reactions, it is useful to linearise the conversion profile over the reaction time, by means of the Levenspiel approach (Figure 18).[126] Thereby, the slope of the new linear

trend is an indication on how intensively the conversion drops over the time on stream, or rather, how fast the catalyst deactivates during the reaction. Henceforth, the slope of that linear trend is assumed to be the deactivation rate of the reaction undergoing study, therefore denoted as k_d. It should be noted that, in a continuous reaction in which the catalyst does not suffer any deactivation phenomena, all the conversion points are constant and, as consequence, also the respective points of the logarithmic function (Figure 18). Therefore, in case of a continuous reaction in which deactivation events do not occur, the gradient of the Levenspiel plot and, hence, the deactivation rate measured is equal to zero.

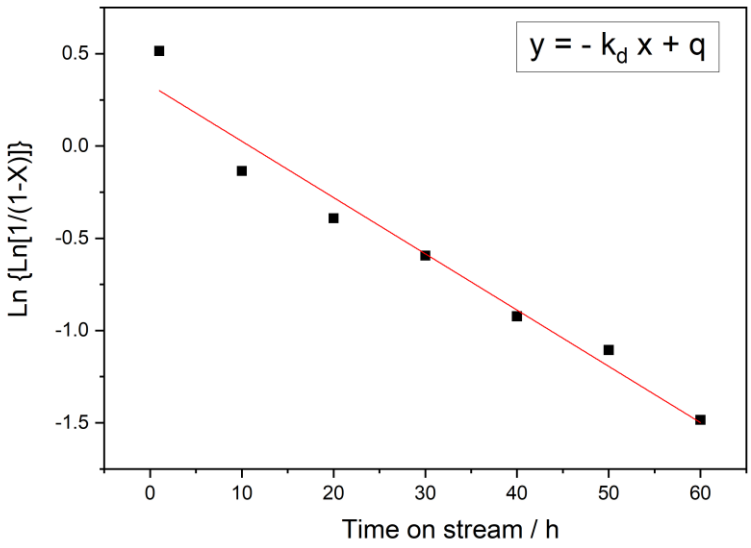

Figure 18 Example of Levenspiel plot obtained by plotting the results of the logarithmic function of consecutive conversion points of a continuous reaction against the time on stream of the reaction itself. In this manner the conversion drop due to catalyst deactivation can be linearised against the time on stream of the reaction and the deactivation rate k_d calculated as the linear gradient of that profile.

In this way, thanks to continuous flow systems, it is possible to observe and quantify catalyst deactivation in one single experiment. Furthermore, this modus operandi allows an experimentalist to compare deactivation rates of reactions conducted in different operational conditions and, hence, to optimise catalyse stability. It is then obvious why continuous flow chemistry allows a more thorough analysis on catalyst deactivation.

In addition, continuous systems, compared to batch reactors, offer a wide array of advantages which make them the preferred solution for industrial scale application. Indeed, the steady state of continuous processes, as previously explained, ensure time invariable reaction conditions, such as concentration, reaction rates, heat and pressure gradients, allowing a more accurate control of the process parameters. The higher level

of process control ensures in turn, improved product quality and enhanced reactor safety. Indeed, one of the most interesting breakthroughs in continuous processes is the in-line analysis of the downstream effluent, which permit to live verify the product quality and promptly intervene on the reaction conditions if deviations from quality standards are detected. The continuous control of the process also allows to identify and prevent hazardous incoming events, such as reactor run-aways. As consequence, continuous systems are considered intrinsically safer than discontinuous ones, also for their lower equipment size/productivity ratio. Indeed, to guarantee equal time productivities, batch reactors should be bigger in size and process higher quantities of chemical compounds, thus increasing operational risks. In addition to the improved safety, reactor volumes minimizations ensure higher levels of scalability, thus facilitating the transfer of processes from R&D to industrial production. The reduction of equipment sizes also decreases mass and heat gradients inside the apparatus, thereby allowing to easier achieve those conditions which optimize the catalyst performances. Furthermore, it must be noted, that in the particular case of heterogeneous catalysis, the continuous reaction is integrated with the continuous separation of the solid catalyst from the products stream, thus dramatically decreasing the cost associated to the product recovery. Accordingly, it is obvious why continuous systems offers the possibility to massively enhance the economic potential and the sustainability of chemical processes.

One of the most used continuous systems to evaluate catalyst performances is the lab scale packed bed tubular reactor. This lab scale apparatus well simulates industrial fixed-bed reactors and, at the same time, permit to obtain accurate kinetic data. In fact, if right precautions are taken, these systems can operate within the conditions used to define the plug-flow fluid dynamic approximation, which allow to describe the occurring reaction with accurate kinetic equation.

1.4.3 Packed bed tubular reactor and plug flow approximation

These kinds of apparatus consist of a tube reactor packed with a given mass of catalytic material in which a continuous flow of reactant solution is fed through, and continuously converted in the target product, which in turn leaves the rector as effluent, (Figure 19).

In these systems the first condition that must be respected in order to obtain reliable and accurate data on the catalyst performance is the so-called *plug-flow* fluid dynamic approximation. In this condition the reacting fluid moves through the reactor tube in lamellar flow like a plug or piston, assuring the equal distribution of the different phases through the catalytic bed. This prevents the formation of preferential fluid channel, in which the effluent might only partially interact with the catalyst bed.

Figure 19 Schematic representation of a lab scale packed bed tubular reactor. The reactants are continuously fed through a tubular reactor packed with a fixed mass of catalyst. Passing through the catalyst bed the reactants are continuously converted in the reaction products, that in turn leave the reactor as effluents.

The condition of lamellar flow generally ensures the absence of temperature, velocity and concentration gradients in the radial direction. As consequence, this fluid dynamic approximation ensures that the solution in contact with catalyst bed is well-mixed in radial coordination and zero-mixed in the axial ones. A fixed-bed tubular reactor that respect the condition of plug flow is denoted as *plug flow reactor* (PFR). Thanks to the plug-flow state, for a given mass of catalyst and a constant reaction solution flow rate, the contact time (τ, Equation 9) of the substrate molecules with the active material inside the reactor is fixed. A useful parameter usually adopted in PFR systems is the reciprocal of the contact time, or rather the Liquid Hourly Space Velocity (LHSV), defined as the fraction of feed exposed to a given quantity of catalyst per unit time, (Equation 10).

Equation 9
$$Contact\ time = \tau = \frac{volume_{(catalyst\ bed,mL)}}{flow\ rate\ (mL\ min^{-1})}$$

Equation 10
$$LHSV = flow\ rate\ _{(feed\ solution)}\ volume^{-1}_{(catalyts)}\ hour^{-1}$$

To ensure a plug flow state inside a tubular reactor the following measures should be taken:

- The reactor diameter (D) must be at least 10 times the catalyst particle diameter (d_p).

  $$\frac{D}{d_p} > 10$$

  in order to avoid preferential effluent stream path near the reactor wall. Indeed, the difference between the packing density in the interior and that near the wall may cause higher local velocity near the wall, resulting in a non-flat radial velocity profile, and possibly also bypassing of effluent along the wall.

- The catalyst bed length should be several hundred particle diameters, in order to preventing effect of axial dispersion.

The selection of the catalyst particle diameters and the reactor sizes it is also important to prevent severe pressure rises along the reactor which can induce catalyst structural damages, causing in turn effluent blockage. Even local pressure drops must be prevented, otherwise a non-constant diffusion of the reacting solution along the catalyst bed can occur, thus falsifying the contact time of the reaction. A good rule of thumb is that the pressure drop should be lower than approximately 20% of the total operation pressure in the reactor.

In PFR systems, *isobaric operation* can be ensured by a thoroughly selection of the bed particle sizes and by the installation of a back-pressure regulator downstream to the reactor.

Moreover, to collect representative experimental data it is important not only to work in well-defined fluid dynamic regime but also assure an *isothermal profile* along the tubular reactor. In fact, according to the Arrhenius equation (Equation 1), the kinetic of the reaction is strongly dependent to the temperature. Thereby, to obtain accurate measures of the catalyst activity the temperature inside the reactor must be intimately known and constant. Furthermore, in a complex chemical scenario, characterized by several parallel and sequential reactions, the temperature of the system also strongly influences the product distribution, thus affecting the catalyst selectivity. In addition, the formation of hot-spots can induce rapid deactivation events along the catalyst bed, threatening the stability of the material. In the worst-case scenario, if the temperature gradients are not controlled, an exothermic reaction can even lead to the run-away of the reactor. In heterogeneous catalytic reactions the most significant temperature profiles arise between the catalyst bed and the effluent liquid phase because of the different thermal conductivity of solid and liquid. In this case the temperature gradient is classified as *extraparticle.* However, also important *intraparticle* temperature profiles can arise if are used too big catalyst particles with unregular geometry. Tight temperature control is therefore necessary to collect accurate measurement, of the activity, selectivity and stability of the catalyst, in addition to assure safe reaction conditions.[127, 128]

To operate isothermally extra precautions must be taken, especially if particularly exothermic or endothermic reactions are performed. In this regard, to avoid intra-reactor temperature gradient, dilutions of the reaction feed and the catalyst bed may be necessary. Indeed, the feeding of an inert substance together with reactants allows to increase the heat removal from the reaction zone. In addition, the catalysts dilution with inert solid particles, having the same size of the catalytic particles, reduces the local hot-spots and improves the temperature distribution along the catalytic bed. Another measure that aids to reduce temperature gradients is decreasing the reactor diameter, which should necessarily be accompanied by the reduction of particle diameter, in order to fulfil the PFR condition.

However, in all the lab scale experiments performed in this work, the temperature gradient due to exo/endothermicity of the reactions can be neglected since only small quantities of reactants were used if compared to the heat power exchange of the equipment employed. Moreover, the small dimension of the reactors, assure uniform temperatures in every points of the apparatus, including the catalyst bed and the catalyst particles.

Ensuring the system works under a specific fluid dynamic regime, at isothermal and isobaric state allows to know and control at any time and at any location the conditions within the reactor. However, prior to collect reliable catalyst kinetic data it must be ensured that the system is not affected by interphase limitations, such as external and internal mass transfer. Indeed, these undesired phenomena might introduce extra resistances to the catalytic process, hence limiting and falsifying the real potential of the catalyst. Therefore, prior to evaluate catalytic performances, including long-term stability, it must be conducted control experiments to identify those operational condition which guarantee the occurring of the correct chemical kinetic regime.

1.4.4 Kinetic regime evaluation

Once the experimental reactor has been set-up, with all the criteria previously described, the first step to follow for a correct estimation of the continuous catalytic performance is the evaluation of the continuous kinetic regime. Indeed, in order to properly investigate the performance of a catalytic material it is essential to know the intrinsic kinetic behaviour of the reaction undergoing study and the catalyst itself.

Intrinsic kinetic data can only be obtained from the system operating in *chemical kinetic regime*, where the only resistance to the chemical reaction is its thermodynamic barrier. This because, during the chemical reaction, may occur different transport limitations which add physical resistance to the already present chemical ones, thus decreasing the overall reaction rate and leading to an underestimation of the catalyst performances.

For instance, according to film theory, when the heterogeneous catalyst is immersed in fluid environments a liquid (gas) static film of solvent is formed around the solid particles. The liquid (gas) film act as a proper barrier for the substrate molecules, which to interact with the catalyst active sites must diffuse thought it according to the mass diffusion law, thus adding a resistance coefficient for the overall process. This phenomenon is known as *external mass transfer*. According to fluid dynamic principles, the liquid film around the catalyst particle becomes thinner at increasing linear velocities, thus decreasing the mass transfer resistance.[129] Hence, it can be proposed to conduct continuous reactions at higher flow rates to nullify the external mass resistance, but in turn longer reactors must be adopted to work at constant contact time. As consequential effect higher pressures arise inside the reactor.

It is clear that a proper fluid dynamic study must be conducted in order to find the optimal operating conditions. This involves monitoring the catalytic activity of several continuous reaction performed with different flow rate but at fixed contact time. To do that the mass of catalyst for each reaction must be adjusted accordingly to the linear velocity adopted, preparing a range of catalyst reactors of various lengths (diameter should be kept constant). As such, if external mass transfer limits the overall process, an increase in conversion will occur with increased flow rates. On the other hand, if conversion is independent of flow rate at a fixed contact time then the system is operating in absence of external mass transfer limitation, (Figure 20). Moreover, it must be kept in mind that higher flow rates avoid back mixing phenomena and help to maintain isothermal condition inside the tubular reactor. Indeed, higher linear velocity help to extract the heat generated or subtracted by the reaction, thus ensuring axial and radial isothermal conditions, and even lower extraparticle temperature gradient. Thereby, in all laboratory scale experiment conducted in tubular reactor it is good practise to use flow rates higher than 0.1 mL min^{-1}. In this manner real plug-flow conditions are typically maintained, and good quality kinetic data are collected.

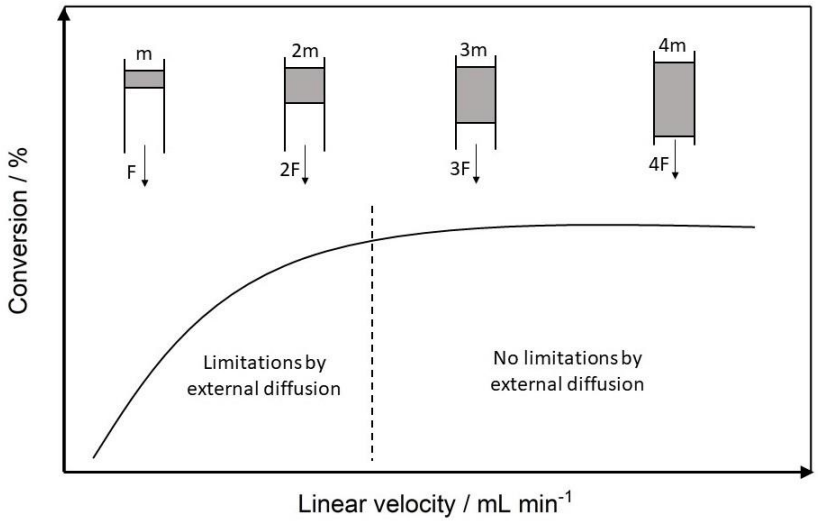

Figure 20 Representation of the effect of the linear velocity in term of mL min^{-1} on the conversion of a continuous reaction. At low linear velocities external diffusion limitations influence the activity of the catalyst. Increasing the linear velocity of the substrate the resistance due to the external diffusion becomes negligible compared to the chemical resistance of the catalytic process, hence the extent of the linear velocity does not more influence the reaction conversion.

In addition to external mass transfer, the overall heterogenous process can be affected by *internal mass transfer*. This occurs when the substrate molecules, once reached the surface of the heterogeneous catalyst, struggles to diffuse inside the solid particles. It follows that for bigger catalyst particles, more likely arise internal diffusion resistances. Furthermore, it must be considered that, in case of highly exo/endothermic reactions,

intraparticle temperature profiles could also arise if too large particles are employed. The simplest way to rule out potential internal mass transfer limitation, is to verify the effect of the catalyst particles sizes on the catalytic activity. To do that, substrate conversion is monitored in several continuous reactions, performed with different catalyst particle sizes, but keeping constant all others reaction conditions, (Figure 21). In the absence of internal mass transfer limitations, the observed conversion should be independent of particle size. Conversely, where internal mass transfer is observed, conversion will decrease. Through this manner Aellig and co-workers demonstrate the presence of internal mass transfer limitations during the liquid phase dehydration of fructose to 5-hydroxymethylfurfural, when the reaction was catalysed by larger particles of Amberlyst-15.[130]

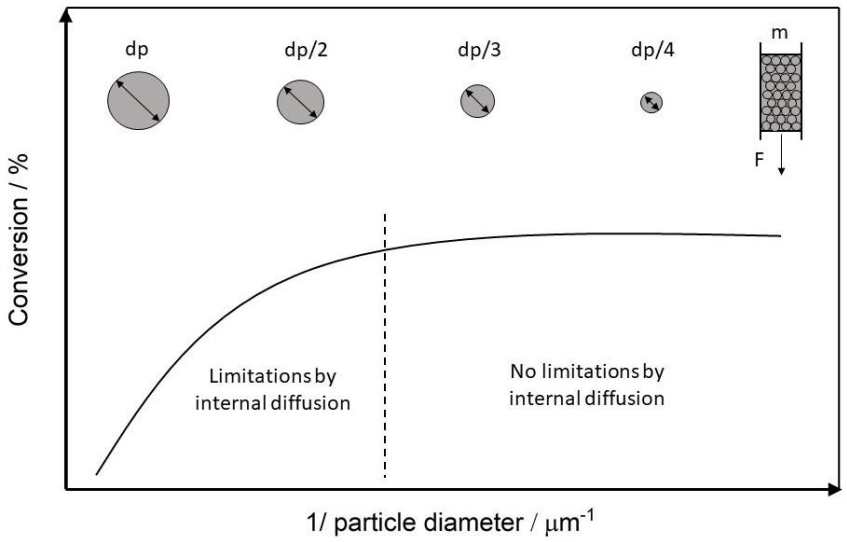

Figure 21 Representation of the effect of the catalyst particles size on the conversion of a continuous reaction. With large catalyst particles the reactants molecules struggle to diffuse through the inner part of the active material, thus decreasing the effective amount of catalyst exploited to assist the reaction, hence returning lower value of conversion. At lower values of catalyst particles diameters, no more internal diffusion limitations occur and reaction conversion values are independent to the particles size of the catalyst.

Usually, in industrial plants, it is preferred to work with the larger catalyst particles which not induce any internal mass and thermal transfer limitation. Indeed, larger catalyst particles ensure lower pressure inside tubular reactors and minimize the potential risk of catalyst bed plugging during continuous operations, thus preserving the catalyst lifetime. In absence of any of interphase limitations the reaction operates in *chemical kinetic regime* and the only resistance to the chemical reaction is the thermodynamic barrier which reactants should overcome to be converted in products. In these conditions, the real intrinsic activity of the catalyst can be measured, and at the same time, the reactor efficiency results optimised under the hydrodynamic standpoint.

1.5 Aim of the thesis

During recent decades, biomass has been considered one of the most valid renewable alternatives to fossil feedstock in the production of chemical commodities. Like petroleum derived substrates, biomass feedstock must be deconstructed into their building blocks and chemically upgraded to create useful platform molecules. In this regard, heterogeneous catalysts have been widely explored by the scientific community as potential materials to upgrade biomass-derivate compounds. However, although some promising heterogeneous catalysed reactions have been developed on laboratory scale to upgrade biomass, intensification studies in which other elements of their industrial applicability are explored, are much less common. Therefore, a lack of knowledge on the real potential of these technologies persists.

Continuous processes are one of preferred solutions by industry to process chemicals due to the several advantages that they possess compared to discontinuous ones, including their easer scalability. Therefore, understanding if a chemical reaction can be conducted in a continuous mode of operation is crucial to evaluate its industrialisation. For these reasons, in this thesis it was attempted to develop continuous processes for heterogeneous catalysed reactions which have shown promising capability to upgrade biomass-derivate substrates in laboratory batch experiments. Furthermore, developing efficient biomass-based processes is imperative to produce cost-effective chemical commodities and thus, to steer the transition from fossil feedstock to renewable resources. As such, particular interest has also been focused on the optimisation of the developed continuous processes to achieve improved performances and thus increasing their potential to be industrially employed. Furthermore, particular emphasis has been addressed to catalyst stability during continuous long-term operation. This catalyst property, although often overlooked in academic research, is paramount to achieve excellent productivity in industrial scale applications. Specifically, due to their commercial interest, throughout the project the following systems were investigated, including formic acid decomposition to hydrogen (Chapter 3), sorbitol dehydration to isosorbide (Chapter 4) and fructose dehydration to furanic compounds (Chapter 5).

1.6 References

1) N. Abas, A. Kalair, N. Khan, *Futures*, 2015, **69**, 31.
2) S. H. Mohr, J. Wang, G. Ellem, J. Ward, D. Giurco, *Fuel*, 2015, **141**, 120.
3) M. Hook, X. Tang, *Energy Policy*, 2013, **52**, 797.
4) Bp, '*Statistical Review of World Energy*', 2020.
5) S. Shafiee, E. Topal, *Energy Policy*, 2009, **37**, 181.
6) IEA, 2007b. World Energy Outlook 2007 China and India. Organisation for Economic Co-operation and Development, International Energy Agency, Paris and Washington, DC.

7) IEA, 2006. World Energy Outlook 2006. Organisation for Economic Co-operation and Development, International Energy Agency, Paris and Washington, DC.
8) W. P. Nel, C. J. Cooper, *Energy Policy*, 2009, **37**, 166.
9) S. Solomon, D. Qin, M. Manning, Z. Chen, M. Marquis, B. Averyt, M. Tignor, H. Miller. IPCC, Climate change: the physical science basis. Contribution of working group 1 to the Fourth Assessment Report of the Intergovernmental Panel on Climate Change. 2007
10) C. O. Tuck, E. Pérez, I. T. Horváth, R. A. Sheldon, M. Poliakoff, *Science*, 2012, **337**, 695.
11) R. A. Sheldon, *Green Chem.*, 2014, **16**, 950.
12) H. A. Krässig, '*Cellulose - Structure, Accessibility and reactivity*', Gordon and Breach Science Publishers, Yverdon, 1993.
13) Y.-H. Percival Zhang, *J. Ind. Microbiol. Biotechnol*., 2008, **35**, 367.
14) W. S.-L. Mock, M. J. Antal, *Ind. Eng. Chem. Res.*, 1992, **31**, 94.
15) M. E. Himmel, S. Ding, D. K. Johnson, W. S. Adney, M. R. Nimlos, J. W. Brady, T. D. Foust, *Science*, 2007, **315**, 804.
16) P. McKendry, *Bioresource Technology*, 2002, **83**, 37.
17) D. M. Alonso, J. Q. Bond, J. A. Dumesic, *Green Chem.*, 2010, **12**, 1493.
18) W. N. R. W. Ishak, M. W. M. Hisham, M. A. Yarmo, T.-Y. Y. Hin, *Renewable and Sustainable Energy Reviews*, 2012, **16**, 5910.
19) T. Kan, V. Strezov, T. J. Evans, *Renewable and Sustainable Energy Reviews*, 2016, **57**, 1126.
20) A. V. Bridgewater, *Biomass and Bioenergy*, 2012, **38**, 68.
21) P. McKendry, *Bioresource Technology*, 2002, **83**, 47.
22) Y. C. Lin, G. W. Huber, *Energy Environ. Sci*., 2009, **2**, 68.
23) G. W. Huber, S. Iborra, A. Corma, *Chem. Rev.*, 2006, **106**, 4044.
24) M. E. Himmel, S. Ding, D. K. Johnson, W. S. Adney, M. R. Nimlos, J. W. Brady, T. D. Foust, *Science*, 2007, **315**, 804.
25) C.-H. Zhou, X. Xia, C.-X. Lin, D.-S. Tong, J. Bertramini, *Chem. Soc. Rev.*, 2011, **40**, 5588.
26) A. Brandt, J. Gräsvik, P. Halletta, T. Welton, *Green Chem.*, 2013, **15**, 550.
27) T. E. Timell, *Wood Sci. Technol.*, 1967, **1**, 45.
28) K. E. Myton, S. C. Fry, *Planta*, 1994, **193**, 326.
29) W. S.-L. Mock, M. J. Antal*, Ind. Eng. Chem. Res.*, 1992, **31**, 94.
30) M. FitzPatrick, P. Champagnea, M. F. Cunninghama, R. A. Whitney, Bioresource Technology, 2010, **101**, 8915.
31) E. Nikolla, Y. Roman-Leshkov, M. Moliner, M. E. Davis, *ACS Catal.*, 2011, **1**, 408.
32) A. Corma, S. Iborra, A. Velty, *Chem. Rev*., 2007, **107**, 2411.
33) H. Kobayashi, A. Fukuoka, *Green Chem.*, 2013, **15**, 1740.
34) D. Martinz, J. Quadros, *Plast. Rubber Compos.*, 2008, **37**, 459.
35) G. Sorda, M. Banse, C. Kemfert, *Energy Policy*, 2010, **38**, 6977.
36) R. Datta and M. Henry*, J. Chem. Technol. Biotechnol*., 2006, **81**, 1119.
37) I. Bechthold, K. Bretz, S. Kabasci, R. Kopitzky, A. Springer, *Chem. Eng. Technol*., 2008, **31**, 647.
38) Y. Roma´n-Leshkov, M. Moliner, J. A. Labinger, M. E. Davis, *Angew. Chem. Int. Ed.*, 2010, **49**, 8954.

39) R. DiCosimo, J. McAuliffe, A. J. Poulose, G. Bohlmann, *Chem. Soc. Rev*., 2013, **42**, 6437.
40) X. Zhang, K. Wilson, A. F. Lee, *Chem. Rev.*, 2016, **116**, 12328.
41) H. Chang, A. H. Motagamwala, G. W. Huber, J. A. Dumesic, *Green Chem*., 2019, **21**, 5532.
42) H. Li, S. Yang, S. Saravanamurugan, A. Riisager, *ACS Catal.*, 2017, **7**, 3010.
43) Z. Zhang, A. A. Donaldson, X. Ma, *Biotechnol. Adv*., 2012, **30**, 913.
44) M. Dusselier, P. Van Wouwe, A. Dewaele, E. Makshina, B. F. Sels*, Energy Environ. Sci.*, 2013, **6**, 1415.
45) T. Ennaert, J. Van Aelst, J. Dijkmans, R. De Clercq, W. Schutyser, M. Dusselier, D. Verboekend, B. F. Sels, *Chem. Soc. Rev*., 2016, **45**, 584.
46) L. Cottier, G. Descotes, *Trends Heterocycl. Chem.*, 1991, **2**, 233.
47) E. de Jong, M. A. Dam, L. Sipos, G.-J. M. Gruter, *ACS Symposium Series*, 2012**, 1105**, 1.
48) A. Gandini, M. N. Belgacem, *Prog. Polym. Sci.*, 1997, **22**, 1203.
49) L. Cottier, G. Descotes, J. Lewkowski, R. Skowronski, *Pol. J. Chem.*, 1994, **68**, 69.
50) C. Thoma, J. Konnerth, W. Sailer-Kronlachner, P. Solt, T. Rosenau, H. W. G. van Herwijnen, *ChemSusChem*, 2020, **13**,3544.
51) N. van Strien, S. Rautiainen, M. Asikainen, D. A. Thomas, J. Linnekoski, K. Niemelä, A. Harlin, *Green Chem.*, 2020, **22**, 8271.
52) M. Caiti, D. Padovan, C. Hammond, *ACS Catal.*, 2019, **9**, 9188.
53) B. Timokhin, V. Baransky, G. D. Eliseeva, *Russ. Chem. ReV.*, 1999, **68**, 73.
54) Y. Nishiyama, P. Langan, H. Chanzy, *J. Am. Chem. Soc*., 2002, **124**, 9074.
55) C. M. Hansen, A. Björkman, *Holzforschung*, 1998, **52**, 335.
56) S. Tolborg, S. Meier, I. Sádaba, S. G. Elliot, S. K. Kristensen, S. Saravanamurugan, A. Riisager, P. Fristrup, T. Skrydstrupc, E. Taarning, *Green Chem*., 2016, **18**, 3360.
57) M. Rose, R. Palkovits*, ChemSusChem*, 2012, **5**, 167.
58) J. Zhang, J. Li, S. Wu, Y. Liu, *Ind. Eng. Chem. Res.*, 2013, **52**, 11799.
59) N. Rey-Raap, L. Sousa Ribeiro, J. J. de Melo Orfao, J. L. Figueiredo, M. F. Ribeiro Pereira, *Appl. Catal. B*, 2019, **256**, 117826.
60) J. J. Bozell, G. R. Petersenb, *Green Chem.*, 2010, **12**, 539.
61) F. Fenouillot, A. Rousseau, G. Colomines, R. Saint-Loup, J.-P. Pascault, *Prog. Polym. Sci*., 2010, **35**, 578.
62) J. N. Cohn, G. Johnson, S. Ziesche, F. Cobb, G. Francis, F. Tristani, R. Smith, W. B. Dunkman, H. Loeb, M. Wong*, N. Engl. J. Med*., 1991, **325**, 303.
63) M. Banu, S. Sivasanker, T. M. Sankaranarayanan, P. Venuvanalingam, *Catalysis Communications*, 2011, **12**, 673.
64) Y. Wang, Y. Pan, Z. Zhang, R. Sun, X. Fang, D. Yu, *Process Biochem.*, 2012, **47**, 976.
65) S. Saravanamurugan, M. Paniagua, J. A. Melero, A. Riisager, *J. Am. Chem. Soc.*, 2013, **135**, 5246.
66) L. S. Scott, *ACS Catal.*, 2018, **8**, 8597.
67) A. Corma, A. Martínez, "*Zeolites in refining and petrochemistry*", Stud. Surf. Sci. Catal, 2005.
68) J. Song, H. Fan, J. Ma, B. Han, *Green Chem*., 2013, **15**, 2619.
69) D. Padovan, C. Parsons, M. S. Grasina, C. Hammond, *Green Chem.*, 2016, **18**, 50413.
70) J.-P. Lange*, Angew. Chem. Int. Ed*., 2015, **54**, 13186.

71) I. Fechete, Y. Wang, J. C. Védrine, *Catal. Today*, 2012, **189**, 2.
72) P. Munnik, P. E. de Jongh, K. P. de Jong, *Chem. Rev.*, 2015, **115**, 6687.
73) J.-P. Lange, *CatTech*, 2001, **5**, 82.
74) V. M. Akhmedov, S. H. Al-Khowaiter, *Catal. Rev.*, 2007, **49**, 33.
75) H. Kobayashi, H. Yokoyama, B. Feng, A. Fukuoka, *Green Chem.*, 2015, **17**, 2732.
76) E. T. C. Vogt, B. M. Weckhuysen, *Chem.Soc.Rev.*, 2015 ,**44**, 7342.
77) B. Smit, T. L. M. Maesen, *Nature*, 2008, **451**, 671.
78) L. Kiwi-Minsker, M. Crespo-Quesada, *Chimia*, 2011, **65**, 699.
79) A. T. Bell, *Science*, 2003, **299**, 1688.
80) M. J. Lundwall, S. M. Mcclure, X. Wang, Z. Wang, M. Chen, D. W. Goodman, *J. Phys. Chem. C*, 2012, **116**, 18155.
81) U. Diebold, *Surf. Sci. Rep*., 2003, **48**, 53.
82) M. Haruta, *Catal. Today*, 1997, **36**, 153.
83) M. D. Argyle, C. H. Bartholomew, *Catalysts*, 2015, **5**, 145.
84) J. A. Moulijn, A. E. van Diepen, F. Kapteijn, *Appl. Catal. A: Gen.*, 2001, **212**, 3.
85) C. H. Bartholomew, *Appl. Catal. A: Gen*., 2001, **212**, 17.
86) L. W. Kroh, *Food Chem.*, 1994, **51**, 373.
87) M. Choura, N. M. Belgacem, A. Gandini, *Macromolecules*, 1996, **29**, 3839.
88) D. C. Elliott, D. Beckman, A. V. Bridgwater, J. P. Diebold, S. B. Gevert, Y. Solantausta, *Energy Fuels*, 1991, **5**, 399.
89) S. Lima, A. Fernandes, M. M. Antunes, M. Pillinger, F. Ribeiro, A. A. Valente, *Catal. Lett.*, 2010, **135**, 41.
90) P. S. Metkar, E. J. Till, D. R. Corbin, C. J. Pereira, K. W. Hutchenson, S. K. Sengupta, *Green Chem.*, 2015, **17**, 1453.
91) K. J. Zeitsch, 'The chemistry and technology of furfural and its many by-products', *Elsevier*, 2000.
92) J.-P. Lange, E. van der Heide, J.van Buijtenen, R. Price, *ChemSusChem*, 2012, **5**, 150.
93) K. Xiong, W.-S. Lee, A.Bhan, J. G. Chen*, ChemSusChem*, 2014, **7**, 2146.
94) B. Katryniok, S. Paul, V. Bellière-Baca, P. Reye, F.Dumeignil, *Green Chem.*, 2010, **12**, 2079.
95) P. Forzatti, L. Lietti, *Catal. Today*, 1999, **52**, 165.
96) P. S. Metkar, E. J. Till, D. R. Corbin, C. J. Pereira, K. W. Hutchenson, S. K. Sengupta, *Green Chem.*, 2015, **17**, 1453.
97) Y. Takeshita, Y. Sato, S. Nishi, *Ind. Eng. Chem. Res.*, 2000, **39**, 4496.
98) B. J. Arena, *Appl. Catal. A*, 1992, **87**, 219.
99) C. Hammond, M. T. Schümperli, S. Conrad, I. Hermans, *ChemCatChem*, 2013, **5**, 2983.
100) T. J. Schwartz, B. J. O'Neill, B. H. Shanks, J. A. Dumesic*, ACS Catal.*, 2014, **4**, 2060.
101) Y. Román-Leshkov, M. E. Davis, *ACS Catal.*, 2011, **1**, 1566.
102) A. Corma, M. E. Domine, S. Valencia, *J. Catal.*, 2003, **215**, 294.
103) R. Gounder, M. E. Davis, *J. Catal.*, 2013, **308**, 176.
104) J.-P. Lange, R. Price, P. M. Ayoub, J. Louis, L. Petrus, L. Clarke, H. Gosselink, *Angew.Chem. Int. Ed.*, 2010, **49**, 4479.
105) C. Hammond, *Green Chem.*, 2017, **19**, 2711.
106) K. Yakabi, K. Milne, A. Buchard, C. Hammond, *ChemCatChem*, 2016, **6**, 1.
107) D. S. Mannel, S. S. Stahl, T. W. Root, *Org. Process. Res. Dev.*, 2014, **18**, 1503.

108) K. P. De Jong, 'Synthesis Of Solid Catalysts', *Wiley-VCH*, 2009.
109) T. W. Hansen, A. T. DeLaRiva, S. R. Challa, A. K. Datye, *Acc. Chem. Res.*, 2013, **46**, 1720.
110) F. Héroguel, G. Siddiqi, M. D. Detwiler, D. Y. Zemlyanov, O. V. Safonova, C. Copéret, *J. Catal.*, 2015, **321**, 81.
111) B. Beverskog, I. Puigdomenech, *Corros. Sci.*, 1997, **39**, 969.
112) D. A. Palmer, P. Bénézeth, C. Xiao, D. J. Wesolowski, L. M. Anovitz, *J. Solut. Chem.*, 2011, **40**, 680.
113) I. Sadaba, M. Lopez Granados, A. Riisager, E. Taarning, *Green Chem*., 2015, **17**, 4133.
114) M. Morad, M. Sankar, E. Cao, E. Nowicka, T. E. Davies, P. J. Miedziak, D. J. Morgan, D. W. Knight, D. Bothell, A. Gavriilidis, G. J. Hutchings, *Cat. Sci. Tech.*, 2014, **4**, 3120.
115) D. M. Alonso, S. G. Wettstein, J. A. Dumesic, *Chem. Soc. Rev.*, 2012, **41**, 8075.
116) A. Cao, R. Lu, G. Veser, *Phys. Chem. Chem. Phys.*, 2010, **12**, 13499.
117) R. C. Tiruvalam, J. C. Pritchard, N. Dimitratos, J. A. Lopez- Sanchez, J. K. Edwards, A. F. Carley, G. J. Hutchings, C. J. Kiely, *Faraday Discuss.*, 2011, **152**, 63.
118) E. K. Gibson, A. M. Beale, C. R. A. Catlow, A. Chutia, D. Gianolio, A. Gould, A. Kroner, K. M. H. Mohammed, M. Perdjon, S. M. Rogers, P. P. Wells*, Chem. Mater.*, 2015, **27**, 3714.
119) D. Padovan, C. Parsons, M. S. Grasina, C. Hammond, *Green Chem.*, 2016, **18**, 50413.
120) P. M. Dove, N. Han, J. J. D. Yoreo, *Proc. Natl. Acad. Sci.*, 2005, **102**, 15357.
121) N. T. S. Phan, M. Van der Sluys, C. W. Jones, *Adv. Synth. Catal.*, 2006, **348**, 609.
122) R. A. Sheldon, M. Wallau, I. W. C. E. Arends, U. Schuchardt, *Acc. Chem. Res*. 1998, **31**, 485.
123) L. Yin, J. Liebscher, *Chem. Rev.*, 2007, **107**, 133.
124) C. Hammond, S. Conrad, I. Hermans, *Angew. Chem. Int. Ed.*, 2012, **51**, 11736.
125) S. Van de Vyver, C. Odermatt, K. Romero, T. Prasomsri, Y. Roman-Leshkov, *ACS Catal.*, 2015, **5**, 972.
126) O. Levenspiel, "*Chemical Reaction Engineering*", 1999, **38**.
127) A. Tanimu, S. Jaenicke, K. Alhooshani, *Chem. Eng. J.*, 2017, **327**, 792.
128) X. Liu, B. Ünal, K. F. Jensen, *Catal. Sci. Technol*., 2012, **2**, 2134.
129) I. W. C. E. Arends, R. A. Sheldon, *Appl. Catal. A: Gen.*, 2001, **212**, 175.
130) C. Aellig, I. Hermans, *ChemSusChem*, 2012, **5**, 1737.
131) L. Kiwi-Minsker, M. Crespo-Quesada, *Chimia*, 2011, **65**, 699.
132) S. Becht, R. Franke, A. Geißelmann, H. Hahn, *Chemical Engineering and Processing*, 2009, **48**, 329.
133) A. J. J. E. Eerhart, A. P. C. Faaij, M. K. Patel, *Energy Environ. Sci.*, 2012, **5**, 6407.
134) D. Welsby, J. Price, S. Pye, P. Ekins, *Nature*, 2021, **597**, 230.
135) K. Huang, X. Peng, L. Kong, W. Wu, Y. Chen, C. T. Maravelias, *ACS Sustainable Chem. Eng*., 2021, **9**, 14480.
136) R. Kajaste, *Journal of Cleaner Production*, 2014, **75**, 1.
137) W. Schutyser, T. Renders, S. Van den Bosch, S. F. Koelewijn, G. T. Beckham, B. F. Sels, *Chem. Soc. Rev*., 2018, **47**, 852.
138) J. Xu, C. Li, L. Dai, C. Xu, Y. Zhong, F. Yu, C. Si, *ChemSusChem* 2020, **13**, 4284.

139) C.-J. Pana, M.-C. Tsai, W.-N. Sub, J. Ricka , N. G. Akaleworka , A. K. Agegnehua, S.-Y. Chenga , B.-J. Hwanga, *Journal of the Taiwan Institute of Chemical Engineers*, 2017, **74**, 154.

140) R. Sheldon, M. Wallau, I. W. C. E. Arends, U. Schuchardt, *Acc. Chem. Res*., 1998, **31**, 485.

Chapter 2 - Techniques

This chapter provides a summary of all the characterization techniques employed in this work to investigate catalysts properties. In addition, the entire range of analytic equipment and procedures exploited to evaluate catalyst performances and to acquire reactions kinetic profile are also described.

2.1 Catalyst Characterization

Catalyst characterization is that experimental phase in which the chemical and physical properties of the catalyst are methodically investigated by exploiting a wide range of techniques. It follows that it is a fundamental step for the intensification of a chemical catalytic process. Indeed, characterization studies permit an experimentalist to understand by which mechanism the catalyst converts the reactants into products and, when integrated with structural analyses, help to investigate which modifications the catalyst undergoes during the chemical reaction. Hence it is a pivotal tool also in the identification and mitigation process of catalyst deactivation. Therefore, a summary of experimental procedures employed to characterize catalysts, as well as the theory behind each technique, is illustrated in the next section.

2.1.1 Pore Size Analysis by Gas Adsorption

Pore size analysis is a characterization technique that is useful to obtain important information on the conformation of solid materials. Indeed, it can return values of a solids surface area, pores dimension and distribution. Generally, porous materials are characterized by different pores dimensions, which can be classified according to their size:

- *Macropores* have widths greater than 50 nm;
- *Mesopores* show dimension between 2 nm and 50 nm;
- *Micropores* are smaller than 2 nm.[28]

Gas adsorption is one of the most employed methods to investigate these material parameters and it is based on the physical interaction of gas molecules with solid surfaces called physisorption. Physisorption is a general phenomenon which occurs whenever an adsorbable gas (the adsorptive) is brought into contact with the surface of a solid (the adsorbent). The intermolecular forces involved are of the same kind as those responsible for the imperfection of real gases and the condensation of vapours.[28] During gas adsorption analyses an inert gas is left adsorbed on the solid sample and, through the measurement of the adsorbed gas volume, it is possible to return information on the surface properties of the material such as surface area, pore width distribution, pure

volume distribution etc.. Despite, at first glance, the adsorption phenomenon could appear intuitive, in the experimental reality it is quite complex since adsorption depends on a large range of variables, including temperature, pressure, structural conformation of the sample, interaction energies between adsorbent and adsorptive, and more.

Nonetheless, through several assumptions, it is possible to qualitatively and quantitatively describe adsorption phenomenon, and hence correlate the amount of gas adsorbed to the surface conformation of the sample. The simplest adsorption model has been described by Langmuir, which consider a uniform solid surface owing identical and discrete number of adsorption sites, which can be progressively occupied by adsorptive gas molecules.[1] However, adsorption is a reversible process, and thus the system is characterized by several equilibrium states in which the fraction of the occupied sites on the surfaces, θ_A, increases if the partial pressure of the gas p_A enhances. The Langmuir model culminate with the *adsorption isotherm*, which assume the maximum of the adsorption as the full coverage of the solid surface by a monolayer of adsorbate molecules, for which $\theta_A = 1$, (Equation 1).

Equation 1, Langmuir equation

$$\theta_A = \frac{v}{v_m} = \frac{K_{eq}^A p_A}{1 + K_{eq}^A p_A}$$

Where: θ_A = occupancy fraction of adsorbate sites on the surface
v = volume of gas adsorbed
v_m = volume of gas adsorbed which constitute the monolayer
K_{eq}^A = adsorption equilibrium constant
p_A = partial pressure of the adsorptive A

During a porosimetry analysis a solid sample of known mass is placed inside a glass tube and an adsorptive gas, generally nitrogen at 77 K, is let adsorbed on it at increasing pressure p, until the gas saturation pressure p_0 is reached. In a second step the gas is left to desorbed, by decreasing the pressure. The instrument continuously measures the amount of gas adsorbed and desorbed, v, as function of the gas equilibrium pressure p. In this way, plotting the measured gas volume, v, against p/p_0 generates the adsorption/desorption isotherm, characteristic of the analysing sample. For a non-porous material which follows the Langmuir assumptions, the adsorption isotherm is well described by the Langmuir equation (Equation 1), which is graphically translated into the first type of isotherm, (Figure 1, I). At low relative pressure, when the occupancy fraction of adsorbate sites, θ_A, is still far from unity, the Langmuir isotherm (Figure 1, I) is characterized by a linear increasing of adsorbed gas in function to its pressure. At greater pressures, a monolayer of adsorbate is formed and, as consequence, the isotherm reports a plateau since no more gas can be adsorbed. However, the reality of materials is far from

the ideal condition of a uniform surface, and the irregular conformation of their structures induces phenomena such as multilayer formation or capillary condensation that cause deviation from the Langmuir isotherm. Indeed, several classes of acquired isotherms can be experimentally obtained, depending to the structural features of the analysed material, which can be classified into six groups (Figure 1).

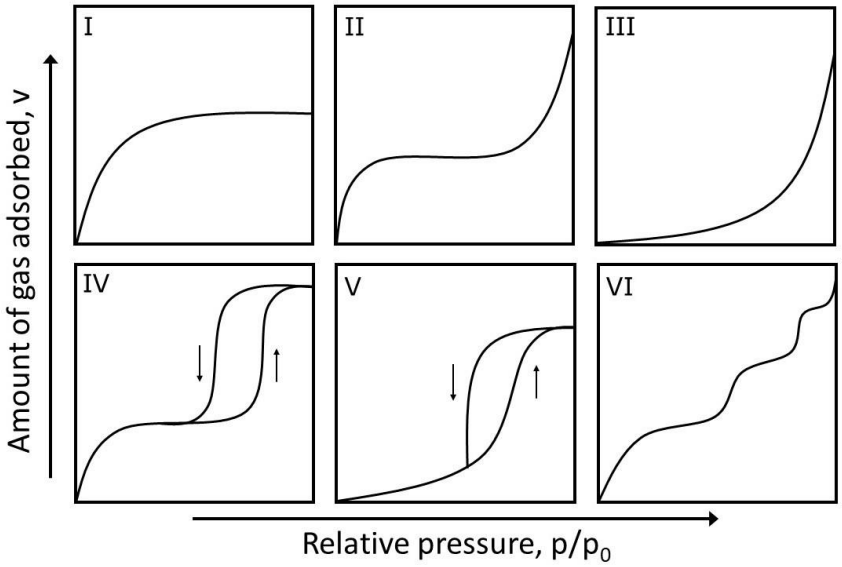

Figure 1 Six type of isotherms obtained by gas adsorption and desorption on sample materials at increasing and decreasing gas relative pressure. From top left to bottom right: Type I isotherm: non-porous or microporous material with low external surface area which follow Langmuir assumption; Type II: macroporous material; Type III: isotherm generate by weak interaction between adsorbate and adsorbent; Type IV: mesoporous materials; Type V: porous material in which weak interaction occurs between adsorbate and adsorbent; Type VI: multilayer adsorption on a uniform non-porous surface.

Type I isotherms (Figure 1) are generated from uniform surfaces which follow the monolayer Langmuir model, or from microporous samples having low external surface area, such as zeolite sieve materials or some porous oxides. Type II isotherms, are the normal form of isotherm obtained with a non-porous or macroporous adsorbent. The third types of isotherms are convex to the p/p_0 axes, are not common and are due to weak interactions between adsorbate and adsorbent. Isotherms number IV are characteristic of mesoporous materials. As it can be seen, the initial part of these isotherms follows the same path of the monolayer Langmuir adsorption (type I) and indeed, it is attributed to the adsorption of the monolayer on the whole material surface. Afterwards, larger amount of adsorbate can be accommodated inside the cavities of the sample, in which the capillary condensation of the adsorbate molecules is induced at pressures near to the saturation pressure p_0. At these conditions, the pores of the material are totally filled by the adsorbate molecules, which, in their condensate phase, form menisci inside the

cavities. During the desorption step of the analysis, the first molecules desorbed are the one situated on the last covering layer, or rather the one that form menisci, which have different energies to the one directly adsorbed on the solid surface. Therefore, the desorption step of the analysis result to be different from the adsorption path and, as a consequence, adsorption isotherms of mesoporous materials are characterized by hysteresis loops. The hysteresis loop provides insight on the sample conformation since the loop profile depends on the material pores structure. For example, vertical hysteresis are attributed to material constituted by agglomerates of solid uniform spheres, hence having narrow pore size distribution, whereas horizontal hysteresis are associated to slit-shaped micropores. Type V isotherms are uncommon and are related to porous materials which have weak interaction with the adsorbate. Indeed, they have the same shape of isotherms III, but present the hysteresis loop of porous materials. The final type of isotherms, type VI, represents stepwise multilayer adsorption on a uniform non-porous surface. The height of each step represents the monolayer capacity for each adsorbed layer.[2]

Accordingly, from the adsorption isotherms, obtained during the porosimetry analysis, can be derived important information on the pore size and structure conformation of the analysed sample.

However, it follows, that the Langmuir model is not suitable to mathematically describe the adsorption on the majority of the materials but can be implemented, with additional assumptions, in order to simulate more complex realities. One of the most employed and affirmed theory, which include multilayers adsorption and adsorbate capillary condensation, is the model described by Brunauer, Emmett and Teller, known as BET theory.[3]

The BET theory of multilayer adsorption permits to describe adsorption isotherms of meso and macroporous materials through the following equation, (Equation 2).

Equation 2, BET equation

$$\frac{1}{v(\frac{p_0}{p}-1)} = \frac{c-1}{v_m c}\left(\frac{p}{p_0}\right) + \frac{1}{v_m c}$$

Where: v = volume of gas adsorbed

p_0 = adsorptive saturation pressure

p = adsorptive partial pressure

c = BET constant

v_m = volume of gas adsorbed which constitute the monolayer

The BET equation represents an adsorption isotherm which has a linear relationship in the range of $0.05 < p/p_0 < 0.35$. Indeed, the data acquired during the analysis, adsorbed gas, (v), and p/p_0, can be plotted as straight line with the left-hand side term of the BET

equation on the y-axis and p/p_0 on the x-axis. The resulting linear trend is called *BET plot* (Figure 2), which takes the following form:

- slope = $\frac{c-1}{v_m c}$
- and intercept = $\frac{1}{v_m c}$

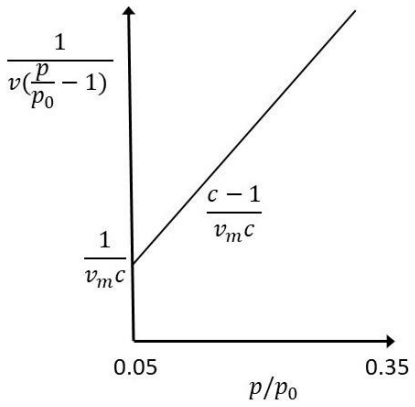

Figure 2 BET plot obtained by plotting the left hand-side term of the BET equation (Equation 2) against p/p_0. From the BET plot it can be determined the slope and the intercept values useful to calculate the volume of gas adsorbed on the monolayer of the sample.

Through the slope and intercept values of the BET plot it is possible to determine the volume of adsorbed gas which constitutes the monolayer v_m, which can in turn be utilised to calculate the surface area of the material. Indeed, according to the assumptions made by Langmuir, Brunauer, Emmett and Teller, the monolayer of the adsorbate is constituted by a continuous layer of adjacent adsorbate molecules. Hence, knowing the volume of the monolayers of gas adsorbed and the cross section of the adsorbate molecules, (s), the total surface area of the sample can be derived (Equation 3):

Equation 3

$$S_{total} = \frac{(v_m N s)}{V}$$

Where: S_{total} = total surface area of the sample
v_m = volume of gas adsorbed which constitute the monolayer
N = Avogadro constant
s = cross section of the absorbed molecule
V = molar volume of the gas adsorbed

Instead, according the BET theory, the c constant exponentially relate to the difference between the heat of the adsorption of the first layer and the second and higher layers and is equal to the heat of liquefaction or heat of vaporization.[28]

In addition to the BET theory, there are several types of models that can be used to facilitate gas adsorption analyses. Each model is based on a different mathematical description, and can therefore be better suited to describe specific materials or to return characteristic information. For example, the Barrett-Joyner-Halenda (BJH) model is based on the modified Kelvin equation and return insights on pore size distribution. Also, several computational methods have been developed such as, Density Functional Theory (DFT) or Monte Carlo simulation (MC). Each method is able to simulate specific gas-solid interaction and return different parameters.[4, 5] For example, in this work DFT method has been used to analyse activated carbons and zeolite catalysts, because of its good capacity of interpreting microporous materials.

Therefore, gas adsorption porosimetry is an extremely useful technique to study catalytic materials because it allows the user to quantify essential parameters that the catalysts performances typically depends, such as total surface area, micro and mesoporous volumes and surface area, hence prose size distribution.

In this work, gas adsorption analysis was exploited to determine surface area and pore volumes of the catalytic materials employed. In particular, gas adsorption analysis was conducted on the pre- and post-reaction catalyst in order to correlate deactivation phenomena to eventual surface areas or pore volumes decreasing.

2.1.2 Powder X-ray diffraction (p-XRD)

Powder X-ray Diffraction (XRD) is a rapid characterization technique that exploits the interaction of the physical structure of the catalyst with X-ray radiations to study specific physical properties of the catalyst itself, such as its crystallinity fraction or the crystallites particles sizes. Furthermore, since physical parameters are strictly correlated to the chemical composition of a specific material, XRD can also be employed to determine chemical reorganization of the active sites, such as oxidation or reduction of metal catalytic centres. For this reason, it is particularly important in catalytic studies since comparison of XRD spectra of pre- and post-reaction samples allows a user to evaluate if some modifications occur to the catalyst during the reaction. In addition, it can be employed to determine if certain materials have the specific features to assist the target chemical reactions.

XRD techniques exploit the possibility of a crystalline material to behave as a diffraction grating when a monochromatic radiation is directed toward it. Indeed, the periodic distance between subsequent atoms planes, which compose the material elementary unit cells, act as slits through which light can be diffracted. The first requirement to observe the diffraction phenomenon is that the wavelength of the incident radiation must have the same order of magnitude of slits width. X-ray electromagnetic waves, which have wavelengths in a range of 0.1-10 Å are specifically suited to interact with crystal lattices.

In addition, X-rays possess enough energy to penetrate solids, thus giving information not only of surface features but also their internal structures.

To generate X-ray radiations in diffractometers, a metallic filament is heated in a cathode X-ray tube to produce electrons, which are accelerated by means of a voltage toward a metallic target (or anode). When the hitting electrons have sufficient energy to dislodge inner shell electrons of the metallic target, these latter ones are ejected. Higher shell electrons of the metallic target immediately decay to replace the ejected inner electrons, thus generating X-ray photons. Thereby, frequencies, energies and wavelengths of the emitted radiations are specific for a given metallic target. However, when the accelerated electrons impact the anode, they are also decelerated, producing a continuous spectra of X-ray radiations, called *white* or *Bremsstrahlung* radiation.

As previously described, to have diffraction, the incident radiation must be monochromatic i.e. be of one specific wavelength (λ), and thus a filter is placed after the X-ray source in order to select the appropriate λ to irradiate the samples. The employment of a copper target anode coupled with a nickel filter ensure a characteristic monochromatic radiation of λ = 1.51 Å, thus called Cu Kα radiation.[6]

In this way the monochromatic radiation is generated and, interacting with the sample, is elastically scattered in several beams which may combine constructively, forming diffraction spots or, destructively, annihilating each other.

According to physical laws, only scattered beams whose difference in path is equal to an integer number (n) of their wavelength (λ) can interfere constructively. In the specific case of crystalline materials diffraction, the path difference of beams scattered by following crystallographic planes, spaced of distance d, is equal to $2d \sin\theta$, where θ is the angle formed between the incident radiation and the perpendicular to the sample, (Figure 3).

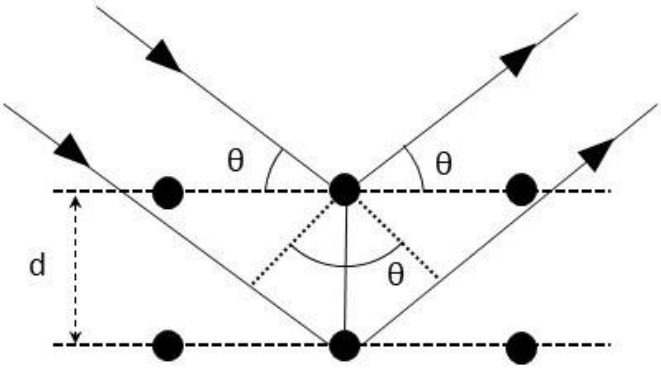

Figure 3 Scheme of diffraction phenomenon generated by the incidence of a monochromatic radiation into a crystalline structure according to the Bragg's law. The incident radiation interacting with the different lattice plane placed at distance d, will generate a diffracted radiation at θ degree.

Hence, to ensure constructive diffractions by crystal lattices, both conditions must be verified, as described by the Bragg equation, (Equation 4).[7]

Equation 4, Bragg equation $$n\lambda = 2d \sin\theta$$

Where: n = integer

λ = wavelength

d = lattice spacing

θ = scattering angle

As consequence, with a given monochromatic radiation and at certain incident angle, only crystallographic planes that satisfy the Bragg condition originate constructive diffraction pattern. Therefore, in order to collect information on all the crystallographic planes present in the materials, during the XRD analysis, the incident angle, θ, is continuously varied by rotating the sample holder together with the detector, in respect to the X-rays source. A peak in intensity is recorded by the detector when the mineral contains lattice planes with d-spacings appropriate to diffract X-rays at that value of θ. In this way diffraction pattern intensities are recorded as function of θ, resulting in the so-called diffractogram.

The signals obtained in an XRD pattern can then be compared with the diffraction patterns present in a large data-bank, allowing the identification of the crystalline phases present within the sample. Analysing the diffractograms of a specific material permits important lattice parameters, such as the distance of its crystallographic planes or if samples are characterized by the same crystallographic planes or not, to be characterised. Moreover, the intensity of the diffraction peaks at a given θ are strictly correlated to the crystallinity of the sample. Thus, it can be evaluated if during the chemical reaction the catalyst has undergone to some amorphization processes or if, instead, it has conserved its structural features. Furthermore, thanks to the Scherrer equation, is possible to determine the size of sub-micrometre crystallites in a solid from the broadening of a peak in a diffraction pattern.[29]

Equation 4.1, Scherrer Equation $$\Theta = \frac{K\lambda}{D\cos\theta_B}$$

Where: Θ = full width at half-maximum of the diffraction peak

K = parameter that depends on the relative orientation of the scattering vector to the external shape of the crystallite.

λ = wavelength of the radiation

D = crystallite size

θ_B = Bragg angle

In this work p-XRD technique was used to determine the crystallinity of the catalysts employed and to ascertain the structural integrity of the post-reaction catalysts. In addition, p-XRD analysis was used to determine oxidation state of nanoparticles in metal based catalyst. Specifically, XRD data were collected at ambient temperature with PANanalytical X'PertPRO X-ray diffractometer using Cu Kα radiation and operated at 40 kV and 30 mA. XRD patterns were recorded between 10°- 80° 2θ at a step size of 0.017. An example of a diffractogram of commercial 5% palladium on carbon is provided in Figure 4. As it can be seen, several intense peaks arise at different θ value since the catalyst is composed by different material with different crystallographic planes.

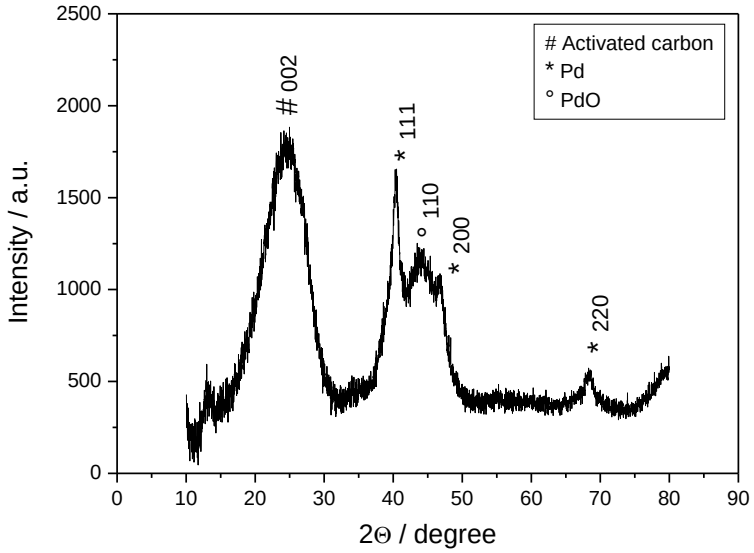

Figure 4 Representative diffractogram of 5% Pd/C obtained by p-XRD analysis.

2.1.3 X-ray Photoelectron Spectroscopy (XPS)

X-ray Photoelectron Spectroscopy (XPS) is a powerful technique that allows qualitative and quantitative characterization of the elements present on the surface of material and in a thickness less than 10 nm from the surface. Furthermore, it can be employed to depict the oxidation state of the species present in the material. Thereby, it is particularly useful in catalysis studies to determine the active surface area of metal supported catalysts, to identify which elements compose the material and if they undergo to some oxidation state changes during the chemical reaction.

According to the photoelectric effect, a surface irradiated by a photon source of sufficiently high energy will emit electrons. This because photons may interact with atomic orbitals transferring its energy to the electrons present, leading to electron emission from the atom. However, the electron is ejected from the atoms core only if the incident photon energy is higher or equal to a threshold level characteristic for each element, which

correspond to the binding energy of the electrons to the atom nuclei. The extra energy possessed by the incident radiation is converted in kinetic energy of the emitted electrons, according to the Equation 5.

Equation 5 $$E_k = h\nu - E_B - \varphi$$

Where: E_K = kinetic energy
hν = energy of the incident radiation
h = Planck's constant (h= 6.62607 x 10^{-34} J)
v = frequency of radiation
E_B = binding energy of the electron
φ= XPS constant

X-rays have sufficient energy to dislodge core electrons of all elements. Hence, measuring the kinetic energy of electrons emitted by a surface hit with X-ray source allows calculation of the binding energy specific of each element, then determine the composition of the studied material.[8] Moreover, the binding energy not only depends to the nature of each element, but it also slightly varies according to the oxidation state.[9] An example of the shift in binding energy due to the oxidation state of the element, is given by palladium (Pd). In fact, whilst a binding energy of 335.4 eV (Pd $3d_{5/2}$) is observed for metallic Pd, a higher binding energy, around 337.0 eV (Pd $3d_{5/2}$), is reported for PdO in which the electrons are more tightly bound to the nucleus due to the higher oxidation state.[10] In addition, when the photoelectric threshold is increased and the radiation intensity is fixed, the amount of electrons emitted by the surface is related to the concentration of the emitting atom. Therefore, XPS could be employed also to quantitatively determine elements on a specific surface, such as in the case of determination of active surface area on metal supported catalysts.

An illustrative XPS spectrum of the Pd region of a fresh Pd on carbon catalyst is shown below (Figure 5), generated by plotting the intensity signal of the expelled photoelectrons against the binding energy. Deconvolution of the experimental signal permits identification of all the intense peaks due to different palladium species present in the sample.

In this work X-ray photoelectron (XPS) analysis was used to gain insight on the chemical nature of the active species of metal-supported catalysts. In particular, XPS spectra were recorded on a Kratos Axis Ultra DLD spectrometer using a monochromatic Al Kα X-ray source. Al X-ray source operating in arrange of 75–150 W and data reordered at pass energies of 160 eV for survey scans, or 40 eV for high resolution scans. All spectra were analysed using CasaXPS (v2.3.17 PR1.1) using Scofield sensitivity factors.

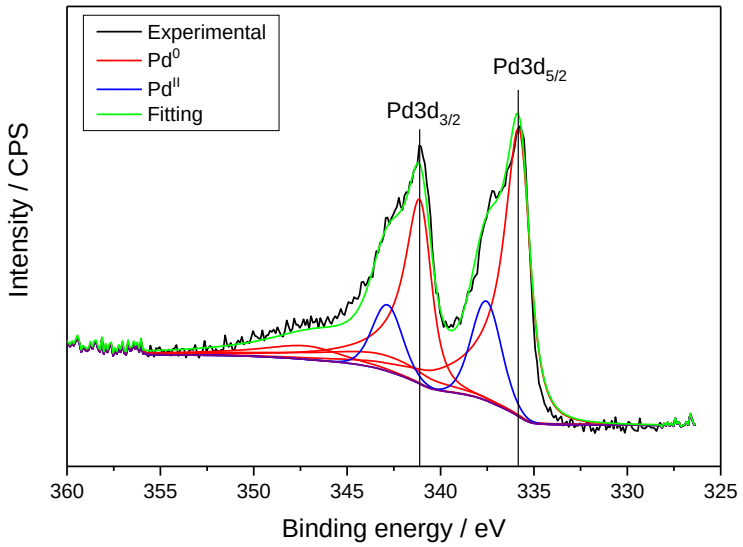

Figure 5 XPS spectrum of the Pd region of a 5% Pd/C sample. The spectrum shows both region of $Pd3d_{5/2}$ and $Pd3d_{3/2}$. In particular it can be observed that in the analysed sample are present both Pd^0 (in red) and Pd^{II} (in blue) which electrons own different binding energy.

2.1.4 Fundamentals of molecular spectroscopy

Spectroscopy constitutes that branch of characterization techniques which exploit the energy exchange between matter and electromagnetic radiations in order to acquire qualitative and quantitative information on the analysed material.

Electromagnetic radiations can be described as a combination of an electric and magnetic field which propagate in the space, perpendicularly to each other, through simple harmonic waves. Accordingly, each radiation is characterized by a wavelength which is the period space over which the wave's shape repeats, which in physics is commonly designated by λ. The frequency of the radiation (*v*) is the reciprocal of its wavelength up to the constant of the speed of light (c), as defined in Equation 6. In turn, the radiation energy is related to its frequency, via the Planck's constant h, (Equation 7). Hence, the radiation energy depends to nature of the radiation itself and is strictly correlated to its wavelength.[11]

Equation 6 $$c = \lambda \nu$$

Equation 7, Planck's equation $$E = h\nu$$

Where: c = speed of light

λ = wavelength

ν = frequency

E = Energy

H = Planck's constant (h= 6.62607 x 10^{-34} J)

The energy of a molecule can be divided into several types of energies: electronic, rotational and vibrational. However, the quantum mechanics approach imposes that the energetic configuration of a molecule is constituted by several discrete levels separated each other by a specific amount of energy (ΔE), (Figure 6). Therefore, only energetic transitions between these quantified levels are allowed, and so become characteristic for each molecule or atom. Accordingly, to permit energetic transitions, a system must absorb or emit the same discrete amount of energy which separate these energy levels.

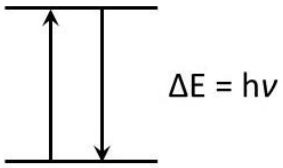

Figure 6 Quantum mechanics energetic configuration of a molecule or an atom. In this configuration are allowed only discrete levels of energy, separated each other by a specific amount of energy ΔE.

It follows that an energetic interaction between electromagnetic radiations and molecules can successfully occur only if the radiation has the suitable energy to fill the energetic gap ΔE between two following energetic levels of the molecule. Since the radiation energy is dependent to the radiation wavelength (Equations 6 and 7), energetic transitions can be promoted by only specific radiations with the opportune wavelength.

Spectroscopic techniques exploit this intrinsic relationship between radiations and molecules. Generally, during the course of spectroscopic analysis the sample is irradiated with beams of different wavelength as a function of time. Accordingly, when a radiation with opportune wavelength hit the sample, the molecules will absorb the radiation and will be excited to an upper energetic level. Acquiring the intensities of the electromagnetic beam as function of the wavelength permits decrease of the incident signal to be detected, which correspond to the radiation absorbed by the sample. Thereby, reading the absorption spectra allows identification at which wavelength the molecules have been excited and then obtaining information on their energetic configuration which is strictly characteristic of their nature.

Conversely, molecules or atoms present in their excited state decay to lower states emitting radiations which frequencies cover the energy gap between the two energetic levels. Hence, emission spectra can be generated recording the intensities of radiation emitted by samples, which were previously excited by electromagnetic source.

In both cases, exploiting the intrinsic relationship between radiations and energetic configuration of samples, spectroscopic analysis provides information regarding the magnetic, vibrational, rotational and electronic properties of the analysed material.

2.1.5 Diffuse Reflectance Infra-red Fourier Transform (DRIFT) Spectroscopy

Infra-red Fourier transform spectroscopy (FT-IR) is a spectroscopic technique used to investigate the vibrational motions of covalent bond which constitute a molecule. In this way it allows detection of specific molecular functional groups present in a sample and hence, to obtain specific qualitative information on a studied material.

The covalent bonds in molecules are not rigid but are free to vibrate like springs. In the same way of every molecular energy, molecular vibrational energies are quantified and subdivided in several energetic levels which generally differ from each other in the order of 2500-25000 nm. Therefore, infrared radiations, which have wavelength in the range of 700-1x10^6 nm, possess suitable frequencies to promote vibrational energy transitions and, thus, permit the molecule to vibrate. Consequently, substances will absorb infrared radiation that corresponds in energy to these vibrations.

Molecules can vibrate in many different ways, depending to their vibrational degree of freedom, which in turn is related to the number of atoms present in its configuration. A molecule composed of n-atoms has 3n degrees of freedom, six of which are translations and rotations of the molecule itself. This leaves 3n-6 degrees of vibrational freedom and 3n-5 if the molecule is linear. Vibrational modes are often given descriptive names, such as stretching, bending, scissoring, rocking and twisting.[12]

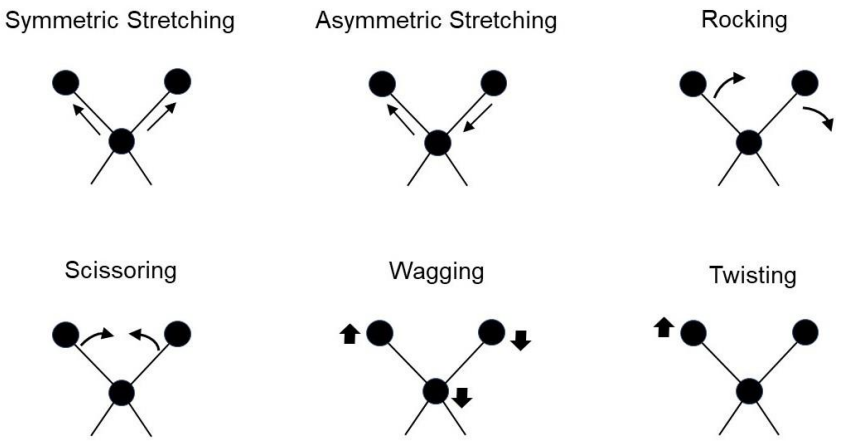

Figure 7 Illustrative vibrational modes of a generic molecule. Symmetric and asymmetric stretching, rocking and scissoring modify molecule bonds within the molecule plane. In contrast, wagging and twisting modify molecule bonds out of the molecule plane.

Stretching, is the vibration mode which elongate or shorten molecular bonds and can occur symmetrically or asymmetrically depending to the relative motion of two adjacent

bonds. *Rocking* and *Scissoring* modify the molecular bond's angles within the molecule plane. Conversely, *Twisting* and *Wagging* alter the bond's angle out of the molecule plane, (Figure 7).

Furthermore, the number of observed vibrations may be decreased by molecular symmetry, spectrometer limitations, and spectroscopic selection rules. One selection rule states that only vibrations that change the electrical dipole moment of molecules induce infrared absorption. For instance, homopolar diatomic molecule, such as O_2, N_2, H_2 are IR inactive, since no vibration motions alter their molecular dipole momentum.

The exact frequency at which a given vibration occurs is determined by the strengths of the bonds involved and the mass of the component atoms,[12] according to the Equation 8 and 9.

Equation 8

$$\nu = \frac{1}{2\pi}\sqrt{\frac{k}{\mu}}$$

Where: ν = frequency (cm^{-1})

k = bond force constant (N / cm)

μ = reduced mass (kg)

Equation 9

$$\mu = \frac{m_1 m_2}{m_1 + m_2}$$

Where: m_1, m_2 = the masses of the two vibrating atoms

It follows that each molecule will absorb specific frequencies characteristic of the bonds that constitute its configuration. Hence more complex molecules will show greater number of absorption bands and functional groups will possess their own characteristic absorption. Therefore, recording IR absorption spectra of samples provides insight on the molecular composition of the material.

During the course of FT-IR analysis, the sample is irradiated with the whole range of infrared wavelengths and depending to its molecular composition will absorb specific radiation frequencies, which allows the transition from vibrational ground state to an excited state. The detector continuously records the intensity of the IR radiation coming from the sample, and by comparison with a reference of negligible absorption, such as KBr, will return the absorption spectrum of the sample.

The IR absorption spectra are plotted as a function of wavenumber (cm^{-1}), the reciprocal of the wavelength, and generally can be distinguished into two parts. The absorption side comprehending the range of wavenumber between 1200-400 cm^{-1} is called *skeletal* where are present all those vibrations related to branched groups in the molecular structures, possessing a large number of vibrational modes. In this region the number of observed

absorptions may be increased by additive interactions between covalent bonds and the molecular configuration in its totality. Therefore, skeletal vibrations are highly sensitive to changes of molecular structure, hence this part of the spectrum is considered the "fingerprint" region, characteristic of the analysing sample. For this reason, it is generally used to identify compounds by comparison of bank-data IR spectra.

For wavenumbers higher than 1200 cm^{-1} the spectra show the *group frequency* region, in which absorptions characteristic of functional group vibrations that are not influenced by the whole molecular structure appear. For instance, the carbonyl functional group (C=O) usually presents an absorption band at ~ 1700 cm^{-1}, whereas for hydroxyl groups (O-H) the band is usually detected at ~ 3500 cm^{-1}. However, the interaction of different functional group must always be considered, even in this part of spectra, since misinterpretation of absorption bands may occur. In this way IR spectroscopy also allows identification of specific functional group in a complex molecule or sample, such in the case of the identification of absorbed substances on a given material.

In order to analyse bulk samples with FT-IR spectroscopy, the diffuse reflectance phenomenon of light by solid surface is exploited, thus originating the Diffusive Reflectance Infra-red Fourier Transform (DRIFT) Spectroscopy. When an IR beam hits the rough surface of the solid sample, it is scattered and reflected in all directions. In DRIFT spectroscopy, an ellipsoid or paraboloid mirror is used to collect and direct all the scattered radiation to the detector that subsequently measure their intensity and evaluate the eventual absorption. Thanks to this technique, IR spectroscopy is the most widely used, and usually most effective, spectroscopic method for chemical characterisation of the surface of heterogeneous catalysts.

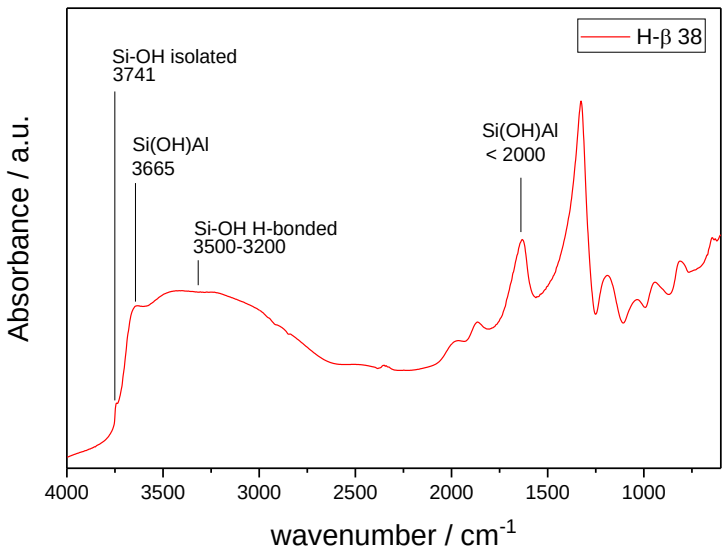

Figure 8 DRIFT spectra of H-β 38 zeolite. It can be observed absorption bands related to several functional group vibration.

For intensification purpose of catalytic processes, DRIFT spectroscopy is a powerful technique because it allows one to detect if some reaction residues remain on the surface of the post-reaction catalyst, and hence, correlate their presence to eventual catalyst deactivation phenomena. Moreover, it can be exploited to investigate the catalyst active sites or general catalysts composition and configuration. An example of DRIFT spectra is illustrated in Figure 8 in which has been analysed H-β 38 zeolite.

In this work DRIFT technique was employed to chemically identify functional groups which characterise the catalyst surfaces and to verify the presence of eventual chemical residues deposited on the post-reaction catalysts. DRIFT spectroscopy was performed in a Harrick praying mantis cell. The spectra were recorded on a Bruker Tensor II spectrometer over a range of 4000-650 cm^{-1} at a resolution of 2 cm^{-1}.

2.1.6 Raman Spectroscopy

Raman spectroscopy is another type of vibrational technique, which is complementary to IR spectroscopy and permits in the same way information on the molecular structure of the analysed material to be obtained.

In Raman spectroscopy, the analysing sample is irradiated with a laser beam with a specific wavelength, which can usually range from the ultraviolet to the visible and near-Infrared depending on the application. The interaction between the electron of the sample and the external electric field of the electromagnetic radiation creates an induced dipole moment within the molecule, which scatter the incident radiation. Depending on how the photons interacts with the molecule can be originated several scattered components with different energies. The *Rayleigh* component, which represents almost the entire fraction of scattered radiation, is generated from an elastic process in which the scattered radiation has the same energy of the incident beam. *Raman* components are instead generated from inelastic interactions and depend on if the scattered radiations have lower or higher energy than the incident beam. *Stokes* or *anti-Stokes* components are produced when the scattered radiation is lower and higher in energy, respectively. Thus, Raman spectroscopy measures the frequency deviances of the scattered radiation from the incident beam. Since frequency differences are due to the vibrational modes of the molecule configuration, molecular fingerprint spectra and bond information can be acquired on the analysed material. Generally, the scattered radiation is collected and sent to an optical filter in which the intense Rayleigh component is filtered out while the rest of the collected light is dispersed onto a detector to obtain high resolution Raman signals. A Raman spectrum is obtained by plotting the intensities of Raman scattered components as function of the shift in frequency of the incident light.

According to quantum mechanical description the Raman effect can be described as follow:

the incident photon, of energy equal to hv_0, interacts with the molecular system which is characterized by vibrational levels separated each others of energy equal to hv_1 . In this way the system is promoted from a vibrational level v = 0 (ground state) to a virtual level of higher energy, equal to E = hv_0. From this virtual level the system can subsequently relax, and decay to the same initial vibrational level v = 0, resulting in an elastic scattering thus originating the *Rayleigh* component. At the same time, the virtual excited system hv_0 might relax to a different vibrational level than the initial one, thus producing scattered radiations with energies different to the incident one, generating the *Raman* components. Specifically, if the frequency radiation is lower than the incident one, *Stokes shifts* are observed. Conversely, *anti-Stokes shifts* occur if decay is to a lower vibrational energy level, (Figure 9).[13]

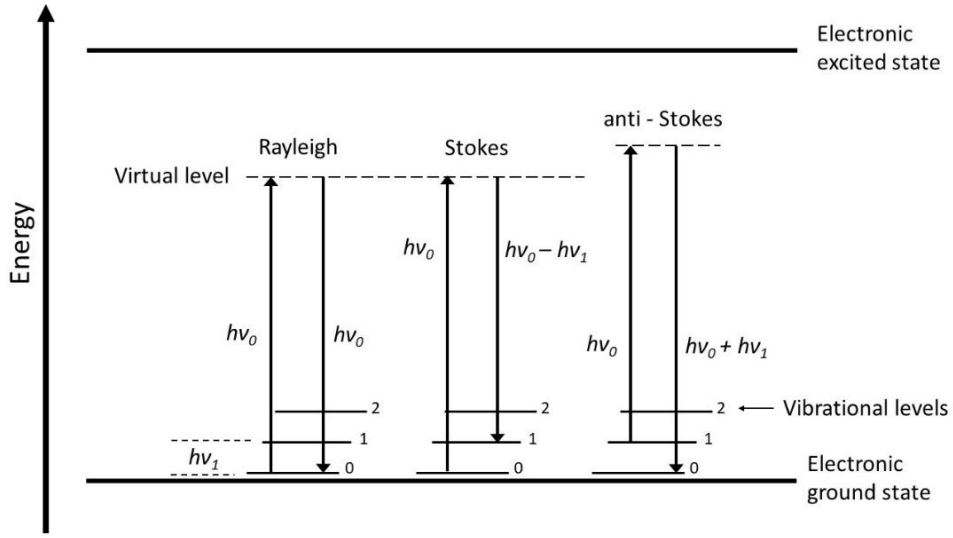

Figure 9 Energetic diagram of a molecule when hit by a radiation. The incident photon promotes the molecule to a virtual energetic level. From this virtual level the molecular system can relax through elastic scattering originating Rayleigh component, or otherwise, through inelastic scattering giving Stokes and anti-Stokes shifts in the so-called Raman effect.

Although IR and Raman spectroscopies are similar in that both techniques provide information on vibrational frequencies, there are many advantages and disadvantages unique to each method. Indeed, selection rules are different for IR and Raman spectroscopies and hence, vibration modes which are not observable by IR analysis can be detected by Raman spectroscopy, and vice-versa. According to quantum mechanics a vibration is Raman-active if the vibration induces a polarizability change of the bond. Polarizability is defined as the tendency of an electric charge distribution, such as the electronic cloud of an atom or a molecule, to modify its original position under the effect

of an external electric field. Indeed, when a molecule is placed in an electric field, such as in the middle of a laser beam, it suffers distortion since the positively charged nuclei are attracted toward the negative pole, and electrons towards the positive pole. This phenomenon induces an electric dipole moment (Figure 10), and the polarizability quantifies its intensity proportional to the electric field, according to the Equation 10:

Equation 10 $$P = \alpha E$$

Where: P = induced dipole
α = molecule polarizability
E = incident electric field

Therefore, the higher the polarizability induced by the vibration, the greater is the dipole momentum generated by the electric field and, as a consequence, the more intense is the Raman effect observed.

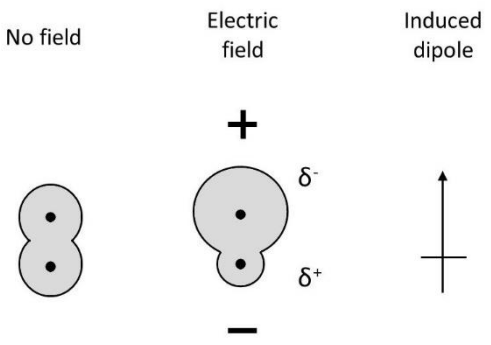

Figure 10 Induced dipole momentum on a polarizable molecule when an electric field is applied to it.

Generally, vibrational transitions which have large Raman intensities often have weak IR intensities and vice versa. If a bond is strongly polarized, a small change in its length such as that which occurs during a vibration has only a small resultant effect on polarization. Vibrations involving polar bonds (e.g. C-O , N-O , O-H) are therefore, comparatively weak Raman scatterers. Such polarized bonds, however, carry their electrical charges during the vibrational motion and this results in a larger net dipole moment change during the vibration, producing a strong IR absorption band. Conversely, relatively neutral bonds (e.g. C-C , C-H , C=C) suffer large changes in polarizability during a vibration. However, the dipole moment is not similarly affected such that while vibrations involving predominantly this type of bond are strong Raman scatterers, they are weak in the IR.[13]
In this way, samples that cannot be analysed with IR spectroscopy are instead measurable with Raman spectroscopy. For instance, totally symmetric vibrations which are IR inactive, such in the case of CO_2, are Raman active. Conversely, it can be exploited

the difference of sensibility of the two spectroscopies to avoid analytic interferences. For example, IR spectroscopy suffers from the strong absorption of water and consequently some bonds that absorb at the same frequencies of water cannot be detected. Conversely, since water is a weak Raman scatterer, samples containing water can be analysed with Raman without interference.

In this work Raman spectroscopy was used to compare the catalytic structure pre-and post-reaction, in order to evaluate if during the reaction the catalyst underwent some structural changes. Raman spectroscopic analysis was performed on a Renishaw inVia Raman microscope with laser excitation wavelengths of 514 nm. Sample measurements were performed inside a Raman cell at 10 mW power, with a total of 256x2 s accumulations.

2.1.7 ^{1}H Nuclear Magnetic Resonance (^{1}H-NMR)

Nuclear magnetic resonance spectroscopy (NMR) is a useful technique for the identification and quantification of organic compounds in solution. NMR analysis provides high resolution NMR spectra in which molecular functional groups are distinguishable, and identical functional groups with differing neighbouring substituents still give different signals. For this reason, besides identification, NMR spectroscopy provides detailed information about the structure, dynamics, reaction state, and chemical environment of molecules. Moreover, the signal area provided by the analysis is proportional to the quantity of molecules present in the solution, and hence by means of a standard reference and a calibration line, NMR can also provide quantitative information.
NMR is a spectroscopic technique based on the magnetic properties of some atom's nuclei. The magnetic properties of a nucleus depend to its *nuclear spin quantum number,* I, which is defined by the number of unpaired nucleons (protons and neutrons) by which is constituted:

- If protons and neutrons are both present in even numbers, such as in the case of ^{12}C, ^{16}O, the nuclear spin is null, $I = 0$.
- If protons are present in even numbers and neutrons in uneven, or vice versa, such in for ^{1}H, ^{19}F, ^{13}C the nuclear spin result to have half-integer values (1/2, 3/2, 5/2).
- Nuclei composed by uneven numbers of protons and neutrons, like ^{2}H or ^{14}N, possess integer nuclear spin.

^{1}H-NMR spectroscopy exploits the magnetic properties of the hydrogen nuclei, which is constituted by only one proton and hence possesses $I = 1/2$.[14]

When a nucleus with a nuclear spin different to 0 rotates around its axes, it generates a magnetic moment, μ, in which the nuclei magnetic state is defined by $2I+1$ degenerate energy levels. In the specific case of ^{1}H, the proton has two degenerate magnetic levels. If an external magnetic field B_0 is applied to the nucleus, the magnetic levels lose their degeneracy, and separate into two quantified levels with different energies. One of these levels will be higher in energy, in which the nucleus magnetic moment is opposed to the external magnetic field, and one of which will be lower, in which the nucleus and external magnetic moments are parallel. The splitting of particles spin in spin groups with different energetic level is called *Zeeman* effect, (Figure 11).

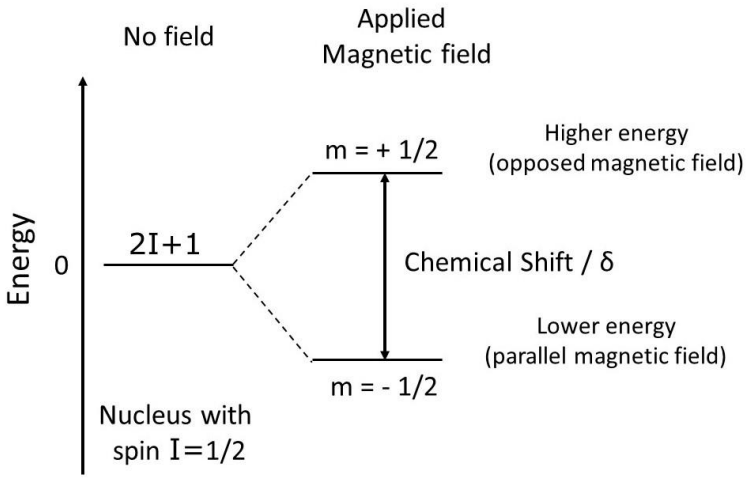

Figure 11 Energetic diagram of a nucleus with spin I = ½ in the absence and presence of an external magnetic field. When an external magnetic field is applied to such nuclei, their degenerate energetic levels are split in two separate energetic levels with different energies.

If the proton, in the lower magnetic level, is perturbated with an appropriate frequency which fills the energetic gap ΔE between the two energy levels, it will invert its magnetic moment, placing itself in the higher energy level. The energy difference ΔE between two split magnetic levels is proportional to the applied magnetic field B_0, according to the Equation 11:

Equation 11

$$\Delta E = \frac{h\gamma B_0}{2\pi}$$

Where: γ = gyromagnetic ratio

h = Planck constant

B_0 = applied magnetic field

However, in the complex chemical system of a molecule, the atom's nuclei are surrounded by cloud of electrons and by other nuclei which also possesses areas of electron density.

When the electronic surrounding of every nuclei is subjected to the external magnetic field B_0, it also generates a weak magnetic moment opposed to the one produced by the nucleus, the intensity of which is strictly correlated to the conformation of the electronic environment. In this way, the electronic cloud around the nuclei behaves as an electromagnetic shield which reduce the local magnetic field B_{local}, felt by the nuclei, the intensity of which can be described by Equation 12:

Equation 12

$$B_{local} = B_0(1 - \sigma)$$

Where: B_{local} = magnetic field felt by the nuclei
B_0 = applied magnetic field
σ = shielding constant

As a consequence of the shielding effect, the energy splitting of the protons magnetic levels will not depend only to the applied magnetic field B_0 but also to the electronic surrounding of every nucleus. Therefore, the same nuclei with different electronic environments, for example a proton in the -CH_3 and CH_2OH systems, will show different splitting energies.
During ^{1}H-NMR analysis, a strong magnetic field is applied to the sample by means of an electromagnet, which induces the splitting of the degenerate magnetic energy levels associated with the ^{1}H nucleus. Afterwards, a radiation with an opportune frequency is sent to the sample in order to promote the protons form the lower magnetic level to the higher one. The energy subsequently released from the excited nuclei during the relaxation toward the lower energy states, is then measured. The NMR spectrum is obtained as a plot of the amount of the intensity as a function of energy, reported in terms of chemical shift and related to a standard reference, usually tetramethylsilane.[14] Accordingly, the chemical shifts of NMR spectra give specific information on the chemical composition and on the molecular configuration of the analysed sample. Figure 12 reports an illustrative ^{1}H-NMR spectra of a formic acid aqueous solution.

In this work, ^{1}H-NMR spectroscopy was used to identify the presence of contaminants in the reaction feedstock and to research eventual reaction residues in water regeneration effluent or water extraction solutions of used catalyst. In particular, ^{1}H-NMR spectra were acquired with a Bruker 500 MHz. Spectra were acquired with D_2O as a deuterated solvent, and the water suppression method was employed.

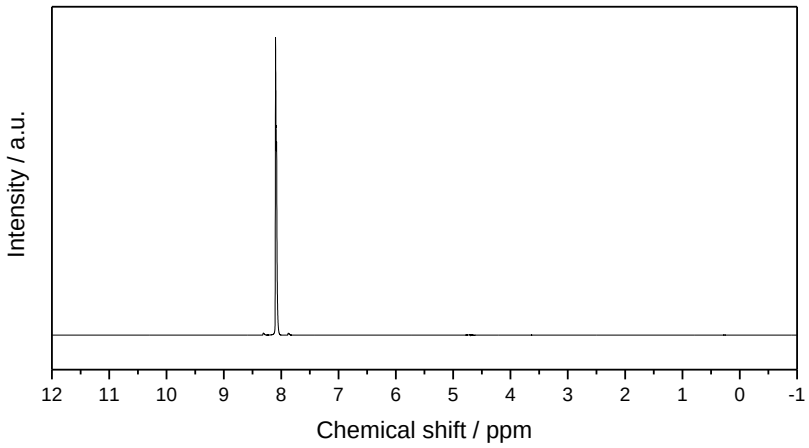

Figure 12 ^{1}H-NMR spectra of distilled formic acid. Due to the identical location of hydrogen atoms inside molecule, only one peak arises from the spectroscopy analysis.

2.1.8 Mass Spectroscopy (MS)

Mass spectroscopy, MS, is an analytical technique in which liquid or gaseous samples are ionized, then separated and detected according to their mass-to-charge ratio (m/z). Typically, samples can be ionized with different sources of energy such as electron beams or plasma environments. Depending on the intensity of the ionization source, these methods can be classified as soft or hard ionization methods. Hard ionization techniques, such as inductively coupled plasma (ICP) (described in the following section), exert on the sample larger amount of energy that together with the ions production, fragment the injected molecule. Soft methods are less likely to break down the chemical species during the ionization process, due to the lower residual energy that remains on the target molecule. Depending on the purpose of the analysis the first or the second ionization method might be chosen. For instance, hard ionizations techniques are preferred for quantitative elemental analysis since they totally ionize samples, and hence produce signals proportional to the real analyte concentration. Additionally, such methods are useful for identification of unknown molecular systems, because the fragments generated during the ionization may be indicative of specific functional groups, although such fragments cannot unfortunately return information on their relative position within the molecule. On the other hand, soft ionization, can be used to determine compound distributions of multicomponent samples, especially when heavy molecules, such polymer or other macromolecules, are analysed.[15]

Once the sample has been ionized, the produced ions are directed toward a mass filter that separates fragments according to their mass-to-charge ratio. In these devices, the charged particles are subjected to electric and magnetic fields which modify their speeds

and direction, respectively. The extent of ion acceleration and deflection depends to their mass to charge ratio, thereby allowing different ion fragments to be discriminated accordingly.

For example, in time-of-flight devices, an electric field accelerates the ions through the same potential, and then measures the time they take to reach the detector. If all the particles have the same charge, the kinetic energies will be identical, and their velocities will depend only to their masses. Ions with a lower mass will reach the detector first.

At present, the most employed mass analyser is the quadrupole mass filter, in which ions are travelled through a radio frequency quadrupole field generated by four magnetic rods, and their path is selectively stabilized or destabilized by oscillating electrical fields. Only ions within a certain range of mass-to-charge ratio are passed through the system and can reach the detector at any time. However, potential changes to the magnetic field allow a wide range of m/z values to be swept rapidly, either continuously or in a succession of discrete hops. In this way the entire m/z range can be analyzed.[16]

The detector is situated after the mass filter, and this is a device capable of detecting charged particles, like a Faraday cup or an electron multiplier, that returns intensity signals depending on the extent of their deflection and proportional to the relative abundance of the ion recorded. In this way the instrument returns a mass spectrum where the ion signal intensity is plotted as function of the mass-to-charge ratios.

Mass spectrometry was used during this work as a selective detection method for a variety of specific characterisation methods, including Temperature Programmed Desorption and Inductively Coupled Plasma Mass spectrometry, as described in the following sections.

2.1.9 Temperature Programmed Desorption Mass Spectrometry (TPD-MS)

Temperature programmed desorption (TPD) is a useful technique which permits the study of the interaction between adsorbed molecules and a substrate surface. In fact, by exploiting the dependence of the substrate-adsorbate interaction with temperature, it can discriminate between processes with different activation parameters, such as activation energy, rate constant, reaction order and Arrhenius pre-exponential factor. For these reasons, TPD is extensively utilised by catalysis scientists to evaluate active sites on catalyst surfaces or to understand the mechanisms of catalytic reactions including adsorption, surface reaction and desorption. The analysis can be conducted under different atmospheres, such as inert or oxidising environment, thus allowing the detection of species evolved under different conditions, thus providing further insights on their chemical nature. For example, TPD conducted under inert atmosphere such as nitrogen or helium allows the detection of chemical species previously adsorbed on the sample. Otherwise, if the analysis is conducted under air or oxygen, all the species present on the

sample will be converted into oxygenated products such as CO_2 and H_2O, thus allowing to determine the total amount of carbon compounds retained on a sample.

During TPD analysis, an aliquot of sample is placed in a quartz tube and heated with a ramp rate, under a selected atmosphere (generally air or nitrogen). By exploiting opportune heating apparatus, such as furnaces, it is possible to precisely programme the heating profile of the analysis according to study desorption phenomena at specific temperatures, heating rates, or even at extended time temperature plateaus. In this way it is possible to mimic the various thermal conditions that the catalyst undergoes during the chemical reaction, or during pre- and post-reaction treatments, such as thermal pre-activation or regeneration, and hence evaluate eventual sample modifications accordingly.

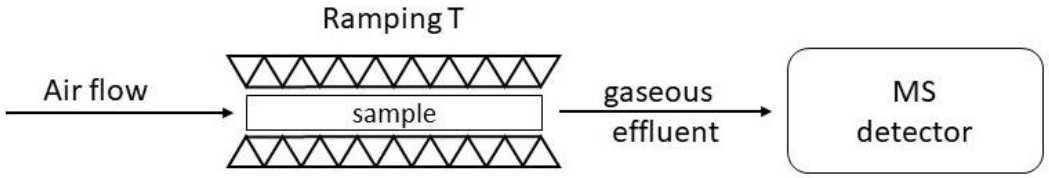

Figure 13 Schematic representation of a typical apparatus used for TPD analysis. The sample is placed in a tube and heated by means of a furnace. Through the sample tube is flowed an oxidizing gas, such as air, and the oxidation products released are injected in a Mass spectroscopy detector.

The TPD technique enhances its potential when it is coupled in-line with a Mass spectroscopy (MS) apparatus, (Figure 13). In TPD-MS analysis all the desorbed products released by sample during the programmed heating are directly injected in a mass spectrometer, which is then able to identify and quantify all the volatile species evolved during treatment. In this way is not only possible to understand which compound were adsorbed on the sample, but also to determine at which specific temperatures they are released. Indeed, thanks to a specific software, MS permit to select specific masses or compounds which signals can be monitored as function of the TPD analysis time. In this way is possible to monitor the signal of substances that are released by the sample at a specific time and, as consequence, to a specific temperature depending to the temperature profile. Therefore, due to its capacity of distinguish different compounds, TPD-MS can be used to gain insight on the thermal reaction mechanism which occur at specific temperature and deduce which phenomena is subject the material. For example, it is possible to detected which substances are released by the material at different temperature, hence determine if the sample is undergoing desorption phenomena or experiences destructive calcination. Moreover, if the programmed heating profile is specifically tuned it is possible to determine the absorption strength of eventual absorbed

substances. Indeed, it can be expected that temperatures at which absorbed substances are released are indicative of the strength at which they were absorbed. For this reasons, TPD-MS is particularly useful for catalyst studies since it permits a user to obtain a broad range of useful information on the catalyst modifications as a function of temperature, and also on specific phenomena which the catalyst undergoes during the chemical reaction.

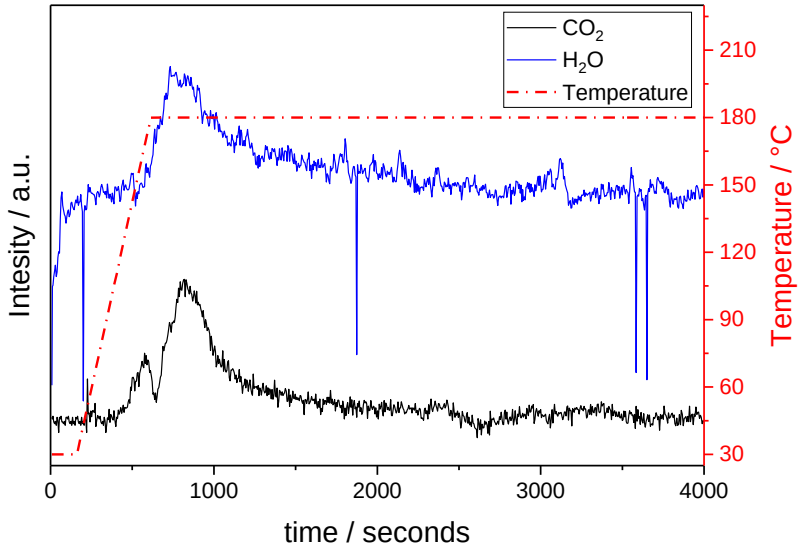

Figure 14 TPD diagram of 5% Pd/C generated by flowing air through the sample with a ramp rate of 20°C/min from room temperature to 180°C. Thanks to a MS detector were recorded CO_2 and H_2O released by the sample at specific temperatures.

An illustrative diagram of TPD-MS is present in Figure 14, in which a supported catalyst of Pd/C is heated from room temperature to 180°C at 20°C /min under air atmosphere. Specifically, the evolution of CO_2 and H_2O are monitored to determine total quantity of retained carbon.

During this work, TPD-MS analysis was employed to verify the presence of eventual carbonaceous compounds retained on the post-reaction catalyst. TPD-MS measurement were carried out on a home-made system formed by a quartz tube heated at 180°C for 3 hours (ramp rate 20°C/min) in a Carbolite EVT 12/450 furnace. The inlet of the quartz tube was connected to a compressed air source, while the outlet was connected to a Hyden QGA mass spectrometer for the online analysis of the gas phase.

2.1.10 Inductively Coupled Plasma Mass Spectroscopy (ICP-MS)

Inductively Coupled Plasma Mass Spectroscopy (ICP-MS) is one of the most sensitive technique used to determine element composition of liquid samples. Theoretically, it is able to detect any element of the periodic table different to argon. At present, state-of-art instruments are currently capable of quantitatively measuring analytes down to 1-10 ng of element per litre, in solution. Therefore, it is usually used to accurately identify chemical

composition of given samples in many research areas. Its excellent performances are due to the efficient plasma ionization technique coupled with the sensitivity of MS detection. Moreover, unlike atomic adsorption spectroscopy, ICP-MS has the advantages of scanning all elements at the same time, thus massively reducing analytical times.

During an ICP-MS analysis, the sample solution is firstly ionized by an Inductively Coupled Plasma (ICP) torch. Solid samples, which cannot be directly injected into ICP torches, must be previously decomposed by means of an *Aqua Regia* digestion, generally assisted by microwaves. Following injection, the sample solution is nebulized in order to have analytes in aerosol form with finely dispersed droplets. In the torch, the high energy plasma atomizes and ionizes more than the 90% of the particles injected which are subsequently directed to a MS device, (Figure 15). Here, the ions produced are separated on the basis of their mass-to-charge ratio and a detector generates an ion signal proportional to their concentration.

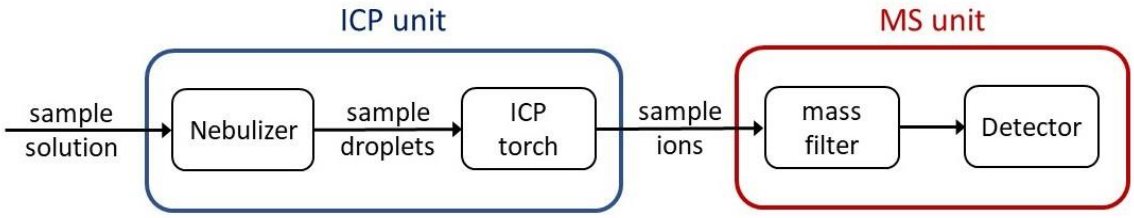

Figure 15 Schematic representation of a ICP-MS apparatus. The sample solution is nebulised and then injected into a ICP torch where it is atomised and ionised. The samples ions are then sended to a MS unit where are saprated throgh a mass filter and then detected.

Inductively coupled plasma (ICP)

Inductively couple plasma is an effective technique of ionization, which is generally used to provide detectable species in atom emission spectroscopy or mass spectroscopy. The high-energy environment, provided by the plasma, permits ionization of all those refractory materials and those analytes which possess high ionization energy that cannot typically be excited by other ionization sources. Plasma media ensure an ionization efficiency higher than 90% for all elements, resulting in the generation of detectable species with just traces concentration of any sample. For these reasons ICP is one of the most exploited and accurate technique for quantification of elemental composition.

ICP torches are constituted by three concentric tubes usually made of quartz, although the inner tube can be composed of sapphire to permit analysis of samples digested with hydrofluoric acid. At the top of the torch is placed an induction coil supplied with a radiofrequency electric current, which generates a magnetic field. A flow of argon is introduced between the two outermost quartz tubes of the torch and an electric spark is applied to induce free electrons in the gas stream. The magnetic field induced inside the

coil is continuously inverted since the supplied electric current is varied with a frequency of 27-41 MHz, equal to 27-41 million cycles per second. As consequence of the changing magnetic field, the generated electrons are continuously accelerated from one side to another of the coil increasing their kinetic energy. The agitated electrons collide at high energy with argon atoms causing electron emission, hence generating argon ions and further electrons. The new charged particles produced are in turn accelerated by the magnetic field inside the coil, thus inducing further collisions and electric species. However, due to the high ionization potential of argon, recombination of electrons with argon ions are likely to occur, returning neutral atoms. However, by increasing the coil electric field frequency, it is possible to enhance the ionization rate until it is equal to the one of ion recombination, generating a balanced state in which a certain concentration of electrons and ions are always present. In this way a high energy ionized gas called a plasma is formed, which is able to sustain itself as long as the electric power is applied to the load coil, by means of the so-called *inductive coupling* phenomenon. The elevated kinetic energy of the charged species inside the plasma, together with their electric potential, produce an energetic environment equivalent to temperatures up to 10,000 K.
Usually, a second flow of argon is fed between the intermediate quartz tube and the central tube of the torch, into which the sample is injected, to ensure a safe distance between travelling analytes and the plasma. Nebulized samples are transported in the core of the plasma by means of a third argon flow, which passes through the central tube of the torch. In this way the analyte aerosol enters in the central channel of the ICP, where it evaporates and the remaining molecules are atomized and then immediately ionized. The high ionization energy of argon ensures that all the electrons generated during the sample ionization are more likely to recombine with argon ions than with the analyte ions, thus leaving the sample as a charged species available for the detection. In addition, many elements own multiple competitive ionization states which can decrease the ionization efficiency. However, the plasma temperature can be specifically tuned to favour the first ionization process against the second, thus increasing the technique efficiency.[17, 18]

In this work ICP-MS technique was used to quantify elemental composition of pre- and post-reaction catalyst, to determine whether active sites leaching occurred during the chemical reaction. Elemental analysis was performed on an Agilent 7500ce ICP-MS. Sample pre-digested in *Aqua Regia* by means of a microwave reactor.

2.1.11 Transmission Electron Microscopy (TEM)

Transmission electron microscopy (TEM) is a microscopy technique which exploits electron wavelengths to form images. Due to the nanometric size of the incident beam wavelength, TEM allow analysis of materials down to the atomic scale. This enables the instrument to capture fine details as a single column of atoms, which is thousands of times

smaller than a resolvable object seen in a light microscope. Due to its high-resolution potential at nanometric levels it is used in various scientific area to investigated material structure compositions. For example, TEM is exploited in catalysis to study atomic details of catalyst structures, such as crystallographic planes, unit cells defects, or single metal nanoparticles.

Theoretically, the optical resolution of an imaging system, d, is defined as the minimum distance between two resolvable points which can be observed. According to physical law, it is strictly correlated to the radiation wavelength used to irradiate the observed object, to the refraction index of the medium in which the light is propagated and to the geometry of the system, (Equation 13).

Equation 13 $$d = \frac{\lambda}{2n\,sin\theta}$$

Where: d = optic resolution
λ = probing photons wavelength
n = refractive index of the medium light propagation
θ = half-angle of the light cone that enters the objective

As consequence, every probing radiation carries an intrinsic limit of resolution correlated with its wavelength. It means that for a given radiation with by which the sample is probed, the optical resolution cannot be enhanced over a certain maximum value.
Electrons, like all matter, have both wave and particle-like properties, and their wave-like properties mean that a beam of electrons can be focused and used as a probing radiation. According to the de Broglie equation (Equation 14), the wavelength of an electron is inversely proportional to its velocity, which in turn depend to the electron kinetic energy.

Equation 14, de Broglie equation $$\lambda_e = \frac{h}{m_e v_e}$$

Where: λ_e = electron wavelength
h = Plank's constant
m_e = electron mass
v_e = electron velocity

For example, electrons with kinetic energy of just 1 volt already possess wavelengths as short as 1.2 nm.[19] It follows that using electron beam as probing radiation for optical systems, resolution can be increased significantly to ultimate reach atomic dimensions. The excellent resolution of transmission electron microscopes is therefore clear.

In TEM the sample must be thinner than 100 nm to permit the electron beam to pass through it and reach the imaging detector. Generally, materials that have dimensions

small enough to be electron transparent, such as powdered substances or nanotubes, can be quickly prepared by sample deposition on support grids. Additionally, samples can be dispersed in light solvent solution and subsequently deposited onto grids. Standard TEM grids are made of copper, molybdenum, gold or platinum, with a thickness and mesh size ranging from a few to 100 μm.[20]

In TEM analysis, the electron beam is generated by a hot tungsten filament, in the same manner as a light bulb, or alternatively by field emission in which electrons are produced by means of an electrostatic effect. Once the beam has been generated, it is typically accelerated by a series of electrostatic plates in order to reach the proper voltage to probe the sample. Generally, the entire apparatus is kept under strong vacuum, typically in the order of 10^{-4} Pa, in order to increase the mean free path of the electrons inside the instrument and to avoid generation of electric arcs.[21]

The electron beam subsequently travels through a condenser lens system, which focuses the radiation to the desired size and location on the sample. In TEM, optical lenses are usually constituted by solenoid coils, which are designed to generate and concentrate magnetic fields into a precise and confined shape. In this way the radiation can be precisely manipulated and focused simply by adjusting the current passing through the electromagnetic coils, allowing a sample to be probed over a wide range of distance and resolution. Indeed, unlike that for an optical microscope, the optical configuration of a TEM can be rapidly changed by enabling, modifying or deactivating electromagnetic lenses, simply via rapid electrical switching. This provides a flexibility of operations that gets further multiplied when lenses are assembled into stacks of independent lenses, each of which can focus, magnify and collimate the beam coming from the previous lens. Additionally, holed thin strips of metals can be placed between one lens and other, generating apertures from which beam components can be discriminated at will. Varying the distance between these apertures and the lenses permits the portion of the electrons beam that reach the next lens or the sample holder to be tuned, thus allowing a wide range of operational control.

Once the electron beam has interacted and passed through the sample, it is back magnified by other magnetic lenses and collected by an imaging detector, which converted the information transported by the radiation to form an image. Example of imaging systems are, phosphor screen for direct observation by the operator, photographic films coupled with Charged-Coupled-Devices and the latest CMOS detectors that permit single electron counts to be detected.[22]

Exploiting the flexibility of the magnetic optical system and the different interactions which may occur between electrons and samples, TEM instruments may operate in many different modes including conventional imaging, scanning TEM imaging (STEM), diffraction spectroscopy, and combinations of these. Once the electron beam has passed

the sample, it forms an image on an imaging device by contrast and, even within conventional imaging, there are many different ways that contrast is produced. For instance, contrast can arise from position-to-position differences in the sample thickness or density, giving the so-called "mass-thickness contrast". When the beam illuminates two neighbouring sample areas with different density or thickness, the heavier region will scatter electrons at wider angles. Tuning the objective apertures, it is possible to block these strongly scattered electrons and, as a result, heavier regions appear darker. These are known as *bright-field* images. Another contrast mode, which is useful to study crystalline materials, is the diffraction contrast, generated when different sample crystallographic structures or orientations are irradiated. In this case, electron beams that probe crystalline structures undergo Bragg scattering and, by tuning the objective apertures, only radiation components which give constructive interaction are projected on the imaging detector, resulting the so-called *dark-field* images. In addition, specific Bragg reflections can be selected or excluded in order to study characteristic crystallographic planes or conformation. Other contrasts mode may arise due to different atomic number, induced quantum-mechanical phase shifts on probing electrons, energy loss of electrons due to their passing through the sample, and more. From each mechanism, different kinds of information can be extrapolated. Hence, TEM is capable of returning an extraordinary variety of nanometric and atomic resolution information, revealing atoms position, crystallinity material composition, atomic structure defects and others. For this reason, TEM is regarded as an essential tool for materials studies.[22]

In this work, TEM was used in conventional imaging mode to study the dimensions and distribution of palladium nanoparticles supported on active carbons. Bright-field images of Pd/C, obtained with various degrees of magnification, are illustrated in Figure 16.

For examination by TEM, samples were prepared by dispersing the catalyst powder in high purity ethanol using ultra-sonication. 40 µl of the suspension was dropped on to a holey carbon film supported by a 300 mesh copper TEM grid before the solvent was evaporated. The samples for TEM were then examined using a JEOL JEM 2100 TEM model operating at 200 kV.

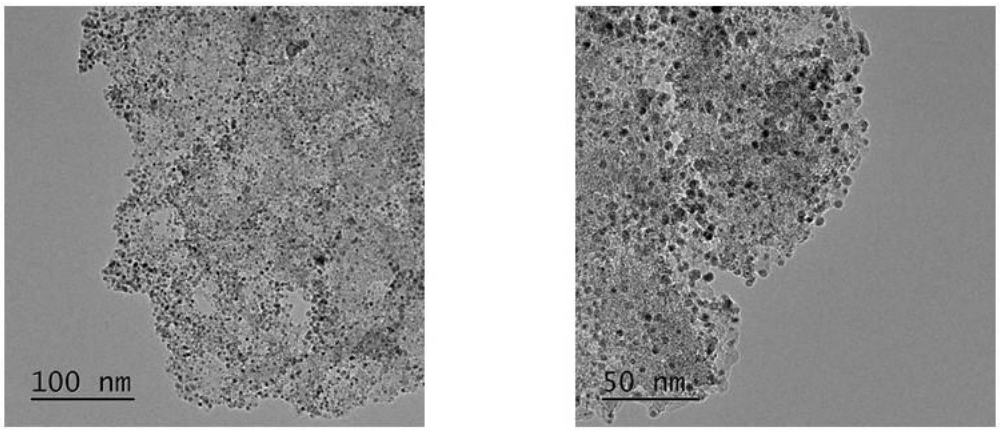

Figure 16 TEM images of commercial 5% Pd/C acquired in bright-field mode at different magnification degrees.

2.2 Product analysis and quantification

In order to know the catalytic potential of a given material, it is a pivotal requirement to test its performance of promoting chemical reactions. Therefore, throughout this work, several reactions were performed and catalytic activity was evaluated by monitoring reactants and (by) products concentration over particular periods of reaction time. A range of analytic techniques was employed to quantitatively analyse the reaction mixture at a given reaction time, in order to kinetically investigate the system under study. A summary of the theory behind every analytical technique is provided in this section.

2.2.1 High Performance Liquid Chromatography

High performance liquid chromatography (HPLC) is a technique exploited to qualitatively separate and quantitatively analyse different components of a reaction mixture. In liquid chromatography, analytes are separated according to their different affinity to the stationary phase, situated in the column, or to the mobile phase known, as the eluent.[23] Components dissolved in the eluent are passed through the column and are retained to a different degree depending to their polarity, charge or dimension, and are thereby separated. The length of time elapsed between the injection of the sample mixture and the elution of a particular compounds is defined as retention time; the stronger the interaction between analyte-stationary phase, the longer the retention time for that analyte will be. Reaction mixture compounds are therefore distinguished by their retention time. Downstream of the column is a detector which returns a signal proportional to the concentration of each single analyte in solution. In this way, a chromatogram of the HPLC analysis is generated, in which at specific retention times appears peak, the area of which is proportional to the amount of compound eluted at that specific time (Figure 17).

Constructing calibration lines with opportune standard references permits correlation of the chromatogram area to the eluted analyte concentration, thereby allowing its quantitative determination.

In this work, refractive index detector (RID) and evaporative light-scattering detector (ELSD) were used as detector modules.

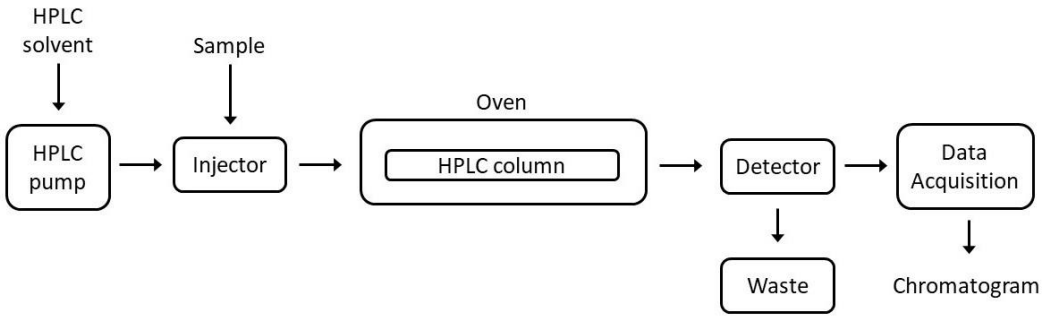

Figure 17 Generic schematic representation of a HPLC system. The eluent and the samples are pushed through all the system by mean of the HPLC pump. The separation of the analytes takes place in the column and the eluted compounds are detected by one or more detector modules.

Refractive Index Detector (RID)

The refractive index (RI) of a solution is proportional to the analyte concertation when the solute is present in a certain range of concentration. Refractive index detector (RID) are devices which measure the refractive index of an analyte relative to the chromatography eluent used as reference. For this reason, RID flow cells are constituted by two parts, one for the sample and one for the reference solvent. During the HPLC analysis, through the sample side is passed the liquid effluent coming from the column, while the pristine eluent used for the HPLC analysis is passed through the reference side. The refractive index of the two solutions is continuously measured and compared. When a particular eluted analyte passes through the detector, the device will measure the difference in refractive index between the sample and the reference, returning a signal proportional to the elute. The refractive index difference appears as a peak in the chromatogram.

Generally, these kinds of devices are used to detect substances with no UV absorption, such as alcohols, sugars, fatty acids, polymers and carbohydrates. RI detectors are considered universal detectors, but they lack sensitivity when the RI of the sample approaches the RI of the mobile phase, and they are temperature dependent.

Evaporative Light-Scattering Detectors (ELSD)

Evaporative light-scattering detectors (ELSD) are destructive detectors, which measure the intensity of the light scattered by residual solid analyte particles. Generally, ELSDs are constituted by a nebuliser in which the chromatographic effluent is transformed in an aerosol of uniform droplet size. Afterwards, the analyte drops are passed through a heated drift tube in which the mobile phase is completely vaporised, without thermally degrading the analytes thanks to the low pressures applied.[24] In this way, the outcoming aerosol is ideally composed only of dry analyte particles, which are subsequently injected into an optical cell. Here, a polychromatic light beam is directed on the incoming solid particles which scatter the incident radiation. The intensity of the light scattered is proportional to the dry particle diameter, D, which in turn can be correlated to the analyte concentration introduced in the detector, (Equation 15).[25]

Equation 15

$$D = D_0 \times \sqrt[3]{\frac{c}{\rho}}$$

Where: D = diameter of dry particle
D_0 = diameter of nebulised droplet
c = concertation of the analyte solution
ρ = density of the dry analyte

In this way, by recording the intensity of the scattered light through a photomultiplier or a photo diode, it is possible to return the concentration of the injected analyte solution. However, depending to relative dimension between the dry particle diameter, D, and the wavelength of the incident radiation, λ, different kinds of scattering occur. For each kind of scattering, the intensity of the scattered light is function to the dry particle diameter with a different order of magnitude. The higher the $\frac{D}{\lambda}$ ratio, the lower the amount of scattered light per unit of particle diameter and, as consequence, per unit of analyte concentration.[26] It follows, that ELSDs do not have a linear response to the analyte concertation (*c*), but response according to an exponential relationship, (Equation 16).

Equation 16

$$A = a \times c^b$$

Where: A = area of the chromatogram peak
a, b = calibration coefficient of the ELSD response
c = analyte concertation

However, by constructing a calibration curve through standard reference solutions, it is possible to determine the ELSD response curve and then correlate the chromatogram peaks to the analyte concentration, (Figure 18).

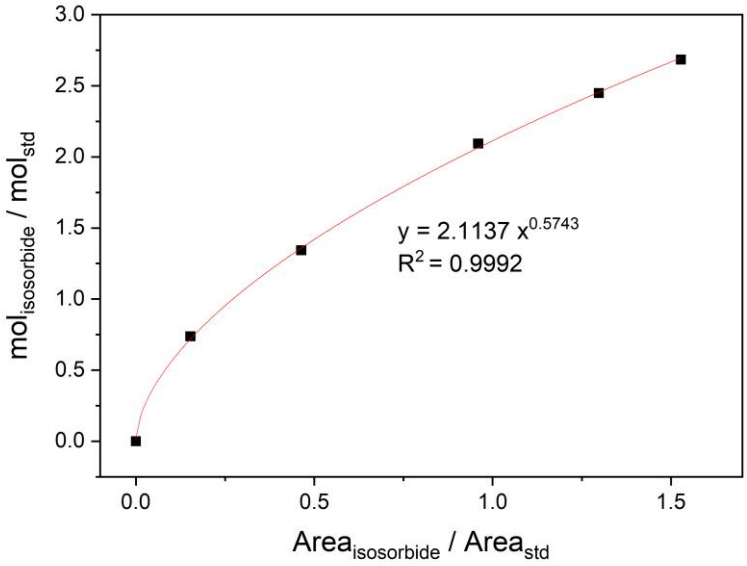

Figure 18 ELSD response curve of isosorbide standard solutions. In order to obtain a more accurate calibration, mols and area values of isosorbide are normalised against mols and area of a cellobiose external standard solution.

ELS detectors are typically used to analyse compounds that cannot be detected by UV/VIS or RI devices. Differently to RIDs, they can operate both in isocratic and gradient elution condition and are 5-10 times more sensitive than RIDs. However, ELS is a destructive technique because the analyte is sacrificed to generate the scattering solid particles, hence ELSDs must be placed at end of an eventual series of detectors.

2.2.2 Gas Chromatography

Gas chromatography (GC) is a useful technique employed to separate and quantify molecules which can be easily vaporised.[27] Gas chromatography exploits the same separation principle of liquid chromatography, but analytes and eluents must be present in the gaseous phase. Liquid analytes, which are not already available in gaseous phase, are vaporized prior to analysis by injection into a heated injection port. As consequence, only those samples possessing relatively low boiling points and which possess sufficient thermal stability can be analysed by GC. Once the analytes have been vaporized, they are transported through a capillary column by a carrier gas (typically helium or nitrogen). GC columns are generally constituted by 10-100 meters of thin fused-silica capillaries of 250 μm inner diameter. Inside the column, the stationary phase, which is coated on the inner surface of the capillary, interacts differently with the eluted compounds according to their polarity. In this way, substances that are retained inside the column with different

strengths are eluted at different retention times. Additionally, the column is placed inside an oven, the temperature of which can be specifically programmed during the analysis in order to enhance the compound separation, (Figure 19). The eluted gas molecules are progressively transported toward a detector, which produces signals proportional to their concentration, thereby generating intensity peaks as function of the compound retention times. In this way, chromatogram plots are returned. Through a calibration line, constructed with accurate reference standard, signal peaks area can be correlated to the concentration of analytes present in the sample.

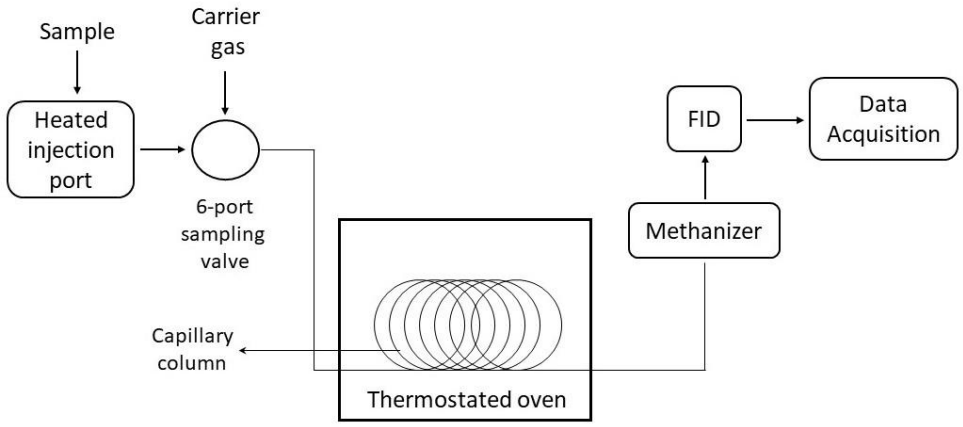

Figure 19 Generic schematic representation of a gas chromatographer with a methanizer unit and FID detector.

One of the most exploited devices to detect analytes in GC analysis is the flame ionization detector, (FID). In these detectors, low oxidation molecules are oxidised with a flame which produces, at the same time, fragmented ions of the analytes. The generated ions are proportional to the amount of analyte injected and are counted by two charged plates with opposite charge, which produce an electrical signal. In order to detect also those molecules with high oxidation state, FIDs are usually coupled with methanizer units. In this apparatus, a broad range of organic molecules, such as CO, CO_2, formaldehyde, formamide and more, can be hydrogenated into methane, which is subsequently detected by the FID. The hydrogenation reaction, assisted by a nickel catalyst and performed in a temperature range between 300 and 380°C, ensures complete conversions of the injected molecules into methane, thus allowing detection limits down to 200 ppb to be reached.

In this project, GC coupled with a methanizer unit was used to analyse the composition of the gaseous mixture produced by formic acid decomposition. In particular, the CO/CO_2 ratio yielded by the reaction was determined, in order to evaluate the selectivity of the decomposition reaction towards dehydration and dehydrogenation respectively.

2.3 References

1) R. Masel, '*Principles of Adsorption and Reaction on Solid Surfaces*', Wiley, 1996.
2) REPORTING PHYSISORPTION DATA FOR GAS/SOLID SYSTEMS with Special Reference to the Determination of Surface Area and Porosity. K. S. W. SING (UK, Chairman); D. H. EVERETT (UK); R. A. W. HAUL (FRG); L. MOSCOU (Netherlands); R. A. PIEROTTI (USA); J. ROUQUEROL (France); T. SIEMIENIEWSKA (Poland). Pure & Appl. Chem., Vol. 57, No. 4, pp. 603—619, 1985.
3) S. Brunauer, P. H. Emmett, E. Teller, *J. Am. Chem. Soc.*, 1938, **60**, 309.
4) M. Thommes, *Chemie Ingenieur Technik*, 2010, **82**, 1059.
5) M. Thommes, K. A. Cychosz, *Adsorption*, 2014, **20**, 233.
6) J. W. Niemantsverdriet, *Spectroscopy in Catalysis*, Wiley-VCH, Weinheim, 2007.
7) W. L. Bragg, *Proc. R. Soc. Lond. A*., 1914, **89**, 468.
8) J. C. Vickerman, I. S. Gilmore, '*Surface analysis: the principal techniques*', Wiley Editor, 2011.
9) D. W. Turner, M. I. Al Jobory, *J. Chem. Phys*., 1962, **37**, 3007.
10) F. Sanchez, D. Motta, A. Roldan, C. Hammond, A. Villa, N. Dimitratos, *Topics in Catalysis*, 2018, **61**, 254.
11) P. Atkins J. de Paula. '*Atkins' Physical Chemistry for the Life Sciences.'* New York: Oxford University Press, 2006.
12) D. C. Harris, M. D. Bertolucci, *'Symmetry and Spectroscopy: an Introduction to Vibrational and Electronic Spectroscopy.'* New York: Dover Publications, 1989.
13) J. R. Ferraro, K. Nakamoto, '*Introductory Raman spectroscopy*', Elseiver, 2003.
14) W. Paudler, '*Nuclear Magnetic Resonance*', Boston: Allyn and Bacon Chemistry Series, 1974.
15) J. H. Gross, *'Mass spectrometry: a textbook'*, Springer, 2006.
16) S. Syed, S. Maher, S.Taylor, *Journal of Mass Spectrometry*, 2013, **48**, 1325.
17) H. E. Taylor, *'Inductively Coupled Plasma-Mass Spectrometry: Practices and Techniques'*, Academic Press., 2001.
18) D. Beauchemin, *Anal. Chem.*, 2008, **80**, 4455.
19) https://advanced-microscopy.utah.edu/education/electron-micro/
20) M. De Graef, '*Introduction to conventional transmission electron microscopy*', Cambridge Uni. Press, 2003.
21) M. A. Hayat, '*Basic techniques for transmission electron microscopy'*, Academic Press Inc., 2012.
22) L. Reimer, '*Transmission electron microscopy: physics of image formation and microanalysis'*, Springer, 2013.
23) L. R. Snyder, J. J. Kirkland, J. W. Dolan, *'Introduction to Modern Liquid Chromatography'*, 3rd Ed., Wiley, 2010.
24) H. Mourey, E. Oppenheimer, *Anal. Chem.*, 1984, **56**, 2427.
25) Principle and practical applications of Shimadzu's ELSD technical report vol.6, Shimadzu Corporation.
26) C. Megoulas, M. A. Koupparis, *Critical Reviews in Analytical Chemistry*, 2005, **35**, 301.
27) W. Jennings, '*Analytical Gas Chromatography*', Elsevier, 1987.
28) M. Thommes, K. Kaneko, A. V. Neimark, J. P. Olivier, F. Rodriguez-Reinoso, J. Rouquerol, K. S. W. Sing, *Pure Appl. Chem*., 2015, **87**, 1051.
29) M. A. R. Miranda, J. M. Sasaki, *Acta Cryst.*, 2018, A**74**, 54.

Chapter 3 - Continuous production of hydrogen from formic acid decomposition over heterogeneous nanoparticle catalysts: from batch to continuous flow

3.1 Introduction

As described in Chapter 1, increasing energy demand from a growing population, combined with increasing awareness of the negative impacts of fossil feedstock and climate change phenomena, have pointed out the urgency of developing new ways to produce energy. In this regard, the oxidation of hydrogen by fuel cells (Proton Exchange Membranes, PEM) represents a promising, clean solution, as they generate electricity and produce water as the only by-product.[1-3] Their application is already established in several sectors ranging from stationary power for buildings to transportation vehicles, including also portable power generators due to the high electricity intensity they can provide compared to their light weight and reduced dimensions.[4]

However, one of the major bottlenecks to use hydrogen for energy applications is its unsafe and inefficient storage. In fact, to achieve high energy densities, gaseous hydrogen is typically compressed and stored in cylinders at high pressure (above 200 bar), making its handling risky and impractical. Alternatively, molecular hydrogen can be liquified, but only at extreme energetic costs, considering that up to 40% of its energy content can be lost due to liquefaction.[5–7] Another major obstacle in using hydrogen as an energy carrier is its currently unsustainable method of production. In fact, industrial hydrogen is manly produced by steam reforming of methane, a finite fossil resource. In this regard, electrolytic water splitting can be considered a much cleaner route for hydrogen production. Yet, despite the abundance of water, this process is currently quite energy inefficient, particularly when non-renewable resources provide the energy to perform water splitting. Industrial hydrogen can also be generated through the water gas shift reaction, in which water is combined with carbon monoxide to produce hydrogen and carbon dioxide. However, hydrogen generated through this process is hardly suitable for PEM application since carbon monoxide impurities retained in the product act as detrimental poison for fuel-cells.

As such, much emphasis has recently been placed to find new method to store or produce hydrogen under more secure and favourable conditions. One of these consist in the physisorbition of hydrogen on different highly porous materials such as zeolites, MOFs, clathrate hydrates, various carbon material and conventional organic polymers.[8-11] In addition, during the last two decades, great scientific attention has been addressed on the catalytic decomposition of various hydrogen-containing molecules (so-called storage compounds), in particular so that molecular hydrogen can be produced for portable fuel-cell devices.[12, 13] Examples of these compounds include solid phase systems, such as

metal and non-metal hydrides[6], amines[7], amides[12], ammonia-like complexes[13], and liquid carriers such as N-ethylperhydrocarbazole[14] or alcohols[15] or formic acid. Lithium and sodium borohydrides, together with ammonia borane, have been screened also as potential compounds due the safe and low-cost technology they require to produce hydrogen. Also hydrous hydrazine represents an interesting solution as hydrogen storage molecule, since the only by-products generated by its decomposition is molecular nitrogen.[16, 17] However, among the numerous well explored options,[14–21] formic acid (HCOOH) is one of the most promising, given the fact it has a relatively high content of hydrogen (4.4 wt.%), and, in contrast with the most physisorbition storage methods, is a stable liquid at room temperature and pressure.[22, 23] This allows the safe and cheap distribution of formic acid through pipes, without the utilization of high-pressure system or road transport like in the case of solid materials, thus minimizing carbon emissions. Although formic acid is currently produced industrially from fossil resources, there are several recent examples in which it can be obtained by the direct oxidation of biomass at high yields.[24-26] For example, BioMetics estimated a large-scale plant, able to process 2000 dry tons of cellulosic feedstock per day with a yield in formic acid up to 50%.[27] Furthermore, formic acid is frequently encountered as a by-product in many biomass-based processes, such as the hydrolysis of 5-hydroxymethyl furfural. In fact, the formic acid production from renewable feedstock is a such established technology that today its ester derivates have been proposed also as bio-alternative for fuels additives.[27] Thus, with the growing scale of biomass processes, there are possibilities of having a large stock of renewable formic acid available in the future. More importantly, if the production of formic acid is performed via biomass conversion, a carbon neutral hydrogen storage cycle can be completed. In fact, during the decomposition of formic acid, hydrogen and carbon dioxide are generated. However, if the carbon dioxide evolved during the process is subsequently captured by plant organisms to generate further biomass, the net carbon amount emitted during the process tends towards zero. Furthermore, several researches have found potential technologies able to capture carbon dioxide and couple it with hydrogen yielding liquid formic acid, in order to use this molecule also as liquid carrier of industrial hydrogen produced in other sustainable ways, Figure 1.[28-30]

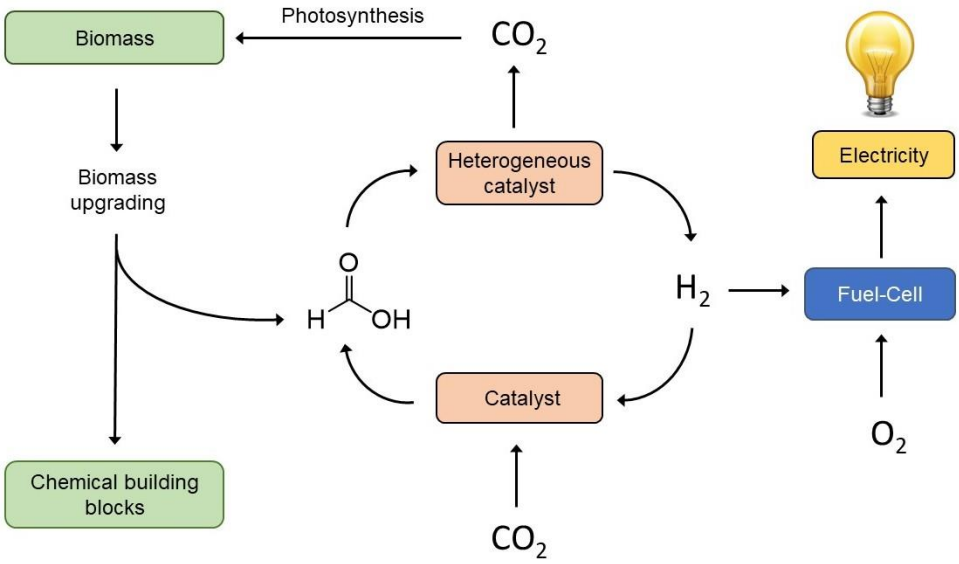

Figure 1 Schematic representation of formic acid as hydrogen storage compound. Formic acid can be decomposed to carbon dioxide and hydrogen, which is then utilised for electricity production by oxidation in fuel-cells, yielding water as the only by product. If formic acid is generated from biomass upgrading technologies the net carbon dioxide emitted during the cycle is theoretically zero. Carbon dioxide can be also recombined with hydrogen yielding formic acid.

Specifically, formic acid decomposition can follow two different pathways: dehydrogenation and dehydration pathways (Scheme 1).

$$HCOOH \rightarrow H_2 + CO_2 \qquad \Delta G = -48.4 \text{ kJ/mol} \qquad (1)$$

$$HCOOH \rightarrow H_2O + CO \qquad \Delta G = -28.5 \text{ kJ/mol} \qquad (2)$$

Scheme 1 Possible formic acid decomposition pathways. Dehydrogenation of formic acid, which is the thermodynamically favoured route, yields hydrogen and carbon dioxide. In contrast, dehydration of formic acid leads to water and carbon monoxide.

The dehydrogenation pathway is the desired route, and leads to hydrogen and carbon dioxide, while the dehydration leads to the formation of water and carbon monoxide, which is a strong poison for the fuel-cell membrane as well for many catalysts. Fortunately, the dehydrogenation route is thermodynamically favoured with a ΔG of -48.4 kJ/mol against the -28.5 kJ/mol of the dehydration reaction. Both reaction pathways are endothermic having a ΔH_1 = 32.09 kJ/mol and ΔH_2 = 28.74 kJ/mol. Considering the enthalpy variation of the two reactions pathways, the dehydrogenation leads to an higher enthalpy increment compared to the dehydration, because of the larger amount of gaseous products that are generated from reaction (1) compared to reaction (2), (ΔS_1 = 270 J/mol K, ΔS_2 = 191 J/mol K).[69]

Therefore, over the past decade, the development of technologies capable of selectively decompose formic acid into hydrogen has been topic of much attention. Once again, one of the best solution able to perform this task have been found via catalysis. In fact, the employment of various metal-based catalysts has been demonstrated as an efficient method to lead the formic acid decomposition towards the dehydrogenation pathway, thus generating hydrogen selectively. Among the screened catalytic materials, some of the most active are homogeneous in nature, employing noble elements such as iridium, ruthenium, and rhodium, among others.[31–35] Despite their excellent catalytic performances, their solubility and requirement for complex and expensive ligands limits their large-scale practicality.[36–39] However, while many heterogeneous catalysts have been studied, many solid catalysts require elevated temperatures (>250°C) and gas phase operation, which also limits their practicality.[40] In several cases, homogeneous and heterogeneous catalysts also require the utilization of stoichiometric equivalents of amines for any catalytic activity to be achieved, evidently undermining their potential.[32–34] A more favourable approach involves the development of heterogeneous catalysts capable of low temperature formic acid decomposition in the absence of external additives.[41–46]

In this regard, supported metallic nanoparticles have been found to be particularly promising in terms of selectivity and activity.[47–49] For example, Dimitratos *et al.* have systematically studied the performance of a commercial Pd on a carbon catalyst (5 wt.% Pd/C) under mild conditions (30−90 °C) and found this catalyst to be one among the best performing in the open literature.[33] However, these studies were performed in batch reactors, which are unable to produce a continuous, stable stream of hydrogen for fuel-cell applications. Furthermore, on a scientific level, such reactors also prohibit a detailed study of the lifetime of the catalyst, which is often its key performance indicator.[39, 50] Accordingly, studies of formic acid decomposition under continuous conditions are an important challenge to determine the true potential of this technology. In respect to this, a handful of reports have recently set about exploring the decomposition of formic acid under continuous conditions over both homogeneous and heterogeneous catalysts in continuous stirred tank (CSTR) mode.[35, 36, 51] Yet, in all of these previous studies, stoichiometric equivalents of amines were employed. Accordingly, it is clear that no heterogeneous catalyst, capable of the continuous, additive-free dehydrogenation of formic acid under mild conditions, has yet been identified.

Moreover, other types of continuous reactors, particularly plug flow reactors (PFRs), have yet to be explored for this chemistry, despite their widespread utilization in other branches of the chemical society and the advantages they offer over CSTRs. Only a single attempt to build this kind of process have been made for formic acid decomposition by Chan *et al.*, in which PtRuBiOx/C catalysts were employed.[44] However, the system suffered of

preferential effluent pathways in the catalytic bed and the catalyst showed rapid loss of activity during the first minutes of reaction. Nonetheless, on a fundamental level, these previous studies have not focused on the structural and chemical changes that catalysts undergo during this catalytic process, nor on the fluid dynamic optimisation of the system. As such, detailed knowledge of the rates of deactivation of catalysts for this reaction, in addition to fundamental knowledge regarding the mechanisms of deactivation, is not available, despite its critical importance.[39, 50] Here, we investigate the continuous production of hydrogen through the decomposition of formic acid over a commercially available Pd/C. Detailed kinetic studies in various reactor modes, including PFR and CSTR, are coupled to a variety of mechanistic and spectroscopic experiments, which permit the generation of structure−activity−lifetime relationships. In addition to providing unique mechanistic insight into this reaction, these studies also allow identification of routes to mitigate deactivation, whilst identifying the optimal reactor mode from a productivity and stability perspective with which future kinetic studies should be performed.

3.2 Experimental

3.2.1 Materials

A commercial Pd (5 wt.%) supported on activated carbon (5% Pd/C) was used as received (Merck-Sigma). Commercial 5% Pd/C was selected as catalyst because showed great activity performances in previous work.[33] Formic acid (98% purity), benzoic acid and acetic acid, succinic acid and D_2O were purchased from Merck-Sigma and used without any purification, unless otherwise stated in the text. Sodium formate was purchased from Merck-Sigma and used without any purification. Dilution of reactants was made in deionized water.

3.2.2 Batch multiple cycles formic acid decomposition

Multiple cycles of formic acid dehydrogenation reaction were carried out in a round bottom flask loaded with 15 mg of Pd/C and 30 mL of water and stirred at 700 rpm with a magnetic stirrer at 50°C and 1 atm. Every cycle of reaction was initiated by adding 0.56 mL of formic acid (to have an initial aqueous formic acid concentration of 0.5 M), and the reaction was run for approximately 2 hours until complete substrate conversion was achieved. Afterward, a fresh aliquot of formic acid was added and a new cycle started. Aliquots from the reaction mixture were collected and the concentration of formic acid analysed by means of HPLC Agilent 1220 Infinity, using a column Agilent MetaCarb 87H 250 × 4.6 mm at 60 °C, 0.45 mL min^{-1}, 0.01 N H_3PO_4 solution in HPLC grade water, equipped with a RI detector.

3.2.3 Continuous PFR formic acid decomposition

Continuous PFR formic acid dehydrogenation reactions were performed in a plug flow, stainless steel, tubular reactor. The reactor was connected to a Cole-Parmer HPLC pump in order to accurately regulate the reactant flow. The catalyst was densely packed such as purchased into a ¼ inch stainless steel tube (4.1 mm internal diameter) and held between two quartz wool plugs, and a frit of 0.5 μm was placed at the reactor exit. The reactor was subsequently immersed in a thermostated oil bath at the desired reaction temperature. Pressure in the system was controlled by means of a backpressure regulator, and a pressure of 5 bar at the end of the system was typically employed. Aliquots of the reaction solutions were taken periodically from a sampling valve placed after the reactor.

3.2.4 Continuous CSTR formic acid decomposition

CSTR formic acid dehydrogenation reactions were performed in a 100 mL two-neck round-bottom flask. The flask was filled with 30 mL of DI water and 45 mg of Pd/C. The reaction temperature was controlled by submerging the flask in an oil bath thermostated at 50°C, and the reaction mixture was stirred at 700 rpm by means of a magnetic stir bar. The two necks of the reactor were sealed by rubber septa. A Cole-Parmer HPLC pump dispensed pure formic acid into the flask at a flow rate of 0.01 mL min^{-1}. Aliquots from the reaction mixture were collected and the concentration of formic acid analysed.

3.2.5 Catalyst regeneration

Thermal catalyst regeneration was performed heating the whole reactor in a combustion furnace (Carbolite MTF12/38/400) to 180°C (20 °C min^{-1}) in air (3 h).

Washing catalyst regeneration was performed by flushing deionised water into the PFR reactor by means of a Cole-Parmer HPLC pump. During the water regeneration treatment the PFR reactor was kept in the oil bath used for the reaction and set at 50°C. Treatment time length and water flow rate were employed as stated in the result and discussion section.

3.2.6 Catalyst characterisation and analytical details

p-XRD, XPS, gas absorption analysis, TEM, Raman Spectroscopy, IR spectroscopy, TGA, TPD-MS, ICP-MS were employed to characterise the fresh, used and regenerated catalyst. ^{1}H-NMR was used to analyse substrate, reaction effluent and supernatant washing solution composition. Formic acid concentration was determined by means of a HPLC equipped with a RI detector using a 0.05 M solution of succinic acid as external standard. Composition analysis of gaseous products generated by the reaction was

performed by means of GC-FID equipped with methanizer unit. Experimental details for each of these methods are fully described in Chapter 2.

3.3 Results and discussion

3.3.1 Kinetic studies: from batch to continuous

As introduced above, commercially available Pd on carbon (5 wt.% Pd/C, henceforth Pd/C) has been identified by Dimitratos *et al.* to be a suitable catalyst for the additive-free decomposition of formic acid under mild conditions (30−90°C).[33] Reusability tests of the catalyst suggested that Pd/C possesses a good degree of stability, since five consecutive uses during “recyclability studies” exhibited less than 5% of loss of performance between cycles. However, classical reusability studies can easily overestimate the potential stability of the catalyst. In fact, as reported by the authors, the recyclability procedure employed implies the separation of the catalyst from the reaction solution through filtration and then, a drying process at ambient temperature for 18 hours. Therefore, for example, if during the first reaction cycle some contaminants are present in the aqueous solution and act as poisons for the catalyst, the pristine solvent introduced in the second cycle could remove such detrimental compounds and thus restore the previously lost levels of performance. Furthermore, the drying treatment conducted for an extended period of time, could induce desorption of volatile species eventually adsorbed by the catalyst during the reaction. Once again, if during the reaction such adsorbed residues inhibit the catalyst activity, the stability performances of the catalyst determined after the drying procedure is falsified.

Therefore, in order to test the real stability potential of Pd/C, this chapter focuses on extending classical reusability experiments by adding fresh aliquots of substrate to a batch reactor once a reaction cycle was completed without removing the catalyst from the reactor between cycles (Figure 2).

In this way, perturbation of the catalyst between “cycles” was minimized. At the beginning of each reaction “cycle” pure substrate was added to the remaining aqueous solution in order to avoid solvent addition, which may decrease the reaction rate of the following cycle. In this way a formic acid-palladium molar ratio equal to 100 was obtained per each reaction “cycle”. In order to calculate precise kinetic parameters, the evaluation of the reaction was followed by conversion of formic acid. Over six “cycles,” the catalyst still retained good initial activity. Indeed, the reaction rate observed during the “sixth” cycle resulted approximately 75% of that of the first.

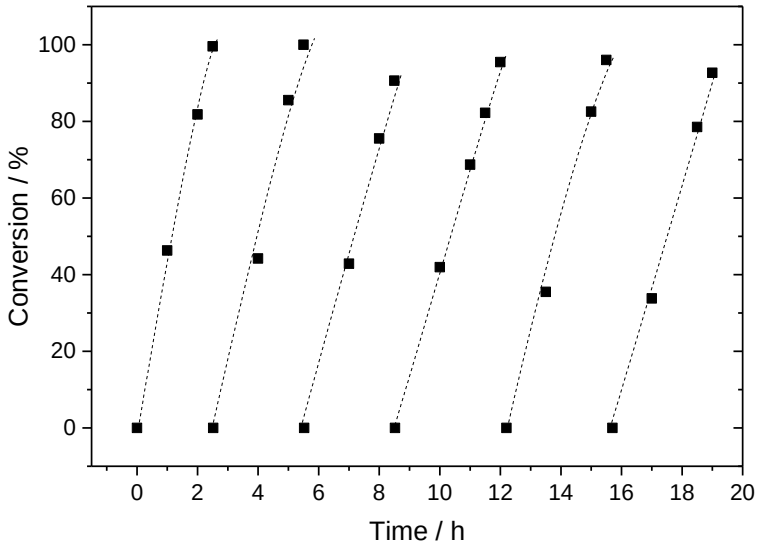

Figure 2 Batch tests of formic acid decomposition over Pd/C with fresh aliquots of formic acid periodically added to the reactor without removal of the catalyst or other treatments. Reaction conditions: Pd/C (15 mg), aqueous formic acid (30 mL, 0.5 M, $mol_{formic\ acid}/mol_{Pd}$ = 2100 per cycle), 50°C, 700 rpm.

Moreover the TOF value calculated in the first reaction hour, 1100 h^{-1}, is in agreement with the one reported by Dimitratos *et al*.,[33] 1600 h^{-1}, confirming the reliability of the results obtained. However, the discrepancy between the TOF calculated and the one reported in literature might be due to several operational conditions, and/or differences in the reaction setup such as different stirring rates, different reactor volume, different magnetic stirrer used and to the different setup optimisation.

This promising first result, in terms of catalyst stability, encouraged the possibility to explore Pd/C for the continuous dehydrogenation of formic acid. Moreover, as already discussed, performing reactions in continuous process is a practical method to gain insights on catalyst deactivation.[39, 50] Among such reactors, PFRs in which the catalyst bed is confined inside a tubular column and the reactant solution is continually pumped over the catalyst bed offer several advantages, including higher rates of reaction, better temperature control, good mass and excellent heat transfer, and facilitated study of the catalytic material post (and during) reaction by (in situ) spectroscopy. Accordingly, a ¼ inch stainless steel tube was packed with Pd/C between two pieces of quartz-wool buds, and an aqueous solution of formic acid flushed through it. However, prior to collecting catalytic data in the continuous set-up, the optimal reaction conditions to allow the system to operate in absence of any mass transfer limitation must first be determined. As mentioned in Chapter 1, this allows an experimentalist to obtain reliable catalytic data and

ensure an accurate interpretation of the measurement. Thereby, to determine the conditions required to operate in chemical kinetic regime, a preliminary kinetic study was performed. To verify the absence of external mass transfer limitation, reactions were performed at 50°C at different linear velocity (LHSV, Equation 1) but at fixed contact time of 35 s. Hence, experiments with flow rate range from 0.1 to 0.5 mL min^{-1} were conducted, adjusting the mass of Pd/C accordingly to maintain the same contact time (Equation 2) in each case.

Equation 1

$$LHSV = flow\ rate_{\ (feed\ solution)}\ volume^{-1}_{(catalyts)}\ hour^{-1}$$

Equation 2

$$Contact\ time = \tau = \frac{volume_{(catalyst\ bed,mL)}}{flow\ rate\ (mL\ min^{-1})}$$

As can be seen from Figure 3, all the reactions conducted with different linear velocity provide the same conversion of 80% at the utilised contact time, within an experimental error of 5%, indicating that in those flow rate (from 0.1 to 0.5 ml min^{-1}) the reaction runs under chemical kinetic regime, thus validating all the following kinetic evaluation. However, in tubular reactions, to have reliable catalyst performance and to avoid back mixing phenomena, it is good practise to have linear velocity greater than 0.1 mL min^{-1} along the catalyst bed. Keeping this golden rule in mind and to have appropriate catalyst amount for post-reaction catalyst characterization, flow rate of 0.25 mL min^{-1} was selected for the following continuous reactions.

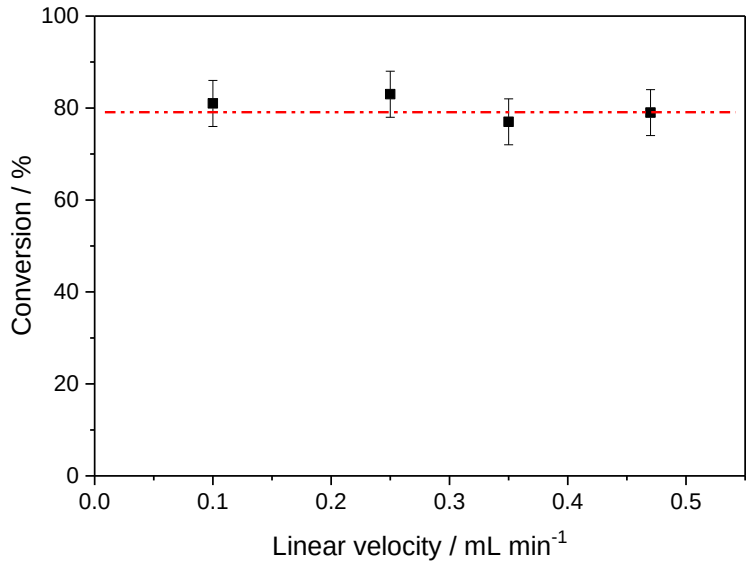

Figure 3 Conversion of aqueous formic acid (0.5 M) at 50°C performed in PFR reactor, linear velocity between 0.10 and 0.50 mL min^{-1} and mass of catalyst between 0.067 and 0.300 g, 5 bar of back pressure.

Another diffusion limiting process that must be considered is internal mass transfer phenomena, in addition to the external ones discussed above. However, the pelletising procedures, required to study such phenomena, might damage the metal nanoparticles and the carbon support of the catalyst, thus falsifying the kinetic results. Nevertheless, the nano-dimensions of the catalyst metal particles, dispersed on a ultra-fine powdery support such as active carbons, ensure that internal mass transfer limitations within Pd/C can be neglected (for detailed description of the phenomena see Chapter 1).

Thereby, once the optimal reaction conditions that allow to work under chemical kinetic regime were evaluated, time on stream experiments were performed in order to evaluate the catalyst stability. To do that, a PFR reactor was packed with 150 mg of Pd/C and a 0.5 M formic acid aqueous solution was fed at 50°C, for a total of 200 minutes of time.

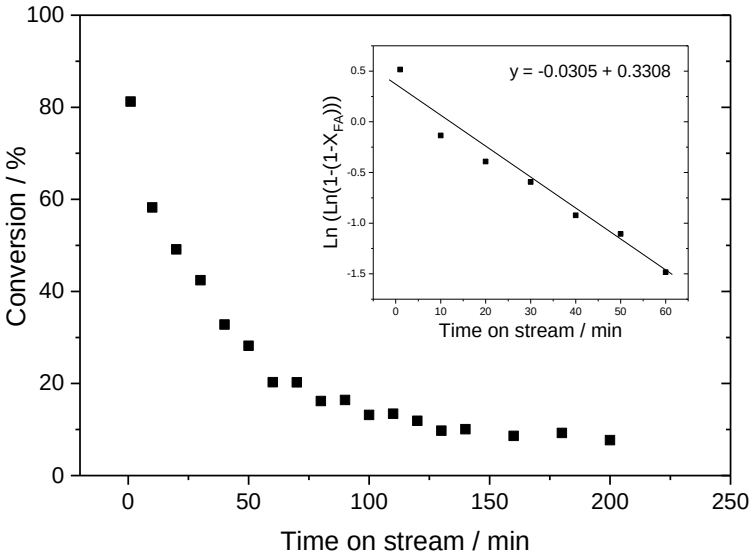

Figure 4 Formic acid conversion as a function of time on stream at 50°C, with the Levenspiel plot to calculate k_d shown in the inset. Reaction conditions: Pd/C (150 mg), 0.25 mL min^{-1} of aqueous formic acid (0.5 M), 50°C, 5 bar.

From the time on stream evaluation (Figure 4) it can be seen that the formic acid conversion is not constant during the continuous decomposition. Indeed, in just 10 minutes of reaction time the formic acid conversion sharply drops from an initial value of 81% to 58%. This clearly indicate that the catalyst loses activity during the continuous process, thereby suffering some deactivation phenomena during the conversion of formic acid. Thanks to the Levenspiel logarithmic plot (Figure 4 inset) the deactivation rate of the catalyst, k_d, was determined and measured equal to 0.031 min^{-1}. Compared to the batch experiment (Figure 2), in which a total TON of 12600 was achieved, the PFR system (Figure 4) is only able to reach a TON of 67, indicating that in the tubular reactor a more rapid catalyst deactivation occurs compared to the batch system. Of course, for the purpose of continuous hydrogen generation this is an negative observation, since after

150 minutes of continuous reaction, the catalyst converts only 10% of the formic acid flowed into the reactor. In order to determine the quantity of gaseous product generated, the volume of the evolved gas from the PFR reaction was monitored by recording the displacement of water in a graduate cylinder. As can be seen from figure 4.A, the rate of gas evolved from the PFR is higher during the first minute of continuous reaction while it decreases as the reaction proceed, confirming the catalyst deactivation observed in figure 4. By comparing the volume of gas produced after 140 minutes of reaction, 204 mL (Figure 4.A), with the theoretical produced amount of gas by considering the overall mols of formic acid converted (Figure 4), 210 mL, it can be stated that all the formic acid converted is transformed in gaseous products. This experiment, combined with the gas composition analysis (Figure 8), confirm the high selectivity of the catalyst towards the formic acid dehydrogenation reaction pathways against the dehydration one, as already reported in previous works.[33]

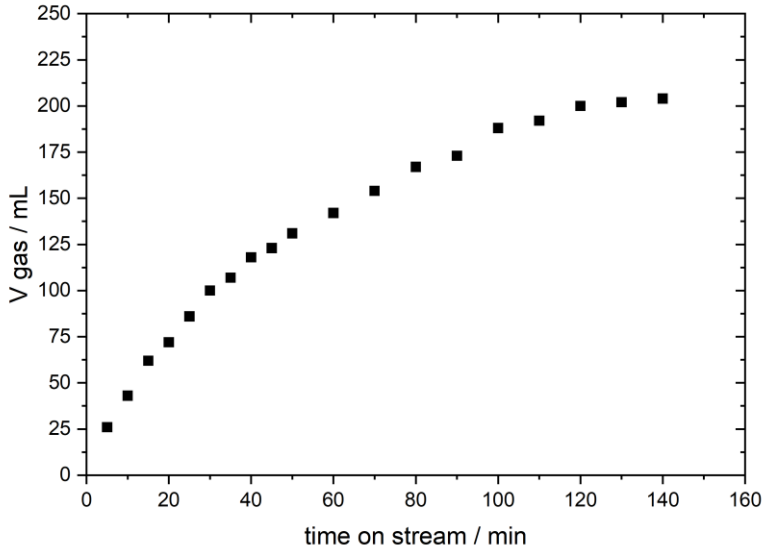

Figure 4.A Measurement of the gas evolved from a PFR reaction in function of the time on stream. Reaction conditions: Pd/C (150 mg), 0.25 mL min^{-1} of aqueous formic acid (0.5 M), 50°C, 1 bar. Volume of the evolved gas from the PFR reaction monitored by recording the displacement of water in a graduate cylinder.

However, in order to allow the use of this reaction system for continuous hydrogen production, a longer catalyst stability must be achieved. Therefore, an extensive study to understand the reason of a such rapid deactivation must be performed, to eventually overcome this detrimental phenomena and thus achieve higher catalyst stability. Hence, in order to evaluate the dependence of the catalyst stability on a variety of physical parameters, continuous decomposition reactions were performed in different conditions and the respective k_d measured. Firstly, it was investigated how the reaction temperature

influence the catalyst deactivation. To do that several continuous reactions were performed in a range of temperature from 50 to 110°C (Figure 5).

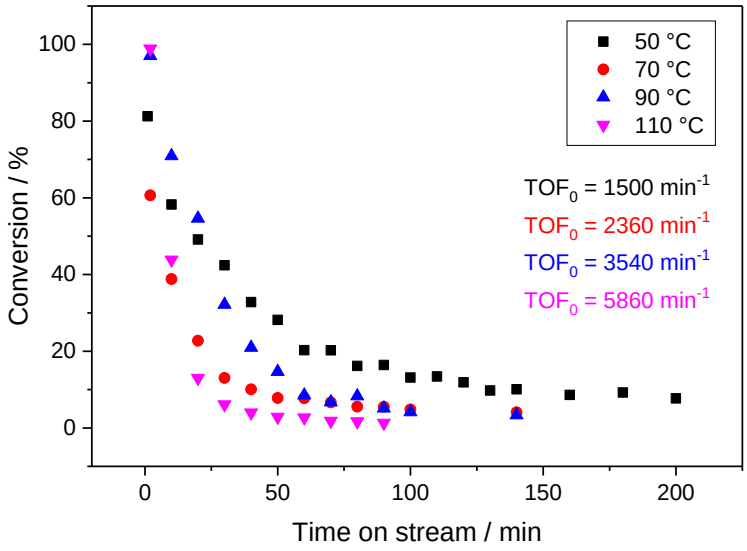

Figure 5 Formic acid conversion as a function of time on stream at different temperatures. Reaction conditions: Pd/C (150 mg), aqueous formic acid (0.5 M), 5 bar. Flow rate and temperature set at (black square) 0.25 mL min^{-1}, 50°C; (red circle) 0.5 mL min^{-1}, 70°C; (blue upward triangle) 0.5 mL min^{-1}, 90°C; (pink downward triangle) 0.85 mL min^{-1}, 110 °C.

For each catalytic experiment, the contact time was adjusted in order that each experiment starts from a similar level of conversion and, hence, the reaction coordinate.[39] Specifically, the mass of catalyst was kept constant at 150 mg whereas the flow of aqueous formic acid solution was progressively increased to 0.50 and 0.85 mL min^{-1} in line with the temperature. Comparison of the performance of the catalyst at each temperature was made by determination of its initial activity, expressed as initial turnover frequency, TOF_0, and rate of deactivation, k_d. By definition, TOF represent how many moles of substrate are converted by a single mole of catalytic active sites per unit time. It follows that higher the TOF, the greater catalyst activity. Therefore, turnover frequency is an important parameter that is useful to compare catalytic performance since express the intrinsic activity of the material in converting the substrate. As expected, increasing the reaction temperature leads to a clear increase in catalytic activity, with the initial turnover frequency (TOF_0) of Pd/C increasing from 1500 h^{-1} at 50°C to 5860 h^{-1} at 110°C. Interestingly, a similar increase for k_d is also observed, from 0.031 to 0.081 min^{-1}, between 50 and 110°C, respectively. In a first instance this trend suggests a temperature dependence for deactivation in addition to catalysis (Table 1).

Table 1 Calculated TOF and k_d from kinetic curve of continuous formic acid decomposition at different temperatures.

entry	T/ °C	TOF/ min^{-1}	k_d x1000/ min^{-1}
1	50	1500 ± 110	31 ± 0.5
2	70	2360 ± 170	43 ± 0.5
3	90	3540 ± 180	59 ± 0.5
4	110	5860 ± 300	81 ± 0.5

Performing reaction at different temperatures allowed to determine an activation energy of 40 kJ/mol which is in agreement with the one reported by Dimitratos *et al*. of 39 kJ/mol.[33] To better evaluate the extent of deactivation and its temperature dependency for reaction performed at slightly different condition, the time on stream data should be compared based on the number of reaction cycles performed, by replotting the data as relative performance as a function of substrate turnover (Figure 6).[70] As relative performance is intended the value of the monitored reaction parameter, in this case conversion, normalised to its initial value and expressed in percentage points.

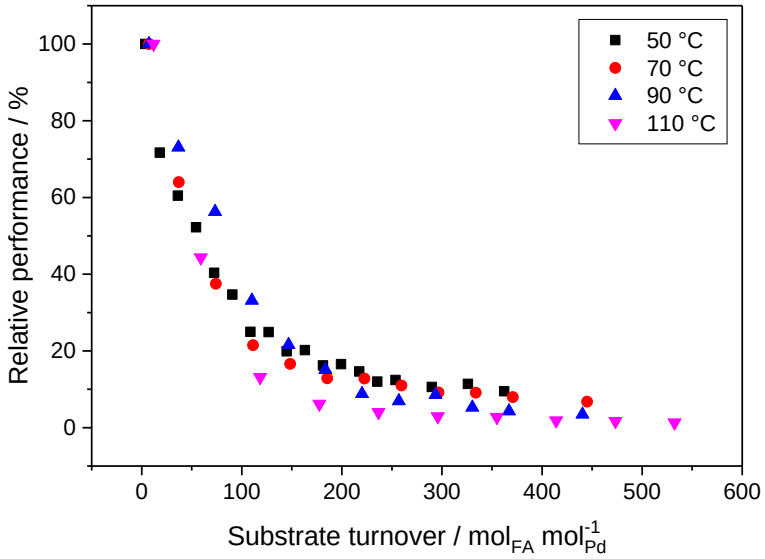

Figure 6 Effect of temperature on the relative performance of Pd/C as a function of substrate turnover. Reaction conditions: Pd/C (150 mg), aqueous formic acid (0.5 M), 5 bar. Flow rate and temperature set at (black square) 0.25 mL min^{-1}, 50°C; (red circle) 0.5 mL min^{-1}, 70°C; (blue upward triangle) 0.5 mL min^{-1}, 90°C; (pink downward triangle) 0.85 mL min^{-1}, 110°C.

In this way, comparison differences due to different initial conversions are nullified. On the other hand, substrate turnover is referred to the moles of substrate which are introduced in the reactor per moles of active sites. In this way, reactions in which are used different amount of catalyst, different feedstock concentration or different feed linear velocity can be compared. In doing so, it can be seen that all points broadly converge on the same

curve, with the partial exception of the highest temperature reaction, 110°C, which appears to deactivate very slightly faster per number of substrate turnovers than reaction at lower temperatures. This observation indicates that deactivation correlates better to the quantity of substrate that has passed over the catalyst rather than to temperature directly. To verify this, several continuous reactions were performed with different initial concentrations of formic acid, 0.25, 0.50, 0.75, and 1.00 M, all at the same temperature of 50°C (Figure 7). In this case, the resulted catalyst relative performances are identical at all the different feed concentrations employed, when compared at the same number of substrate turnovers.

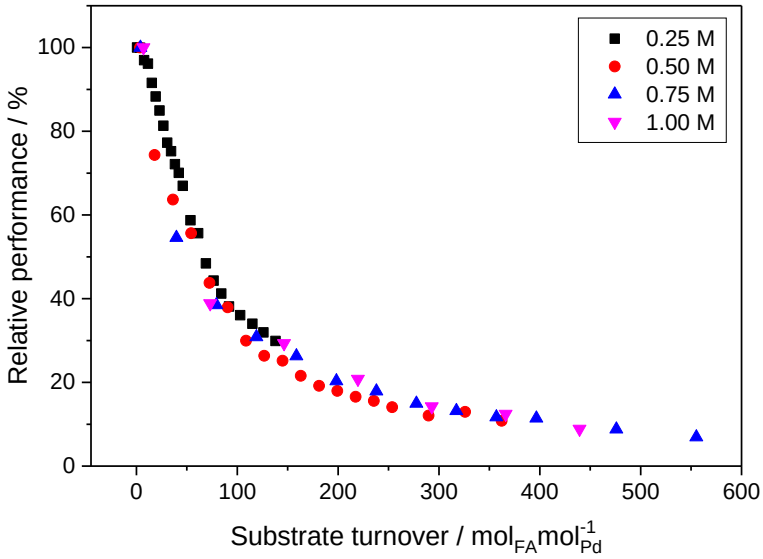

Figure 7 Effect of formic acid concentration on the relative performance as a function of substrate turnover during continuous formic acid decomposition. Reaction conditions: Pd/C (150 mg), 50°C, 5 bar. Different aqueous formic acid concentration and flow rate: (black) 0.25 M and 0.12 mL min^{-1}, (red) 0.5 M and 0.25 mL min^{-1}, (blue) 0.75 M and 0.38 mL min^{-1}, (pink) 1 M and 0.5 mL min^{-1}.

This strict correlation of loss of activity to the number of substrate turnovers suggests that deactivation might relate to a reaction-based stimulus, such as effects related to the reactants, products, by-product(s), or to deposition of residues. Indeed, other solvothermal deactivation causes, such as sintering and/or lixiviation of the metal, would more likely correlate to temperature and time.

Furthermore, to ascertain the catalyst selectivity, the gas effluent of a typical continuous reaction was collected and analysed. Indeed, as previously introduced, the decomposition reaction of formic acid is characterized by the competition between dehydrogenation, the thermodynamically favoured pathway which produce H_2 and CO_2, and dehydration, which instead yield H_2O and CO. The continuous decomposition reaction assisted by Pd/C showed a remarkably selective behaviour toward the dehydrogenation pathway, reporting a CO_2/CO ratio equal to 100,000:1, (Figure 8).

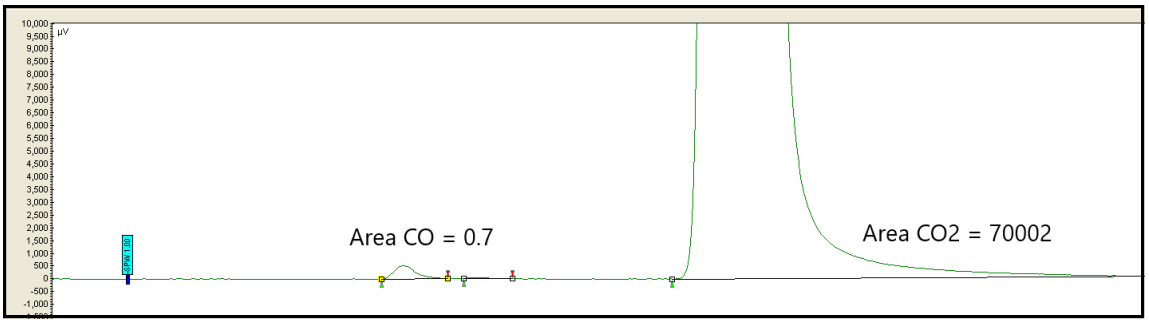

Figure 8 Gas composition analysis of the effluent of the formic acid decomposition reaction. The analysis was conducted by means of a GC-FID equipped with a methanizer unit. Reaction condition: Pd/C (150 mg), 0.25 mL min^{-1} of aqueous formic acid (0.5 M), 50°C, 180 min time on stream, 5 bar.

Hence, this initial series of kinetic experiments resulted to be really important to gain insight on the continuous decomposition of formic acid, allowing the study of the catalyst activity over a variety of different reaction parameters as temperature, linear velocity and feed concentrations. Unfortunately, Pd/C has not showed long-term stability features, but the continuous set-up employed for the kinetic study has permitted to observe a strictly correlation between catalyst deactivation and substrate turnover, giving preliminary clues on the eventual loss of activity reasons. It must be noted that the same correlation between deactivation rate and substrate turnover would have been much more difficult and time consuming if studied in discontinuous systems, thereby confirming the primary importance of lab scale continuous reactors in the investigation of catalyst stability.

As mentioned in the catalyst deactivation paragraph, the pursuit of treatments able to restore the catalyst activity features, are precious experimental procedures because, in addition to the practical aspect, they allow one to obtain useful information on the deactivation mechanisms. Therefore, different regeneration catalyst treatments were attempted on the exhausted Pd/C in order to restore the lost activity features and to gain insights on the deactivation reasons.

3.3.2 Catalyst regeneration

To better understand the causes of Pd/C deactivation, and identify how to prevent it from occurring, attempts to regenerate the catalyst were made. Other than having an obvious practical value, this also allows determination of whether deactivation is permanent or reversible and provides an indirect way of studying the type of deactivation involved. Thus, in order to regenerate the catalyst, thermal treatment of the reactor bed was attempted. This is probably the most common way to regenerate the catalyst, since high temperature treatment can typically remove any unwanted and harmful substances from the catalyst surface. It is worth specifying that the heating procedure was carried out on the whole

tubular reactor without removing the catalyst, thus avoiding any perturbation due to the handling and to exposure at the atmosphere. Hence, the post-reaction tubular reactor was treated in a furnace at 180°C for 90 minutes, 20°C min^{-1}, under air atmosphere.

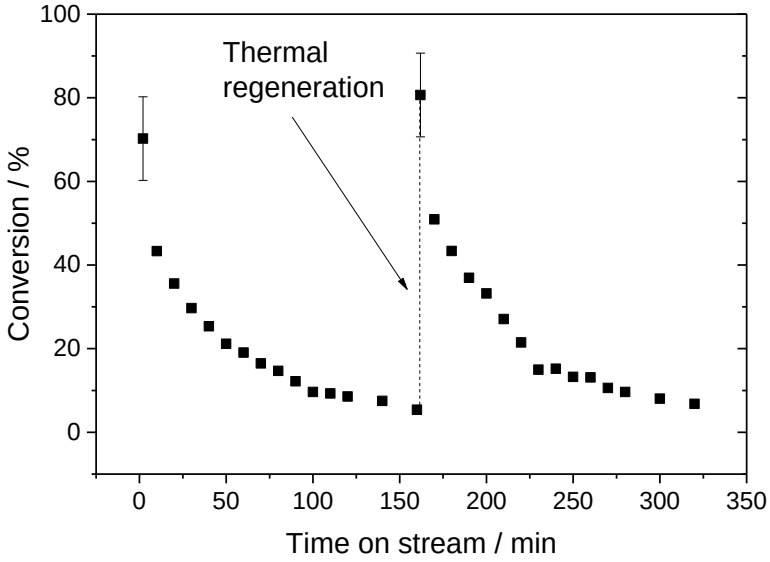

Figure 9 Formic acid conversion as a function of time on stream of fresh and regenerated catalyst, regenerated by heating the reactor at 180°C for 90 min in static air. Reaction conditions: Pd/C (150 mg), 0.25 mL min^{-1} of aqueous formic acid (0.5 M), 50°C, 5 bar.

As it can be seen from the two time on stream plots (Figure 9), the catalyst completely recovered its initial activity after the regeneration procedure, demonstrating the reversible nature of the deactivation phenomena. In order to get insight of the deactivation rate before and after the regeneration treatment, the respective k_d were calculated resulting 0.0258 and 0.0269 min^{-1}. With less the 5% of difference between the two constants, we can state that the deactivation rate before and after the regeneration is unchanged. This experiment, other than indicating the reversibility of deactivation, strongly point out that the catalyst does not undergo to substantial changes during the regeneration treatment, given that its subsequent kinetic and deactivation properties remain the same. We can therefore start to hypothesis that deactivation might happen by poisoning or coking, as suggested before by the dependency of deactivation from a reaction-based stimulus, such as substrate turnover, and its reversible nature.

Before starting to characterise the deactivated catalyst with physical techniques, a second regeneration protocol was investigated. Indeed, the carbon support can be easily degraded by the calcination conditions in which the catalyst is regenerated. Despite after thermal regeneration the catalyst still provides 100% of the performances showed in the first reaction, some degradation of the carbon support might have occurred during the calcination, compromising the catalyst stability after several regeneration cycles. Therefore, washing regeneration procedure was attempted to restore the catalyst activity. Usually, the first choice of "washing agent" is the solvent of the reaction. Thereby, in this case, the used catalyst was flushed with stream of pure water (2.5 ml min^{-1}) for 150 minutes at the same reaction temperature, 50°C.

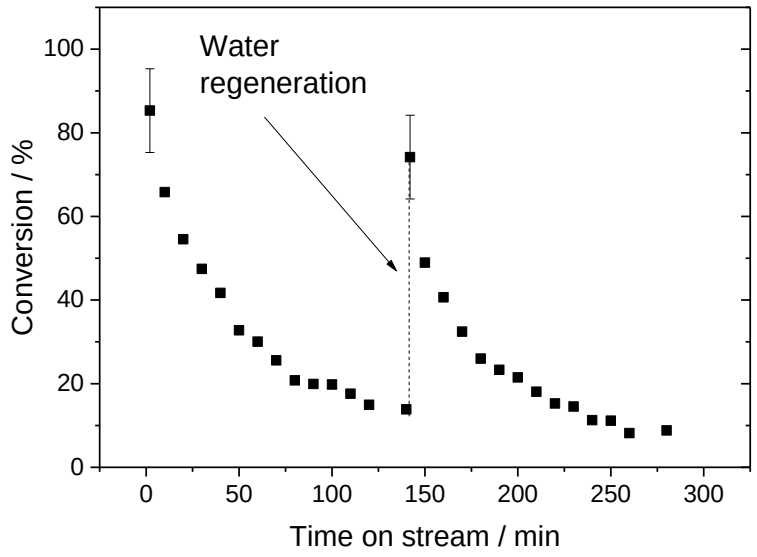

Figure 10 Formic acid conversion as a function of time on stream of fresh and regenerated catalyst regenerated by flushing the reactor with 2.5 mL min^{-1} of water for 150 min at 50°C. Reaction conditions: Pd/C (150 mg), 0.25 mL min^{-1} of aqueous formic acid (0.5 M), 50°C, 5 bar.

Figure 10 demonstrates that the activity after washing went back up to a value of about 90% of the initial activity of the fresh catalyst. As found following thermal regeneration, the calculated k_d of the first and second cycles have less than 5% of difference, at 0.0258 and 0.0265 min^{-1} for the fresh and regenerated catalyst, respectively. The same values of k_d, and the equal initial activity of the two continuous reactions subsequently performed, confirm that the catalyst does not undergo permanent changes neither during the decomposition reaction, nor during the washing regeneration. In very good agreement with previous experiments, the catalyst seems to recover its initial characteristic. Therefore, some permanent deactivation mechanism, such as leaching, or structural deteriorating of the catalyst support can be rejected at first. It must be noted that, during this regeneration procedures, any perturbation of the catalyst bed can be neglected since it involves just a swapping of the reactor feed. The possibility of restoring the catalyst

activity without taking out the solid catalyst form the reactor or without dismantling the continuous plant is of course a precious advantage for industrial scale production, in which any process dead-time corresponds to a massive loss of economic potential. As such, the ability to restore the catalyst activity with just a water flow at mild condition represent a promising regeneration protocol even for industrial scale application. Moreover, the employed regeneration solvent, water, is cheap, abundantly available in nature, environmentally sustainable and can be handled without particular safety dispositions since it is non-toxic, not flammable and not corrosive. In addition to the practical advantages of water washing as regeneration process, it also represents an interesting tool to study the rapid deactivation that occur to Pd/C. Indeed, differently from the heating regeneration, washing procedures are normally milder and thus it is presumed that only weakly bonded compounds are removed when a flow of water is passed over the catalyst. In this case, conducting water regeneration processes for shorter time length or with weaker flow rates should restore the catalyst activity in milder scale. Hence, to study the influence of these two parameters on the regeneration extent they provide, different sets of washing regeneration protocols were carried out on the used catalyst. In particular, the deactivated catalyst was washed with different time length treatments (60, 90 and 150 min) and with different water flow rates (1.0 and 2.5 mL min^{-1}).

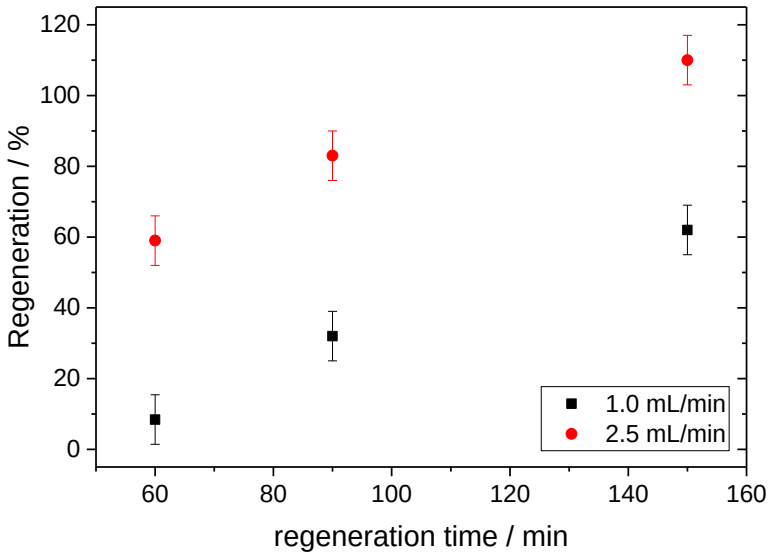

Figure 11 Percentage of regeneration obtained as a function of the time of the water regeneration process at two flow rates. Black squares: 1.0 mL min^{-1}, red circles: 2.5 mL min^{-1}, 50°C.

From Figure 11 it can be noted a linear dependence of the regeneration extent to the time length of the washing protocol. Indeed, washing the exhausted catalyst for 60 minutes with 1.0 mL min^{-1} of water permits to re-gain the 9% of the catalyst initial activity, against the 60% of recovery obtained in 150 minutes. In addition to the time length dependence, it can be noted also the remarkably higher recovery was achieved when faster solvent

linear velocities were used. In fact, the 30% of regeneration obtained by washing the inactive catalyst with 1.0 mL min^{-1} of water for 90 min, is more than doubled if 2.5 mL min^{-1} of solvent is used for the same length of time.

However, the regeneration dependence on the flow rate extent can be either due, to the higher amount of water flushed over the exhausted catalyst, or to the stronger mechanical forces applied by the faster effluent. Therefore, to better comprehend the mechanism of the washing regeneration treatment was investigated the activity recovery dependence on the amount of water passed over the exhausted catalyst bed.

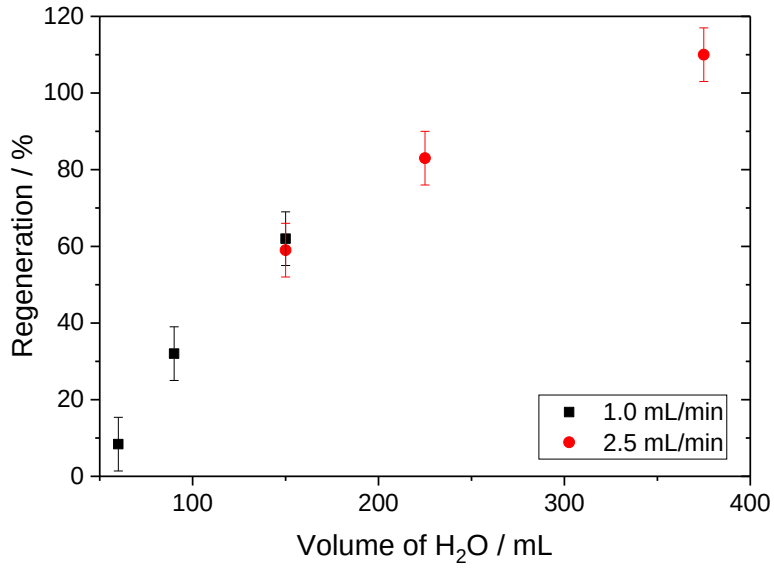

Figure 12 Percentage of regeneration obtained as a function of the total amount of water used during the regeneration. Black squares: 1.0 mL min^{-1}, red circles: 2.5 mL min^{-1}, 50°C.

From Figure 12 it can be seen an incredibly linear correlation between the amounts of solvent passed over the catalyst and the extent of activity re-gained. From this plot is clear that the main parameter which affect the catalyst regeneration is the amount of water passed thought it, not the time length of the process, nor the solvent flow rate employed as first instance observed. Indeed, it can be noted that the same regeneration extent of 60% can be achieved passing 150 mL of water on the deactivated catalyst, both with 1.0 or 2.5 mL min^{-1} of flow rate. This indicates that it is more likely that the solvation properties of water restore the catalyst performance rather than the mechanical forces applied by the liquid effluent, otherwise the regeneration extend would be dependent on the linear velocity of the regeneration flow. The dependency on the amount of water rather than the time of the treatment might have more than a practical implication. Indeed, it can be conjectured that there is some kind of stoichiometric relationship between water molecules and catalyst contaminants, thus suggesting active sites poisoning or reaction residues deposition on the catalytic surface as deactivation cause.

It is important to mention that a spontaneous regeneration of the catalyst simply by removal from the reactor can be ruled out by a control experiment performed by removing a spent catalyst from the reactor, leaving it to dry at room temperature overnight (16 hours), and then re-examining its activity. This procedure resulted in no regeneration being observed. As such, it is clear that thermal treatment or washing is necessary for reactivation of the catalyst and that the deactivated catalyst remains inactive upon removal from the reactor, an important consideration for further spectroscopic study.

In agreement with the hypotheses made from the previous kinetic analysis, both regeneration treatments points toward some chemical species or particles present on the catalyst surface which inhibit the reaction, and which are desorbed by thermal degradation/evaporation or by washing. However, the presence of contaminants (poison or coke), and their chemical nature and their relationship with deactivation must be verified. Indeed, as already described, catalyst deactivation is a complex phenomenon which, commonly, is the synergetic result of several processes. Therefore, to better understand the deactivation process and to truly identify the reason of the rapid inhibition of Pd/C during formic acid decomposition, deeper studies must be performed. In particular, characterisation analyses were conducted on the pre- and post- reaction catalyst to have a deeper knowledge of the transformations that the material undergoes during the continuous reaction.

3.3.3 Identification of the active species

To better understand deactivation of the catalyst, and to propose methods to mitigate its impact, it is necessary to generate structure−activity−lifetime relationships through correlation of the kinetic observations to characterization of the catalyst. Accordingly, a variety of techniques were used to study the physical and chemical nature of the fresh catalyst and its active sites. In addition, characterization analyses were conducted on the deactivated and regenerated material to follow the catalyst transformation during the course of the reaction and along the regeneration treatments. In particular, to obtain more information on the deactivation process, it is important to understand which chemical species are responsible of the catalyst activity. Indeed, the reasons why Pd/C was selected to continuously decompose formic acid was its promising stability features showed in multi cycles batch reaction. However, little is known about this commercial catalyst. For example, the supplier does not report the metal oxidation state of the nanoparticles supported on the active carbon, which is known to be a discriminating feature for catalytic purposes. In this regard, considering that the main product of the formic acid decomposition is hydrogen, it is possible that eventual metal nanoparticles present in their oxidised phase are reduced in situ during the continuous reaction, and the resulted reduced phase be inactive. This would agree well with the kinetic analysis

previously performed which relate the deactivation to a reaction-based stimulus, such as the reaction product. Therefore, a combination of XRD and X-ray Photoelectron Spectroscopy (XPS) analysis was conducted to determine the metal phase composition of the commercial catalyst. In addition, used and water regenerated catalysts were analysed to verify if some chemical transformations of the nanoparticles occur during the decomposition reaction and regeneration treatment. The catalyst material regenerated through the water treatment was employed for these studies, since the thermal regeneration process, performed at 180°C under air atmosphere, likely oxidises the metal nanoparticles, thus leading to a misinterpretation of the features which restore the catalyst activity. XRD patterns of the fresh and used catalysts are shown in Figure 13.

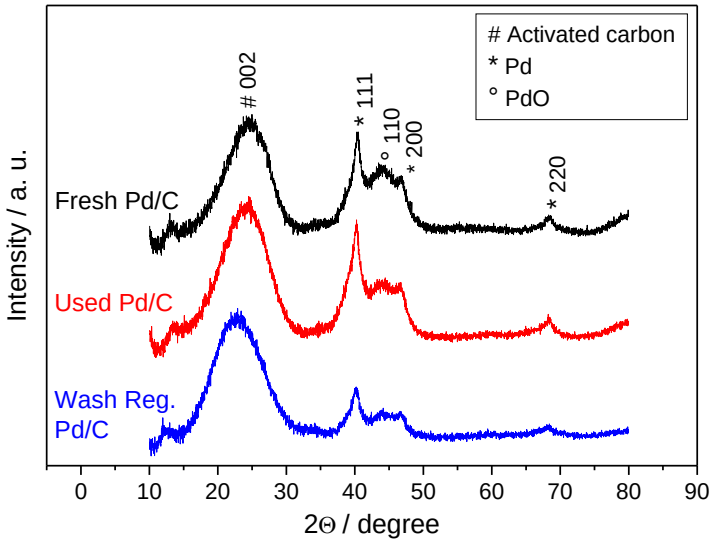

Figure 13 XRD analysis of the fresh, used and washing regenerated Pd/C.

The broad diffraction peak at 2θ = 24.7° is related to the carbon support, in particular, to the (002) planes of the activated carbon.[52] The diffraction peaks at 2θ = 40.4° and 46.8° correspond respectively to the (111), and (200) characteristic planes of the face-centered cubic structure of Pd. Instead, the peak at 43.8° corresponds to PdO (110).[53] Hence, it can be stated that the commercial catalyst is characterized by the presence of both metal phases of palladium, Pd metallic (Pd^0) and its oxidized phase PdO. Furthermore, the characterisation of the used catalyst indicates the decrease of the intensity of the diffraction peaks at 2θ = 43.8° and the increment of the diffraction peaks at 2θ = 40.4° ascribed to (111) of Pd, suggesting the reduction of PdO to metallic Pd by the in situ generated hydrogen. As expected, the water regeneration process does not re-establish the oxidation properties of catalyst, since the 40.4° peak associated to PdO does not result in the regenerated catalyst spectra.

Furthermore, to quantify the fraction of the oxidised and reduced phase in the commercial catalyst, and then to measure the nanoparticles reduction extent due to the hydrogen generation, a XPS study was performed on the fresh, used and regenerated Pd/C. XPS

analysis, focused on the Pd(3d) region (Figure 14), revealed two main peaks at 335.4 and 340.7 eV in the fresh, used and regenerated samples, corresponding to the Pd $3d_{5/2}$ and Pd $3d_{3/2}$ transitions, respectively. These peaks are assigned to the presence of Pd^0. Whereas, the peaks at 337.0 and 342.3 eV correspond to Pd^{II}, PdO being the most probable species.[54] Deconvolution of these peaks allows to quantify the relative amount of Pd^0 and Pd^{II}. In line with previous studies, the fresh catalyst shows a mixed distribution of 78% Pd^0 and 22% Pd^{II}. After use in the PFR, only metallic Pd^0 is detected on the catalyst, likely due to the in-situ reduction of the metal nanoparticles by the generated hydrogen. In a first instance, the decrease of Pd^{II} at the end of the reaction could be correlated to the loss of activity. However, no recovery of Pd^{II} is observed also when the catalyst is fully regenerated.

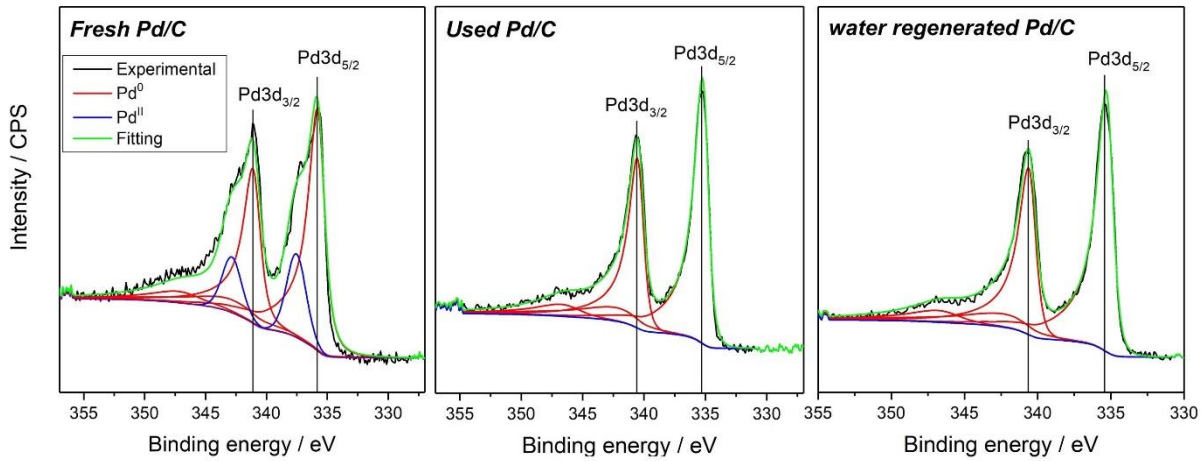

Figure 14 From left to right: XPS of Pd region of fresh, used, and the catalyst regenerated by washing.

These observations strongly suggest that changes in the oxidation state of Pd do not correlate to catalytic performance. To verify this, and hence to study the effect of Pd oxidation state on catalytic activity, a series of pre-treatments were performed on the fresh catalyst prior to operation in the PFR. Specifically, the catalyst was treated in 5% H_2/Ar atmosphere at 250°C, 5°C min^{-1}, for 3 hours to reduce the metal nanoparticles prior to reaction. Similarly, the catalyst was oxidised in same condition under an air atmosphere. XPS analysis showed that during reduction, the percentage of Pd^{II} decreased from the 22% of untreated catalyst to 13%, (Table 1).

Table 1 Palladium nanoparticles oxidation state fraction as calculated from XPS, for the untreated, reduced and oxidized catalyst sample.

entry	sample	Pd^0 / %	Pd^{II} / %
1	untreated	78	22
2	H_2 treated	87	13
3	Air treated	75	25

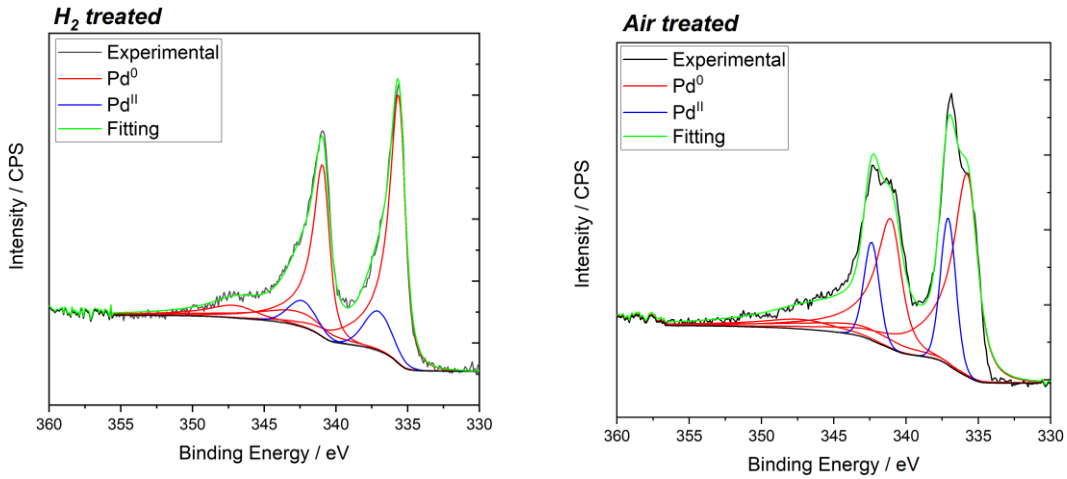

Figure 14.A XPS of Pd region of catalyst treated in 5% H_2/Ar atmosphere at 250°C, 5°C min^{-1}, for 3 hours (Left) and treated in air at 250°C, 5°C min^{-1}, for 3 hours (Right).

The initial activity of the reduced catalyst was found to be slightly higher, about 10% of increased initial activity (Figure 15), indicating that metallic Pd is likely to be the most active species.

This result confirms that the catalyst deactivation cannot be ascribed to the in-situ reduction of metal nanoparticles. Unfortunately, the air treatment was not as effective, showing a modest increase in Pd^{II} fraction from 22 to 25%. As expected from this small change, no obvious changes in activity and stability can be detected, thereby the activity of Pd^{II} cannot be verified. However, the poor oxidation which the nanoparticles undergo during the calcination treatment, confirm the negligible changes of the catalyst properties during the thermal regeneration, explaining why the thermal regenerated catalyst shows the same activity and deactivation rate of the original one. Furthermore, a comparison of the reaction time on stream performed with the commercial, reduced and oxidised catalyst shows that all the three catalysts deactivate with the same rate of 0.0290 min^{-1}, (Figure 15). When combined, these studies indicate that deactivation of the catalyst cannot be attributed to the oxidation state changes of Pd nanoparticles observed during operation.

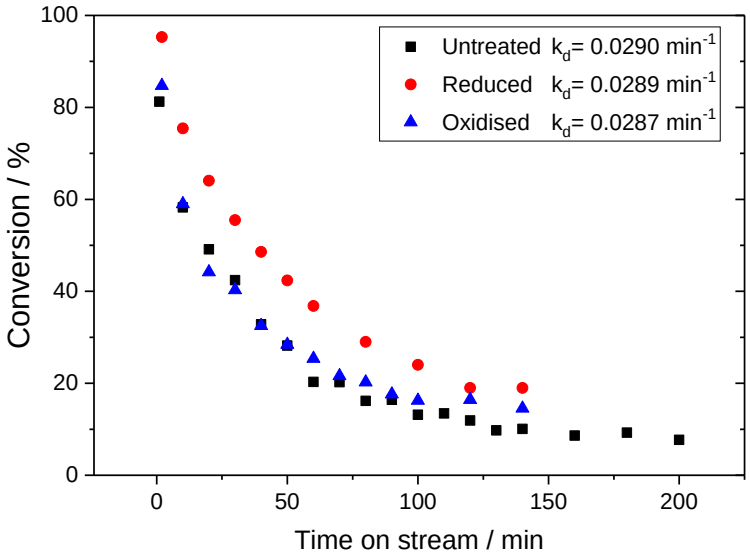

Figure 15 Kinetics comparison of the formic acid decomposition assisted by untreated, reduced and oxidised Pd/C. Reduction treatment at 250°C with 5% H_2 in Ar for 3 h, and oxidation treatment at 250°C in air for 3 h. Decomposition reaction conditions: 150 mg of catalyst, 0.25 mL min^{-1} of a 0.5 M formic acid solution, 50°C, 5 bar back pressure.

3.3.4 A closer look to the metal nanoparticles

As mentioned before, deactivation phenomena are complex and often are the result of combination of multiple causes. So far, kinetics experiment suggested that poisoning or coking can be one possible candidate as part of the deactivation phenomena responsible for this system. However, as indicated by previous studies, the catalytic performances of metal nanoparticles strongly correlated with their dimension and dispersion on the support, hence these parameters cannot be ignored in an accurate study.[55-57] In particular, it is also demonstrated that hydrogen, main product of the reaction under study, can remove the oxygen functional group of the carbon support, leading to lower adhesion of the nanoparticles on the catalyst surface, thus favouring their migration and reorganization.[58] Furthermore, Parkinson *et al.* have shown that low concertation of CO, one of the potential by-product of formic acid decomposition, may induce in chemical-assisted sintering of Pd nanoparticles at room temperature.[59] Hence, the sintering deactivation phenomenon must be thoroughly considered during formic acid decomposition by Pd/C. The best characterization technique that can be employed to investigate this detrimental effect is Transmission Electron Microscopy (TEM), which is able to scan at high resolution nanometres scale of the catalyst surfaces. In this way, images of metal nanoparticles can be acquired permitting to determine the average particles diameters and the particles distribution on the investigated portion of the catalyst surface. Through comparison of data acquired on fresh, used and regenerated catalyst it

is thereby possible to verify if sintering of the nanoparticles is occurred during the reaction or the regeneration treatment. TEM was then used to get an insight on the dimension and distribution of the Pd particles of the fresh (Figure 16 A), deactivated (B), and regenerated (C) catalysts.

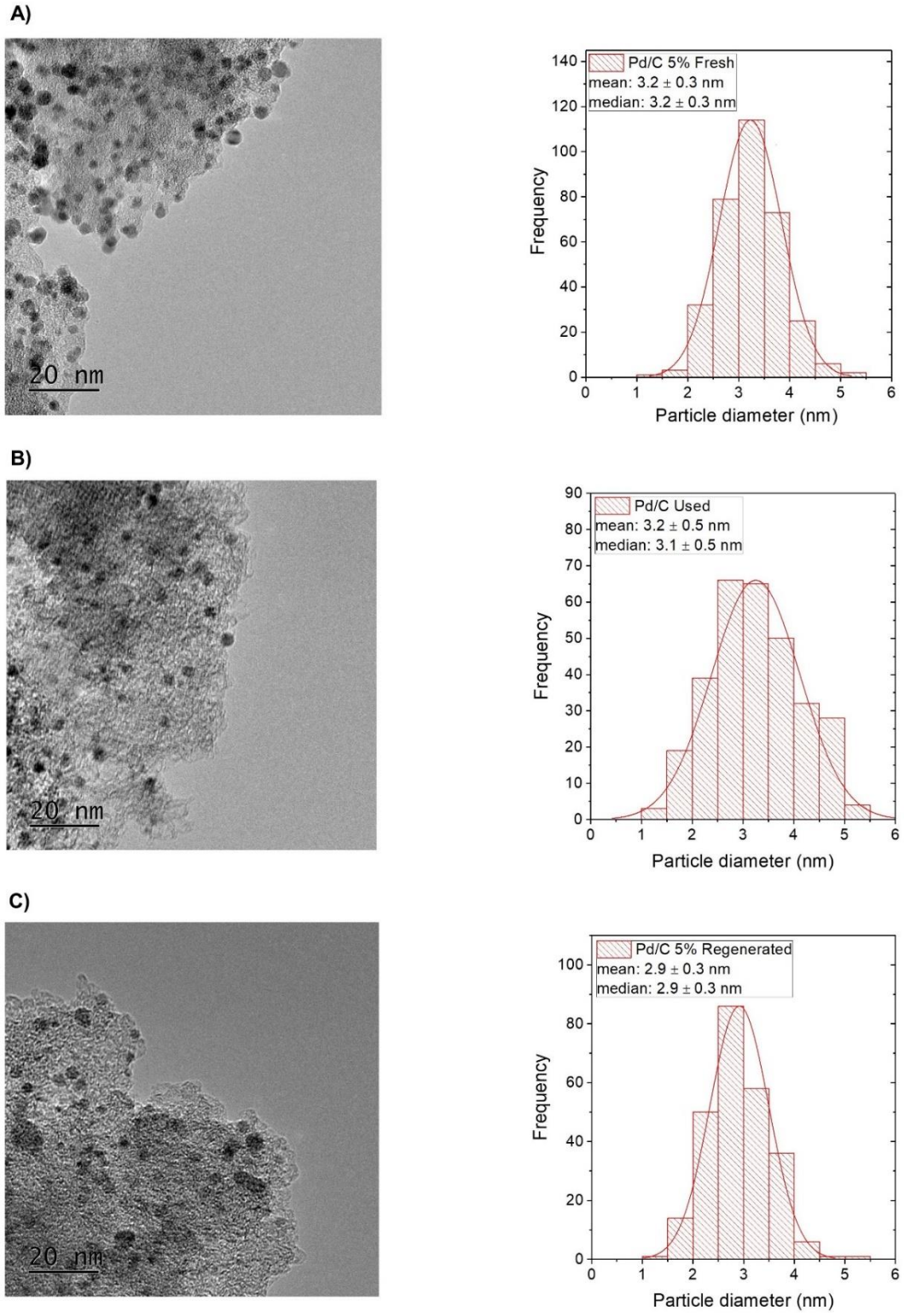

Figure 16 From top to bottom: TEM images and particle size distribution, of (A) fresh, (B) used, and (C) the catalyst regenerated by washing.

By analysis of the distribution of particle dimensions, shown in Figure 16 A−C, it can be seen that all the samples possess an average particle size of 3.2 nm, and rather narrow distributions. Upon deactivation, the average size is maintained on the same value but the size distribution becomes slightly broader. In particular on the deactivated catalyst, the population of particles between 4 and 5 nm is higher than on the fresh catalyst. Although the metallic state, in which all the Pd nanoparticles are converted during the reaction, is known to be the most stable species against leaching, an elemental analysis by ICP-MS must be performed on the fresh and used catalyst to rule out this as reason of the slight changes in particle distribution.[60] Given that the same amount of Pd was found in all samples, this indicates that an actual restructuring event occurs during reaction, as opposed to size-specific leaching (Table 2).

Table 2 Elemental analysis on fresh and used catalyst carried out by inductively coupled plasma (ICP-MS) after samples digestion in *aqua regia* mixture.

entry	sample	Pd wt %
1	Fresh	4.60
2	Used	4.59
3	Water reg.	4.65

However, since on the deactivated catalyst the majority of the nanoparticles still conserve a diameters size between 2.5 and 3.5 nm, the rapid deactivation observed during the reaction is unlikely to be fully related to this effect. In fact, the degree of change in particle size and distribution following reaction, and later regeneration, is extremely modest and likely points toward other factors being more dominant in respect to deactivation. Therefore, the sintering of the Pd nanoparticles can be rejected as a major cause of deactivation. Moreover, the elemental analysis conducted on the fresh and used catalysts (Table 2), confirm that leaching of the active phase into the liquid phase does not occur during continuous operation, as indicated by the lack of change in Pd content of the catalysts. Hence, also the leaching of Pd particles can be rejected as major cause of catalyst deactivation and further investigations must be performed to fully understand the phenomenon.

3.3.5 Investigation of fouling as cause of catalyst deactivation

Another presumable cause of deactivation during heterogeneous catalysis is fouling, which relates to the deposition of reaction residues on the catalyst surface and/or within its pores.[40-43] In such cases, deactivation is often related to the physical amount of reactant converted and hence typically correlates with substrate turnover as opposed to time on stream, which could explain the preliminary kinetic analyses. To verify the presence of some coke particles formed on the catalyst surface and among the catalyst structure

during the reaction, porosimetry analysis was conducted on the fresh, deactivated and regenerated Pd/C. This characterization technique permits measurement of the surfaces area and the pore volume of the catalyst structure, which consequently decrease if some residual reaction materials are deposited on the catalyst because of the reaction. Moreover, by means of porosimetry, precious information can be obtained on the structure of the active carbon, support of the catalyst. Surface area and porosimetry analysis conducted on the fresh catalyst revealed that the majority of the available surface area (1006 $m^2\ g^{-1}$) is microporous in nature (735 $m^2\ g^{-1}$), while only a smaller fraction of the area is mesoporous (Table 3, entry 1).

Table 3 Surface Area and Porosimetry Data Obtained by Nitrogen Adsorption Isotherm Analysis. All values calculated by applying the DFT method to the nitrogen adsorption isotherms (77 K).

entry	sample	S_{DFT} / m^2g^{-1}	S_{micro} / m^2g^{-1}	V_{micro} / m^3g^{-1}
1	fresh	1006	735	0.28
2	flushed in H_2O (t_0)	717	525	0.20
3	used	171	42	0.01
4	washed regen. 80%	707	517	0.20
5	washed regen. 30%	584	412	0.15
6	Thermal regen.	864	608	0.20

Since the kinetic protocol involves flushing the catalyst with water prior to introducing the substrate, and knowing that water can adsorb strongly on this type of support and may itself result in a significant loss of surface area, the sample flushed with water prior to switching to the feed solution was also measured. As can be seen (Table 3, entry 2), a decrease of microporous area of 30% compared to the untreated catalyst occurs simply due to start-up of the reactor in water, prior to introduction of formic acid. For the sake of further comparison, the porosity values of this sample are considered to be representative of the t_0 state of the catalyst. Following continuous operation, a dramatic decrease in the micropore area is observed, reducing by 92% of the t_0 value (Table 3, entry 3). Clearly, deactivation of the catalyst is accompanied by a significant loss of micropore area. Loss of surface area and pore volume can be ascribed mainly to two kind of phenomena: deposition of unwanted material on the catalyst surface (fouling), or changes of the catalyst physical structure. The latter is obviously a more dramatic effect and often is not reversible. However, it is important to ensure that no dramatic structural changing of the carbon support have taken place during the continuous reaction. The integrity of the catalyst structure can be verified by the combination of several characterization techniques. The XRD analysis already performed on the fresh and deactivated catalyst (Figure 13) does not suggest any damaging of the carbon support, although the partially amorphous nature of the catalyst does not allow a clear evaluation on the status of the

material by means of this technique. Further evidence on the carbon support can be obtained by the Raman spectroscopy, (Figure 16).

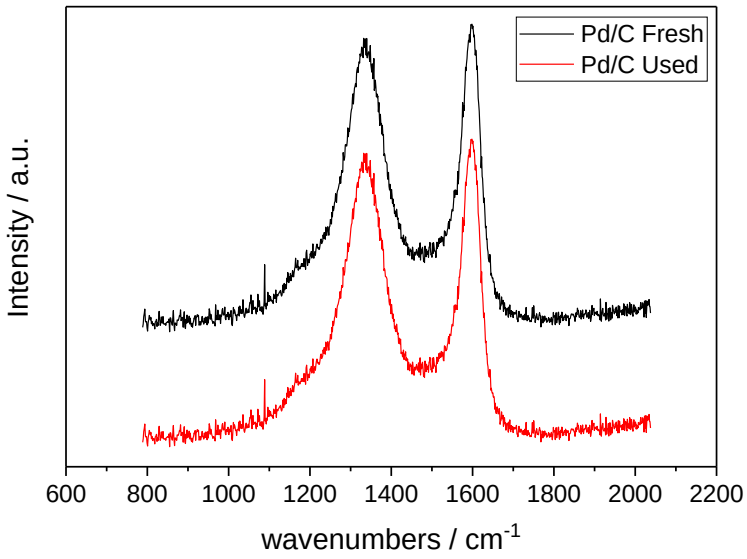

Figure 16 Raman spectra of fresh and used catalyst.

The relatively equal peak intensities for D and G bands (1350 and 1590 cm^{-1}, respectively) is indicative of the amorphous disorder of the carbon support.[61-63] Especially, it is clear that no differences arise on the spectra of the pre- and post-reaction catalyst, confirming that no changes of the catalyst structure occur during the reaction.

Another evidence that the catalyst conserves its structure during the reaction comes from the hysteresis shape of the nitrogen isotherms of the deactivated catalyst, which indicate the microporous nature of the material remains after reaction (Figure 17).[64, 65]

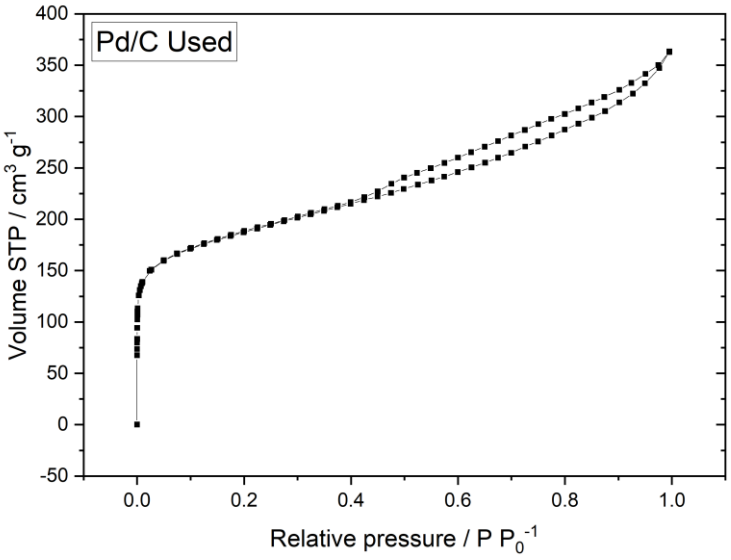

Figure 17 N_2 adsorption and desorption isotherm of used Pd/C.

Therefore, all the characterization techniques employed confirm no apparent changes of the carbon support and consequently, different phenomena must account for the observed loss of surface area and micropores volume upon reaction.

To further verify a possible trend between deactivation and loss of micropore area, samples of Pd/C were further measured following partial (30%, 80%, Figure 11) regeneration by washing and full regeneration by thermal treatment (Table 3, entries 5 and 6). As can be seen, washing regeneration of the catalyst is accompanied by significant restoration of microporous area, and the recovery of microporosity is even greater following thermal regeneration, likely due to the removal of the water molecules contributing to the initial loss of porosity at t_0. These observations further indicate that deactivation and porosity may be related. However, it is notable that the recovery of porosity and the extent of regeneration by washing are not linearly correlated. In fact, while only 30% of the activity is initially recovered after washing regeneration for 90 min at 1.0 mL min^{-1}, around 75% of the t_0 microporosity has been restored. Taken together, these experiments strongly indicate that surface area is a determining property for the activity of this material, and its loss is detrimental for activity. However, at least one other factor contributes to deactivation, and this event requires more extensive washing in water to be mitigated than loss of porosity alone.

To understand the nature of the evident loss of catalyst surface area along the reaction, a variety of experiments were performed on deactivated samples of Pd/C in order to research the presence of some residual materials deposited on it. First, FT-IR analysis of the fresh, used and washing regenerated catalysts were performed (Figure 18).

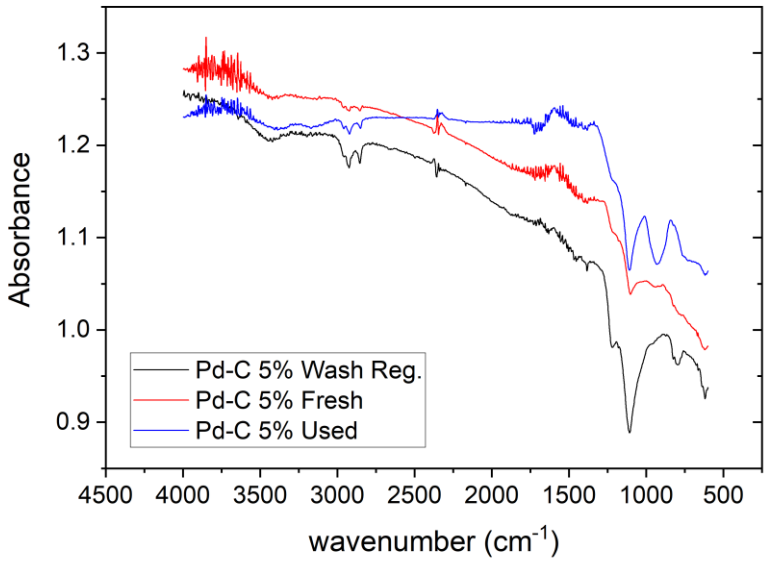

Figure 18 IR analysis of Fresh, Used and Wash Regenerated catalyst.

Nonetheless, no signals that can be attributed to reaction residues were observed. Accordingly, to verify if some reaction residues were washed out during the water regeneration treatment, aliquots of the regeneration effluent were collected and analysed by ^{1}H-NMR. However, the high degree of dilution resulted in no indicative signals being observed, even though calibration of the ^{1}H-NMR for formic acid with an internal standard (tetramethylsilane) showed a detectability limits <0.005 M, (Figure 19).

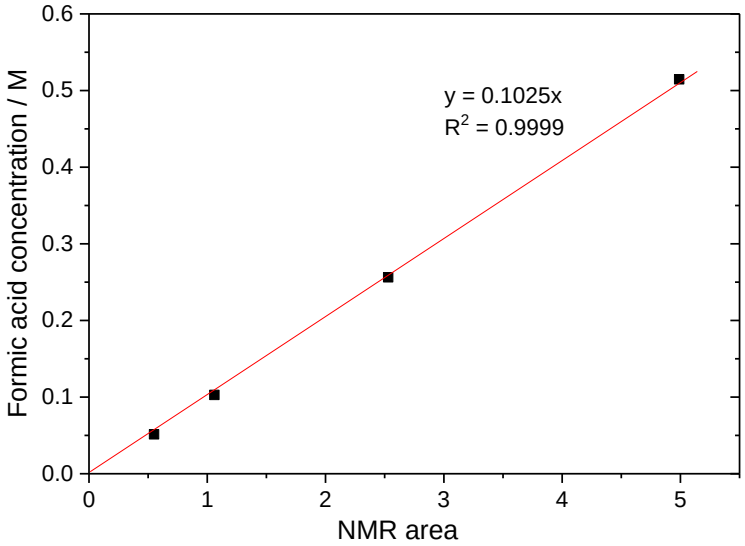

Figure 19 Calibration curve obtained of the response of ^{1}H-NMR signal to different concentration of formic acid.

Thermogravimetric analysis (TGA) were also performed on the exhausted catalyst in order to detect and quantify the sample mass loss ascribed to desorption or degradation of eventual residual species by means of calcination, accordingly with the regeneration

thermal treatment. Unfortunately, TGA of the used and fresh catalyst did not show any differences (Figure 20).

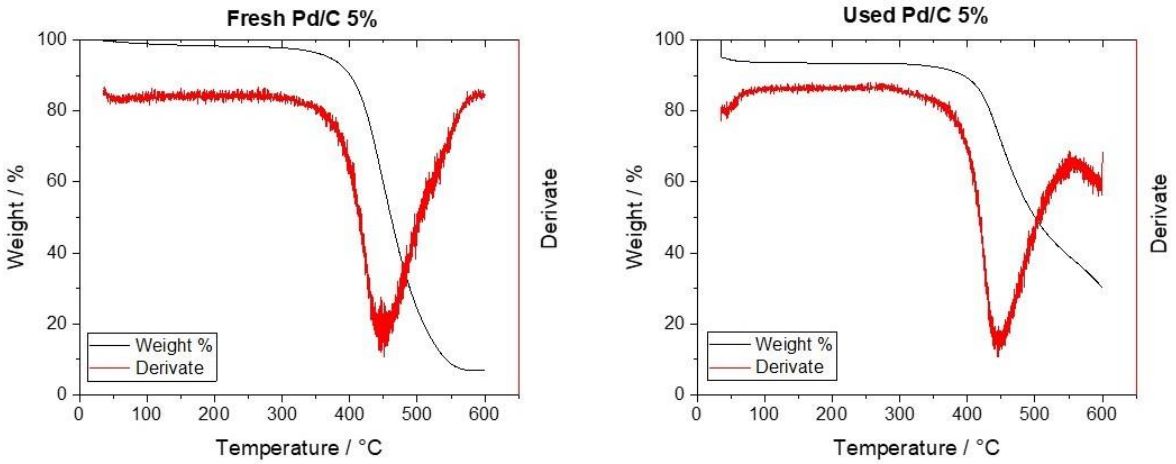

Figure 20 Thermogravimetric profile of (left) Fresh and (right) Used Pd/C 5%. Analysis conditions: air 50 mL min^{-1} 30-600°C, 5°C min^{-1} ramp rate.

The low amount of the catalyst used for the analysis (10 mg) combined with the small amount of eventual reaction residues might have compromise the sensitivity of the technique. The negligible mass loss detected with the TGA analysis should not be considered as evidence of a lack of residual species present on the catalyst surface. Indeed, due to the microporous nature of the catalyst support, even small quantities of residue can cause substantial loss of activity.

Accordingly, the gaseous effluent generated during thermal regeneration was monitored by mass spectrometry (akin to temperature programmed desorption mass spectrometry, TPD-MS, Figure 21).

During thermal regeneration in air, only CO_2 was found to evolve from the deactivated catalyst. When compared to the fresh catalyst, it can be seen that the used sample evolves a much larger quantity of CO_2. Moreover, the different evolution profiles also indicate that different species are present in the sample after reaction. The first signal of CO_2 evolving at 10 min is present both in the used and in the fresh catalyst, and may originate from the same species, albeit at a higher level of concentration in the used catalyst. However, major differences can be observed at later times. In particular, the used sample exhibits a well-defined evolution at 14.5 min, and a broader release at 15.5 min, while in the fresh sample these evolutions are absent, and only a smaller, broader evolution is observed at 13.5 min. Taken together, these analyses reveal that oxidizable carbonaceous material remains on the catalyst post-reaction and that its removal is achieved at a relatively low temperature in line with the facile thermal regeneration process identified. To further verify whether this carbonaceous residue is related to a loss

of activity, the TPD-MS profile of the catalyst regenerated by washing in water was monitored. As it can be seen, the carbonaceous residue present on the used catalyst is no longer present on the catalyst washed by water (and which exhibits activity), indirectly verifying that the presence of this residue is related to loss of activity.

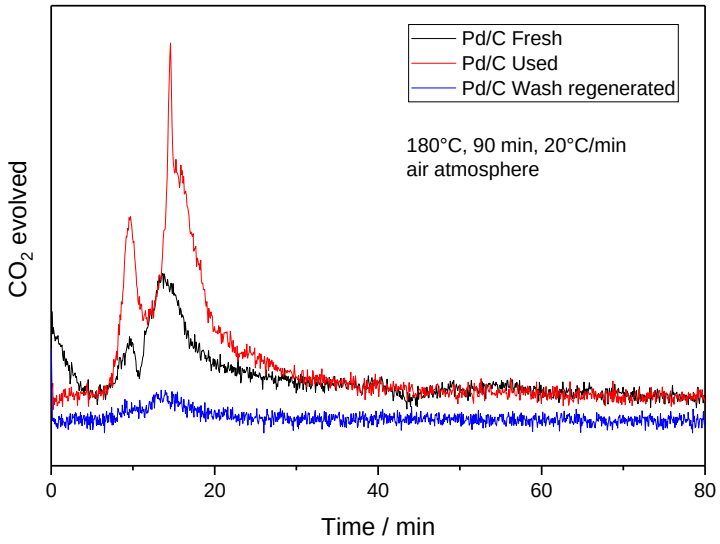

Figure 21 MS signal of CO_2 (M/Z = 44) evolved during heat treatment of used (red), fresh (black), and wash regenerated catalyst (blue). Conditions: air flow, 20°C min^{-1}, 180°C for 3 h.

Having confirmed the presence of reaction residues on the exhausted catalyst, attempts to verifying their nature were made. Indeed, understanding which chemical species are retained on the catalyst after the reaction permits one to deduce where they come from, thus allowing to limit their introduction in the system.

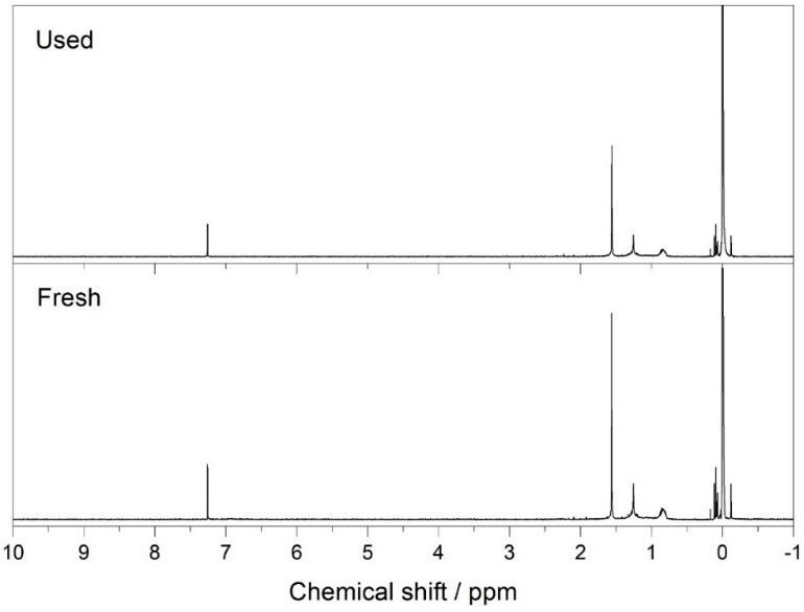

Figure 22 ^{1}H-NMR spectra of D_2O extraction on used (top) and fresh (bottom) catalyst.

Unfortunately, although washing regeneration clearly removes the carbonaceous residue, attempts to detect the residue in the effluent by washing in D_2O prior to ^{1}H-NMR analysis were also unsuccessful (Figure 22), indicating that either (i) the residual carbon is present below the detectability limit of the instrument and/or (ii) the (re)addition of a solvent allows the retained carbonaceous species to react over the catalyst.

On the basis of the detectability limit of ^{1}H-NMR, and the ability of the catalyst to operate at room temperature, we favour the final hypotheses as reasons for why no carbonaceous species can be extracted from the catalyst post reaction. Although these studies do not provide direct identification of the residue(s) retained on the catalyst, they indicate that low molecular weight carbonaceous species that readily result in CO_2 formation in the presence of air must be retained on the catalyst. Since pore fouling is only partially responsible for deactivation (*vide supra*), these residues must also provide additional contributors to deactivation, most likely through active site poisoning.[41-44, 46, 66]

3.3.6 Investigation of poisoning as cause of catalyst deactivation

Poison molecules can be the reactants and products or by-products and impurities present in the feed. In each of these cases, poisoning often relates to the amount of reactant processed and, like fouling, thus often correlates to substrate turnover, in agreement with our kinetic data. Especially for biomass-derived platform molecules, poisoning is often described as a problematic issue for catalyst stability and activity.[67] Therefore, to gain insight into the potential poisons present in the system, and hence indirectly identify the residues present on the used catalyst, poisoning experiments were performed.[39] The most likely poison molecules consistent with the TPD-MS analysis include CO, CO_2, and formic acid (or derivatives thereof), although the potential negative role of feed contaminants and other reaction products (H_2) cannot be overlooked. To first verify the presence and role of feed contaminants, ^{1}H-NMR was carried out on the formic acid solutions used for reaction.

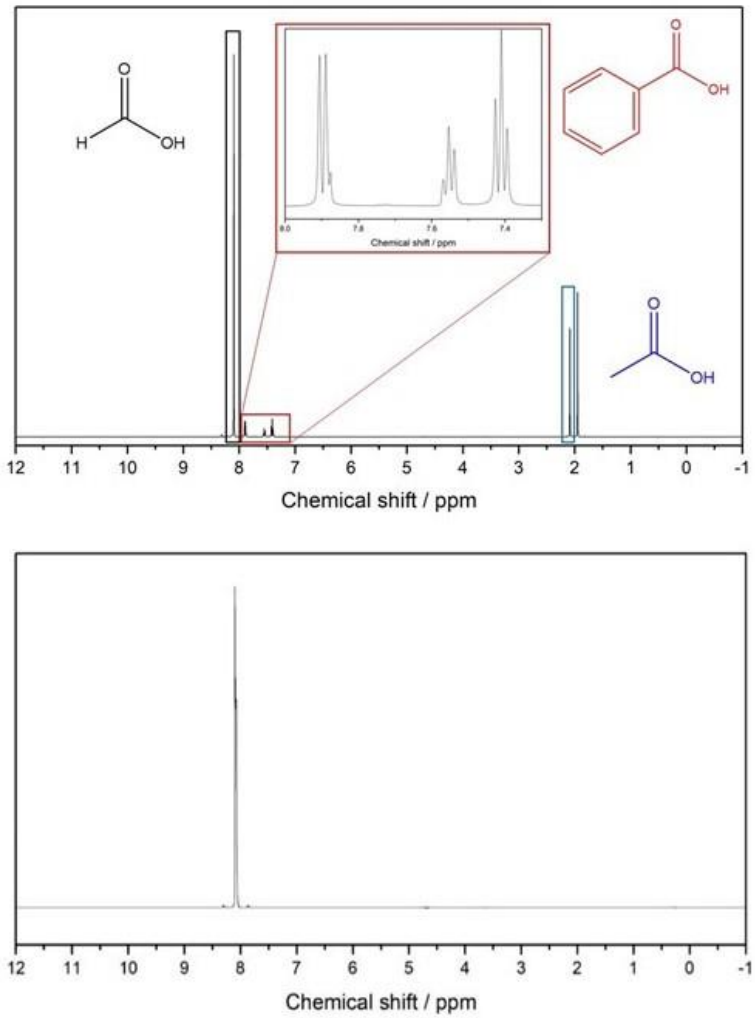

Figure 23 ^{1}H-NMR spectra of (top) commercial and (bottom) distilled formic acid acquire with a 400 MHz NMR.

This revealed low, but non-negligible, concentrations of acetic and benzoic acid (Figure 23, top), which evidently may contribute to deactivation. Therefore, commercial formic was purified through distillation, its composition verified by means of ^{1}H-NMR analysis (Figure 23, bottom) and then the purified substrate was employed as feedstock for a continuous dehydration reaction. However, it was observed that utilizing a distilled and purified solution of formic acid did not change the deactivation rate of the catalyst (k_d), implying that the impurities present in the feed did not affect the catalyst performance under the experimental conditions employed, (Figure 24).

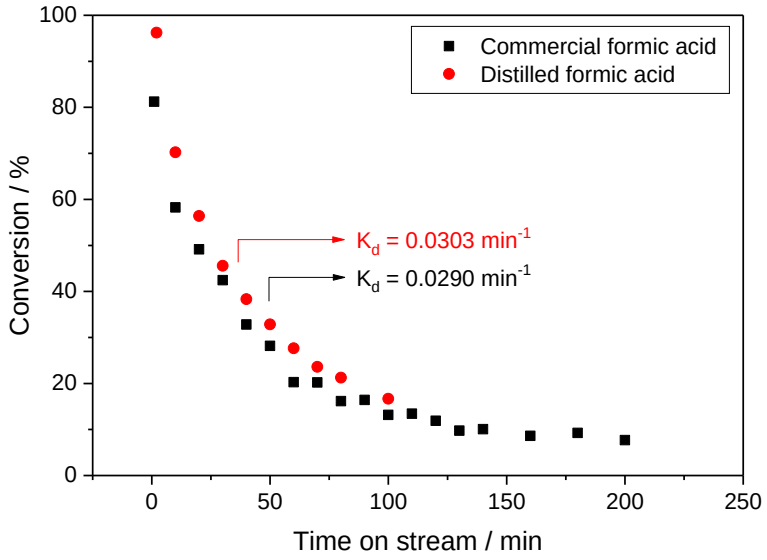

Figure 24 Conversion of formic acid as function of time before and after purification by distillation. Deactivation constant, k_d, have been calculated using the approach of Levenspiel. 0.5 M formic acid aqueous solution, 0.25 mL min^{-1}, 150 mg Pd/C, 50°C, 5 bar.

Although the low concentrate contaminants present in the feedstock did not affect the decomposition reaction, it is important to verify their impact at higher concentration, since during the continuous process they can accumulate inside the tubular reactor and cause eventual side-effects when longer reaction are conducted. Therefore, increasing quantities of acetic and benzoic acid were added inside the 0.5 M formic acid feed solution and then tested in a decomposition reaction at usual condition. Commercial formic acid reported 3% of impurities but without indicating the ratio of acetic and benzoic acid present. Accordingly, the effect of the two impurities was investigated individually for each acid and then using a combination of the two acids in a 1:1 mass ratio mixture. It must be noted that the weight percentage (wt.%) of the added contaminants is related to the amount of formic acid used to prepare the feedstock solution and not to the entire mass of solution.

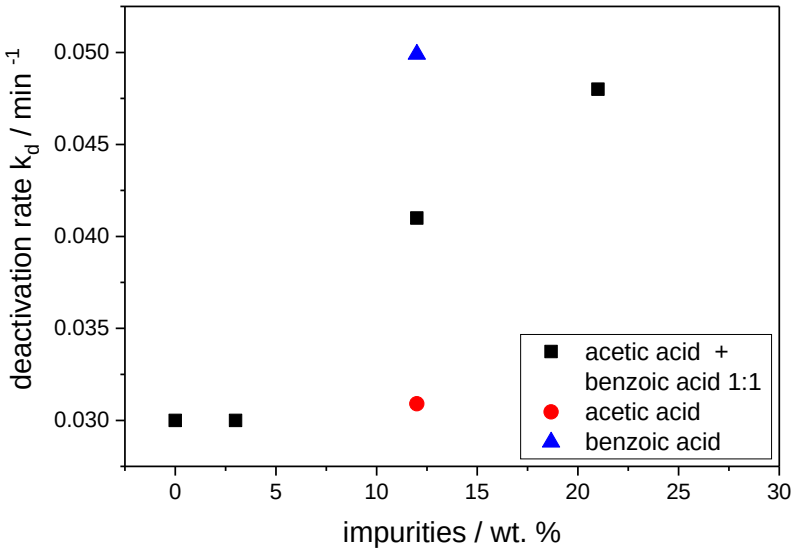

Figure 25 Deactivation rate of decomposition reaction as a function of increasing organic acids impurities present in the reaction feedstock. The weight percentage of impurities is related to the amount of formic acid to prepare the solution feedstock. Decomposition reaction condition: 0.5 M formic acid aqueous solution, 0.25 mL min^{-1}, 150 mg Pd/C, 50°C, 5 bar.

As can be seen from Figure 25, the higher amount of impurities clearly deactivates the catalyst more rapidly. Indeed, an increased impurities amount from 3% to 12% causes the k_d value to increase from 0.0300 min^{-1} to 0.0400 min^{-1}, if both contaminants are added in the feedstock. Furthermore, the deactivation rate linearly increases to 0.0476 min^{-1} if 21 wt.% of impurities are present. However, the individual addition of one single contaminant indicates that the main role in the poisoning effect is played by benzoic acid, whereas acetic acid only plays a negligible effect. Indeed, when benzoic and acetic acid are singularly added in an equal amount of 12%, deactivation rates of 0.0499 and 0.0309 min^{-1} are observed, respectively. This demonstrate that only benzoic acid can strongly inhibit catalyst performance, in line with other dehydrogenation studies in which aromatic compounds are reported as coke precursor.[68]

Although the presence in the feedstock of this organic acid clearly inhibits the catalyst activity, it must be noted that only at high concentration it affects the catalyst stability, as demonstrated by the same k_d value expressed by reactions performed with purified or 3% impure formic acid. Therefore, the limited concentration of benzoic acid in the commercial formic acid cannot be ascribed as the main reason of the rapid deactivation observed in the first minutes of the continuous decomposition reaction assisted by Pd/C. Hence, further poisoning investigation must be performed. Despite the analysis conducted on the feedstock impurities has not been successful in the identification of the main catalyst poison, it is however useful for eventual future long-time reactions, in which purified formic acid solution must be employed to avoid benzoic acid accumulation along the catalyst

bed. In addition to impurities, reactants and products can also result in poisoning of the catalyst. In regards to poisoning by the products (H_2 and CO_2, Figure 26), treatments in both a H_2 atmosphere (5% H_2/Ar atmosphere, 20 mL min^{-1}, 250 °C, 3 h) and CO_2 (100% CO_2, 20 mL min^{-1},25 °C, 3h) appeared to be slightly beneficial toward activity (Figure 26).

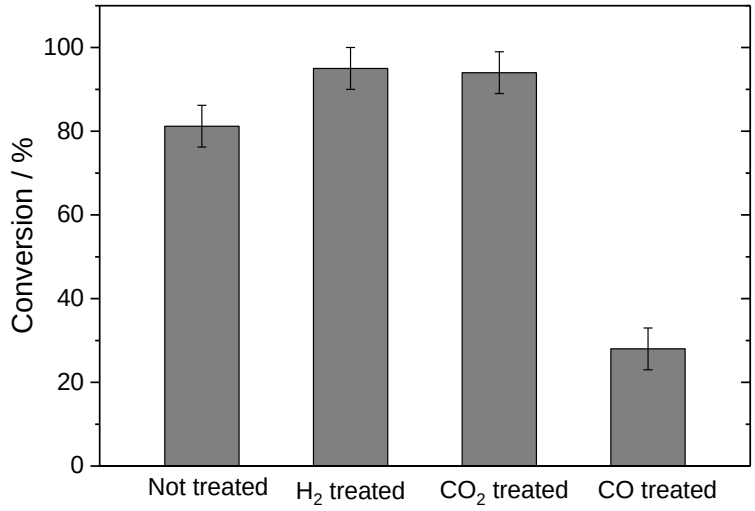

Figure 26 Initial activity of Pd/C for formic acid dehydrogenation following various pretreatment procedures. H_2 treated: 5% H_2/Ar atmosphere at 250°C, 20 mL min^{-1}, 3 h, 5°C min^{-1}. CO_2 treated: flushed with 100% CO_2 (20 mL min^{-1}) at 25°C, 3 h. CO treated: flushed with 10% CO - He (20 mL min^{-1}) at 25°C, 3 h.

Thus, poisoning by product molecules is unlikely to account for deactivation of the catalyst, and the carbonaceous residue present on the used catalyst is clearly not CO_2 itself.

Many works in literature indicate that Pd nanoparticle-based catalysts are particularly susceptible to CO poisoning.[44-47, 66] This is particularly relevant in this case, since competition between dehydrogenation and dehydration is present (Scheme 1). Although, gas composition analysis demonstrates that only trace amounts of CO are formed during this process (Figure 8), checking the susceptibility of the catalyst to CO poisoning is still of relevance during extended operation, where gradual accumulation and poisoning can occur. Accordingly, a fresh catalyst was packed into the reactor and treated in a flow of 10% CO in helium (20 mL min^{-1}) for 3 hours, after which time, the feed was switched to the reaction solution and an otherwise-standard continuous flow reaction performed.

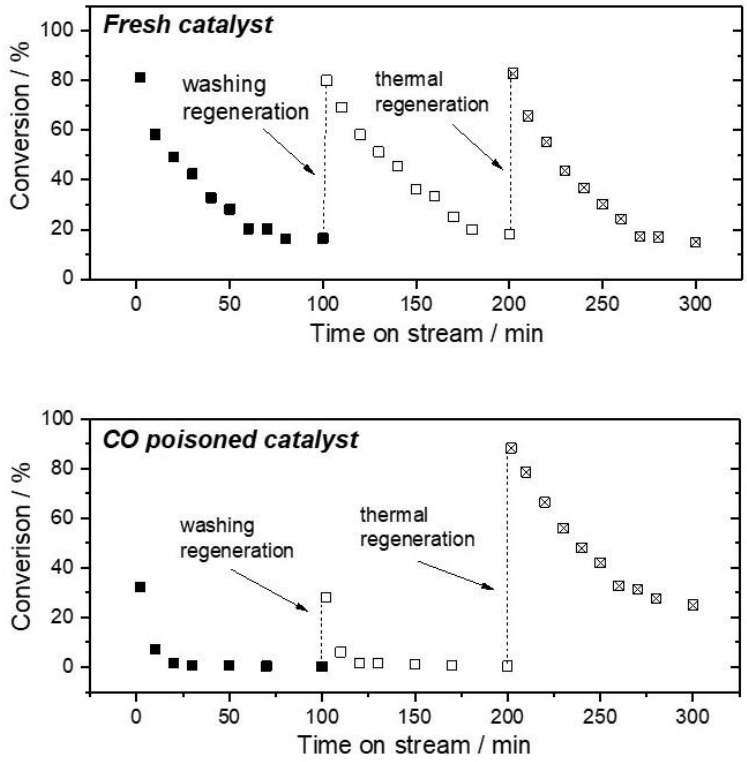

Figure 27 Formic acid dehydrogenation over Pd/C as (top) an untreated catalyst and (bottom) a CO-poisoned catalyst. In the latter, the reaction was started after treating the catalyst with a stream of CO (10% of CO in He, 20 mL min^{-1}, 3 h). In both cases, washing regeneration was performed after 100 min (2.5 mL^{-1} min, 150 min at 50°C), and a thermal regeneration was performed prior to a third cycle by heating the reactor in static air at 180°C for 90 min. Reaction conditions: Pd/C (150 mg), 0.25 mL min^{-1} of aqueous formic acid (0.5 M), 50°C, 5 bar.

As it can be seen, the initial activity of the catalyst after CO poisoning is dramatically lower than the untreated catalyst, with an initial conversion of only 32% achieved, compared to a ca. 80% value observed for the untreated sample (Figure 26). This result clearly indicates that CO is an effective poison of the catalyst. However, while washing regeneration is sufficient to restore full activity of the catalyst between typical reaction cycles (Figure 27, top), in the case of the CO-treated catalyst, washing only restores the additional amounts of activity lost during the reaction cycle itself; i.e., washing regeneration does not restore activity to ca. 80% conversion and hence is not able to mitigate CO poisoning (Figure 27, bottom), in line with the non-poisoned catalyst. This strongly indicates that although CO is an effective poison of the catalyst, CO poisoning is not the principal reason behind the loss of activity of Pd/C during the experiments performed in this study, since the mode(s) of deactivation observed during reaction is amenable to washing regeneration.

Although washing regeneration is unable to reverse CO poisoning, thermal regeneration is still feasible (180 °C, 90 min), with this treatment restoring the catalyst to its standard level of activity. On the basis of this, we can conclude that during the reaction, CO

poisoning does not give the main contribution to deactivation, as demonstrated by the fact that the activity between cycles can be totally recovered by washing, while CO poisoning itself cannot be removed by simply washing the catalyst with water.

In addition to impurities, by-products, and products, poisoning by substrate is also possible. In fact, acids such as formic acid are well-established poisons for nanoparticle-based catalysts, due to their ability to chelate strongly to the metal centres. In fixed bed reactors, deactivation events that are dependent on the concentration of reactants, such as fouling or poisoning, often involve specific parts of the catalyst bed, since the reactant concentration is space dependent rather than time dependent, as is the case of batch reactors. Indeed, in plug-flow systems the concentration of the reactants decreases from the front of the reactors till the end, whereas products concentration increases along the reactor length. Hence, deactivation due to poisoning by formic acid would be more severe at the front of the catalyst bed, rather than at the end. Thus, to probe the deactivation of different parts of the reactor, a reaction was performed with a typical mass of catalyst (150 mg), but with the total amount of catalyst split in two reactors placed in series.

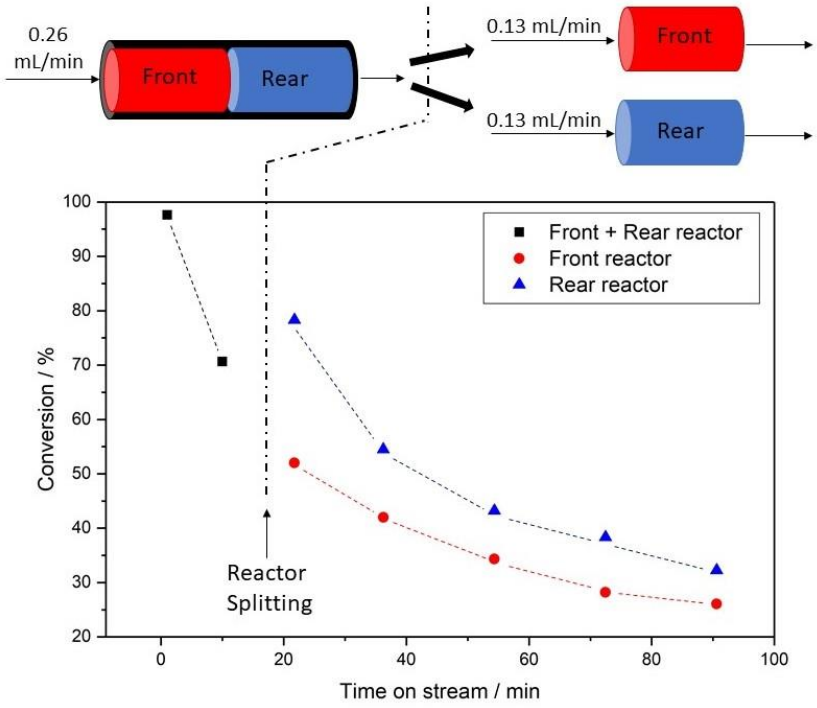

Figure 28 Performance of Pd/C for formic acid decomposition measured at different spaces of the catalytic bed. Reaction condition: first 10 min of reaction carried out with two reactors in series. Total amount of Pd/C 150 mg, 0.26 mL min^{-1} of aqueous formic acid (0.5 M), 50°C, 5 bar back pressure. After 10 min, the reaction was stopped and the two reactors separated. The reaction was then continued in duplicate, with both “half” beds tested under otherwise identical conditions: Pd/C (75 mg), 0.13 mL min^{-1} of aqueous formic acid (0.5 M), 50°C, 5 bar.

The reaction was initially run through the two reactors in series until the conversion of formic acid dropped from 95 to 70%, when the reaction was paused, and the two reactors separated. Subsequently, both “half” beds of catalysts were tested individually as two separate reactors, halving the flow rate in order to keep constant the contact time. If the catalytic bed had experienced homogeneous deactivation, the same value of initial activity would be found in both the reactors in the second part of the experiment. Instead, it is clear that the second (rear) catalyst bed exhibits much higher activity then the first (front) catalyst (Figure 28). The higher initial activity can be attributed to a lower degree of deactivation of the catalytic bed initially located in the rear half of the reactor, where the concentration of the reactant is lower. Accordingly, since deactivation of the catalyst is dependent on both substrate turnover and space, and is worst at the beginning of the reactor bed, it is likely that deactivation of the catalyst occurs from an effect related to the presence of the reactant, rather than (by)products.

Notably, of all the species present in the reactor, only formic acid can also be responsible for pore fouling, since the products and by-products of the reaction are all gaseous, and should readily be liberated from the catalyst. Poisoning by formic acid would also result in the evolution of CO_2 during thermal regeneration, in line with MS analysis.

In the case of formic acid, many theoretical reports on the mechanism suggest this reaction first involves deprotonation of formic acid on the surface of the metal, followed by desorption and release of H_2 and CO_2.[33, 48, 49] Formate anions possess a higher chelating strength than their protonated counterparts, making them a possible candidate as a poisoning agent.

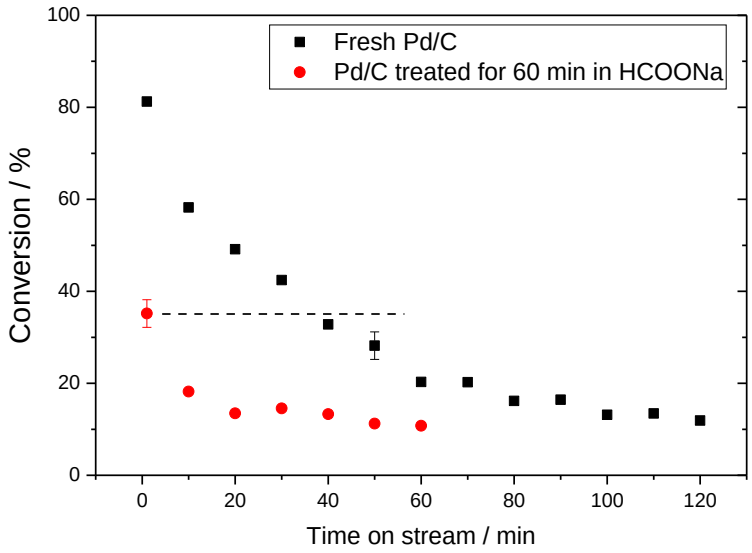

Figure 29 Performance of Pd/C for formic acid decomposition measured following pretreatment in an aqueous solution of HCOONa (0.5 M, 60 min, 0.25 mL min^{-1}). Reaction conditions: Pd/C 150 mg, 0.25 mL min^{-1} of aqueous formic acid (0.5 M), 50°C, 5 bar back pressure.

To probe the possible influence of the formate anions, a reaction was performed following pretreatment of the catalyst in an aqueous solution of sodium formate (Figure 29). We note that sodium formate itself does not result in the production of much H_2 and hence allows the impact of products of the reaction on deactivation to be minimized. In this case, the initial conversion level of the catalyst after treatment for 60 min in aqueous sodium formate was consistent with that typically observed after 45−60 min on stream, confirming the formate anions is the genesis of poisoning in this system.

Moreover, the catalyst poisoning by formate anions agrees well with all the evidences acquired from the previous experiments. Indeed, the poisoning by formate strongly correlate with the amount of feed introduced in the system, hence is in line with the deactivation dependence to substrate turnover confirmed by kinetic experiments. Absorbed formate anions can be subsequently converted in coke, which in turn occupies the catalyst micropores, decreasing their volumes and reducing the whole surface area. Calcination treatments are able to transform both the coke formed and the formate residues in CO_2, generating higher gas evolution when post-reaction catalyst is analysed by TPD-MS experiments. Furthermore, formate anions, accordingly with their electrolytic nature, can be easily washed out from the catalyst bed with a water treatment. The formate compounds as poison cause also explain why ^{1}H-NMR analysis of the regeneration effluent and D_2O extraction of the exhausted catalyst bed did not detect any residue substances, despite the high sensibility of the technique employed. Indeed, it can be conjectured that the remaining formate molecules retained on the catalyst surface, when in contact with large amount of water recombine in their acid form, which are able to react at room temperature with the regenerated catalyst, yielding in H_2 and CO_2 which promptly leave the solution as gaseous products. In addition, the substrate deactivation does not induce any sintering of the metal nanoparticles as demonstrated by TEM analysis and it is not correlated with the oxidation sate of the metal active sites as confirmed by XPS analysis.

3.3.7 Achieving continuous performance

When combined, the spectroscopic, kinetic, and mechanistic studies presented in this section clearly indicate that deactivation of the catalyst during the continuous conversion of formic acid to hydrogen relates to poisoning and fouling due to the presence of the substrate, formic acid. Since the substrate is an essential component of the reaction system, and it cannot necessarily be avoided during the reaction, this makes continuous operation of the system very challenging.

With the aim of maximizing durability of the system, and hence permitting true continuous operation to be achieved, we reasoned that continuous performance should be feasible by running in a continuous stirred tank mode (CSTR), where the steady state

concentration of formic acid can be minimized by operating the system at a level of conversion as close to 100% as possible. To do that, the rate of formic acid conversion must match the rate of formic acid addition, so that a steady state concentration of zero is achieved. To achieve this, pure formic acid was flown into a round bottom flask filled with 60 mL of water and the catalyst at 50°C. Despite not reaching full conversion, the catalyst exhibited much higher levels of stability in the CSTR, with the relative activity of the catalyst after over 2000 turnovers comparable to its activity at t_0, (Figure 30).

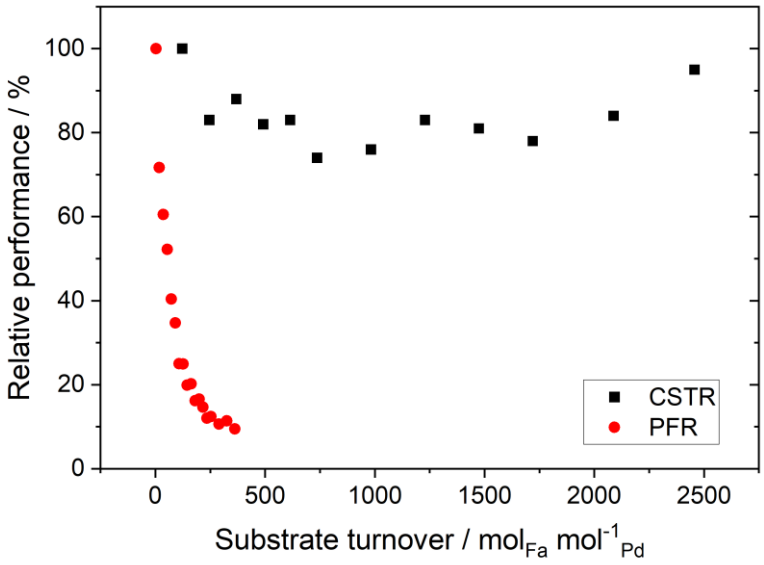

Figure 30 Comparison of Pd/C performance during formic acid dehydrogenation in CSTR and PFR. In particular relative performance of the catalyst as a function of substrate turnover in the two systems. CSTR reaction conditions: Pd/C (45 mg), 0.01 mL min^{-1} of pure formic acid, 60 mL of reactor volume, 50°C, 800 rpm. PFR reaction conditions: Pd/C (150 mg), 0.25 mL min^{-1} of aqueous formic acid (0.5 M), 50°C, 5 bar back pressure.

Because of its increased stability, more formic acid could be converted in CSTR than the PFR, as clearly shown in Figure 31, thus demonstrating how the choice of reactor and conditions can remarkably improve catalyst stability.

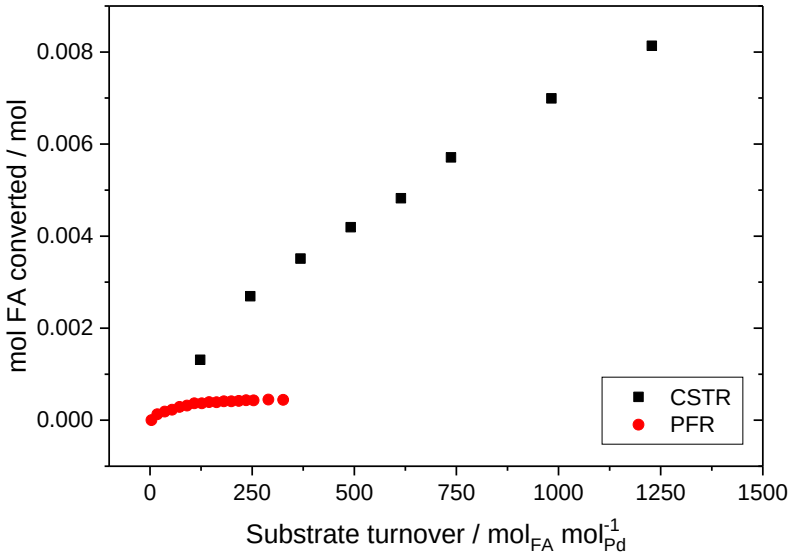

Figure 31 Comparison of Pd/C performance during formic acid dehydrogenation in CSTR and PFR. In particular cumulative moles of formic acid converted in the two systems as a function of substrate turnover. CSTR reaction conditions: Pd/C (45 mg), 0.01 mL min^{-1} of pure formic acid, 60 mL of reactor volume, 50°C, 800 rpm. PFR reaction conditions: Pd/C (150 mg), 0.25 mL min^{-1} of aqueous formic acid (0.5 M), 50°C, 5 bar back pressure.

In light of the fact that the activity can be recovered by washing the catalytic bed with water, it can be hypothesized that, in the CSTR, the constant stirring and the better dispersion of the catalyst in a higher volume of water account for a similar effect observed after washing, mitigating the deactivation of the catalyst. However, it should be added that despite the superior performance of the CSTR in terms of stability and overall productivity, the lower catalyst-to-volume ratio and the decreased steady state concentration of formic acid do compromise the initial space−time−yield of the reactor by an order of magnitude.

3.4 Conclusions

The promising stability showed by Pd/C in consecutive reaction cycles, performed in discontinuous systems for a total of 600 substrate turnover, has prompted its utilisation for promoting formic acid decomposition in continuous processes. Hence, in this chapter a PFR system was constructed and utilised to thoroughly investigate the kinetic aspect of the decomposition reaction. Despite Pd/C has expressed remarkably selectivity in favouring only the dehydrogenation reaction at 50°C, its activity has been halved after 25 minutes of continuous operating. This unacceptable catalyst stability for continuous hydrogen generation, have spurred the investigation of the reasons of such rapid deactivation.

Thanks to the time on stream analysis, performed in continuous reactors, it was observed that Pd/C deactivation is strictly depended to the substrate turnover, even when different reaction temperatures or feedstock concentrations were used. The correlation between catalyst deactivation and substrate turnovers has suggested that deactivation may relate

to a reaction-based stimulus, such as effects due to reactants, products, by-product(s), or to deposition of residues. Characterisation techniques performed on fresh, used and regenerated catalyst have excluded the in-situ formation of inactive chemical species and metal nanoparticles sintering during the continuous reaction.

Successful attempts to regenerate the exhausted catalyst bed were made by use of aerobic thermal treatments, or trough water washing, thereby pointing toward reversible causes of deactivation rather than irreversible, thus excluding metal lixiviation or collapse of the catalyst structure.

The catalyst regeneration extent achieved by means of water washing was shown to be strongly dependent on the amount of water used, rather than to the time length of the treatment or to the flow rate employed. This indicated that solvation properties of water are more beneficial for the catalyst regeneration than the linear velocities forces applied by the solvent stream on the inactive catalyst bed, suggesting stoichiometric relationship between eventual reaction residues and deactivation.

A common deactivation phenomenon which is dependent to the reaction operating is the deposition of coke on the catalyst surface. In fact, porosimetry analysis have demonstrated a decreased catalyst surface area and micropores volume on the used Pd/C than to fresh one. Characterization techniques such as XRD and Raman spectroscopy have demonstrated that the collapse of the catalyst structure during reaction does not occur, thus confirming the correlation between the reduced surface area and the catalyst deactivation.

Attempts to identify the nature of the residual species present on the catalyst surface, such as ^{1}H-NMR analysis of the reaction effluent or D_2O extraction of the used catalyst were made but no substances were detected in the washing solution. Conversely, TPD-MS analysis demonstrate the presence of extra carbonaceous material on the used catalyst, confirming the fouling hypothesis. However, the regeneration extent of deactivated catalysts, achieved by means of the water washing treatment, did not linearly correlated with the recovery of the catalyst surface area. Accordingly, fouling is to be considered only a partial cause of the whole catalyst deactivation phenomena and other reasons of deactivation must be present.

Feed impurities poisoning experiments excluded feedstock contaminants as cause of deactivation since commercial and purified formic acid showed the same deactivation rate. In addition, poisoning by the products H_2 and CO_2 was rejected by means of performing continuous reactions prior catalyst treatment in both, H_2 and CO_2 atmosphere. Conversely, CO has been demonstrated as a strong poison for Pd/C, in agreement with other studies performed on metal nanoparticles. However, a water regeneration process conducted on a CO-poisoned catalyst after a decomposition reaction cycle, demonstrated that the flush of water is able to restore only the catalyst performances lost during the

reaction cycle, and not to remove the CO molecules strongly physi- or chemisorbed to the metal nanoparticles. Thereby, since the water regeneration process has been demonstrated as able to fully restore the performance of inactive Pd/C, CO must be considered not responsible for the deactivation arisen during the decomposition reaction. Indeed, GC composition analysis of the gaseous reaction effluent demonstrated that only negligible quantities of CO are produced during formic acid decomposition, thus likely to be not the primary reason of the rapid deactivation showed by the catalyst.

Other reasons of catalyst poisoning have been conjectured, like by the reaction substrate itself. Indeed, organic acids are known to have strong chelating behaviour toward metal nanoparticles. Continuous reaction in which the reactant concertation is length depended, such as the one performed in tubular reactor, are the best system in which verify this hypothesis. In fact, if the main reason of catalyst poisoning is the reactant, the front part of the PFR, in which the reactant concentration is higher, should suffer much more deactivation than the rear part. A two-step experiment confirmed that after 10 minutes of decomposition reaction the front part of the PFR resulted to be less active than the rear part, demonstrating formic acid as main poison for Pd/C.

The deactivation by formic acid well agrees with all the other evidences resulted from previous investigations. Indeed, formic acid can be decomposed to CO_2 if treated in air at high temperature, as demonstrated by TPD-MS analysis, and can be washed out from the catalyst surface by means of a water flow and can generate the carbonaceous compounds which reduce catalyst surface area. In addition, the formic acid cause agrees well with all the kinetic experiments performed, since the deactivation rate is strictly dependent to the substrate turnover. A further kinetic experiment, performed with sodium formate, demonstrated that the reason why formic acid induces such a rapid deactivation should be attributed to the strong chelating properties of the formate anions. Accordingly, attempts to improve catalyst stability were made conducting the continuous reaction in a stirred tank reactor. In fact, the intrinsic feature of CSTR systems permit to conduce the reaction in a steady state condition in which pure formic acid is introduced in the system at the same rate at which it is decomposed, thus allowing an average formic acid concertation close to zero inside the reaction vessel. In this way the deactivation has been minimized and a stable continuous reaction has been conducted for over than 2000 turnover number. As a confirm of the higher catalyst stability, the CSTR reaction has allowed to continuously convert 27 times more formic acid than the reaction performed in PFR.

In addition to the higher hydrogen productivity and the process improvements achieved, the remarkable result of this work is the key role that continuous kinetic studies have played in the identification of the deactivation causes. Indeed, thanks to the PFR system, the causes of deactivation have been understood, the deactivation dependence on the

substrate turnover has been identified, and it has been possible to follow, and then compare, deactivation rates of reactions performed in different reaction conditions.
Most importantly, the tubular reactor has permitted to study the catalyst deactivation dependence along to the reactor length and not to the reaction time, which demonstrate formic acid as the main responsible species for the catalyst poisoning. To observe the same deactivation dependence to the substrate turnover in batch or CSTR processes, a larger number of experiments would have been necessary, but identification of which reaction compounds inhibit catalyst activity would have not been possible.
In discontinuous systems, kinetic studies in which the catalyst is treated with a likely poison solution prior the reaction, such as sodium formate, would have required two-step experiments and the catalyst separation from the poisoning environment thus prejudicing the reliability of the test. Conversely, the set-up of the tubular reactors permits to conduct these kinetic experiments in a one-step reaction in which it is only swapped the reaction feed, thus preventing catalyst perturbation due to the catalyst extraction from the reaction environment and its separation from the reaction solution.

To conclude, it must be stated that for the continuous generation of hydrogen to be employed as supply for fuel cell, Pd/C does not seem the most promising solution. Indeed, despite higher hydrogen productions have been achieved utilizing stirred tank reactors, the low catalyst-to-volume ratio of these systems discourages their implementation in portable and practical devices. Thereby, if this solution is still wanted to be adopted as electricity source, more stable catalysts must be designed to continuously decompose formic acid in small tubular reactors. Otherwise, different renewable molecules can be studied as chemical storage for hydrogen. In this term one proposed compound is urea, because it can be decomposed in hydrogen, nitrogen and carbon dioxide, and nowadays is considered the larger organic waste produced by industrial breeding.

3.5 References

1) S. Park, J. M. Vohs, R. J. Gorte, *Nature*, 2000, **404**, 265.
2) S. Z. Baykara, *Int. J. Hydrogen Energy*, 2005, **30** 545.
3) A. F. Dalebrook, W. Gan, M. Grasemann, S. Moret, G. Laurenczy, *Chem. Commun.*, 2013, **49**, 8735.
4) M. M. Mench, '*Fuel Cell Engines'*, Wiley-VCH, Weinheim, Germany, 2008.
5) C. Christodoulou, G. Karagiorgis, A. Poullikkas, N. Lymberopoulos, E. Varkaraki, *The Cyprus Journal of Science and Technology*, 2005, **4**, 72.
6) J. Graetz, *Chem. Soc. Rev.*, 2009, **38**, 73.
7) J. Shen, L. Yang, K. Hu, W. Luo, G. Cheng, *Int. J. Hydrogen Energy*, 2015, **40**, 1062.
8) Z. Yang, Y. Xia, R. Mokaya, *J. Am. Chem. Soc.*, 2007, **129**, 1673.
9) H. Dai, B. Xia, L. Wen, C. Du, J. Su, W. Luo, G. Cheng, *Appl. Catal. B*, 2015, **165**, 57.
10) H. P. Veluswamy, R. Kumar, P. Linga, *Appl. Energy*, 2014, **122**, 112.
11) H. Furukawa, O. M. Yaghi, *J. Am. Chem. Soc.*, 2009, **131**, 8875.

12) Y. Nakamori, G. Kitahara, A. Ninomiya, M. Aoki, T. Noritake, S. Towata, S. Orimo, *Mater Trans*, 2005, **46**, 2093.
13) Z. H. Lu, H. L. Jiang, M. Yadav, K. Aranishi, Q. Xu, *J. Mater. Chem.*, 2012, **22**, 5065.
14) Z. Wang, I. Tonks, J. Belli, C. M. Jensen, *J. Organomet. Chem.*, 2009, **694**, 2854.
15) A. Iulianelli, P. Ribeirinha, A. Mendes, A. Basile, *Renew. Sustain. Energy Rev.*, 2014, **29**, 355.
16) S. S. Tafreshi, A. Roldan, N. H. De Leeuw, *Faraday Discuss*, 2017, **0**, 1.
17) L. He, Y. Huang, X. Y. Liu, L. Li, A. Wang, X. Wang, C. Y. Mou, T. Zhang, *Appl. Catal. B*, 2014 **147**, 779.
18) F. Joó, ChemSusChem, 2008, **1**, 805.
19) J. F. Hull, Y. Himeda, W. H. Wang, B. Hashiguchi, R. Periana, D. J. Szalda, J. T. Muckerman, E. Fujita, *Nat. Chem.*, 2012, **4**, 383.
20) B. Loges, A. Boddien, F. Gartner, H. Junge, M. Beller, *Top. Catal.*, 2010, **53**, 902.
21) B. Loges, A. Boddien, H. Junge, M. Beller, *Angew. Chem. Int. Ed.*, 2008, **47**, 3962.
22) H. Junge, A. Boddien, F. Capitta, B. Loges, J. R. Noyes, S. Gladiali, M. Beller, *Tetrahedron Lett.*, 2009, **50**, 1603.
23) B. Loges, A. Boddien, H. Junge, J. R. Noyes, W. Baumann, M. Beller, *Chem. Commun.*, 2009, 4185.
24) C. Fellay, P. J. Dyson, G. Laurenczy, Angew. Chem. Int. Ed., 2008, **47**, 3966.
25) D. J. Morris, G. J. Clarkson, M. Wills*, Organometallics*, 2009, **28**, 4133.
26) A. Corma, S. Iborra, A. Velty, *Chem. Rev.*, 2007, **107**, 2411.
27) S. W. Fitzpatrick, *BioMetics, Inc.*, Report No. DOE/CE/41178, U.S. Department of Energy: Washington, DC, 2002.
28) Z. Xu, N. D. McNamara, G. T. Neumann, W. F. Schneider, J. C. Hicks, *ChemCatChem*, 2013, **5**, 1769.
29) Tian W., Dezhang R., Zhibao H., Zhiyuan S., Fangming J., Mingwei C.,Luyang C. *Green Chem.*, 2017, **19**, 716
30) X. Zeng, F. Jin, Z. Huo, T. Mogi, A. Kishita, H. Enomoto, *Energy Fuels,* 2011, **25**, 2749.
31) M. Grasemann, G. Laurenczy, *Energy Environ. Sci.*, 2012, **5**, 8171.
32) A. Boddien, H. Junge, *Nat. Nanotechnol.*, 2011, **6**, 265.
33) F. Sanchez, D. Motta, A. Roldan, C. Hammond, A. Villa, N. Dimitratos, *Topics in Catalysis*, 2018, **61**, 254.
34) A. Majewski, D. J. Morris, K. Kendall, M. Wills, *ChemSusChem*, 2010, **3**, 431.
35) P. Sponholz, D. Mellmann, H. Junge, M. Beller, *ChemSusChem*, 2013, **6**, 1172.
36) A. Boddien, B. Loges, H. Junge, F. Gartner, J. N. Noyes, M. Beller, *Adv. Synth. Catal.*, 2009, **351**, 2517.
37) M. Czaun, J. Kothandaraman, A. Goeppert, B. Yang, S. Greenberg, R. B. May, G. A. Olah, G. K. Surya Prakash, *ACS Catal.*, 2016, **6**, 7475.
38) Q. Y. Bi, X. L. Du, Y. M. Liu, Y. Cao, H. Y. He, K. H. Fan, *J. Am. Chem. Soc.*, 2012, **134**, 8926.
39) C. Hammond, *Green Chem.*, 2017, **19**, 2711.
40) D. Padovan, L. Botti, C. Hammond, *ACS catal.*, 2018, **8**, 7131.
41) C. H. Bartholomew, *Applied Catalysis*, 2001, **212**, 17.
42) L. Zhang, N. A. Seaton, *Chemical Engineering Science*, 1996, **51**, 3257.
43) J. P. Lange, *Angew. Chem. Int. Ed.*, 2015, **54**, 13186.
44) C. Hu, S. W. Ting, J. Tsui, K. Y. Chan, *International journal of hydrogen energy*, 2012, **37**, 6372.
45) D. Lin, Z. Shouzhong, *Journal of Power Sources*, 2011, **196**, 9369.

46) J. Grunes, J. Zhu, M. Yang, G. A. Somorjai, *Catalysis Letter*, 2003, **86**, 157.
47) J. Liu, F. R. Lucci, M. Yang, S. Lee, M. D. Marcinkowski, A. J. Therrien, C. T. Williams, E. C. H. Sykes, M. Flytzani-Stephanopoulos, *J. Am. Chem. Soc.* 2016, **138**, 6396.
48) Y. Wang, Y. Qi, D. Zhang, C. Liu, *J. Phys. Chem. C.*, 2014, **118**, 2067.
49) J. A. Herron, J. Scaranto, P. Ferrin, S. Li, M. Mavrikakis, *ACS Catal*., 2014, **4**, 4434.
50) S. L. Scott, ACS Catal. 2018, **8**, 8597.
51) A. Majewski, D. J. Morris, K. Kendall, M. A. Wills, *ChemSusChem*, 2010, **3**, 431.
52) C. Hu, J. K. Pulleri, S. W. Ting, K. Y. Chan, *Int. J. Hydrogen Energy*, 2014, **39**, 381.
53) A. K. Datye, J. Bravo, T. R. Nelson, P. Atanasova, M. Lyubovsky, L. Pfefferle, *Appl. Catal. A*, 2000, **198**, 179.
54) X. Wang, G. W. Qi, C. H. Tan, Y. P. Li, J. Guo, X. J. Pang, S. Y. Zhang, *Int. J. Hydrogen Energy*, 2014, **39**, 837.
55) K. P. de Jong, '*Synthesis Of Solid Catalysts*', Wiley-VCH Verlag GmbH & Co. KGaA, 2009.
56) F. Héroguel, G. Siddiqi, M. D. Detwiler, D. Y. Zemlyanov, O. V. Safonova, C. Copéret, *J. Catal.*, 2015, **321**, 81.
57) T. W. Hansen, A. T. DeLaRiva, S. R. Challa, A. K. Datye, *Acc. Chem. Res*., 2013, **46**, 1720.
58) J. H. Vleeming, B. F. M. Kuster, G. B. Marin, F. Oudet, P. Courtine, *J. Catal.*, 1997, **166**, 148.
59) G.S. Parkinson, Z. Novotny, G. Argentero, M. Schmid, J. Pavelec, R. Kosak, P. Blaha, U. Diebold, *Nat. Mater.*, 2013, **12**, 724.
60) P. Albers, J. Pietsch, S. F. Parker, *Journal of Molecular Catalysis A: Chemical*, 2001, **173**, 275.
61) A. C. Ferrari, J. Robertson, *Phys. Rev. B,* 2000, **61**, 14095
62) F. Tuinstra, J. L. Koening, *J. Chem. Phys*., 1970, **53**, 1126.
63) J. Schwan, S. Ulrich, V. Bathori, H. Erhardt, S. R. P. Silva, *J. Appl. Phys.*, 1996, **80**, 440.
64) REPORTING PHYSISORPTION DATA FOR GAS/SOLID SYSTEMS with Special Reference to the Determination of Surface Area and Porosity. K. S. W. SING (UK, Chairman); D. H. EVERETT (UK); R. A. W. HAUL (FRG); L. MOSCOU (Netherlands); R. A. PIEROTTI (USA); J. ROUQUEROL (France); T. SIEMIENIEWSKA (Poland). Pure & Appl. Chem., Vol. 57, No. 4, pp. 603—619, 1985.
65) K. S.W. Sing. *Advances in Colloid and Interface Science*, 1998, **76**-**77**, 3.
66) L. Dai, S. Zou, *J. Power Sources*, 2011, **196**, 9369.
67) Z. Zhang, J. E. Jackson, D. J. Miller, *Bioresour. Technol*., 2008, **99**, 5873.
68) M. D. Argyle, C. H. Bartholomew, *Catalysts*, 2015, **5**, 145.
69) K. Mori, M. Dojo, H. Yamashita, *ACS Catal.,* 2013, **3**, 1114.
70) J. Font Freidea, T. D. Gamlinb, C. Grahamc, J. R. Hensmanb, B. Nayc, C. Sharpc, *Topics in Catalysis*, 2003, **26**, 3.

Chapter 4 - Developing a continuous process for isosorbide production from renewable sources

4.1 Introduction

As discussed in Chapter 1, most of the chemical goods currently required by our society are typically manufactured by conversion of fossil carbon source. However, since fossil feedstocks are not a renewable source of carbon atoms, they are considered a limited resource destined to run out in the next few decades. Furthermore, the intensive exploitation of fossil resources has already been established as one of the main factors which contribute to the increasing concentration of CO_2 in the atmosphere, causing alarming environmental issues.[1-3] Therefore, the scientific community is exploring renewable alternatives to replace fossil sources. In this context, an important target is to establish sustainable and productive biorefineries, which produce value added compounds utilising biologically available materials as carbon sources.[4] The principal starting materials suitable for conversion in a biorefinery are hemicellulose and lignin, since they are naturally available renewable resources, and their structures can be broken-down into smaller constituents like glucose, xylose and many organic alcohols.[5, 6] These compounds can subsequently be converted into important platform molecules, such as ethanol, glycerol, sorbitol, lactic acid, succinic acid and more.[7] Amongst them, sorbitol, a sugar alcohol produced by glucose hydrogenation, is considered one of the top platform molecules derived from biomass,[8-10] with an estimated 2020 annual production of 2.3 million tons.[11] Sorbitol derivatives are utilised in several industrial sectors as fuels, plastic precursors, detergents, emulsifiers, antioxidants and pesticides.[8] Moreover, sorbitol can be consecutively dehydrated into isosorbide, an added value molecule employed in several industrial applications.[9, 12] For example, isosorbide, with its double ring shape and hydroxyl groups (Scheme 1), could replace the toxic bisphenol A in the large market of epoxy resins, yielding polymers with special mechanical performances.[13, 14]

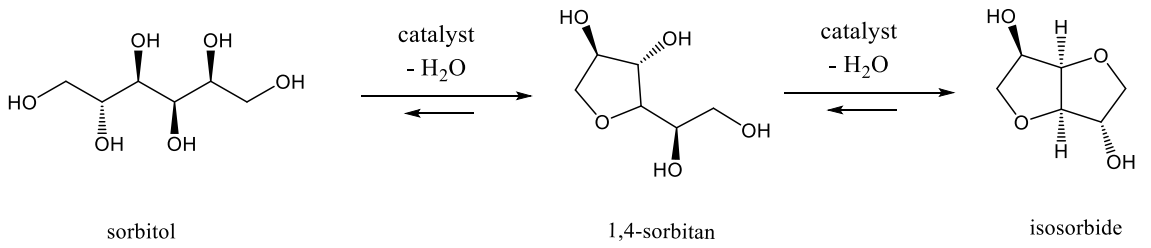

Scheme 1 Sorbitol dehydration to isosorbide via 1,4-sorbitan.

Furthermore, for its chiral properties, isosorbide has been exploited widely by the pharmaceutical industry in the challenging synthesis of pure enantiomeric drugs and healthcare products. Isosorbide derivates also find applications as organic solvents, surfactants, and additives capable of replacing harmful plasticizers such as phthalates. In addition, isosorbide is used for the synthesis of its mono and dinitrate derivates, compounds that are widely employed in medicine as vasodilators in cardiologic disease treatments.[15] Alongside these applications, the opportunity to use isosorbide to synthesise special fuels or biofuel additives has also been explored.[16]

At present, isosorbide is mainly produced through sorbitol dehydration performed by mineral acids such as H_2SO_4, HCl or p-toluenesulfonic acid.[17-19] These liquid acids provide good isosorbide selectivity but constitute a corrosive hazard for the reaction vessel, and result in several post-reaction operations being required to recover the pure product and treat the generated toxic waste. For such reasons, solid catalysts, typically preferred by chemical industries for their facile recovery and potential reusability in multiple reaction cycles, have been identified as a promising alternative to these liquid acids in the context of sorbitol dehydration. In fact, several classes of heterogeneous catalysts have recently been explored for sorbitol dehydration, in order to improve the isosorbide production from both an economic and environmental standpoint.[20-36] Amongst the investigated catalysts are included acid resins, molten salts, zeolites, bimetal catalysts, phosphates and sulphate oxides.[20-36] In this context, an extensive screening of solid acids has been performed in solvent-free batch conditions where the dehydration reaction was conducted by adding the catalyst into melted sorbitol.[20-27] For example, Hwang *et al.*[20] have thoroughly analysed different Brønsted and Lewis solid acids to correlate the acid strength, expressed as pKa, to the catalyst activity. Amongst the investigated Brønsted acid, p-toluensulfonic acid and methansulfonic acid were shown to be particularly active reaching an isosorbide yield over 60% after one hour reaction at 160°C. Whereas $Ti(SO_4)_2$ and $Zr(SO_4)_2$ resulted to be the most promising Lewis acids for the conversion of sorbitol in solvent-free condition, with an isosorbide selectivity of 68% and 65%, respectively. Fukuoka *et al.* explored the potential of aluminosilicate materials to produce isosorbide in melted sorbitol at 130°C in batch reactors.[21] Several zeolites with different structures and various Si/Al ratio have been screened, such as H-β, H-USY, H-ZSM-5, and H-Mordenite (H-MOR). At these reaction conditions, the most promising catalyst resulted to be H-β with a Si/Al ratio equal to 76, reported to be able to achieve an isosorbide yield of 76% after one hour of reaction.[21] The production of isosorbide in melted sorbitol as reaction medium, has been also investigated, employing other catalytic materials such as sulphated tin oxide,[22] sulphated titania,[23] sulphated zirconia,[24] and hydrophilic sulphated micro bead of silica,[25] which are capable to achieve isosorbide selectivities of 65%, 70%, 61% and 84%,

respectively. Moreover, the family of sulfonic polymeric resins has also been widely explored as solid acids to assist the sorbitol dehydration in solvent-free conditions. For example, Maireles-Torres *et al*. studied different commercial resins such as Amberlyst 35, Amberlyst 70 and Purolite (CT275, CT269, PD206) by using melted sorbitol at 140°C.[26] However, despite the best isosorbide yield of nearly 35% has been achieved by Purolite CT275, all the other sulfonic resins investigated exhibited comparable performances in terms of isosorbide productivity. Other sulfonic resins, such as Amberlyst 15 and Nafion, have also been studied in solvent-free media, exhibiting an isosorbide yield of 40% and 66%, respectively.[27, 28]

Although some solid catalysts have provided promising yields and productivities in solvent-free batch conditions, several disadvantages are prevalent and many challenges remain. For example, the high levels of substrate concentration attained in the melted phase lead to several undesirable reaction events, including sugar degradation processes,[37] and fouling of the catalyst.[38] Unfortunately, these phenomena might result in decreased catalyst longevity, which is considered a pivotal catalyst property for industrial application. Furthermore, the high viscosity of melted sorbitol represents a substantial hurdle for continuous operation, which is an important target given that such reactors provide several advantages for large scale processes (see Chapter 1).

Therefore, to overcome the disadvantages related to the solvent-free systems, sorbitol dehydration was also performed in the presence of reaction solvents. For example, Li and Huber investigated the dehydration of a 5 wt.% aqueous sorbitol solution promoted by SiO_2–Al_2O_3, reporting 60% of isosorbide yield after 25 hours of batch reaction at 245°C.[29] Furthermore, the activity of other classes of aluminosilicates materials was also screened for the production of isosorbide from sorbitol aqueous solutions.[30] Among the tested zeolites, promising results were achieved by the β type zeolites with a Si/Al ratio equal to 75, reportedly capable to achieve an isosorbide yield of 80% after 2 hours of dehydration reaction at 200°C.[30] Notably, Shirai *et al.* explored the opportunity to dehydrate sorbitol in the absence of any catalytic material, in which the reaction is only assisted by water at elevated temperature e.g. 317°C, achieving an isosorbide yield of 57% after 1 hour of reaction. It was proposed that the ability of the high temperature water to dehydrate sorbitol is due to the increasing self-ionisation rate reached by water at high temperatures, yielding a concentrated solution of proton and hydroxide ions, responsible for sorbitol dehydration.[39] Even hydrated molten salts were employed as reaction media to assist the isosorbide production in batch processes. The most promising resulted to be a 70 wt.% $ZnCl_2$ aqueous solution at 220°C, converting 69% of sorbitol into isosorbide.[40, 41]

Despite interesting results of isosorbide productivity were achieved in lab scale batch systems, continuous reactors are still the preferred solution for industrial scale operations, since they can provide several major advantages, including improved process and safety

control, higher level of mass and heat transfer, faster rates of reaction, minimised reactor volumes and higher levels of scalability.[42] For such reasons, sorbitol dehydration assisted by heterogeneous catalysts, was recently explored also in continuous systems.[31-36] However, to the best of my knowledge, the few continuous processes reported up to date were all performed in vapour-phase fixed bed reactors. In these systems, an aqueous sorbitol solution is pumped in a preheating zone and then, the generated vapor, is transported through the catalyst bed by a carrier gas as nitrogen. For example, Huang *et al.* tested plenty of solid acids such as sulphated copper oxides, metal (IV) phosphates and tungstophosphoric acids (PW) supported on various metal oxides.[31-33] Among the solid acids tested, particularly promising resulted to be sulphated copper oxide obtained from the calcination of $CuSO_4$ at 650°C, able to achieve an isosorbide selectivity of 67% in 4 hours of continuous reaction at 200°C.[31] Also 30 % PW/SiO_2 represents a promising catalyst since, in 6 hours at 250°C, provides an isosorbide selectivity of 45%.[32] Titanium phosphate reported a full conversion of sorbitol at 300°C, however, after only 3 hours of continuous reaction, losses of activity were observed.[33] Niobium and tantalum oxides modified with phosphoric acid also provided good isosorbide selectivities of 62 and 48% respectively, but reporting poor stability features.[34, 35]

As previously anticipated in Chapter 1, a promising catalyst for industrial purposes, in addition to high activity and selectivity, must also demonstrate excellent levels of stability. In fact, the economic potential and sustainability of any catalytic process intimately depends on the ability of the catalyst to be continuously used without loss of performance over a substantial period of time. Although critical to the commercial prospect of an heterogeneous catalytic system, this performance indicator is often overlooked, especially in academic literature.[37, 42] In fact, all the continuous studies previously reported do not evaluate the stability of the catalyst for long term operation.[31-35] Conversely, Xi and co-workers have synthesised a niobium phosphate-based catalyst able to dehydrate sorbitol with stable performances up to 60 hours of reaction time,[36] then first evidences of catalyst deactivation start to appear. However, it should be stated that the long-term reaction was conducted at 100% of sorbitol conversion, which prohibits promptly detection of any loss of catalyst activity before 60 hours of reaction, thus, providing not reliable stability results. Nonetheless, the loss of activity was attributed to the formation of carbonaceous materials on the surface of the catalyst, usually known as coke, which hamper the interaction between the substrate and the active sites. In fact, although vapour-phase reactors provide the benefits of continuous operation, such an approach is hampered by the poor volatility and low thermal stability of sorbitol, which complicates stable operation of the reactor in the vapour-phase, and unnecessarily degrades a valuable carbon resource, consequently resulting in low levels of reactor productivity.[43] Furthermore, the inert gas carriers utilised in vapor-phase reactors to transport the substrate molecules through the

catalyst bed, highly dilute the reaction feed, returning low values of substrate turnover even when long reaction times are employed. For example, when niobium phosphate catalyst starts to lose its activity after 60 hours of reaction, only 4.5 substrate turnovers is achieved.[36] This indicate that the catalyst begins to lose activity when just a few molecules of sorbitol have been converted into isosorbide, demonstrating that the catalyst is highly susceptible to some deactivation phenomena, dramatically affecting isosorbide productivity.

Therefore, despite the demand for isosorbide, efficient continuous processes catalysed by solid acids have not yet been developed. In this context continuous liquid-phase systems, in which the substrate is dissolved into a solvent, are a possible way to overcome the challenges faced by the continuous vapour-phase systems previously mentioned, whilst also allowing continuous operation of the reactor in a simpler manner than can be achieved for solvent-free systems. Indeed, the presence of liquid media allows the employment of optimal substrate concentrations throughout the catalyst bed and, at the same time, prevents high viscosity and temperature disadvantages typically encountered for solvent-free reactions. In addition, liquid systems are ideal to upgrade biomass-derivate molecules since lignocellulosic feedstocks are typically treated via hydrolysis and, therefore, the generated products are typically found in diluted aqueous streams.[44-50] In this way, the liquid-phase processes employed to valorise renewable platform molecules could be directly coupled with lignocellulose decomposition treatments, thus avoiding expensive intermediate product separation steps. Moreover, performing liquid-phase continuous reactions presents an opportunity to gain insights into the reaction kinetics of the process, an investigation topic that, although essential for industrial productivity, sustainability and profitability,[37, 42, 51] has been overlooked in the continuous scenarios previously reported.[31-35] Furthermore, since previous works have highlighted the propensity of sorbitol dehydration catalysts to lose performances along the reaction course,[30, 33, 35] a catalyst deactivation study should also be performed.

For these reasons, the scope of this thesis chapter is to explore sorbitol dehydration assisted by a heterogeneous catalyst in a liquid-phase continuous flow reactor which, to the best of my knowledge, has not previously been attempted. Particular attention is placed on kinetic aspects of the system, including long-term continuous operation to probe catalyst stability. Preliminary batch studies, essential to identify a suitable catalyst and optimal reaction conditions for initial continuous applications, have also been performed and included in this chapter.

4.2 Experimental

4.2.1 Materials

Sorbitol (≥98%), Cellobiose (≥98%) Amberlyst 36 dry, $CuSO_4 \cdot 5\ H_2O$ (≥98%), H_2SO_4 (≥97%), and HCl (37%) were purchased from Sigma-Aldrich. MeOH (≥99.5%) was supplied by Fisher Scientific. All zeolites, beta, ZSM-5, Y, Ferrierite, Mordenite were purchased from Zeolyst and calcinated in their H^+ form by calcination in air at 550°C for 6 hours, 5°C min^{-1} ramp rate, prior to their use.

4.2.2 Kinetics studies

Discontinuous sorbitol dehydration reactions were performed in a 50 mL Parr stainless-steel autoclave set at the desired temperature, autogenic pressure and at 800 rpm. The autoclave liner was previously charged with 20 mL of sorbitol solution of selected concentration and the desired amount of catalyst. The impeller of the reactor was set in motion only when the desired temperature was reached. At the end of the reaction, the autoclave was cooled in an ice-bath. Aliquots from the reaction mixture were collected and the concentration of sorbitol, 1,4-sorbitan and isosorbide was analysed by means of HPLC-ELSD

Continuous sorbitol dehydration reactions were performed in a plug flow, stainless steel, tubular reactor. The reactor was connected to an Agilent HPLC pump in order to accurately regulate the reactant flow. Long term reactions were performed with a Cole-Parmer HPLC pump. In order to avoid flow obstruction by the catalyst bed, zeolite beta-38 was pelletised, prior to loading into the reactor, in a uniform 60-100 μm diameter grains. Then the catalyst pellets were densely packed into a ¼ inch stainless-steel tube (4.1 mm internal diameter), held between two quartz wool plugs, and a frit of 0.5 μm placed at the reactor exit. The reactor was subsequently placed inside a furnace (Carbolite EVT 12/450, Carbolite MTF12/38/ 400) for long term reactions and set at the desired temperature. Pressure in the system was controlled by means of a backpressure regulator, typically set at 40 bar. Prior to start feeding effluent substrate to the reactor, reactor was conditioned for 30 minutes by flowing 0.5 mL/min of MeOH at reaction temperature and pressure. Aliquots of the reaction mixture were periodically withdrawn from a sampling valve placed after the reactor. Catalyst regeneration was performed heating the whole reactor in a combustion furnace (Carbolite MTF12/38/ 400) at 650°C (20°C min^{-1}) in air for 6 hours.

4.2.3 Catalyst characterisation and analytical details

p-XRD analysis, IR spectroscopy and TGA, were employed to characterise fresh, used, and regenerated catalysts. Specific surface area and microporous volume were determined from nitrogen adsorption isotherms by using DFT method. Experimental details for each of these methods are fully described in Chapter 2. Concentration of sorbitol, 1,4-sorbitan and isosorbide were analysed by means of HPLC equipped with ELS

detector employing a 0.05 M cellobiose solution as external standard. Each sample was analysed under the following conditions: Agilent Hiplex-Ca column, 0.75 mL min^{-1} HPLC water flow, 80°C. ELSD condition: T nebuliser = 35°C, T evaporator = 35°C, 1.60 SLM nitrogen flow.

4.3 Results and discussion

4.3.1 Batch study

Before developing the continuous liquid-phase reactor it is necessary to study the sorbitol dehydration in a discontinuous process. Indeed, discontinuous operations present much less parameters to be tuned and controlled when compared to continuous processes, thus, offering the opportunity to better understand the reaction dependence to certain process parameters, such as temperature or substrate concentration. Moreover, since the concentrations employed in batch systems is time dependent, rather than space dependent as in continuous apparatus, the determination of the products distribution over the reaction time can be accurately performed by means of few simple experiments. Thus, preliminary studies were conducted in discontinuous modus operandum to gain insights into the sorbitol dehydration reaction.

As illustrated in the introduction of this chapter (page 129), sulfation is a widely used technique to improve the acidity of solid catalysts in order to generate active materials able to promote acid catalysed reactions. In fact, most of the best performant catalysts able to dehydrate sorbitol present sulfonic functionalities such as CuSO,[31] sulphated tin oxide,[22] sulphated titania,[23] sulphated zirconia,[24] and sulfonated micro bead silica.[25] Amberlyst is a commercial sulfonated acid resin which exhibited great potential to dehydrate sorbitol too.[27] Indeed, its sulfonated functionalities confer to the resin the optimal acid sites to assist the broad range of chemical reactions that require acid sites to take place. In particular, the scientific community has explored Amberlyst as potential catalyst for the upgrading of numerous biomass-derived molecules. In fact, the dispersed sulfonic groups on its polymeric framework led to active but not degrading acid sites, making the material compatible with the fragile carbohydrate derivates. Furthermore, its polystyrene-divinylbenzene structure makes Amberlyst insoluble in water, one of the most common media in which biomass conversion is performed, thus, allowing to use this material as heterogeneous catalyst.[44-50] For example, Centi *et al*. reported that Amberlyst 15 converts cellulose in glucose and 5-hydroxymethylfurfural (HMF) in aqueous media at 190°C, meanwhile Alonso and co-workers employed this acid resin to upgrade corn stover to levulinic acid.[46, 52] Also, Amberlyst 15 resulted to be suitable to assist the esterification of succinic and levulinic acid and it is currently adopted in the synthesis of butyl lactate.[53, 54] Nevertheless, for the purpose of this work of developing a continuous liquid-phase system, the most interesting application of Amberlyst 15 has been reported by Aellig and

co-workers, who conducted the dehydration of fructose in continuous fixed-bed reactors.[55] Therefore, due to its great compatibility with biomass derivates and to its promising acidity, Amberlyst 15 has been selected as a suitable heterogenous catalyst to study sorbitol dehydration in discontinuous systems. For this preliminary study, water has been employed as reaction solvent since it can restrain larger amounts of sugars than all organic solvents, it is not toxic, nor flammable, it is cheap, naturally available and it is environmentally respectful. Furthermore, as reported by Shirai *et al.* the aqueous media can have a beneficial effect on sorbitol dehydration because of the self-ionization of water at high temperature.[39] Moreover, most of the recent studies performed on sorbitol dehydration assisted by solvents have been conducted in aqueous environment.[29-36] In this way, selecting water as reaction solvent for this preliminary study also offers the opportunity to compare the performances of our batch system to the ones reported in literature.

However, prior to acquiring catalytic data, it must be established the reaction is operated the chemical kinetic regime, thus, to not underestimate the catalyst performance. Indeed, as described for continuous systems (see Chapter 1), also in batch reactors external mass transfer limitations that add extra resistance to the chemical process may occur. In these systems, the extent of mass transfer limitation is strictly affected by the liquid agitation inside the reactor vessel, hence, to the impeller stirring velocity. In fact, at elevated solution agitation, the thickness of the static fluid layer, that surrounds the catalyst particles, is expected to decrease, thereby reducing mass transfer limitations. Therefore, to ascertain the chemical kinetic regime, several batch reactions were first conducted at various stirring rate, in a range from 0 to 1350 rpm, in otherwise identical conditions (Figure 1).

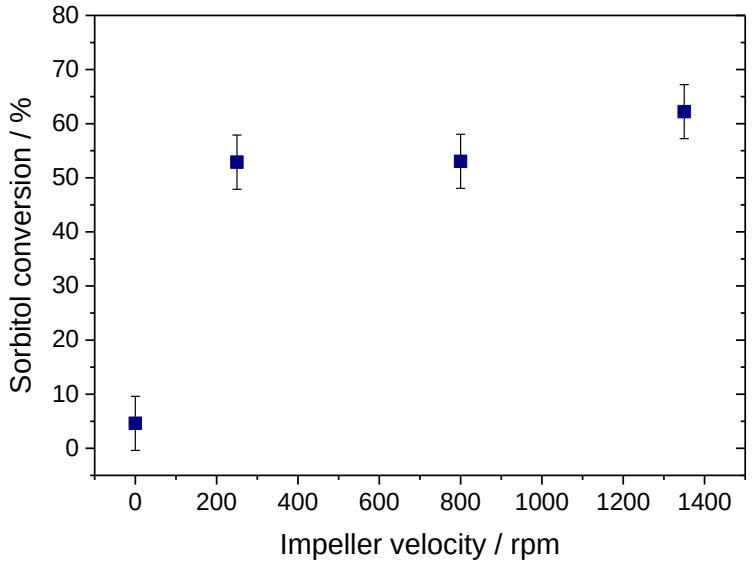

Figure 1 External mass transfer limitation test. Batch reactions were performed adding 0.500 g of commercial Amberlyst 15 in a stainless-steel Parr autoclave with 20 mL of 5 wt.% sorbitol aqueous solution ($moles_{acid\ sites}/moles_{sorbitol}$ = 0.5). The system was heated at 200°C and the reactions conducted at autogenic pressure for 1 hour at different impeller velocity: 0, 250, 800, 1350 rpm.

As expected, in absence of any solution agitation the reaction does not occur, showing a negligible sorbitol conversion of 4%. Conversely, as soon as the impeller is set in motion at 250 rpm the reaction conversion reaches a value of nearly 54%, which is maintained constant up to 800 rpm. At higher agitation, 1350 rpm, the conversion slightly increases reaching a value of 62%. However, it must be considered that, in this latter case, fragments of the solid catalyst particles were observed in the post-reaction mixture, indicating that the higher forces exerted by the impeller might have damaged the heterogeneous catalyst. However, it can be acknowledged that for all the employed velocities, the sorbitol conversion obtained is constant within the experimental error of ± 5%. Therefore, it can be concluded that no external mass transfer phenomena limit the proceeding of the dehydration reaction when performed in batch reactors at stirring velocities higher than 200 rpm. Hence, to ensure to work in chemical kinetic regime and, at the same time, to preserve the catalyst integrity, all the following batch reactions were conducted at 800 rpm. Notably, the effect of internal mass transfer limitation cannot be studied since the fragile nature of the Amberlyst 15 impedes to pelletise the catalyst in bigger diameter particles.

Subsequently, time online experiments were performed to study the dehydration reaction evolution and the product distribution over the reaction time.

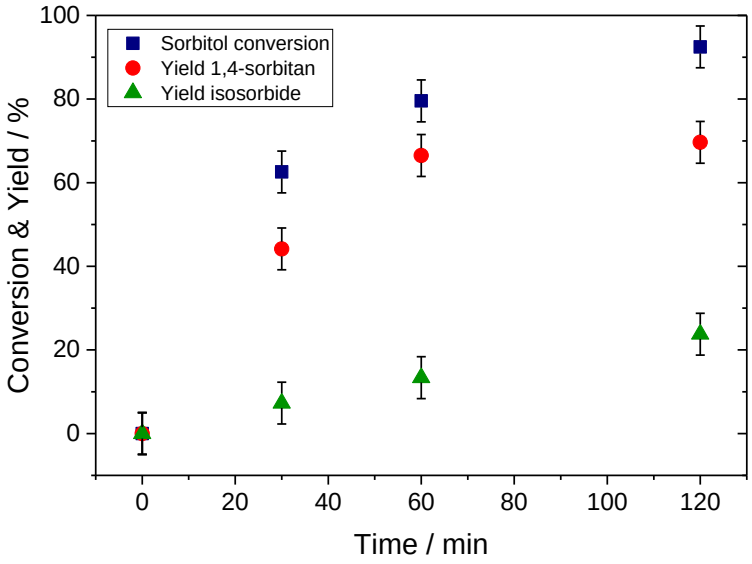

Figure 2 Sorbitol dehydration performed in autoclave. Reaction condition: 20 mL of 5 wt.% sorbitol aqueous solution, 0.500 g of Amberlyst 15 ($moles_{acid\ sites}/moles_{sorbitol}$ = 0.5), 200°C, 800 rpm, autogenic pressure.

A blank test was also conducted at the same conditions albeit without any catalytic material, to truly elucidate the activity of the catalyst in promoting the dehydration reaction. In the absence of any solid acids no conversion of sorbitol was detected, even after 2 reaction hours at 200°C. Conversely, Amberlyst 15 provided almost full sorbitol conversion at 200°C in 2 hours reaction time (Figure 2), confirming the promising potential of this polymeric resin in promoting dehydration reactions. However, a poor isosorbide selectivity was achieved, 24%, suggesting the requisition of a more intensive study of the reaction parameters.

Therefore, the effect of the reaction temperature on sorbitol dehydration was investigated (Figure 3).

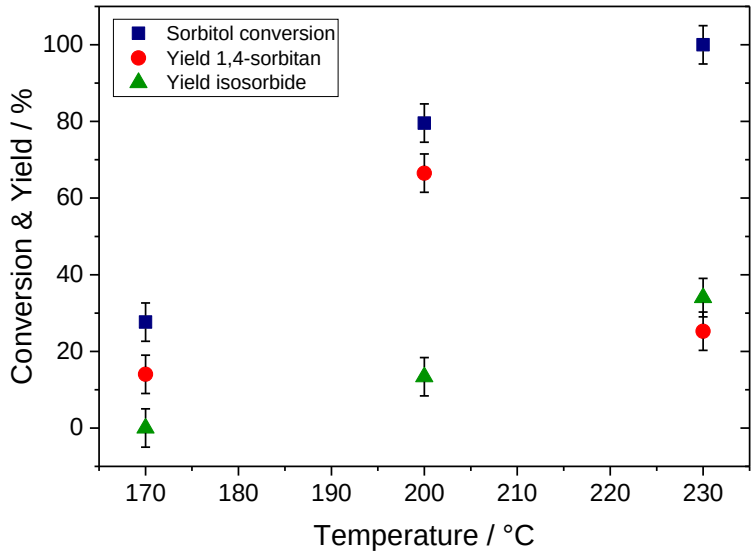

Figure 3 Sorbitol dehydration performed at different reaction temperature. Reaction condition: 20 mL 5 wt.% sorbitol aqueous solution, 0.500 g Amberlyst 15 ($moles_{acid\ sites}/moles_{sorbitol}$ = 0.5), 1 hour, 800 rpm, autogenic pressure.

Performing the reaction at 170°C, it can be seen that 27% of sorbitol conversion is achieved and only the product of the first dehydration step (Scheme 1), 1,4-sorbitan, is produced, with a yield of 14%. At higher temperature, 200°C, sorbitol conversion and 1,4-sorbitan yield increased to 80% and 67% respectively, but, most importantly, first quantities of isosorbide were detected, with a yield of 13%. Further rising in temperature was found to benefit the proceeding of the second dehydration step, since at 230°C, the isosorbide yield enhanced to 34%, whereas the intermediate 1,4-sorbitan yield dropped to 25%. Accordingly, this experiment highlights the key role that temperature plays to promote the consecutive dehydration of 1,4-sorbitan to isosorbide (Scheme 1). Since the purpose of this experiment was to screen different reaction temperatures in order to understand the behaviour of the reactant, the intermediate product and the terminal product, reaction by-products and reaction carbon balances were not reported and discussed (For carbon balance discussion see Figure 14). Performing the reaction at different temperatures, also allowed to determine the apparent activation energy for the overall sorbitol dehydration by means an initial rate method based on conversion values and assuming a first-order kinetics of the dehydration reaction as reported in previous batch studies (Figure 4).[27]

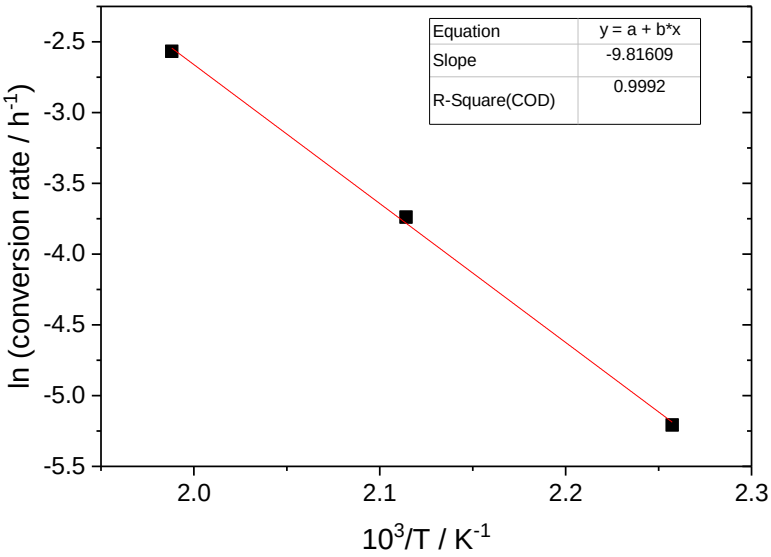

Figure 4 Apparent temperature dependence for sorbitol dehydration reaction performed in batch reactors. Reaction condition: 20 mL 5 wt.% sorbitol aqueous solution, 0.500 g Amberlyst 15 ($moles_{acid\ sites}/moles_{sorbitol}$ = 0.5), 1 hour, 800 rpm, autogenic pressure. Conversion rate of reactions were determined by means of an initial rate method based on conversion values obtained at 1 h reaction time and assuming a first-order kinetics: conversion rate = ln(1-X)/t, where X the conversion value obtained at the reaction time t.

The apparent activation energy calculated of 81 KJ/mol is not in the range of diffusion and is in accordance with the value reported by Fukuoka *et al*.[21] and Jhung *et al.*.[27] This suggests the reliability of the acquired data, ensuring that the reactions were performed in chemical kinetic regime, in absence of any interphase limitation.[56]

In addition to the reaction time and temperature, also the substrate concentration might play an important role on the reaction outcome. Therefore, 1, 5 and 10 wt.% of sorbitol aqueous solution were tested, and the mass of catalyst was adjusted accordingly, in order to maintain a constant $moles_{acid\ sites}/moles_{sorbitol}$ ratio of 0.5 (Figure 5).

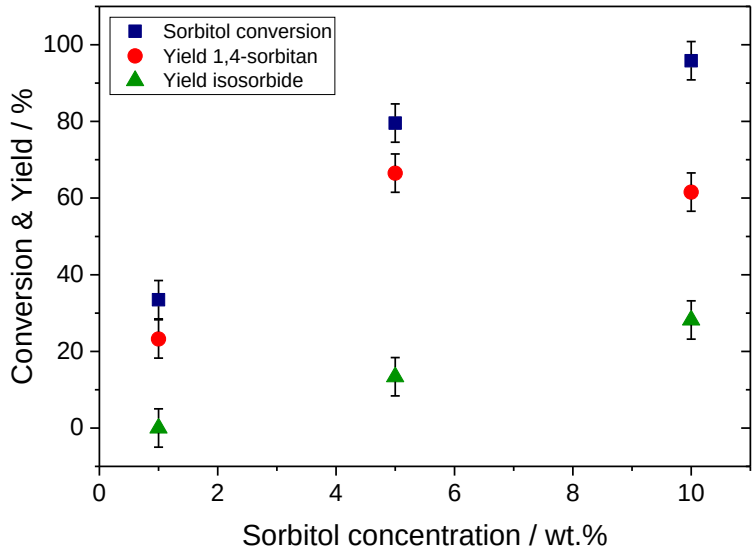

Figure 5 Study of substrate concentration effect on the reaction outcome. Reaction condition: 20 mL sorbitol aqueous solution at different wt.%, $moles_{acid\ sites}/moles_{sorbitol}$ = 0.5, 1 hour, 200°C, 800 rpm, autogenic pressure.

As expected, increasing both substrate and catalyst concentration led to a higher reactivity, beneficial favouring both sorbitol conversion and isosorbide yield. In fact, by increasing the sorbitol concentration from 1 to 5 wt.% the sorbitol conversion was enhanced from 33 to 76% and the isosorbide yield from 0 to 13%. Further intensification of the substrate concentration up to 10 wt.% led to a sorbitol conversion of 96% and to a isosorbide yield of 28%, while the yield of 1,4-sorbitan resulted to be decreased from 67 to 61%.

To also evaluate the impact of the amount of acid sites on the dehydration outcome, several reactions were performed with different amounts of catalyst (Figure 6), otherwise keeping constant all the remaining reaction parameters.

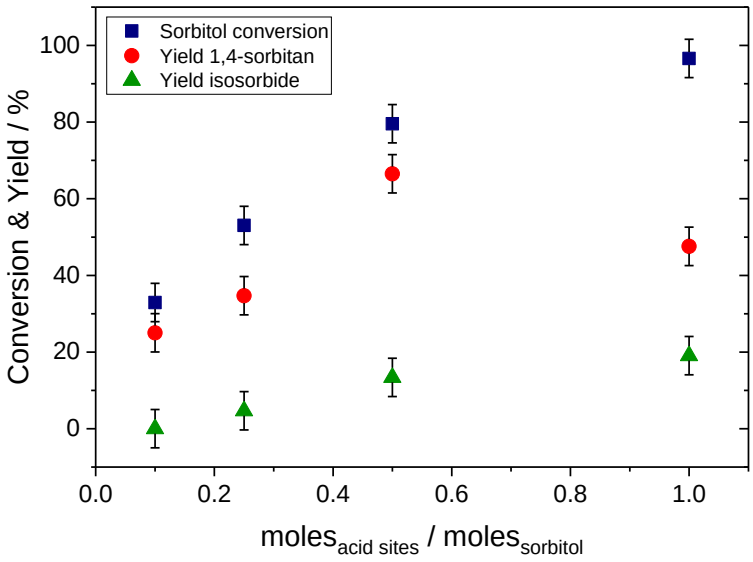

Figure 6 Effect of different moles of active sites per moles of substrate on the reaction outcome. Reaction condition: 20 mL sorbitol 5 wt.% aqueous solution, 1 hour, 200°C, 800 rpm, autogenic pressure.

In agreement to various studies reported in the literature, the acidity of the environment resulted to play a key role in the success of the full dehydration.[20, 21] In fact, it can be noted the linear dependence of sorbitol conversion and isosorbide yield to the amount of acid sites present in the reaction environment. Specifically, increasing the ratio of $moles_{acid\ sites}/moles_{sorbitol}$ from 0.1 to 1.0 led to an enhancement in sorbitol conversion from 33% to 98% and in isosorbide yield from 0% to 20%. It can also be noted that when $moles_{acid\ sites}/moles_{sorbitol}$ have been intensified from 0.5 to 1.0, the yield of the intermediated 1,4-sorbitan has dropped from 67% to 48%, favouring the isosorbide yield increase from 11% to 20%.

From all the experiments conducted above, it is clear that to generate substantial amounts of isosorbide, the reaction must reach high conversion values at which is mainly produced the intermediate 1,4-sorbitan, and then the second dehydration step takes place converting 1,4-sorbitan into isosorbide (Scheme 1). In fact, it can be deduced by the results of these experiment, that only when most of the sorbitol molecules have been consumed, the acid sites present in the reaction environment are able to exert their activity towards the intermediate 1,4-sorbitan, thus, converting it into isosorbide. As such, it can be ascertained that the determining step for isosorbide production is the second dehydration step (Scheme 1), rather than the first one.

These preliminary discontinuous experiments show that full conversion of sorbitol, and hence satisfactory isosorbide yield, can only be achieved at harsh reaction conditions such as long rection time (Figure 2), elevated temperature (Figure 3), high substrate

concentration, (Figure 5) or large amount of acid sites (Figure 6). Unfortunately, these conditions might result detrimental for the acid catalyst itself, threatening its stability and activity during long-term continuous processes. In fact, as reported by Siril and co-workers, Amberlyst 15 can lose up to 40% of its acid sites after only six hours of hydrothermal treatment at 200°C.[57] Therefore, to assess the catalyst stability, a hot-filtration experiment was performed. The reaction was conducted for 45 min at 200°C, afterwards it was stopped and the solid catalyst separated from the reaction mixture by filtration. Then the reaction was continued with the aqueous solution only. If the catalyst has not been damaged during the first 45 min of reaction, both the sorbitol conversion and products yield should not increase during the reaction after the filtration. Since, after the filtering of the catalyst (Figure 7), the sorbitol conversion increased from 61% to 93% it is clear that during the first 45 min of reaction the polymeric resin had dispersed some of its acidic sites into the reaction mixture, which are responsible for the reaction progress even in absence of the solid catalyst.

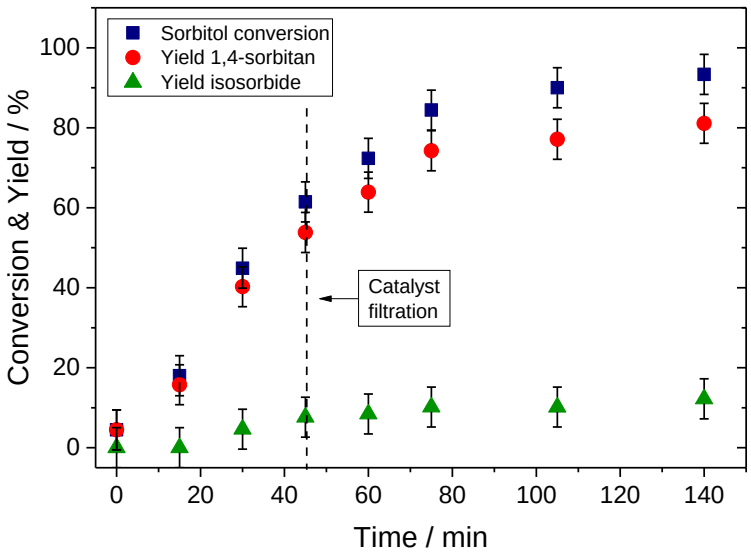

Figure 7 Hot-filtration test. For the Initial 45 minutes of the reaction performed in autoclave at with 0.500 g of Amberlyst 15, 20 mL 5 wt.% sorbitol aqueous solution at 200°C, 800 rpm. Following 45 minutes of reaction, the catalyst was filtered from the reaction mixture and the supernatant introduced into the autoclave to proceed the reaction at the condition reported.

Of course, the leaching of the catalyst must be considered a not-acceptable feature for the development of a continuous process, since after long term reactions the active sites might be fully washed out from the catalyst bed, thus, losing all its activity. Therefore, Amberlyst 15 was considered a not suitable catalyst for this process and a screening of different solid materials is crucial to be conducted in order to find active catalysts with stable features, also at the harsh conditions at which the sorbitol dehydration must be performed. Hence, the following section of this chapter will focus on the screening of other heterogeneous catalysts, to identify the best one to employ for continuous operations.

4.3.2 Catalyst screening

Despite several heterogeneous catalysts have already been screened for sorbitol dehydration,[20-36] the most interesting ones were utilised in solvent-free media, an option hardly applicable for continuous operation purposes.[20-28] Indeed, most of the studied solvent-free reactions were performed close to the melting point temperature of sorbitol (95°C), in order to provide a liquid phase, but, at the same time, to avoid the easy degradation of sugar derivates that can easily occur at elevated temperatures. These conditions imply to work in a highly viscous liquid medium that might prevent to operate in continuous apparatus or threat the catalyst stability during long term reactions. Therefore, a screening of various catalytic materials in liquid-phase condition is required, since the presence of a solvent might highly affect the catalyst performances. In this regard, focus was place on zeolites in their proton forms, in which the Brønsted acid sites are represented by protons that balance the negative sites created by the aluminium atoms. Because the aluminium atoms are strongly incorporated inside the mineral framework, we hypothesised a lower leaching behaviour of the acid sites and, thus, a greater stability than Amberlyst 15. Accordingly, an array of zeolites with different framework structures and SiO_2/Al_2O_3 molar ratios (indicated in parentheses) was selected and tested for sorbitol dehydration (Figure 8). In addition, sulphated copper oxide (CuSO), obtained by calcination of $CuSO_4$ (650°C, 5h, 20°C/min) was also explored, since it was reported as a promising catalyst for sorbitol dehydration.[31] Furthermore, the activity of Amberlyst 15 was used to benchmark the explored catalysts, since all the previous batch studies were performed employing this acid resin. Control experiments using mineral acids such as H_2SO_4 and HCl were also performed, in order to compare the catalytic performance of zeolites to those of the liquid acids currently employed for isosorbide production. Each batch reaction was performed at constant $moles_{acid\ sites}/moles_{sorbitol}$ ratio, by varying the amount of the catalyst accordingly. Notably, for zeolites, the moles of active sites were considered equal to the moles of Al present in the material framework. Furthermore, each zeolite was tested in its H^+ form following calcination in air at 550°C for 6 hours, at a ramp rate of 5°C/ min.

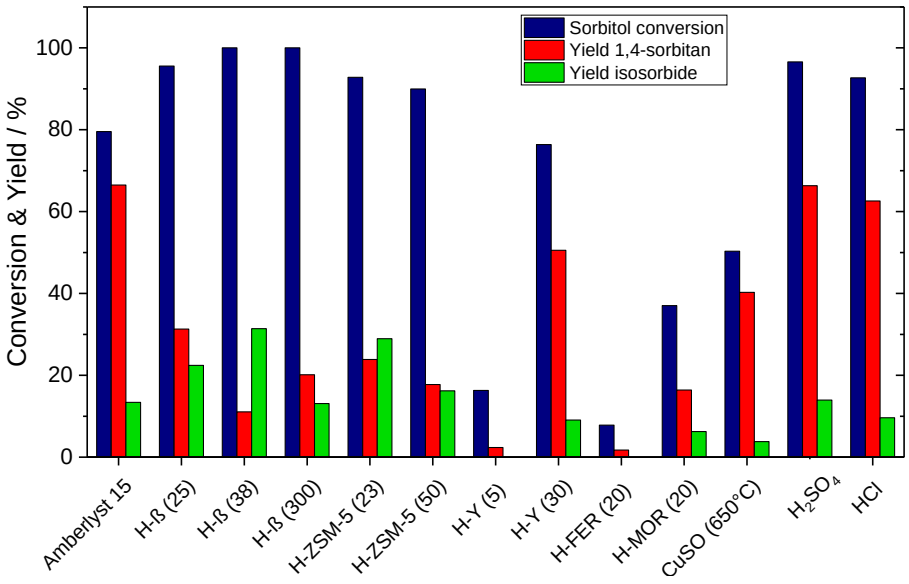

Figure 8 Sorbitol conversion (blue bars), 1,4-sorbitan yield (red bars) and isosorbide yield (green bars) achieved by different solid and liquid acid catalysts during sorbitol dehydration. Reaction conditions: 20 mL of aqueous sorbitol (5 wt.%), $moles_{acid\ sites}/moles_{sorbitol}$ = 0.5, 200°C, autogenic pressure, 1 hour. Acid sites loading data were taken from commercial catalysts suppliers.

As shown in Figure 8, depending on the frame topology and the aluminium content, the zeolite materials explored in this study exhibited a wide range of activity and selectivity. Specifically, H-β and H-ZMS-5 were the most promising materials, achieving isosorbide yields even greater than those achieved by the mineral acids and Amberlyst 15. Conversely, poor isosorbide yields were observed for H-Y, H-Ferrierite (H-FER) and H-Mordenite (H-MOR), which may be ascribed to several reasons such as different pore structures, hydrophilicity, or even to hydrothermal instability of the materials.[21, 30] Regarding the SiO_2/Al_2O_3 molar ratio, the isosorbide productivity trend observed in Figure 8 is in good agreement with previous works, as zeolites with intermediate aluminium content showed the best performance.[21, 30] In particular, for the H-β series, maximum isosorbide yield was achieved for the material possessing a SiO_2/Al_2O_3 ratio of 38. The superior performances exhibited by zeolites which possess intermediate aluminium content can be explained considering the dual effect that the SiO_2/Al_2O_3 ratio plays on the aluminosilicates properties. In fact, at lower SiO_2/Al_2O_3 ratios, the acid density of the material is increased, which is already demonstrated as a key features for catalysts which promote dehydration reactions.[21, 30] On the other hand, decreasing the SiO_2/Al_2O_3 ratio, the hydrophilicity of the material increases, which thermodynamically discourage the removal of the water molecules formed during the dehydration reaction. Accordingly, aluminosilicates with intermediate SiO_2/Al_2O_3 ratio exhibit the best performances in producing isosorbide.

Conversely, sulphated copper oxide (CuSO) does not seem really promising to dehydrate sorbitol in liquid phase reaction. Moreover, at the end of the reaction, CuSO resulted to be fully dissolved in the reaction media, thus resulting not suitable for continuous purposes. It must be observed that, in all the materials tested, except for Amberlyst 15, the carbon balance was not complete, indicating that other products than 1,4-sorbitan and isosorbide were created during the sorbitol dehydration, but since the purpose of the test was just a performances screening, they were not identified.

From the materials explored in Figure 8, zeolite H-β (38) achieved the best isosorbide yield (31 %). The superior catalytic performance exhibited by H-β (38) indicates that this catalyst is able both to convert sorbitol, and assist the dehydration of the reaction intermediate, 1,4-sorbitan (Scheme 1), unlike other catalysts (e. g. H-Y (30)) which appear less able to facilitate the second dehydration, resulting in high selectivity toward 1,4-sorbitan. Based on these findings, H-β (38) was selected as primary catalyst to perform the sorbitol dehydration reaction. To better understand the performance of H-β (38) and identify how the choice of conditions affects catalyst productivity a condition optimisation study was performed in batch reactors employing H-β (38) as catalytic material.

4.3.3 Conditions optimisation with H-β (38) in batch reactors

From the last catalyst performance screening, the zeolite H-β (38) resulted to be, at equal reaction conditions, the best material able to favour the production of isosorbide, in agreement with previous works.[21] In fact, at the reaction conditions employed, H-β (38) entirely converted the substrate sorbitol reporting isosorbide and 1,4-sorbitan yields of 30% and 11%, respectively. Therefore, in order to maximize the production of isosorbide, the catalytic activity of this promising material was studied more intensively. Although during the catalyst screening H-β (38) provided 100% sorbitol conversion, in the process of studying a catalytic reaction it is good practise to use a catalyst amount which does not lead to a full conversion of the substrate, otherwise the catalytic activity of the studied material can be underestimated. Moreover, operating at reaction conditions that return high or maximal conversion values does not allow the intrinsic kinetic behaviour of the catalyst to be correctly evaluated.[42] Therefore, the amount of H-β (38), employed for the dehydration reaction, was decreased from 3.25 g to 0.25 g to find the optimal mass of catalyst to be used during the catalytic study. Hence, several dehydration reactions were performed employing different amounts of catalyst and in otherwise identical conditions (Figure 9).

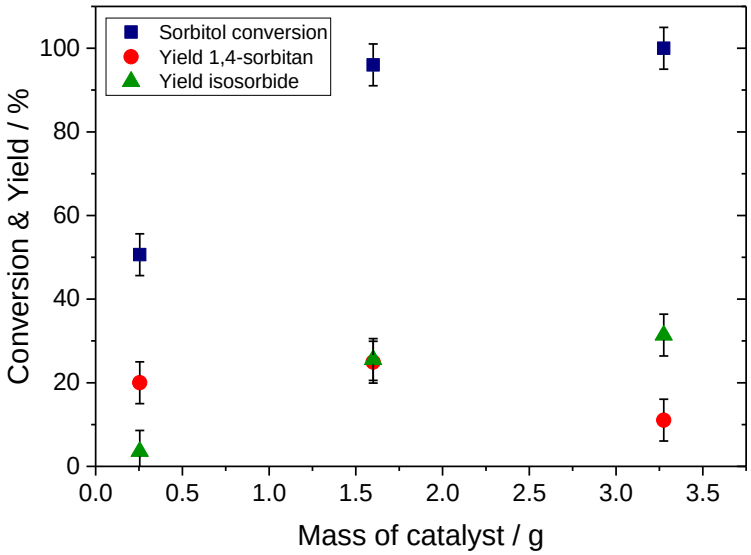

Figure 9 Sorbitol dehydration reaction performed with different amounts of H-β (38). Reaction condition: 20 mL of sorbitol 5 wt.% aqueous solution, 1 hour, 200°C, 800 rpm, autogenic pressure.

By decreasing the mass of catalyst from 3.25 g ($moles_{acid\ sites}/moles_{sorbitol}$ = 0.5) to 1.60 g ($moles_{acid\ sites}/moles_{sorbitol}$ = 0.25) the resulted sorbitol conversion can be considered unvaried within the experimental error of ± 5%. This result suggests that over 1.60 g the whole mass of catalyst is not promoting the sorbitol dehydration, making useless a portion of catalyst present in the reaction environment. Furthermore, it can be stated, that neither the isosorbide production is largely affected by the lower mass of H-β (38) employed, since only a slightly decrease from 30% to 27% of isosorbide yield is reported when the amount of catalyst is more than halved from 3.25 g to 1.60 g. Since the mass of the catalyst is directly correlated to the amount of acid sites present in the reaction environment, this plot also indicates that using too large amounts of H-β (38), some of its acid sites are not exploited in the conversion of the substrate and so, do not contribute to the reaction outcome. Of course, for the optimisation of a catalytic process, conditions in which an excess of catalyst is used must be avoided. In fact, in this way, not only precious material is wasted but the extra active sites present in the reaction environment might favour consecutive or side-reactions, especially when highly functionalised substrates are used, such as in the case of biomass-derived compounds. Conversely, if the mass of catalyst is further reduced to 0.25 g, the sorbitol conversion decreases from 96% to 51% and the isosorbide yield is reduced from 26% to 4% indicating that the whole amount of the zeolite actively participates to the reaction. For such reason, 0.25 g ($moles_{acid\ sites}/moles_{sorbitol}$ = 0.04) of zeolites H-β (38) were used in the following catalytic tests performed in batch conditions. In particular, to identify the evolution of the sorbitol dehydration reaction over the reaction time, several dehydration reactions were performed in batch reactors at increasing reaction time (Figure 10).

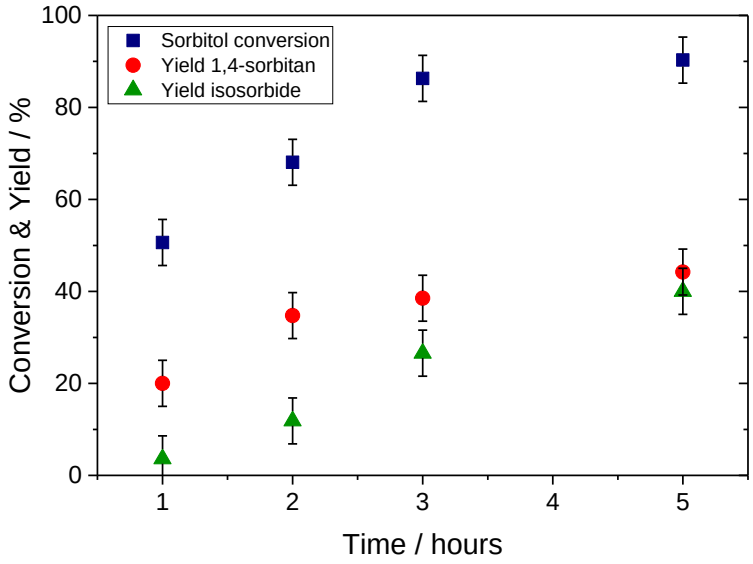

Figure 10 Time online of sorbitol dehydration assisted by H-β (38). Reaction performed in autoclave with 20 mL of sorbitol 5 wt.% aqueous solution, 0.25 g of catalyst, 200°C, 800 rpm, autogenic pressure.

From the time online evaluation obtained it can be noted the sharp linear relationship between isosorbide yield and reaction time, since extending the reaction time from 1 to 5 hours, the isosorbide yield progressively increases from 4 to 40%. Conversely, 1,4-sorbitan yield demonstrates a weaker dependence to the reaction time, since already at the first hour of reaction it showed a 20% value, reaching then in a gentler manner only a 44% value in 5 hours of reaction. It must be noted that, also when the dehydration reaction is assisted by the aluminosilicate catalyst, substantial isosorbide yields are achieved only at maximal conversion of sorbitol. In fact, during the last two hours of reaction sorbitol conversion only increases from 86% to 90%, and 1,4-sorbitan yield from 38% to 44%, whereas isosorbide yield strongly enhances from 26% to 40%. Accordingly, this trend suggests that even with zeolite catalysts, harsh reaction conditions must be adopted to selectively produce isosorbide from sorbitol, such as long reaction times, high temperatures, or large amounts of catalyst that in addition to decrease the efficiency of the process might degrade the fragile renewable substrate. One of the possible reasons for the difficult production of isosorbide is the aqueous media in which the reaction was conducted. Indeed, the huge amount of water present in the reaction environment could rehydrated isosorbide favouring the hydrated compound 1,4-sorbitan or even sorbitol. Indeed, since water is the main co-product of the dehydration reaction, when present in large amount in the reaction environment, it may shift the thermodynamic equilibrium toward the reagent, in this case sorbitol and 1,4-sorbitan. The detrimental role of water when present in the reaction environment may be further supported by the decreased

isosorbide yield obtained when using aluminium-rich zeolites, which are more hydrophilic.[21, 30] For example, a drop in isosorbide yield from 31% to 22% was observed when replacing H-β (38) with H-β (25) (Figure 8). Therefore, to avoid the aqueous media, it was explored methanol as solvent for the sorbitol dehydration. To have a whole comprehension of the effect of methanol on the reaction outcome different methanol aliquots were added to the reaction aqueous solvent. Due to the lower sugar solvating properties of methanol when compared to water, and its higher vapour pressure, these reactions were performed with a 3.2 wt.% sorbitol solution at 170°C, differing from the previous tests conducted in water with 5 wt.% sorbitol solution at 200°C. Progressive additions of methanol to the reaction solvent resulted to be beneficial for sorbitol conversion and isosorbide selectivity only when the ratio MeOH/H_2O exceed 50%. In particular it can be stated that water acts as a real detrimental element for the dehydration reaction since only a 10% of its presence reduce the sorbitol conversion from 95% to 76% and especially impoverish isosorbide selectivity from 47% to 14% (Figure 11).

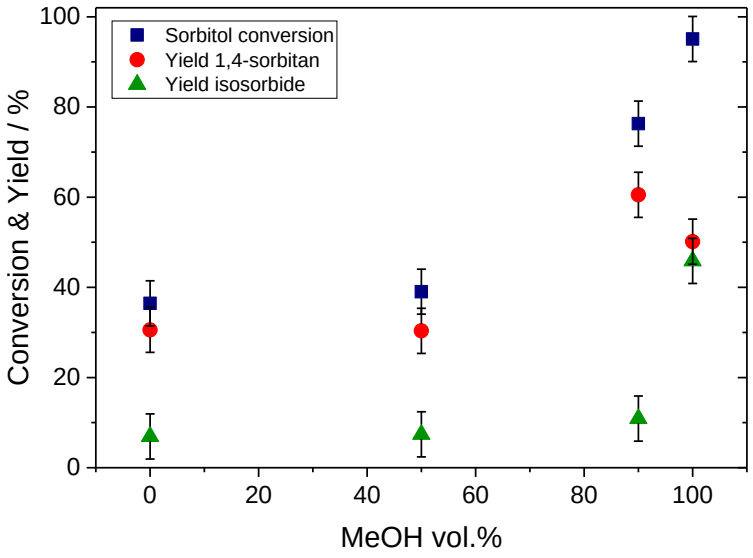

Figure 11 Effect of MeOH concentration in the reaction solvent. Reaction conditions: 3.2 wt.% sorbitol in MeOH/H_2O of various ratios, 20 mL volume, 0.25 g of H-β (38), 5 hours, 170°C, 800 rpm, autogenic pressure.

The substantial improvement in isosorbide yield detected following removal of water (100% MeOH, Figure 11) supports the hypothesis that water inhibits the consecutive dehydration of 1,4-sorbitan to isosorbide. In addition to the improved catalytic performance observed in methanol, replacing aqueous media with this solvent is also favoured for industrial scale application, since its lower enthalpy of vaporisation facilitates downstream separation and recovery of isosorbide. Use of methanol as reaction solvent instead of water also results in higher yields even at milder reaction conditions. Indeed, 45% isosorbide yield was achieved in methanol at 170°C, whilst only 7% of isosorbide yield was observed in water at 170°C at the same reaction time of 5 hours (Figure 11).

The productivity enhancement observed in methanol constitutes a major improvement for the development of a continuous dehydration system, as it allows satisfactory isosorbide yield to be achieved in reduced reaction times and hence, contact times during continuous operation. Accordingly, pure methanol was used as solvent for the remainder of the study.

4.3.4 Continuous reaction

Following the preliminary investigation performed in batch reactors on the reaction conditions and on the catalyst materials, continuous operation of the sorbitol dehydration reaction was explored in a Plug Flow Reactor (PFR). Understanding the kinetic relevance is a basic requirement for the good optimization of continuous systems, since it could lead to great improvements to the process productivity (see Chapter 1). Therefore, preliminary experiments focused on ensuring kinetic relevance of the PFR reactor, ruling out possible external and internal transfer limitations.[42, 51] Hence, a PFR lab scale reactor was constructed by packing a defined amount of H-β (38) inside a ¼ inch stainless steel tube and flowing through it a sorbitol methanol solution (feed). Moreover, to avoid flow obstruction by the catalyst bed, the zeolite was previously pelletised in a uniform 60-100 μm diameter grains. The linear velocity of the substrate solution inside the catalyst bed can be varied modifying the flow of the solution feed pumped through the reactor. Hence, in order to investigate the kinetic relevance of the reaction, a range of reactor columns containing different amounts of catalyst were prepared, and the activity of each was monitored at a fixed contact time (tau, τ Equation 9, Chapter 1) by scaling the flow rate appropriately. Additionally, for each specific mass of catalyst, the substrate flow rate was also varied during the reaction, to generate contact time profiles. However, to correctly evaluate the phenomena, the sorbitol conversion values achieved at different linear velocities were compared at the same contact time, τ (Figure 12 black dashed line).

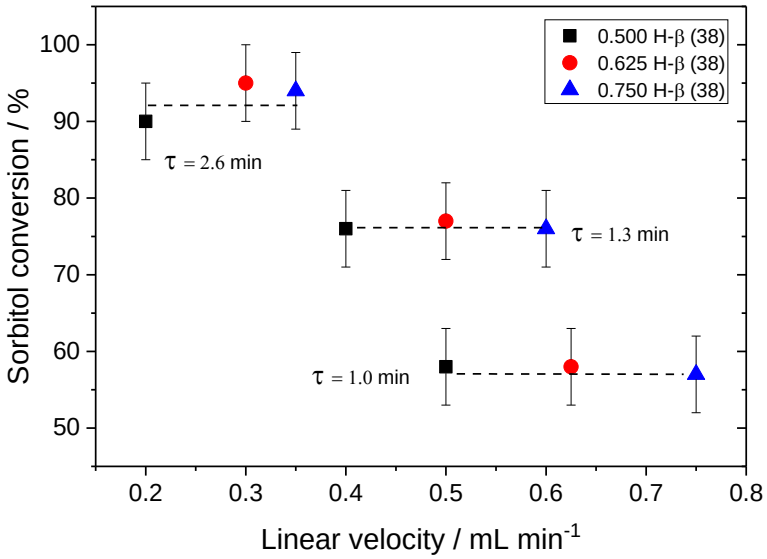

Figure 12 External diffusion limitation study. Each reaction was performed by adjusting the mass of catalyst and flow of sorbitol (3.2 wt.% in MeOH) to maintain a fixed contact time, at 200°C, 40 bar back pressure.

As shown in Figure 12, no substantial variation of sorbitol conversion was observed at different substrate linear velocities, considering the experimental error of ± 5%. Therefore, the effect of external diffusion limitation can be considered negligible for substrate flow rates down to 0.20 mL min^{-1}, ensuring kinetic relevance of the reactor.

As a resistance effect on the reaction rate, it must be considered also the internal diffusion limitation that may occur when substrate molecules find difficulties to diffuse inside large catalyst particles.[42, 51] It follows that for bigger catalyst particles the internal diffusion resistance is greater, which may negatively affect the substrate conversion. On the other hand, in continuous processes, it is discouraged working with too fine particles that might lead to backmixing phenomena or to blockages of the substrate solution flow. Furthermore, if some carbonaceous by-products are formed throughout the reaction, smaller the catalyst particles higher the probability for these carbon compounds to be trapped inside the catalyst bed, so greater the catalyst deactivation or the occlusion failure. Hence, to optimise the continuous operation, the biggest catalyst particles that do not induce conversion decreasing must be found. Therefore, a kinetic study was performed using identical catalyst masses and reactant flow rates, but varying the average particle size of H-β (38).

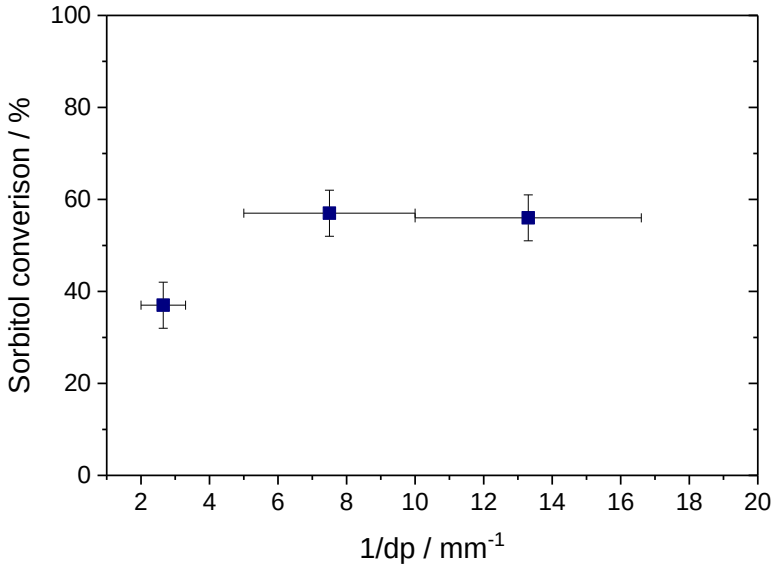

Figure 13 Internal diffusion limitation study. Each reaction was performed with 0.75 g of H-β (38), 0.75 mL min^{-1} of 3.2 wt.% sorbitol in MeOH at 200°C, 40 bar back pressure using catalyst particle size from 60 to 500 µm. 1/dp refers to 1/diameter of the catalyst particles (1/mm).

From Figure 13 it can be observed that with catalyst particles of diameter 60-100 µm, which correspond to a 1/dp (diameter of the particle) value of 12.5 mm^{-1}, 56% of sorbitol conversion was achieved. This value of conversion is constant if the particle diameter is increased to 100-200 µm, but rapidly decrease to 36% if particle diameters of 300-500 µm are adopted. It is clear that internal diffusion limitation phenomena start to occur with a catalyst pellets size over 200 µm. In this circumstance, the substrate molecules struggle to reach the inner core of the pellets and thus the whole amount of catalyst inserted in the bed of the reactor is not fully exploited to convert sorbitol. Accordingly, all further experiments were conducted with catalyst particles between 60-100 µm.

Following optimisation of the kinetic parameters of the reaction, the effect of contact time on the progress of the dehydration reaction was investigated. In this case, continuous reactions were conducted using 0.750 g of catalyst in order to achieve longer contact times (≤8 mins) whilst avoiding linear velocities low enough to induce external diffusion limitation (Figure 12).

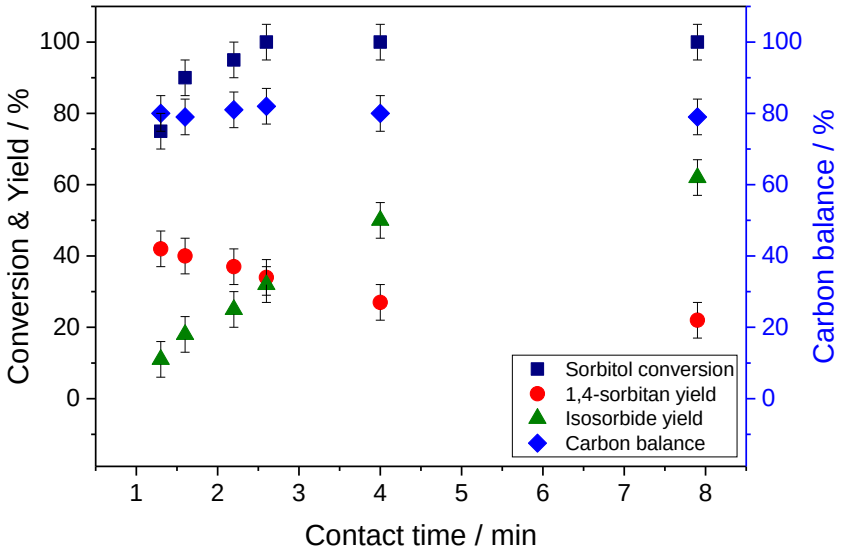

Figure 14 Sorbitol dehydration at different contact time. Each reaction was performed with fresh catalyst, 0.750 g of H-β (38) 60–100 μm, 3.2 wt.% sorbitol in MeOH at different flow rates, 200°C, 40 bar back pressure.

As observed in Figure 14, increasing the contact time was beneficial for the second step of the reaction, resulting in improved yield and selectivity to isosorbide, in agreement with the time online analysis performed on the batch process (Figure 10). In all cases, enhanced isosorbide yield was achieved without affecting the overall carbon balance, an interesting aspect for the isosorbide industrial production. Notably, the carbon balance of 80% observed at all contact times indicates that carbon balance was lost from competing reaction pathways, likely due to the formation of several by-products such as, 1,5-anhydrosorbitol, 2,5-anhydromannitol, isomannide and isoidide, small quantities of which have previously been detected.[25, 39, 40]

Having benchmarked the impact of contact time, continuous sorbitol dehydration was subsequently performed for an extended reaction period to evaluate catalyst stability. For this study, a contact time of 2.6 min was chosen. Although this contact time limited the selectivity towards isosorbide (as shown in Figure 14), maintaining conversion values below 100% ensured an excess catalyst regime was avoided, thereby allowing any potential deactivation events to be immediately detected. Indeed, in the presence of excess catalyst, a significant amount of deactivation might occur before the reaction conversion decreases below 100%.[42] Building on the previous kinetic studies (Figure 12), 0.50 g of catalyst and a flow rate of 0.20 mL min^{-1} were chosen to achieve the desired contact time, so as to balance linear velocity requirements and reactor pressure drop. In order to let the system equilibrate after reaction starting, first reaction points were collected after 2 hour the feed was injected into the reactor.

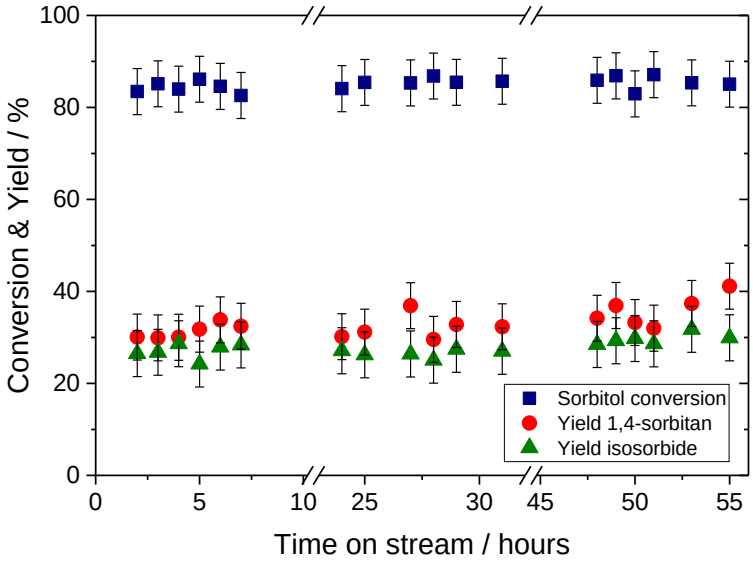

Figure 15 Continuous sorbitol dehydration. The reaction was performed in a PFR at a flow rate of 0.20 mLmin^{-1} of 3.2 wt.% sorbitol in MeOH through 0.500 g of H-β (38) (60–100 μm). Contact time of 2.6 min, at 200°C and 40 bar back pressure.

At these conditions, continuous dehydration of sorbitol was successfully achieved (Figure 15) at mild temperature, achieving 82% sorbitol conversion and an average of 28% isosorbide yield. It should be noted that H-β (38) exhibited excellent stability for the entire reaction progress (55 hours), differently from other catalysts employed in continuous gas-phase reactions, which begin to lose activity during the first hours of reaction.[33] A total isosorbide productivity of 9670 $g_{isosorbide}/kg_{catalyst}$ was achieved over 55 hours, greater than those achieved in the gas-phase continuous systems (Table 1),[31-36] thus showing the benefits of liquid phase continuous operations for isosorbide production. However, we note that this value is an underestimation of the potential productivity of the system, since deliberately limiting the reactor to <100% conversion decreases the isosorbide selectivity (vide supra), and the good stability observed suggest longer term operational to be feasible, which would further boost the productivity values obtained during continuous operation.

Table 1. Comparison of performance for previously investigated continuous systems for sorbitol dehydration.

catalyst	catalyst weight / g	Type of reactor	Temp. / °C	Time on stream / h	stability	sorbitol conversion / %	isosorbide yield / %	isosorbide production $g_{isosorbide}$ / $g_{catalyst}$	Ref.
H-β (38)	0.5	liquid-phase PFR	200	55	stable up to 55 h	85	28	9.67	this work
CuSO	1.5	vapour-phase fixed bed	250	4	not reported	100	48	0.502	31
30% PW[a]/SiO_2	0.5	vapour-phase fixed bed	250	6	not reported	96	54	1.30	32
SnPO	0.5	vapour-phase fixed bed	300	22	conversion decreases after 1 h	72	47	1.96	33
H_3PO_4 modified Ta_2O_5	0.5	vapour-phase fixed bed	225	6	not reported	98	47	1.44	35
H_3PO_4 modified Nb_2O_5	0.5	vapour-phase fixed bed	225	5	activity and selectivity decrease after 5 h	100	63	1.55	34
$NbOPO_4$	2.0	vapour-phase fixed bed	220	60	unknown because of conversion > 100%	100	50	2.12	36

[a] PW = $H_3PW_{12}O_{40}$

4.3.5 Catalyst characterization

As previously mentioned, stability is an essential feature for industrial applicability of catalysts, since it is translated in reduced amount of catalyst used, in enhanced purity product, in less intensive downstream operations and thus, in massive economic and sustainability advantages. However, it is well known, that during the chemical process catalysts may suffer some chemical or physical transformations that might affect their long-term stability (see Chapter 1). For such reason, it is crucial to investigate the integrity of the catalyst after the chemical reaction in order to detect eventual incipient deactivation phenomena. For example, although H-β (38) preserved its catalytic performance for 55 hours on stream (Figure 15), prolonged operational time might induce gradual changes to the catalyst, which may later contribute to deactivation over longer reaction periods. For

example, the high pressure exerted inside the continuous process might damage the crystallinity structure of the aluminosilicate materials thus decreasing their catalytic performances. In fact, from kinetic studies alone, structural changes to the catalyst or deposition of carbonaceous residues cannot be excluded. Therefore, to further understand the stability of H-β (38) during continuous isosorbide dehydration, characterisation of the catalyst after 55 hours on stream was undertaken. To ensure structural integrity of the zeolite framework after reaction, X-Ray Diffraction (XRD) analysis was performed on the used catalyst, in addition to control samples (i.e. fresh H-β (38) and H-β (38) treated in MeOH: 0.25 $mLmin^{-1}$, 200°C, 24 hours, 40 bar).

Table 2. Full width at half maximum (FWHM) of XRD patterns of Fresh, MeOH treated and Used H-β (38) and calculated relative crystallinity.

peak / 2Θ degree	**FWHM**			**Relative crystallinity[a]**	
	Fresh H-β (38)	MeOH treated H-β (38)	Used H-β (38)	MeOH treated H-β (38)	Used H-β (38)
7-8	1.071	1.095	1.109	1.022	1.035
22-23	0.583	0.562	0.578	0.963	0.991

[a] relative crystallinity = $\frac{\mathrm{FWHM}^{2\Theta=n}_{\mathrm{catalyst}}}{\mathrm{FWHM}^{2\Theta=n}_{\mathrm{Fresh\ catalyst}}}$

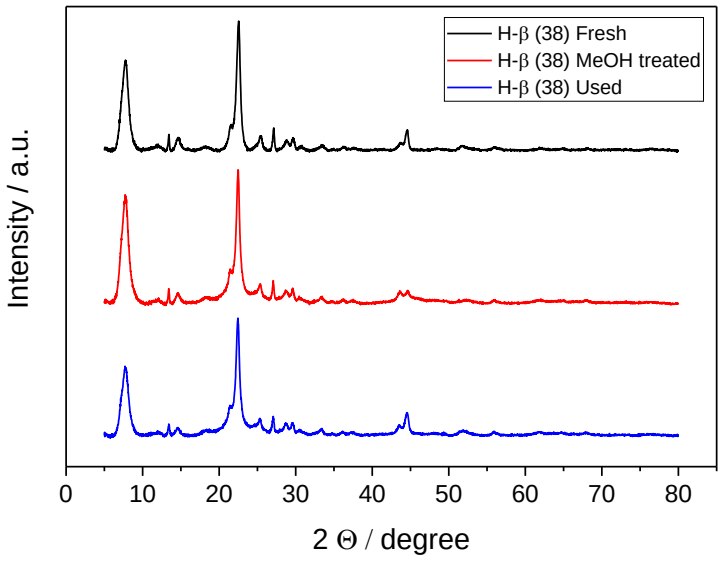

Figure 16 XRD diffraction patterns of fresh (top), MeOH treated (middle) and used (bottom) H-β (38). MeOH treated catalyst conditioned with 0.25 mLmin^{-1} of MeOH at 200°C, 24 hours, 40 bar. Used catalyst conditions: 0.25 mL min^{-1} 3.2 wt.% sorbitol MeOH solution, 200°C, 40 bar, substrate turnover = 127.

XRD analysis of the fresh and used catalysts, and the control sample treated in MeOH, revealed no changes in the XRD pattern of these samples, confirming that the zeolite preserves its crystalline structure even after 55 hours of reaction (Table 2 and Figure 16).

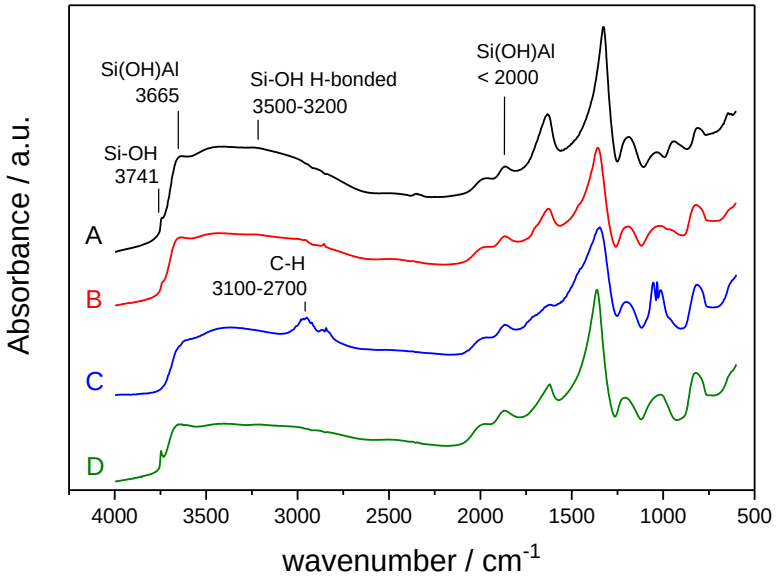

Figure 17 IR spectra of A) fresh, B) MeOH treated (24 h, 0.25 mL min^{-1} MeOH, 200°C, 40 bar), C) used and D) regenerated (6 h, 650°C, 5°C/min, air) H-β (38) (60–100 µm). Reaction conditions of used catalyst: 0.25 mL min^{-1} 3.2 wt.% sorbitol in MeOH, 200°C, 40 bar back pressure, substrate turnover = 127.

Diffuse Reflectance Infrared Fourier Transformation (DRIFT) analysis of the samples was also performed (Figure 17). As expected, the IR spectrum of fresh catalyst (Figure 17) showed the characteristic absorption bands of silanol groups and bridged Brønsted acid sites at 3741, 3665 and 3500-3200 cm^{-1}.[58-61] Specifically, the absorbance narrow band at 3741 cm^{-1} can be attributed to the ν(OH) stretching of the terminal Si-OH group.[58] At 3665 cm^{-1} can be noted a narrow band assigned to the ν(OH) stretching of the Si(Al)OH Brønsted sites.[58] Whereas the broad absorption between 3500-3200 cm^{-1} can be due to the presence of the ν(OH) bonds of Si-OH groups H bonded, which width and intensity depends on the water amount absorbed by the zeolite.[59] The absorption between 2000-700 cm^{-1} instead, can be assigned to the ν(OH) stretching and δ(OH) bending of the Si(OH)Al groups, typical of the aluminosilicates Brønsted material.[60, 61] In addition to these absorption bands characteristic of aluminosilicate materials, the IR spectrum of the used catalyst exhibited a new band in the range 3100-2700 cm^{-1}, which could be attributed to the presence of carbonaceous species retained by the catalyst during operation (coke).[62] To verify the carbonaceous nature of such species, the used catalyst was calcined in air at 650°C for 6 hours with a ramp rate of 5°C min^{-1}, and denoted for simplicity as regenerated catalyst. The IR spectrum of the regenerated catalyst did not show vibrations associated with C-H stretches, confirming that during the heat treatment the carbonaceous species trapped on the catalyst were removed, thus restoring the pristine catalyst.

However, TGA analysis of the fresh and used catalysts suggested that the total quantity of carbonaceous residue deposited during reaction was very low, which likely accounts for the high level of stability exhibited by the catalyst (Figure 18).

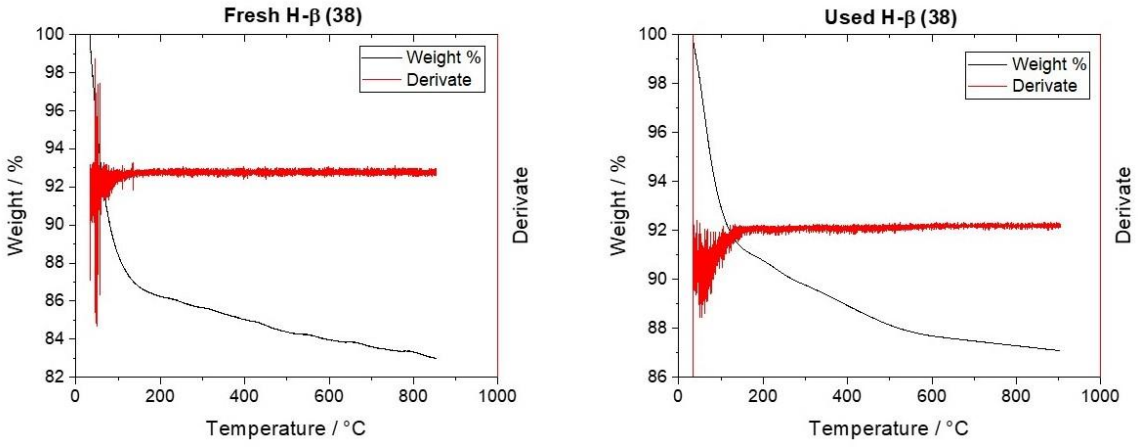

Figure 18 Thermogravimetric profile of (Left) Fresh and (Right) Used H-β (38). Analysis condition: air 50 mL min^{-1}, 30-850°C, 5°C min^{-1} ramp rate.

To investigate whether the small amount of carbonaceous residue detected on the used catalyst was generated as a consequence of the solvent or the substrate, H-β (38) was treated with a 0.25 mL min^{-1} flow of MeOH for 24 hours at 200°C and 40 bar (in the absence of the substrate), and subsequently dried overnight. The IR spectrum of the MeOH treated catalyst exhibited the same absorptions of the fresh catalyst but no band in the C-H region, confirming that the band at 3110-2750 cm^{-1} relates to formation of carbonaceous species arising from reactive components of the system (reactants, (by)-products), and not simply the solvent (Figure 17). In order to investigate coke formation during the reaction, the used catalyst was recovered at different stages of the continuous process, notably after 21 and 146 substrate turnovers, and characterised via porosimetry analysis (we note for reference that the total number of turnovers after 55 hours was 211). The DFT surface area of the catalyst decreased rapidly at increasing levels of substrate turnover (Table 3). Indeed, after only a short time on stream (21 turnovers) the catalyst surface area was already reduced to 75% of its initial value, decreasing further to 28% of the initial value after extended times on stream (146 turnovers). The micropore volume of the catalyst was equally affected during continuous operation (Table 3).

Table 3. Surface Area and Porosimetry Data Obtained by Nitrogen Adsorption Isotherm Analysis[a]

Entry	Sample	S_{NLDFT} / $m^2\ g^{-1}$	S_{micro} / $m^2\ g^{-1}$	S_{meso} / $m^2\ g^{-1}$	V_{micro} / $mL\ g^{-1}$
1	Fresh pelletised	724	641	83	0.15
2	Used (21 st[b])	543	462	81	0.10
3	Used (146 st[b])	202	128	74	0.04
4	Regenerated	612	530	82	0.14

[a]All values calculated by applying the DFT method to the nitrogen adsorption isotherms (77 K). [b]Substrate turnovers.

Porosimetry analysis further demonstrated the efficiency of the heat treatment to remove the carbonaceous residues from the zeolite pores, in accordance to the IR analysis. In fact, after the thermal treatment, the surface area and micropore volume of the framework were almost fully restored. These findings suggest that deposition of carbonaceous residue causes fouling of the catalyst during continuous operation, either through accumulation in the micropores, or by deposition on the surface and/or interparticle voids. However, despite the changes in porosity described in Table 3 and the formation of carbonaceous species on the catalyst (Figure 17), no loss of catalytic activity was observed at long reaction time (Figure 15). This excludes fouling as being a major contributor to the catalyst deactivation over the reaction period presented in Figure 15.

4.4 Conclusion

In this work, the feasibility of performing sorbitol dehydration to isosorbide over heterogeneous catalysts in continuous liquid-phase reactors was explored. Building on previous biomass upgrading works, Amberlyst 15 was selected as suitable material to preliminary study the sorbitol dehydration reaction in batch systems. Although the promising activity showed by this acid catalyst in converting sorbitol, a hot-filtration experiment revealed poor stability of the polymeric resin when employed at the high temperatures required by the dehydration reaction to obtain satisfactory isosorbide yield. Therefore, different zeolite catalysts were screened with the purpose to find a resistant active material for sorbitol dehydration. Amongst a range of zeolites with different shape and acidity, H-β (38) zeolite exhibited the best catalytic performance and was therefore identified as the most suitable material for continuous applications. A preliminary batch investigation of this reaction also demonstrated that aqueous reaction environments inhibit the full dehydration of sorbitol to isosorbide. Substitution of the aqueous reaction media with methanol increased isosorbide yield to a maximum of 46%, despite operating at milder conditions (170 °C). Diagnostic kinetic studies performed on the continuous system indicated that diffusion limitations are negligible for flow rates of 0.20 mL min^{-1} and above, and catalyst particle sizes smaller than 250 μm. Optimisation of the continuous reactor allowed isosorbide yields of up to 60% to be obtained without compromising the overall carbon balance. A long-term kinetic experiment performed at conditions suitable for deactivation studies (sub-maximal conversion) was successfully performed over H-β (38) zeolite in a plug flow reactor. Over a 55 hours period of continuous operation, no loss of activity was detected, demonstrating the excellent stability of the catalyst. The high catalyst stability, together with the good isosorbide yield reached in the continuous liquid-phase system, allowed an isosorbide production of 9.67 $g_{isosorbide}/g_{catalyst}$ to be achieved. This value is the best production value achieved by a continuous sorbitol dehydration reaction system to date (Table 1), and was achieved despite the reaction being deliberately performed at sub-maximal conversion, was undertaken at temperatures at least 50°C lower than previous reports, and was terminated prior to the catalyst experiencing any loss of activity. Although no loss of activity was observed up to 55 hours of time on stream, characterisation analyses performed on both fresh and used catalyst revealed coke deposition on the postreaction catalyst. However, the total quantity of carbonaceous residue as determined by TGA was negligible, and since no loss of activity accompanied this deposition, catalyst fouling cannot be considered as a major reason of deactivation over this reaction timeframe. Moreover, heat treatment of the used catalyst was found to be an efficient method to almost completely restore the initial material, removing the carbonaceous species deposited on the catalyst throughout reaction.

In the introduction of this thesis (Chapter 1) it has been illustrated that heterogeneous catalysts technologies have been one of the most exploited solutions over the last century to upgrade fossil-based feedstock to platform molecules for the production of chemical commodities. Therefore, a wide knowledge is currently available on such materials and strong developments have been performed over the century on heterogenous catalysed processes to achieve maximum efficiency and productivities. For this reason, heterogeneous catalysts have been thoroughly explored over the last decades as potential materials also to upgrade biomass-derived substrates, thus, to exploit the already designed industrial engineering solutions to process fossil feedstock. However, this chapter demonstrate that as consequence of the different chemical nature of biomass-derived compounds to the fossil ones, the engineering solutions developed over the last century to maximise productivity of fossil-based processes are not suited for the new renewable substrates. For example, most of the zeolite catalysed industrial processes which upgrade crude oil are gas-phase based,[63-65] due to high stability that the catalyst shows under such reaction conditions and to easy recovery of the final product. However, in this chapter has been demonstrated that gas phase approaches, although to the best of my knowledge the only continuous solution explored in literature to dehydrate sorbitol, are not the best option to process biomass-derived compounds. In fact, if the whole catalytic process for sorbitol dehydration is redesigned employing a liquid-phase, more appropriate to the chemical nature of biomass-derived compounds, enhanced process productivities can be achieved. Therefore, if competitive processes and thus inexpensive products are wanted to be generated from biomass-derived molecules, the development of the catalytic process needs to be fully redesigned and tailored accordingly to new biomass substrates requirements. For this reason, although over the last decades extensive research on biomass valorisation have been conducted, there still might be promising solutions that have not been properly investigated from an intensification perspective and thus may not appear to be competitive with the current fossil-based technologies. Therefore, in light of the current environmental emergency of switching from fossil to renewable resources, intensification studies also on lab scale are becoming much more crucial. Furthermore, in this chapter it emerged how the achievement of improved process productivities is the results of the synergic optimisation of every aspect of the chemical reactions. In fact, in order to obtain a more efficient process to continuously dehydrate sorbitol many aspects of the process have been addressed and studied. Starting from the exploration of a more suitable phase in which to process the feedstock, to the selection of the more appropriate catalyst to develop the continuous system, to the screening of more efficient reaction solvents and to the optimisation of fluid dynamic conditions which return more efficient processes.

4.5 References

1) B. Török, T. Dransfield, *"Green Chemistry: An inclusive approach"*, Elsevier, 2017, 211.
2) A. Berg, K. Findell, B. Lintner, A. Giannini, S. I. Seneviratne, B. van den Hurk, R. Lorenz, A. Pitman, S. Hagemann, A. Meier, F. Cheruy, A. Ducharne, S. Malyshev, P. C. D. Milly, *Nat. Clim. Change*, 2016, **6**, 869.
3) S. C. Doney, V. J. Fabry, R. A. Feely, J. A. Kleypas, *Annu. Rev. Mar. Sci.*, 2009, **1**, 169.
4) M. Fitzpatrick, P. Champagne, M. F. Cunningham, R. A. Whitney, *Bioresour. Technol.*, 2010, **101**, 8915.
5) R. J. Henry, *Plant Biotechnology Journal*, 2010, **8**, 288.
6) A. Corma, S. Iborra, A. Velty, *Chem. Rev.*, 2007, **107**, 2411.
7) H. Kobayashi, A. Fukuoka, *Green Chem.*, 2013, **15**, 1740.
8) J. J. Bozell, G. R. Petersenb, *Green Chem.*, 2010, **12**, 539.
9) J. Zhang, J. Li, S. Wu, Y. Liu, *Ind. Eng. Chem. Res.*, 2013, **52**, 11799.
10) T. Werpy, G. Petersen, "*Top Value Added Chemicals From Biomass*", 2004, **1**.
11) N. Rey-Raap, L. Sousa Ribeiro, J. J. de Melo Orfao, J. L. Figueiredo, M. F. Ribeiro Pereira, *Appl. Catal. B,* 2019, **256**, 117826.
12) C. Dussenne, T. Delaunay, V. Wiatz, H. Wyart, I. Suisse, M. Sauthier, *Green Chem.*, 2017, **19**, 5332.
13) F. Fenouillot, A. Rousseau, G. Colomines, R. Saint-Loup, J. P. Pascault, *Prog. Polym. Sci.*, 2010, **35**, 578.
14) M. Yokoe, K. Aoi, M. Okada*, J. Polym. Sci.*, 2005, **43**, 3909.
15) J. N. Cohn, G. Johnson, S. Ziesche, F. Cobb, G. Francis, F. Tristani, R. Smith, W. B. Dunkman, H. Loeb, M. Wong, *N. Engl. J. Med.*, 1991, **325**, 303.
16) M. Rose, R. Palkovits, *ChemSusChem*, 2012, **5**, 167.
17) F. W. Lichtenthaler, *"Occurrence, Structures and Chemistry"*, Ullmann's Encyclopedia of Industrial Chemistry, 2010, 617.
18) B. Kamm, P. R. Gruber, M. Kamm, *"Biorefineries Industrial Processes and Products"*, Ullmans Encyclopedia of Industrial Chemistry, 2015, 1.
19) H. Schiweck, A. B. Roland Vogel, E. Schwarz, M. Kunz, C. Dusdutois, A. Clement, C. Lefranc, B. Lüssem, M. Moser, S. Peters, *"Sugar Alcohols"*, Ullman's Encyclopedia of Industrial Chemistry, 2012, 1.
20) A. A. Dabbawala, D. K. Mishra, G. W. Huber, J. Hwang, *Applied Catalysis A: General*, 2015, **492**, 252.
21) H. Kobayashi, H. Yokoyama, B. Feng, A. Fukuoka, *Green Chem*., 2015, **17**, 2732.
22) A. A. Dabbawala, D. K. Mishra, J. Hwang, *Catalysis Communications*, 2013, **42**, 1.
23) A. Nazmul, A. K. Dinesh, K. Mishra, J. S. Lee, J. Hwang, S. H. Jhung, *Chemical Engineering Science,* 2013, **93**, 91.
24) N. A. Khan, D. K. Mishra, I. Ahmed, J. W. Yoon, J. Hwang, S, H. Jhung, *Applied Catalysis A: General*, 2013, **452**, 34.
25) J. Shi, Y. Shan, Y. Tian, Y. Wan, Y. Zheng, Y. Feng, *RSC Adv.*, 2016, **6**, 13514.
26) M. J. Ginés-Molina, R. Moreno-Tost, J. Santamaría-González, P. Maireles-Torres, *Applied Catalysis A: General*, 2017, **537**, 66.
27) N. A. Khan, D. K. Mishra, J. Hwang, Y. Kwak, S. H. Jhung, *Res. Chem. Intermed.*, 2011, **37**, 1231.
28) M. Yabushita, "Acid-Catalyzed Dehydration of Sorbitol to 1,4-Sorbitan", Springer, 2016.
29) N. Li, G. W. Huber, *Journal of Catalysis*, 2010, **270**, 48.

30) R. Otomo, T. Yokoi, T. Tatsumi, *Chemical. Applied Catalysis A: General*, 2015, **505**, 28.
31) J. Xia, D. Yu, Y. Hu, B. Zou, P. Sun, H. Li, H. Huang, *Catalysis Communications*, 2011, **12**, 544.
32) P. Sun, D. H. Yu, Y. Hu, Z. C. Tang, J. J. Xia, H. Li, H. Huang, *Korean J. Chem. Eng.*, 2011, **28**, 99.
33) M. Gu, D. Yu, H. Zhang, P. Sun, H. Huang, *Catal. Lett.*, 2009, **133**, 214.
34) X. Zhang, D. Yu, J. Zhao, W. Zhang, Y. Donga, H. Huang, *Catalysis Communications*, 2014, **43**, 29.
35) Z. Tang, D. Yu, P. Sun, H. Li, H. Huang, *Bull. Korean Chem. Soc.*, 2010, **31**, 3679.
36) J. Xi, Y. Zhang, D. Ding, Q. Xia, J. Wang, X. Liu, G. Lu, Y. Wang, *Applied Catalysis A: General*, 2014, **469**, 108.
37) J. Lange, *Angew. Chem. Int. Ed*., 2015, **54**, 13186.
38) C. H. Bartholomew, *Appl. Catal. A*, 2001, **212**, 17.
39) A. Yamaguchi, N. Hiyoshi , O. Sato, M. Shirai, *Green Chem.*, 2011, **13**, 873.
40) R. M. de Almeida, J. Li, C. Nederlof, P. O'Connor, M. Makkee, J. A. Moulijn, *ChemSusChem*, 2010, **3**, 325.
41) J. Li, A. Spina, J. A. Moulijn, M. Makkee, *Catal. Sci. Technol*., 2013, **3**, 1540.
42) C. Hammond, *Green Chem.*, 2017, **19**, 2711.
43) E. Taarning, C. M. Osmundsen, X. Yang, B. Voss, S. I. Andersen, C. H. Christensen, *Energy Environ. Sci.*, 2011, **4**, 793.
44) R. Rinaldi, F. Schüth, *ChemSusChem*, 2009, **2**, 1096.
45) X. Zhang, K. Wilson, A. F. Lee, *Chem. Rev.*, 2016, **116**, 12328.
46) P. Lanzafame, D. M. Temi, S. Perathoner, A. N. Spadaro, G. Centi, *Catal. Today*, 2012, **179**, 178.
47) I. Delidovich, K. Leonhard, R. Palkovits, *Energy Environ. Sci.*, 2014, **7**, 2803,
48) T. Ennaert, J. V. Aelst, J. Dijkmans, R. De Clercq, W. Schutyser, M. Dusselier, D. Verboekend, B. F. Sels, *ChemSocRev.*, 2016, **45**, 584.
49) C. O. Tuck, E. Pérez, I. T. Horváth, R. A. Sheldon, M. Poliakoff, *Science*, 2012, **337**, 695.
50) R. A. Sheldon, *Green Chem.*, 2014, **16**, 950.
51) C. Perego, S. Peratello, *Catalysis Today*, 1999, **52**, 133.
52) D. M. Alonso, J. M. R. Gallo, M. A. Mellmer, S. G. Wettstein, J. A. Dumesic, *Catal. Sci. Technol.*, 2013, **3**, 927.
53) M. Petrini, R. Ballini, E. Marcantoni, G. Rosini, *Synth. Commun.*, 1988, **18**, 847.
54) S. Dassy, H. Wiame, F. C. J. Thyrion, *Chem. Technol. Biotechnol.*, 1994, **59**, 149.
55) C. Aellig, I. Hermans, *ChemSusChem*, 2012, **5**, 1737.
56) D. Padovan, C. Parsons, M. S. Grasina, C. Hammond, *Green Chem.*, 2016, **18**, 50413.
57) P. F. Siril, H. E. Cross, D. R. Brown, *Journal of Molecular Catalysis A: Chemical*, 2008, **279**, 63.
58) R. Hajjar, Y. Millot, P. P. Man, M. Che, S. Dzwigaj, *Phys. Chem. C*, 2008, **112**, 20167.
59) C. Pazé, A. Zecchina, S. Spera, A. Cosma, E. Merlo, G. Spanò, G. Girotti*, Phys. Chem. Chem. Phys*., 1999, **1**, 2627.
60) C. Pazé, S. Bordiga, C. Lamberti, M. Salvalaggio, A. Zecchina, G. Bellussi, *J. Phys. Chem. B*, 1997, **101**, 4740.
61) A. Zecchina, G. Spoto, S. Bordiga, *Phys. Chem. Chem. Phys.*, 2005, **7**, 1627.
62) J. Cejka, N. Filková, B. Wichterlová, G. Eder-Mirth, J. A. Lercher, *Zeolites*, 1996, **17**, 265.
63) M. Stöcker, *Microporous and Mesoporous Materials*, 2005, **82**, 257.
64) C. R. Marcilly, *Topics in Catalysis*, 2000, **13**, 357.

65) S. Matar, L. F. Hatch, “Chemistry of petrochemical processes”, Gulf professional Publishing, 2001, 2.

Chapter 5 - Study of continuous fructose dehydration in MeOH/H_2O solvent media. An attempt to couple fructose dehydration with glucose isomerisation.

5.1 Introduction

In the previous study focused on isosorbide production from renewable feedstock, described in Chapter 4, use of an alcoholic solvent, such as MeOH, was pivotal for the development of an efficient continuous process to dehydrate sorbitol. In fact, replacement of the aqueous media, in which sorbitol dehydrations were usually conducted, with MeOH, led to an enhanced catalyst activity and selectivity, thus remarkably improving the productivity of the continuous process. Another dehydration reaction with large industrial interest for biomass upgrading, is fructose dehydration, since this process leads to promising platform molecules such as furanic-based compounds. As described in Chapter 1, furanics are a family of oxygenated 5-membered closed-ring compounds that can be converted into many derivates which find application in polymer science, industrial solvents and renewable fuels, amongst many other areas.[1-3] First of all is 5-hydroxymethylfurfural (HMF), obtained from the three-fold dehydration reaction of fructose (Scheme 1) which, in the last decade, has been refereed as the "sleeping giant" of renewable chemistry, due to its suitability to be converted in many industrial intermediates, including 2,5-furandicarboxylic acid (FDCA).[4] FDCA is a closed-ring bifunctional carboxylic acid considered as a potential renewable substitute of terephthalic acid, the primary monomer of polyethylene terephtalate (PET), which represent the most widely produced monomer in the bulk chemistry industry.[5, 6] Furthermore, using FDCA as monomer led to polymers with enhanced performances compared to terephthalic acid such as gas barrier properties and mechanical resilience.[7, 104] Moreover, HMF can be transformed into *p*-xylene, the fossil precursor of terephthalic acid, thus also allowing the production of a renewably-derived PET. To have an idea of the economic potential and sustainability impact that furanic compounds might have, it must be considered that only the demand of *p*-xylene is approximately 3 x10^7 t per year.[8] HMF is also a key intermediate in the production of promising resin cross-linkers such as 2,5-bis(hydroxymethyl)furan or 2,5-diformylfuran.[9, 10] In addition, the potential of HMF derivatives as solvents and fuels has been reported.[11] In fact, 2,5-dimethylfuran is an alternative biofuel, with a volumetric energy density comparable to gasoline. Other interesting compounds that are obtained from the consecutive rehydration reaction of HMF are levulinic and formic acid (Scheme 1).[12] In fact, levulinic acid is considered one of the top 10 building blocks derived from biomass[13, 14] since it can be employed as a precursor for the production of bio-solvents[15], monomers,[16-18] agrochemicals,[19]

fuels[20-25] and starting materials for the preparation of a variety of pharmaceutical compounds.[14, 26]

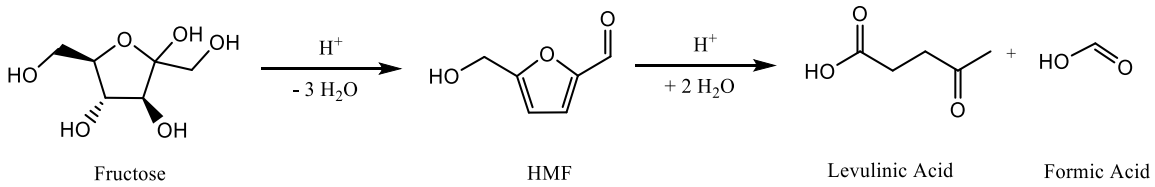

Scheme 1 Fructose dehydration reaction to HMF and consecutive HMF rehydration to levulinic and formic acid. Both reactions are acid catalysed.

For these reasons, dehydration of fructose to HMF has gained increasingly interest during the last decades of scientific research,[27] reaching a point at which more than 10000 scientific articles and patents have been published over the past 10 years, and approximately 1000 papers are published annually on HMF production.[3] In fact, a very broad range of different processes for furanics production from renewable sources have been explored, either assisted by homogeneous or heterogeneous catalysts, performed in aqueous[47] or organic solvents, both in mono or multiphasic systems,[28, 29] or even supported by a range of additives such as ionic liquids.[30] Specifically, acid catalysed dehydration of fructose resulted the most convenient and efficient method for preparing HMF. As consequence, many types of acid catalysts have been screened for this process, such as mineral acids,[31, 32] strong acid cation exchange resins,[33-36] H-form zeolites[37, 38] and supported heteropolyacids.[39] However, acid catalysts possessing Brønsted functionalities have been shown to be the most efficient to promote fructose dehydration. Nevertheless, despite this vast knowledge gained on fructose dehydration and some promising catalytic performances have been achieved, the persistent exploration of new methods for HMF production points out that efficient and competitive technologies to produce furanics from biomass feedstock have not yet been found. In fact, another crucial step to obtain the aforementioned wide range of valuable products from biomass, and hence to open new chemical pathways from renewable resources, is converting the aldose form of glucose in the ketose form fructose via isomerisation reactions. Indeed, as already described in Chapter 1, glucose is the monomer of the most abundant non-edible biomass fraction cellulose, thus being much more available in nature than fructose. However, the aldose sugar form of glucose is much more reluctant to undergo dehydration than the keto-form fructose.[40, 41] In fact, only 23% yield of furanic products is obtained when glucose is dehydrated using Brønsted acid catalysts, compared to the 99% of yield achieved when fructose is used as substrate in the same reaction conditions.[42] Hence, in order to produce a substantial amount of furanics from glucose, the only efficient chemical pathway to pursue is a multistep reaction in which glucose is isomerised into fructose, and then fructose is dehydrated to furanics. Furthermore, each step is promoted by different types of active species: the isomerization step requires, for example, Lewis acid functionalities, whereas the

dehydration step requires Brønsted acid sites,[43-45] thus impeding the use of the same active material to promote the overall multistep reaction from glucose to furanics. For this reason, attempts have been made in coupling together glucose isomerisation and fructose dehydration in one-pot reaction by introducing a mixture of Lewis and Brønsted acid catalysts in the same reaction environment. For example, Pagán-Torres *et al.* assessed a wide range of known Lewis acidic metal ions in combination with HCl, and found $AlCl_3$ to be the most effective, generating yields of 62% of furanics starting from glucose.[46] $CrCl_3$ has been observed to be an equally effective Lewis acid generating yields of 58% with HCl as the co-catalyst.[47] Also several kind of bifunctional catalysts, characterised by Lewis and Brønsted active sites, have recently attempted to be synthesized. For example, as described in Chapter 1, zeolites are materials that potentially support both Lewis and Brønsted acid functionalities. Therefore, a range of aluminosilicate materials have been screened in their pristine or modified form to assist the production of HMF from glucose. In this regard, H-, Fe- and Cu-ZSM-5 zeolites have been tested returning a 42% HMF yield by using a biphasic NaCl (20 wt.%) aqueous solution/methyl isobutyl ketone (MIBK) system.[48] In addition, synthetised beta zeolites reported HMF yield up to 72%, but only when used in presence of DMSO and THF.[49] Post synthetic Nb beta zeolites have shown 82 % HMF yield when used in a biphasic water/MIBK system and in presence of NaCl.[50] MCM-41 silica containing ZrO_2 generated 23% of HMF starting from glucose operating in a biphasic medium of water/MIBK.[51] Also silicoaluminophosphate (SAPOs) catalysts have been tested for glucose conversion to furanics in one-pot reaction, returning 94% HMF yield if γ-valerolactone (GVL) was used as reaction solvent.[52] Phosphated Ti and Zr oxides have been screened as well returning 90% HMF yield if used in a 1-methyl-2-pyrrolidone (NMP) reaction environment.[53-55] Although promising HMF yields were obtained with these bifunctional materials, acceptable catalytic activities were observed only when toxic or high boiling solvents such as MIBK, GVL, DMSO, NMP, and dimethylformamide were used. Also, a series of heteropolyacids were synthesised to promote the glucose one-pot reaction to furanics. Nevertheless, also in this case, acceptable HMF amount were observed only when high boiling and expensive additives such as ionic liquids or DMSO were employed.[56-59] Attempts to promote furanics production from glucose have been performed also with Cr-based coordination polymer catalysts, reaching HMF yield up to 81%, but only when biphasic systems supported by concentrate NaCl solution (10 wt.%) were employed.[60] Despite some of these bifunctional synthesised catalysts providing promising furanics yields in one-pot glucose reactions, important technical disadvantages still persist for their employment in large scale intensified processes. For example, using heavy metal based active sites, such as Cr, causes dangerous environmental and health issues in case of catalyst leaching or poor metal recovery in the case of homogeneous catalysis. Likewise, the use of concentrate saline solution in the development of biphasic systems results in process design and maintenance impediments. Furthermore,

the high boiling solvents and additives, required by most of the aforementioned bifunctional catalysts to achieve acceptable furanics yield, imply operating the separation and product recovery downstream units at high temperatures, thus threatening the thermolabile furanic compounds.[61] Moreover, the introduction of high temperature separation units makes the recovery of HMF very energy demanding, thus limiting the economic feasibility of the process. In fact, the separation and purification of HMF has been reported as one of the most important challenges in the scale-up of industrial HMF production.[61] Specifically, it has been reported that the employment of such high boiling solvents and additives is required due to the stabilisation effect they provide on glucose, fructose and furanics,[62-66] which otherwise would undergo to a series of competitive side reactions, thus decreasing process selectivity and productivity. For example, when glucose is heated at elevated temperatures and in a Brønsted acidic environment, such as the one required for fructose dehydration, it tends to form disaccharides, anhydrosugars and insoluble polymers which do not subsequently go to furanics.[67-69] On the other hand, the Lewis acid functionalities required to promote glucose isomerisation, also favour fructose side-reactions, thus decreasing furanics yield.[45, 69, 70] Therefore, although positive steps forward with respect to furanics production from glucose have been achieved in recent years, there still exists a blockade to further progress as a result of the side reactions that tend to occur when glucose and fructose are processed with both Lewis and Brønsted acid sites. Hence, in the perspective of designing a process for furanics production from glucose, the promotion of the two single reactions, glucose isomerisation and fructose dehydration, by a mixture of the two acid catalysts or by a bifunctional catalyst must not be pursued due to the side-reactions issues afore described. An alternative way to combine these two individual reactions is an integrated process where the two reactions, isomerisation and dehydration are conducted individually. In fact, integrated processes can be defined as the combination of more individual reaction units into a single system that operate under unified control (Scheme 2), leading to several industrial advantages such as reduced operational dead time, increased time and space productivity, more efficient quality product supervision, which also makes them today the most attracting process design to be developed.

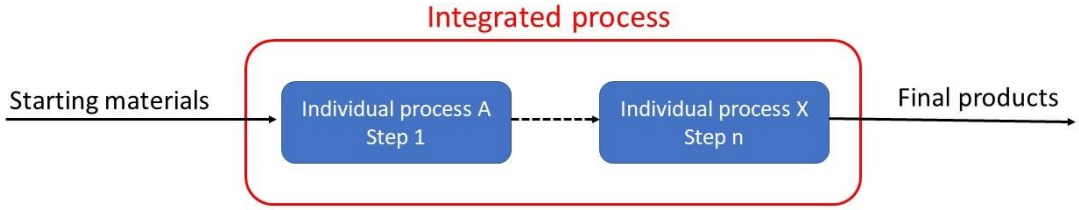

Scheme 2 Schematic representation of an integrated process constituted by n individual process units. Each individual unit constitute a step of the overall integrated process required to transform the initial starting materials to the end final products.

In this way, in such a process design, the two individual reactions, isomerisation and dehydration, can be catalysed by their own specific acid active sites and conducted at their optimum reaction conditions. Specifically, glucose isomerisation can be conducted at low temperatures (<180°C), ensuring that the precious glucose substrate is not degraded and that the reaction be assisted by a Lewis acid catalyst. Whereas, the second reaction step, fructose dehydration, can be performed at higher temperatures and catalysed by Brønsted acid catalysts. In this way fructose does not even interact with Lewis acid sites responsible of fructose side-reactions.

A significant breakthrough in developing integrated processes is the possibility of conducting all or most of individual reaction steps in continuous modo operandi thus to continuously process the outlet stream of the first reaction step as inlet of the consecutive step. Recently, metal incorporated zeolites such as Sn or Hf-beta have been proposed has promising catalyst for continuous glucose isomerisation.[71-80] These heterogeneous catalysts exhibited unprecedented single-pass fructose yields and selectivity features, with excellent continuous long-term stability performances that no chemical or biological catalysts has yet been able to achieve.[80] Furthermore, compared to enzymes, the bio-alternative catalysts employed for glucose isomerisation, zeolites can tolerate larger variations of operational conditions such as temperature, reaction solvent, pH and feedstock impurities, thus returning much solid and constant catalytic performances along reaction times.[81-89] The possibility of employing these heterogeneous catalysts for continuous glucose isomerisation in larger ranges of reaction parameters open the possibility to couple glucose isomerisation with following chemical steps required to obtain valuable platform molecules, such as fructose dehydration, thus allowing to conceptualise an integrated process for furanics production from glucose. Conversely, due to the strict reaction conditions which enzymes require to operate, hypothetical integration of these bioprocesses with further upgrading reactions would be more problematic. For example, the incompatibility of enzymes to operate with many organic solvents would prevent an operational flexibility also in the downstream processes such as fructose dehydration. In such cases, a product recovery unit placed after the first step of glucose isomerisation would be required, together with the introduction of other auxiliary solvents to

aids the second step of fructose dehydration. On the other hand, if the two consecutive reactions processes can operate with the same reaction solvent and if any by-products do not interfere with the second reaction step, intermediate product recovery or separation units can be avoided, thus highly enhancing the sustainability and economic potential of the overall process. The recent studies conducted on promoting glucose isomerisation with Hf and Sn hetero-substituted zeolites, have shown that best performance of catalyst productivity and stability are achieved by introducing slightly amount of water in the conventional MeOH reaction solvent. In fact, Padovan *et al.* have demonstrated that upon the addition of 1-10 wt.% water to the conventional sugar/MeOH feed, reactivity was found to increase by a factor of 2.5, and catalyst stability improved by 1 order of magnitude.[90] The ability of these promising catalysts to better work with small amounts of water has a tremendously impact also on process intensification perspectives, since it allows to increase the poor sugar solubility showed in pure alcoholic environments. For example, glucose solubility more than doubles if 10 wt.% of water is introduced in pure MeOH and is 5 times improved if the water amount is extended up to 20 wt.%.[91] Increasing the sugar solubility in the reaction media allows to process much more concentrated feedstock streams resulting in a boost to space-time process productivities.

For these reasons, if fructose dehydration can be conducted in a MeOH/H_2O environment too might open the interesting opportunity to couple the reaction with the glucose isomerisation catalysed by metal substituted zeolites and thus to develop an integrated process from glucose to furanics. The good results obtained on sorbitol dehydration described in Chapter 4, allows the hypothesis that MeOH is a great alcoholic solvent in which to conduct fructose dehydration too. However, amongst the literature investigated systems for furanics production from fructose, very few have been conducted in MeOH environment.[40, 92] Thus, there is no extensive knowledge on this type of systems currently available. Moreover, not one of these studies consider how water aliquots affect the dehydration reaction. Unfortunately, previous works conducted using other type of solvents point out that water presence in the rection environment is highly detrimental for fructose dehydration and furanics productions.[93-99] In fact, has been reported that the presence of an aqueous environment decreases catalyst activity and, especially, strongly threaten furanics stability due to their tendence to be rehydrated in consecutive products such as levulinic and formic acid, or even to useless products such as humins. As such, even small quantities of water in the MeOH media might strongly affect the product distribution obtained at the end of the dehydration reaction and thus threaten the process efficiency. Therefore, to truly evaluate the chance of coupling fructose dehydration with glucose isomerisation a study on the fructose dehydration reaction performed in MeOH/H_2O media is crucial to be conducted. Furthermore, understanding the water tolerance of such a process is pivotal also for intensification purposes. In fact, it must be considered that for each molecule of fructose dehydrated into HMF, three molecule of

water are produced. Hence, in the future perspective of processing high concentrated sugar streams, substantial amount of water might be formed as coproduct of the dehydration reaction.

Therefore, this chapter will assess the impact of water on the fructose dehydration reaction when conducted in an MeOH media, thus allowing evaluation of the potential of coupling this reaction with the glucose isomerisation reaction assisted by incorporated beta zeolites. First, reaction screening will be performed in batch reactors to understand how furanics production is affected by the variation of operational parameters, such as water presence, reaction temperature and type of catalyst employed. Then, once the reaction conditions have been understood and optimised to allow a substantial furanic productivity to be achieved, conduction of fructose dehydration in continuous modo operandi will be explored. In fact, all the previous fructose dehydration studies performed in MeOH have been conducted only in batch reactors which, as previously anticipated, are not the favoured system for the design of an integrated process or bulk scale chemical manufacture. Therefore, only a partial or even naught knowledge of continuous fructose dehydration performed in alcoholic/aqueous environment is currently available. As consequence, at the current time, an accurate feasibility evaluation of coupling continuous glucose isomerisation with continuous fructose dehydration can not be performed. Therefore, studying continuous fructose dehydrations in a MeOH/H_2O media might enable precious information to be obtained, which can lead to the design of new strategic processes to produce high valuable platform molecules from renewable resources.

5.2 Experimental

5.2.1 Materials

Fructose (≥98%), glucose (≥98%), Amberlyst 15, H_2SO_4 (≥97%), and HCl (37%) tetraethyl orthosilicate (TEOS, 98%), tetraethylammonium hydroxide (TEAOH, 35%), $HfCl_4$ (≥99.5%) were purchased from Sigma-Aldrich. MeOH (≥99.5%) and HF (50%) were supplied by Fisher Chemicals. Zeolite beta 38 and 300 were purchased from Zeolyst and calcinated in their H^+ form by calcination in air at 550°C for 6 hours, 5°C min^{-1} ramp rate prior to their use.

5.2.2 Catalyst synthesis

The hydrothermal synthesis of metal incorporated BEA zeolites was performed according to the following protocol: 30.6 g of TEOS, was added to 33.1 g of TEAOH, under careful stirring, resulting in the formation of a two-phase mixture. After 60-90 min, a single phase was obtained, and the desired amount of the metal source ($HfCl_4$) dissolved in 2.0 mL of H_2O was added dropwise. The solution was then left for several hours under stirring until

a viscous gel was formed. Formation of the final solid gel was achieved by addition of 3.1 g of hydrofluoric acid (HF) in 1.6 g of demineralized H_2O. The molar composition of the final gel was; 1.0 Si: 0.005 Hf: 0.02 Cl^- : 0.55 TEA^+: 0.55 F^- : 7.5 H_2O. The obtained gel was transferred to a Teflon lined stainless steel autoclave, and heated at 140°C for a total 7 days. The crystals obtained were filtered and washed with deionised water. Removal of the organic template was achieved by calcination at 550°C (2 °C min^{-1}) for 6 h under static air.

5.2.3 Kinetics studies

Batch fructose dehydration reactions were performed in a Anton Paar Microwave reactor. Each batch reaction was conducted adding 5 g of substrate solution in a 10 mL glass vial with the proper amount of catalyst. Reactions were performed at the reported temperature, autogenic pressure and 800 rpm. At the end of the reaction the reaction vials were cooled to 50°C by air flow. Aliquots from the reaction mixture were collected for quantification analysis.

Continuous fructose dehydration reactions were performed in a plug flow, stainless steel, tubular reactor. The reactor was connected to an Agilent HPLC pump in order to accurately regulate the reactant flow. The catalyst was packed into a ¼ inch stainless-steel tube (4.1 mm internal diameter), held between two quartz wool plugs, and a frit of 0.5 µm was placed at the reactor exit. The reactor was subsequently placed inside an aluminium block, heated by an electrical resistance and the temperature was controlled by means of a temperature controller and a thermocouple. Pressure in the system was controlled by means of a backpressure regulator, typically set at 40 bar. Aliquots of the reaction solutions were taken periodically from a sampling valve placed after the reactor.

5.2.4 Analytical details

The concentration of fructose, methyl fructoside and glucose were determined by means of HPLC equipped with ELS detector, and a 0.5 wt.% sorbitol solution was used as external standard. Was used an Agilent Hiplex-Ca column7.7 x 300 mm at 80°C, 0.75 mL min^{-1}, using HPLC water as an eluent. HMF, MMF and furfural concentration were quantified using an HPLC Agilent 1220 Infinity LC using a column Agilent MetaCarb 87H 250 × 4.6 mm at 65°C, 0.45 mL min^{-1}, in 0.01 M H_3PO_4 water solution as an eluent, equipped with a variable wavelength detector (VWD) at 254 nm. Methyl levulinate and levulinic acid concentrations were quantified by GC equipped with FID using a 0.5 wt. % biphenyl solution as external standard. Formic acid concentration was calculated from stoichiometric ratio of methyl levulinate and levulinic acid concentration.

5.3 Result and discussion

5.3.1 Fructose dehydration in batch system, screening of reaction conditions.

To gain insight on the fructose dehydration reaction, a preliminary study was performed in batch systems. In fact, as mentioned in previous chapters, discontinuous reactions are affected by a restricted number of parameters compared to continuous ones, thus offering the opportunity to quickly gather information on intrinsic reaction aspects such as temperature dependence and product distribution evolution over reaction time.

Although the scientific community has thoroughly studied furanics productions from fructose, and thus information on the influence of reaction conditions may be already found in literature, acquiring ones own catalytic data is crucial to have a reliable benchmark values to which future novel results can be compared. Moreover, only a few of those studies were conducted in alcoholic solvents which, as described, is the main element to evaluate the integration of fructose dehydration with the novel glucose isomerisation reactions catalysed by metal incorporated zeolites. Furthermore, the few studies conducted on fructose dehydration in alcoholic solvents report furanics yields at different reaction conditions but do not place much emphasis on the nature of the generated by-products, which instead, is essential to comprehend the whole range of chemical pathways that occur together with fructose dehydration. In fact, having the knowledge of which direction the chemical process takes, as a function of reaction conditions, is pivotal to develop a selective and efficient industrial process. To date, investigations on fructose dehydration in a mixture of alcoholic/aqueous media have never been performed or reported. Furthermore, some dehydration by-products such as levulinates, generated by consecutive rehydration of HMF, possess industrial interest too. In this way, there might be reaction conditions which do not returning the highest furanics production, but may be more economically attractive since they generate a full mixture of valuable compounds. In other words, the furanics yield optimum might not coincide with the economic optimum of the whole process. For this reason, knowing the distribution of products generated by fructose dehydration in alcoholic/aqueous environment, as function of different reaction parameters, it is of pivotal importance to make an accurate economic evaluation of the industrial process. Therefore, a series of reaction conditions such as reaction temperature, reaction time and type of acid catalyst employed have been screened in batch reactors. As described in Chapter 4, due to its dispersed acid functionalities and water insoluble structure, Amberlyst 15 has shown great chemical suitability in assisting biomass upgrading reactions. Moreover, some scientists have already gained interesting results by using this polymeric resin for continuous dehydration systems.[33-36] For these reasons, and for its easy commercial availability, Amberlyst 15,

was chosen as heterogeneous catalyst to preliminary screen different operational conditions for fructose dehydration.

Literature studies have reported that dehydration reactions are strongly temperature dependent processes.[36] However, depending on the reaction environment, such as reaction solvent and type of catalyst used, the temperature optimum at which is obtained the highest furanics yield may vary substantially. In fact, higher temperatures improve furanics formation rate but, at the same time, also increase rates of side reactions, such as products and substrates decomposition, especially when thermolabile biomass derivates are processed. For this reason, the product distribution yielded at the end of the reaction might change considerably depending to the process temperature. Therefore, to gain insights on how the reaction temperature affects fructose dehydration in alcoholic/aqueous environment, a series of batch reactions were conducted using 1 wt.% fructose solution in 95:5 wt.% MeOH/H_2O media at different temperatures (Figure 1). Prior to that, a control experiment performed by stirring a 1 wt.% fructose solution at 180°C for 10 min revealed that only the temperature effect is not able to produce any furanic compound (Figure 7 entry 1). Conversely when an acid catalyst such as Amberlyst 15 is introduced in the reaction environment furanic compounds start to form at low temperature such as 110°C (Figure 1).

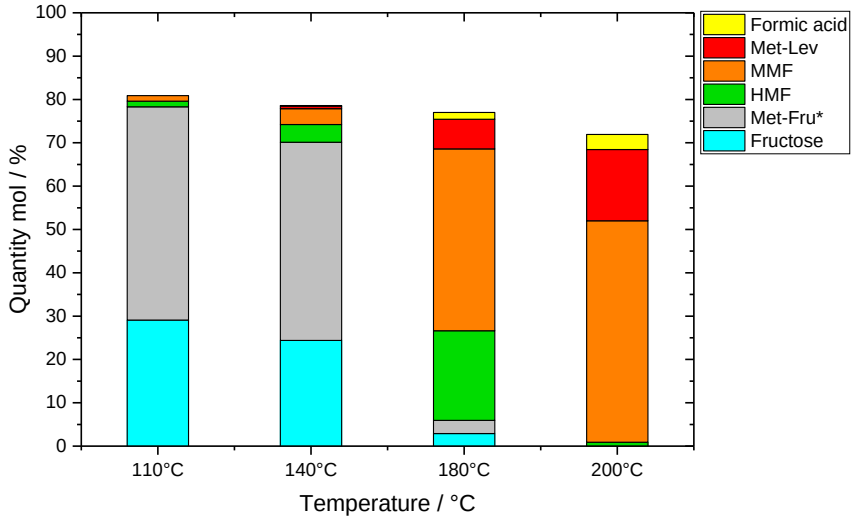

Figure 1 Product distribution at different reaction temperatures, 110°C, 140°C, 180°C and 200°C. Batch reactions were performed adding 0.0100 g of commercial Amberlyst 15 in 5 mL of 1 wt.% fructose 95:5 wt.% MeOH/H_2O solution. $mol_{acid\ sites}/mol_{fructose}$ = 0.200. Each reaction was conducted by means of a microwave reactor for 10 min under autogenic pressure. *Methyl fructoside (Met-Fru) quantification made by means of methyl glucoside calibration curve and checked with the kinetic experiment showed in Figure 3.

Furthermore, as Figure 1 shows, it can be noted that when the reaction is performed in an alcoholic media such as MeOH, in addition to HMF, a series of etherification products arise, such as methyl fructoside, 5-methoxymethylfurfural (MMF) and methyl levulinate. It

is worth to mention MMF has lower boiling point than HMF, thus simplifying the separation and recovery of furanic compounds at the end of the dehydration reaction.[40]

Unfortunately, methyl fructoside, is not available on the market, thus its quantification can not be performed by means of constructing a calibration curve with standard solutions, as done with all other reaction products. Therefore, approximate quantification of methyl fructoside was attempted by using the calibration curve of its aldose isomer, methyl glucoside. Although this represents a potential source of quantification error, the ability of even roughly estimate amounts of methyl fructoside might offer precious insights to study the fructose dehydration reactions performed along this chapter. However, in order to determine the reliability of using such a method to quantify methyl fructoside, amounts of methyl fructoside were generated via fructose methylation at very mild reaction condition, and quantified with methyl glucoside calibration curve. Due to the mild reaction condition at which fructose methylation reaction was conducted, and to the very facile methylation of fructose to methyl fructoside reported in other studies,[101, 102] methyl fructoside is assumed to be the only product generated.

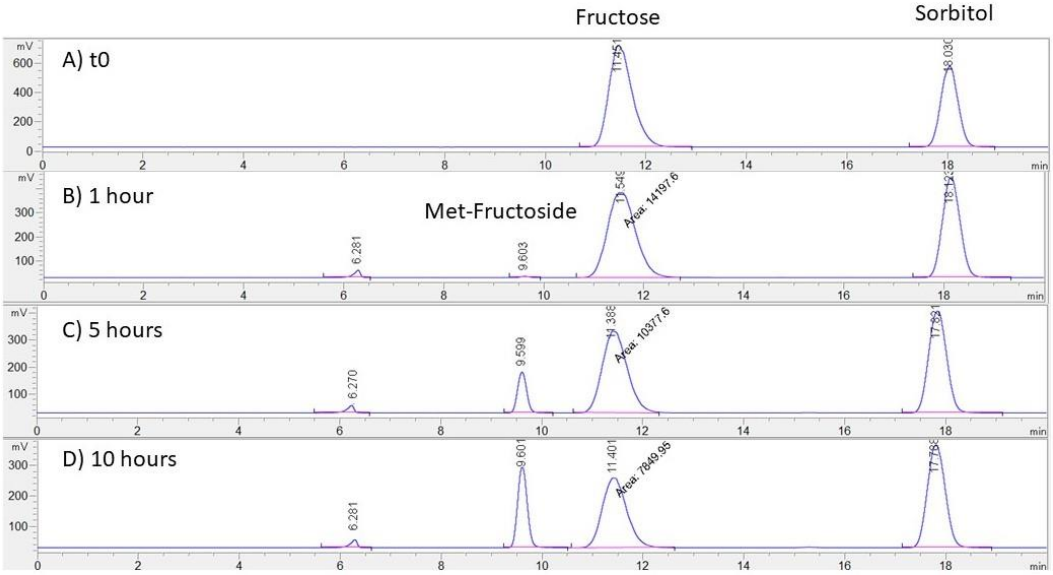

Figure 2. HPLC-ELSD chromatograms of A) 1 wt.% fructose solution and samples reaction withdrawn at B) 1 h, C) 5 h and D) 10 h after the addition of HCl. Methylation of fructose was performed by adding 0.165 mL of 0.5 M HCl to a 10 mL 1 wt.% fructose methanol solution, and slowly stirred at 25°C.

As such, the real methyl fructoside yield can be considered equal to the fructose conversion observed, and the evolution of this value can be compared to the one calculated with the methyl glucoside calibration curve (Met-Fru*). Specifically, methylation of fructose was performed by adding 0.165 mL of 0.5 M HCl to a 10 mL 1 wt.% fructose methanol solution, thus resulting in 4 mM HCl acid environment. The resulted acid solution

was slowly stirred at 25°C and samples were periodically withdrawn and analysed by means of HPLC-ELSD.

Figure 2A shows the HPLC-ELSD chromatograms of the 1 wt.% fructose in methanol solution prior to the addition of HCl. Accordingly, in the chromatogram appear only two chromatographic peaks, one at 11.4 min and one at 17.7 min retention time, respectively related to fructose and sorbitol used as external standard. Figure 2B, 2C and 2D are instead related to HPLC-ELSD chromatograms of the fructose methylation reaction samples withdrawn 1, 5 and 10 hours after the addition of HCl. As can be observed in the chromatograms of each reaction point, two additional peaks arise: one at 6.2 min and another at 9.6 min, thus can be attributed as consequence of the addition of HCl to the fructose methanol solution. However, observing the reaction point chromatograms, it is clear that only the peak at 9.6 min gradually increases as function of the reaction time, resulting in a very sharp peak after 10 h reaction. Whereas the peak at 6.2 min preserves a constant dimension as function of the reaction time. Therefore, it can be stated that only the compound eluted at 9.6 min is the main product of the fructose methylation, whereas the peak at 6.2 min appears to be related to a species that is quickly formed after HCl addition but its amount is not depended to the reaction time. Thus, it might be attributed to an impurity inserted during the addition of HCl, or a product that is rapidly formed but only to a minor quantity. For this reason, only the 9.6 min chromatographic peak was assigned to methyl fructoside as product yielded from the fructose methylation reaction. Accordingly, that peak was integrated with the methyl glucoside calibration curve to calculate an approximate yield, indicated as Y Met-Fru*.

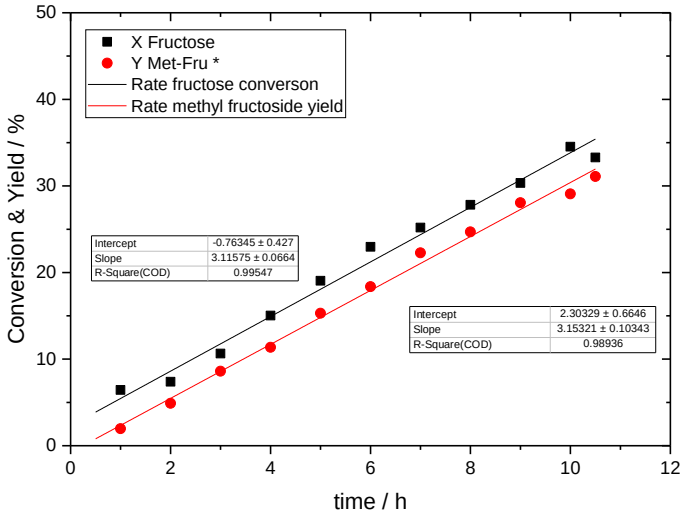

Figure 3. Methylation of fructose. The reaction was performed by adding 0.165 mL of 0.5 M HCl to 10 mL of 1 wt.% fructose in 95:5 MeOH/H_2O solution. Reaction temperature 25°C. Samples were periodically withdrawn and analysed with HPLC-ELSD. Y Met-Fru* calculated by means of methyl glucoside calibration curve.

That approximated yield was then compared with the conversion of fructose which, as previously discussed, can be considered equal to the real value of the methyl fructoside yield and thus the discrepancy between the two data can be evaluated.
As Figure 3 shows, quantifying methyl fructoside with methyl glucoside calibration results in an underestimation of the compound since for all the reaction points analysed the yields of methyl fructoside determined (Y Met-Fru*) was lower than fructose conversions. However, the average difference between fructose conversion and methyl fructoside yield resulted to be 3.3%, a discrepancy that can be considered acceptable due to the fact that methyl fructoside is not the target product of this work and its quantification will be mainly used to understand the evolution of dehydration reactions. A further check on the truthfulness of methyl fructoside as sole product of the fructose methylation reaction was conducted by calculating kinetic rates of fructose conversion and methyl fructoside yield (Figure 3). In fact, if methyl fructoside is the very sole product yielded by the fructose methylation reaction, methyl fructoside generation rate should match the fructose consumption rate. By interpolating the rection points of Figure 3, and considering the fructose methylation reaction to be a first-order reaction as reported in previous studies,[101] the same rate constant of 0.053 min^{-1} was determined by interpolating the Met-Fru* yield points and the fructose conversion points. Therefore, the equal kinetic rate of fructose and methyl fructoside strongly indicate that methyl fructoside was the only product generated by the fructose methylation reaction, suggesting that the assumption that methyl fructoside yield must match fructose conversion if the analytical method used for methyl fructoside quantification would be error free is valid. Since the difference between fructose conversion and methyl fructoside yield calculated with the calibration curve of methyl glucoside has been considered acceptable for the aim of this work, from now on, amounts of methyl fructoside were calculated by using the methyl glucoside calibration curve, thus indicated as Met-Fru*.

As Figure 1 shows, the substrate conversion and the products distribution yielded by dehydrating fructose is strongly influenced by the reaction temperature. In fact, at low reaction temperatures, 110°C and 140°C, the substrate conversion reaches values of 70 and 75% respectively, yielding methyl fructoside as main reaction product. Although at low temperatures the amount of furanics detected were negligible, it can be noted that increasing the reaction temperature by a further 30°C caused the overall furanics yield (HMF & MMF) to improve from 3 to 8%. Thereafter, the dehydration temperature was increased to 180°C and, at this condition, an almost complete conversion of fructose was achieved, producing only negligible amounts of methyl fructoside and an abundant presence of HMF and MMF. In fact, at 180°C, the overall furanics production reached the value of 63% yield. In addition to these compounds also small quantities of methyl levulinate and formic acid were generated, with a yield of 7 and 2% respectively. Further

increasing the temperature to 200°C led to higher yields of MMF, methyl levulinate and formic acid (51%, 16% and 4% respectively) than those obtained at 180°C, but with a poorer production of HMF (1%), thus yielding a lower overall furanics yield of 52%. In this way, it can be already observed that there is a temperature optimum at which an highest furanics production is achieved and, at these specific operational conditions, resides around 180°C. Furthermore, it must be noted that in none of the reactions performed a full carbon balance was achieved, suggesting the formation of other chemical species during fructose dehydration such as aldol-condensation or degradation by-products.[50, 52, 64, 103] Nonetheless, by GC analysis the presence of consecutive furanics rehydration products such as levulinic and formic acid were not detected. It is also worth to observe that increasing the reaction temperature the carbon balance of the reaction is not strongly affected. Indeed, conducting the reaction at 200°C compared to 110°C, induce a carbon balance loss by only 8%, from 80% to 72%.

For the further screenings of fructose dehydration conditions, 180°C was selected as working temperature since at this condition both furanics species, HMF and MMF, are generated in acceptable amounts, and it is possible to detect other compounds involved in the reaction, including the substrate and by-products. Therefore, starting from this condition, it is possible to observe how other reaction parameters such as reaction time and presence of different water aliquots affect the main chemical pathways that occur during fructose dehydration.

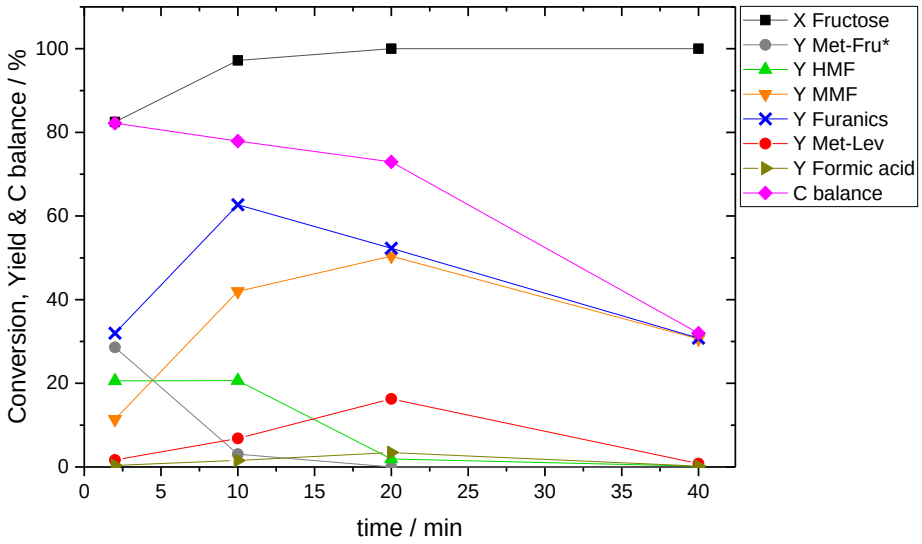

Figure 4 Fructose dehydration performed in discontinuous systems. Batch reactions were performed adding 0.0100 g of commercial Amberlyst 15 in 5 mL of 1 wt.% fructose 95:5 wt.% MeOH/H_2O solution. $mol_{acid\ sites}/mol_{fructose}$ = 0.200. Each reaction was conducted at 180°C under autogenic pressure.

Therefore, with the purpose of further investigating the spectra of reactions involved in this process, several batch fructose dehydration were conducted at different reaction time

(Figure 4). For ease of comparison, the total furanics yield (blue crosses), defined as the sum of HMF and MMF yields, has been included as reaction product.

From the time online experiment (Figure 4) it is possible to observe the high reactivity exhibited by fructose at 180°C in a 95:5 wt.% MeOH/H_2O reaction environment and in presence of a Brønsted acid catalyst as Amberlyst 15. In fact, at these reaction conditions, 83% of the substrate is already converted in 2 minutes reaction time. Furthermore, from this time online evaluation it is possible to appreciate fructose methylation as the first reaction that take place in the MeOH/H_2O environment. In fact, at the shortest reaction times (2 min) the prevalent compound detected in the reaction mixture is methyl fructoside, at a yield of 29%, against the 21% yield of HMF and 11% of MMF. Increasing the reaction time at 10 min resulted in almost the entire substrate being converted, and the yield of methyl fructoside decreasing from 29% to 3%, indicating its transformation in other compounds. However, it must be stated that is not clear if methyl fructoside undergoes dehydration, thus yielding MMF directly (Scheme 3, blue pathway) or if the consumption of methyl fructoside during the reaction course is due to a shift of the eventual thermodynamic equilibrium between fructose and methyl fructoside caused by fructose dehydration to HMF, which is subsequently methylated (Scheme 3, red pathway).

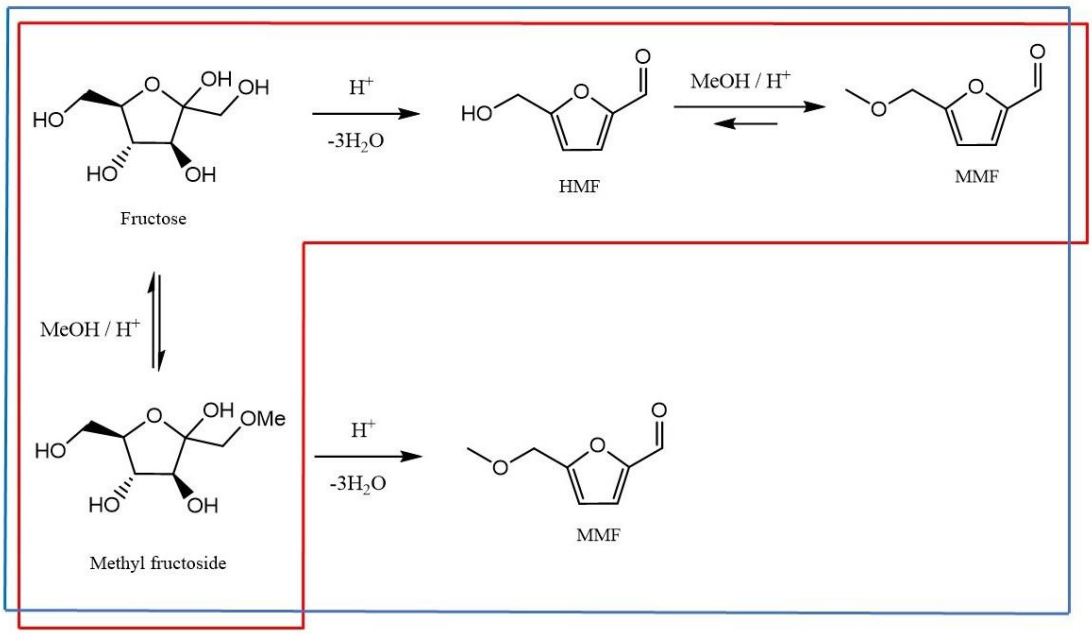

Scheme 3 Two possible chemical pathways of the furanics formation from ketose sugar forms. Both pathways consider the formation of methyl fructoside as methylated product of fructose by an equilibrium reaction, the dehydration of fructose to HMF and its consecutive methylated product MMF. However, the blue pathway also allows the direct dehydration of methyl fructoside to MMF, whereas the red pathways reject that hypothesis.

Nonetheless, since the final purpose of this work is evaluating the performance of fructose dehydration in an alcoholic/aqueous environment, the susceptibility of methyl fructoside

to be dehydrated into furanics was not further investigated since whatever reaction pathway occurs, it led to the desired products. However, with a more thorough investigation it might be understood which chemical pathway is preferred. Although it is not still exactly understood which chemical reaction pathway led to the furanics formation when fructose dehydration is conducted in MeOH environment, the fact that when reactions are performed at harsher condition such as high temperature (Figure 1) or long rection time (Figure 4) full conversion of fructose and zero methyl fructoside yield were observed shows that dehydration reaction from ketose in MeOH media is a one-way reaction an not an equilibrium. Conversely, increasing the reaction time from 2 to 10 min, the HMF yield remain constant at 21%, whereas the MMF yield increases to 42% and slight amounts (7%) of methyl levulinate started to appear. Further incrementing of the reaction time to 20 minutes resulted in complete methylation of HMF into MMF, also suggesting the consecutive dehydration product nature of MMF. Furthermore, the fact that when the dehydration reaction is conducted at the harshest conditions such as long reaction times (Figure 4) or high reaction temperatures (Figure 1), the only furanic compound detected is MMF suggests that the chemical relation which link the two furanic compounds is not an equilibrium but most likely a one-way reaction. Or, if the reaction between HMF and MMF is equilibrium limited, it is largely shifted toward the methylated product due to the high presence of methanol as reaction solvent. However, it can be affirmed that, in the conditions at which the dehydration reaction has been conducted so far, a conversion of MMF to HMF is not observed. Despite the increment of MMF, the reaction time extension to 20 min, yielded a decreasing furanics production, from 63 to 52%. Since the quantity of methyl levulinate generated at 20 min also increased to 16%, it can safely be assumed that methyl levulinates is the consecutive product formed from furanics. However, it is not possible to identify if methyl levulinate is produced by the rehydration of MMF, or by the methylation of levulinic acid formed as rehydration product of HMF. In fact, it is possible that both reaction pathways take place. It must be also noted that longer reaction times induce stronger decomposition of valuable products, since a progressively lower carbon balance is detected if the reaction is elongated from 2 to 20 min. Further increment of reaction time to 40 min results in a decomposition of all the species involved in the dehydration reaction as the dropping of their yield and the carbon balance suggests.

In this way, both reaction temperature dependence and time online experiments confirm there is an operational window in which furanics yield is maximised and that must be considered in the future attempt of developing a competitive continuous process for furanics production.

Having understood the evolution of products from fructose dehydration with respect to reaction temperature and time, several batch reactions were performed with different

amount of water to investigate the effect of the aqueous environment on the products stability and on the overall reaction development. Specifically, the reaction condition were selected from the experiments previously described (Figure 1 and 4) which returned the highest furanic yield, in particular 180°C and 10 min contact time, but in presence of different amounts of water (Figure 5).

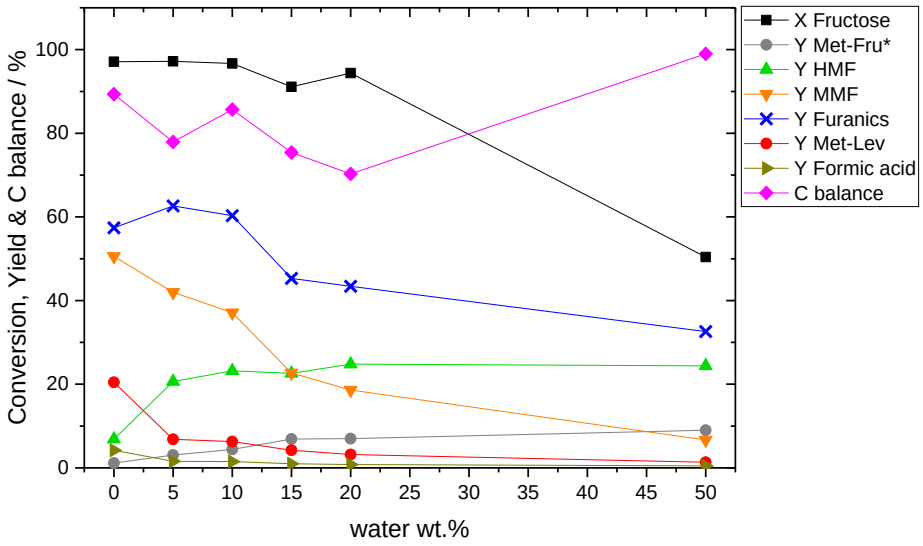

Figure 5 Fructose dehydration batch reactions performed at increasing water aliquots inside the methanol reaction media. Batch reactions were performed adding 0.0100 g of commercial Amberlyst 15 in 5 mL of 1 wt.% fructose methanol solution with different amount of water wt.%. $mol_{acid\ sites}/mol_{fructose}$ = 0.200. Each reaction was conducted at 180°C under autogenic pressure for 10 min reaction time.

From Figure 5 it can be appreciated how the product distribution obtained from fructose dehydration is affected when progressive water amounts are added in the methanol solvent. Compared to the reaction performed in only methanol, performing fructose dehydration with 5 wt.% amount of water (Figure 5) increased the HMF yield from 7 to 21% and decreased the MMF yield from 51 to 42%, thus obtaining a similar overall furanics yield of nearly 60%. However, it can be appreciated how the yield of consecutive products such as methyl levulinate decreased from 21 to 7%. Therefore, the addition of 5 wt.% of water seems to mitigate consecutive reactions such as the etherification of HMF to MMF and the ring opening of furanics to levulinates, thus not threating furanics stability. This is clearly in contrast to what has been reported in literature to date, where water is reported to decrease the overall yield of furanics by favouring rehydration to levulinates and formic acid.[93-99] Having observed that conducting the fructose dehydration reaction in MeOH allowed the furanic compounds to tolerate the presence of 5% of water, higher water amounts were introduced in the reaction environment. Surprisingly, even working with 10 wt.% of water, furanics stability was not compromised, since an overall furanics

yield of 60% was still obtained. It can be observed, that also in this case, the increment of water amount in the reaction environment discourages the methylation of HMF to MMF. In fact, upon passing from 5 to 10 wt.% the HMF yield increased from 21 to 23%, and MMF yield drops from 42 to 37%. However, the yield of methyl levulinate only decreased from 7 to 6%. Considering the final purpose of this work, or rather evaluate the potential of developing a continuous process for furanics production form glucose, the possibility of introducing 10 wt.% of water in the reaction environment without affecting the stability of furanics, highly increases the economic appealing of the process. In fact, working in presence of 10 wt.% of water in the reaction media allows the concentration of sugar in the reaction stream to be doubled compared to when methanol is used as solvent alone, thus offering the opportunity to boost the catalyst time productivity of the whole integrated process. Moreover, it must be considered that for each fructose molecule dehydrated to HMF, 3 molecule of water are generated, thus in the optic of an intensified furanics production which process high concentrated sugar streams, the final reaction mixture of the dehydration reaction might contain substantial amounts of water. Hence, knowing the system is able to tolerate up to 10 wt.% of water without compromising furanics stability is a huge breakthrough for future process intensification targets.

To determine the maximal amount of water that can be tolerated, larger amounts of water were added to the reaction environment to evaluate if furanics stability and productivity can be further enhanced. As Figure 5 shows, passing from 10 to 15 wt.% of water, furanics stability decreased from 60 to 45%. Specifically, it can be noted that the furanic species most affected by the introduction of 15 wt.% of water is MMF, the yield of which decreased from 37 to 22%, whereas HMF yield maintained a constant value of 23%. Further increment of water (20 wt.%) led to a further MMF yield decreasing, 19%, and to a slightly increment of HMF yield, 24%. Notably, methyl levulinate yield progressively decreased to 3%. Hence, the product distribution trend obtained as function of water addition from 0 to 20 wt.% suggests that water presence mitigates HMF consecutive reactions which lead to MMF and methyl levulinate. Conversely, in this water range utilised (0-20 wt.%) fructose conversion always resided around an average value of 95%, indicating water did not have a strong effect on fructose dehydration at these levels. Hence the amount of water was increased up to 50 wt.% to evaluate if larger presence of water also affects conversion of fructose. As Figure 5 shows, the most affected reaction performance indicator by the presence of 50 wt.% of water is exactly fructose conversion which drops to 50% compared to the average value of 95%, obtained by working in the range of 0-20 wt.% water. Furthermore, it can be noted that, also in this case, progressive water additions improve the yield of the direct fructose dehydration product HMF, whereas it decreases the amount of compounds formed by HMF consecutive reactions (i.e. MMF, methyl levulinate and formic acid). Hence, the whole trend of product distribution obtained as function of water

amount introduced in the reaction environment suggests that the water presence decrease all the reaction kinetic rates involved in the process of fructose dehydration rather than merely the furanics stability. Therefore, to verify if substantial amounts of furanic compounds can be achieved even in the presence of high amounts of water, a time online experiment was conducted in presence of 50 wt.% H_2O/MeOH environment (Figure 6).

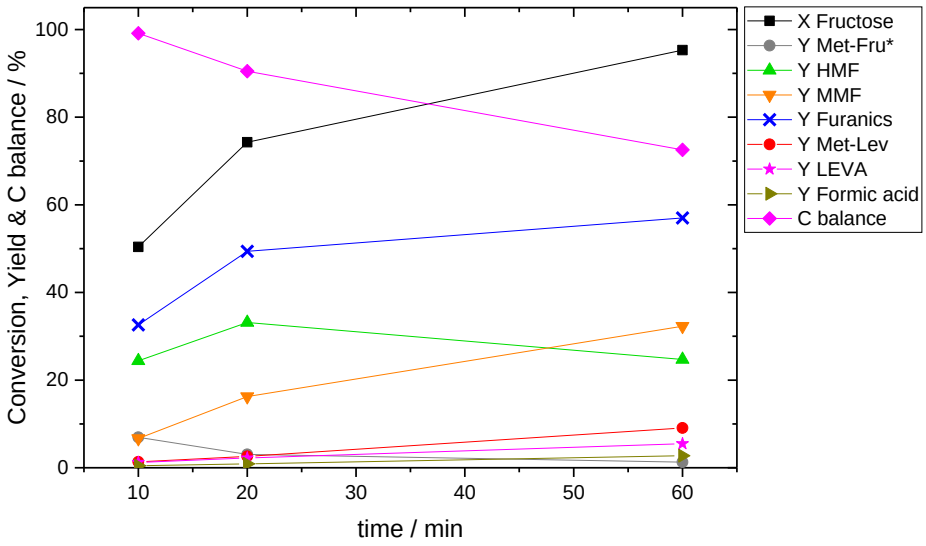

Figure 6 Fructose dehydration performed in discontinuous system. Batch reactions were performed adding 0.0100 g of commercial Amberlyst 15 in 5 mL of 1 wt.% fructose 50:50 wt.% MeOH/H_2O solution. $mol_{acid\ sites}/mol_{fructose}$ = 0.200. Each reaction was conducted at 180°C under autogenic pressure.

Interestingly, the time online experiment performed in presence of 50 wt.% of water (Figure 6) shows that extending the reaction time up to 60 minutes it can be achieved a surprisingly furanics yield of 57%, with an acceptable carbon balance value of 73%, meaning that the dehydration products in an alcoholic media are able to tolerate a high amount of water. In fact, such value of carbon balance is comparable to the one obtained in presence of 5 wt.% of water at similar furanics yield (Figure 4, 10 min of reaction, 63% furanics yield, 78% carbon balance). Furthermore, it is worth to note that in presence of this high concentrated aqueous environment small amount of levulinic acid starts to form. In contrast, when smaller amounts of water were present, only its methylated form, methyl levulinate, was detected. This might indicate that i) there is an equilibrium between levulinic acid and methyl levulinate, which in the presence of larger quantities of water is less shifted toward the methylated form; or ii) that in higher presence of water HMF starts to be rehydrated in levulinic and formic acid; or iii) both of the above. Looking at the trend of the reaction carbon balance with respect to the time online profile (Figure 4 and 6) and to respect with the amount of water present in the reaction feed (Figure 5) it can be

observed that the loss of carbon balance is much more affected by the reaction proceeding to higher degrees of conversion than simply the amount of water. In fact, the lowest values of carbon balance were detected when high fructose conversion was achieved and, conversely, great values of carbon balance were reached in correspondence of lower values of substrate conversion. This, again, is a good evidence that in alcoholic solvent the presence of water is not the main reason for product degradation but, conversely, confirms that dehydrations products might tolerate aqueous aliquots if reaction conditions are properly tuned.

5.3.2 Batch catalysts screening

Having understood the role that the main reaction parameters play in the reaction outcome and having identified the set of conditions which returns high furanics yield, a screening of different acid materials was performed to evaluate which catalytic properties can maximise furanics production. In this regard, selected heterogeneous catalysts with different kind of acid sites were used including Amberlyst 15, which possesses only Brønsted functionalities, and zeolites that possess both Brønsted and Lewis acid sites. Amongst aluminosilicate materials, Beta type zeolites were employed due to their great performances in dehydrating sorbitol (as described in Chapter 4). These beta type minerals were tested at two different SiO_2/Al_2O_3 molar ratios to understand how the quantity and strength of acidic sites affect the dehydration reaction. Furthermore, a metal incorporated zeolite which showed great glucose isomerisation performances,[80] hydrothermal Hf-beta, was tested to ascertain if just by operating at higher temperature, compared to the one usually adopted for glucose isomerisation (110°C), it is possible to catalyse fructose dehydration as well with the same catalyst. It must be noted that Hf-beta is the only catalyst tested which does not own Brønsted functionalities but only Lewis one, since during its synthesis aluminium precursor where not introduced. In addition, two homogeneous catalysts H_2SO_4 and HCl) were also tested. Both homogeneous catalysts were introduced in a proper amount to return the same number of acid functionalities of Amberlyst 15. Nevertheless, in the first place, a blank test was performed in absence of any catalyst to properly evaluate the catalytic properties of the investigated materials and to understand if only heating the substrate fructose in an alcoholic environment returns any active effect.

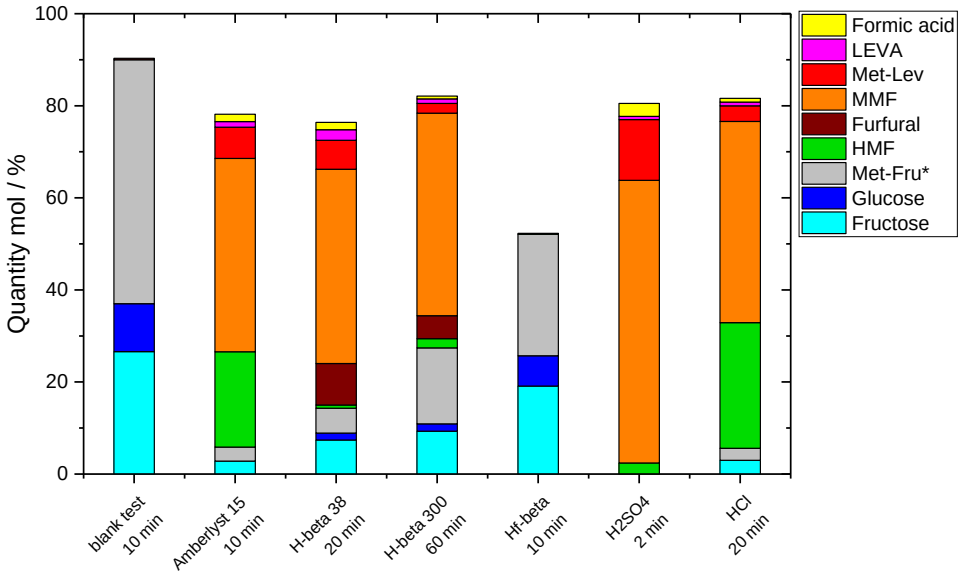

Figure 7 Screening of different acid materials in assisting batch fructose dehydration. Each reaction was performed with 5 mL of 1 wt.% fructose solution in 95:5 wt.% MeOH/H_2O at 180°C and autogenic pressure. For Amberlyst 15 and homogeneous acids the catalysts were added accordingly to have $mol_{acid\ sites}/mol_{fructose}$ ratio equal to 0.200. For zeolites the catalysts were introduced in amount equal to 0.0100 g. For each catalyst is reported the reaction time which provide the best performances in terms of furanics yield.

As Figure 7 shows, in the absence of any catalyst but just stirring and heating at 180°C for 10 minutes, using a 1 wt.% fructose solution in 95:5 wt.% MeOH/H_2O solution, 75% of the fructose present in the feed was converted, resulting in formation of a 10% yield of glucose and 53% yield of methyl fructoside. However, no furanic compounds were formed. This blank reaction highlights the fact the sugar substrate in an alcoholic media is particularly reactive and that the methylation of fructose occurs even in absence of any active material. Therefore, as a consequence of this result, it is highly probable that, even in presence of an acid catalyst, the first reaction that takes place during furanics production from fructose is the methylation of the substrate, as previously hypothesised. It is also important to underline that, although formation of this methylated compound is facile, the dehydration reaction is still able to proceed to furanics, as showed in the previous time online experiments (Figure 1). From the catalyst screening performed (Figure 7), it is clear that to have an acceptable formation of furanics high temperature conditions alone are not sufficient, but the presence of an acid material is compulsory. In fact, all the catalysts screened provide a furanics yield higher than 42%, although in different reaction times. Among the material tested, zeolites were found to be the least active and selective catalysts, as they did not produce more than 46% of furanics. Moreover, it can be noted that when beta zeolites are used as catalyst, the predominant furanic compound is MMF, and only traces of HMF were produced. Although zeolites with

different SiO_2/Al_2O_3 molar ratio were used in equal masses and thus, different amount of acid sites were introduced in the reaction environment, a clear activity difference for the same aluminosilicate framework but with different aluminium loading is observed. In fact, the same beta zeolite framework generates 42% of furanics yield in 20 min reaction time when a SiO_2/Al_2O_3 molar ratio equal to 38 is used, whereas it takes three times longer to produce similar furanic quantities if present in a SiO_2/Al_2O_3 molar ratio of 300. Interestingly, it can be observed that zeolites are the only tested catalyst which also yield furfural, as already reported by Moreau *et al.*.[100] Unfortunately, Hf-beta zeolite, a catalyst used to promote glucose isomerisation, did not yield furanics even at high reaction temperatures of 180°C. In fact, it yielded mainly glucose and methyl fructoside, in an analogous manner to the blank test described above. Conversely, it shows that at these reaction conditions, at which all other catalysts tested are able to produce substantial amount of furanics, Hf-beta, damages fructose substrate, returning a poor carbon balance of 50% in just 10 min of reactions, as other literature works report.[45, 69, 70] Hence, this result confirms that, to not waste a precious amount of carbon atoms, fructose should not interact with the isomerisation catalyst at high temperatures, thus highlighting the need of a two-step integrated process. On the other hand, Amberlyst 15 resulted the most active and selective heterogeneous catalyst among the screened ones, returning a 63% furanics yield, of which 21% was in the form of HMF and 42% in the form of MMF. Hence, it can be also observed how the kind of acid active sites, Brønsted or Lewis, not only affect the catalyst activity and selectivity, but also which furanics compound is mainly generated. In fact, from this early screening it seems that Lewis acid sites are more prone in promoting methylation reactions, compared to Brønsted acid sites, as catalysts possessing Lewis acid sites returned higher amounts of methyl fructoside and MMF, and generated only negligible amounts of HMF. Amberlyst 15 is also the only heterogeneous catalyst tested which showed comparable selectivities to the homogeneous ones. H_2SO_4 resulted the most active material, able to reach 64% of furanics yield in only 2 min reaction time, whereas HCl returned 71% furanics yield but in 20 min reaction time. Remembering that H_2SO_4 and Amberlyst 15 were introduced accordingly to return the same proton amounts, and that they own the same sulfonic functionalities, the difference in reactivity between the two (same yield of furanics but 5 times faster with H_2SO_4) can be attributed to the usually higher reactivity of homogeneous catalysts than the heterogeneous analogues, due to the more intimate interaction of chemical species when present in the same phase. Conversely, the activity difference arisen between H_2SO_4 and HCl might be attributed to the effect of the counter anions on the dehydration reaction. In fact, for both homogeneous acids it can be assumed they are fully dissociated in the reaction system due to their extremely high dissociation rates (pKa HCl = $1.3x10^6$, pKa_1 H_2SO_4 = $1.3x10^3$, pKa_2 H_2SO_4 = $1.2\ x10^{-2}$) and, since they have been introduced accordingly to have the same mol_{acid}

$_{sites}$/mol$_{fructose}$ ratio, it can be concluded that in the two reaction systems are present the same amount of free protons. Therefore, what differs from the two reactions is only the acid counter anions, SO_4^{2-} or Cl^-. Therefore, observing the activity of the two catalyst and the product distribution they generate, it can be concluded that the two anions have a different effect on the reaction outcome. Indeed, when SO_4^{2-} ions are present in the reaction media, the fructose dehydration proceeds with an higher reaction rate compared to the reaction in which are present Cl^- (it must be also noted that, due to the bifunctionality of H_2SO_4, to have an equal number of free protons in the two reaction systems the number of SO_4^{2-} ions is the half of the Cl^- ones). Therefore, also from this comparison, the strong capacity that sulfonic functionalities can promote dehydration reactions is clear, as mentioned in Chapter 4. In fact, as further support of this observation, it can be noted that, although the sulfonic acid resin Amberlyst 15 is a heterogenous catalyst, and thus should have lower intrinsic reactivity than homogeneous catalysts as proven by its milder activity than H_2SO_4, it is almost two times more reactive than HCl. In fact, Amberlyst 15 produced comparable furanics yield of HCl but in the half of reaction time. The great reactivity of sulfonic functionalities coupled with the heterogeneous features of Amberlyst 15, confirmed the good choice of this catalyst as active material with which the fructose dehydration reaction condition can be screened. Moreover, it must be noted that, at the reaction time at which all catalysts have showed the best furanics production, comparable values of carbon balance were obtained, in the range of 78 - 80%. The sole exception is made for Hf-beta zeolite, which returned a poor 50% of carbon balance, underlining the detrimental effect that Lewis acid sites have on fructose at high temperature. Nevertheless, in no reaction mixture analysed were compounds different from those reported above detected by GC analysis, thus excluding retro aldol products of fructose as being responsible for the lower carbon balance.

Due to the promising activity and selectivity showed by Amberlyst 15 and H_2SO_4, these two catalysts were chosen to further investigate the possibility to develop a continuous process for fructose dehydration in alcoholic/aqueous media.

5.3.3 Continuous reactions

Having collected precious information on fructose dehydration in batch reactors, such as reaction conditions and active materials dependence, the possibility of performing the reaction continuously was explored in a Plug Flow Reactor (PFR). Due to the great furanics quantities yielded in the batch screening, Amberlyst 15 was selected as heterogeneous catalyst to attempt such a process. Thus, a PFR lab scale reactor was constructed by packing a defined amount of Amberlyst 15 inside a ¼ inch stainless steel tube and flushing through it a 1 wt.% fructose solution. In order to evaluate any possible differences on the catalyst performances by conducting the reaction in batch or

continuous modo operandi, the reaction conditions already screened in the preliminary batch study were adopted, such as 1 wt.% fructose solution in 95:5 wt.% MeOH/H_2O media at 180°C. In this continuous set up the pressure was fixed to 30 bar by placing a back-pressure regulator after the tubular reactor. Although in the same reaction condition in batch reactors Amberlyst 15 has showed the maximum of furanics yield at 10 min (Figure 4), in continuous processes the time scale at which the catalyst shows the best performance might be very different. In fact, as already discussed in Chapter 1, 3 and 4, in continuous processes the interaction between the catalyst and the substrate molecules might be different from the ones that occur in batch systems and several fluid dynamic phenomena might compete with the chemical reaction affecting the final product distributions. Therefore, a range of contact times was investigated to find the residential time at which furanics production result maximised in such PFR process.

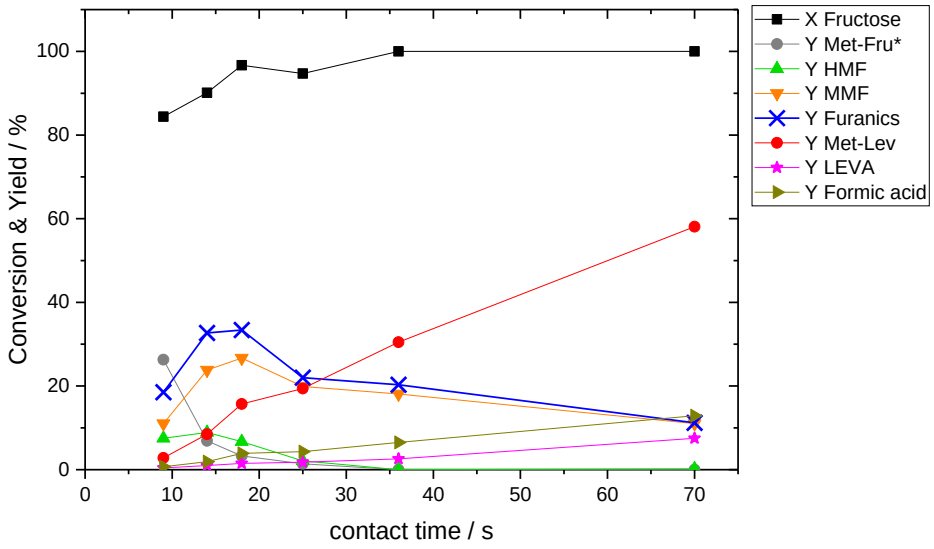

Figure 8 Fructose dehydration performed in plug flow reactor. The continuous reaction was performed by introducing 0.300 g of commercial Amberlyst 15 in a ¼ inch stainless steel tube and flushing through it a 1 wt.% fructose solution in 95:5 wt.% MeOH/H_2O media. The effluent flow was varied between 0.25 and 2 mL min^{-1} accordingly to have the contact times reported in the figure. The reaction was conducted at 180°C and 30 bar by using a back-pressure regulator.

As Figure 8 illustrates, in the reaction condition investigated, the furanics yield as function of contact time shows a volcano plot trend, likewise to that observed in batch systems as function of contact time. In fact, the catalyst provided the highest furanics productivity between 14 and 18 s of contact time (τ), retuning a value of 33% of yield. For τ shorter than 14 s the interaction between the substrate molecules and the catalyst resulted not sufficient to return a satisfactory furanics yield, generating methyl fructoside as main product, specifically 26% of yield in 9 s of contact time. Conversely, for τ longer than 18 s, consecutive reactions start to be predominant, consuming furanic products and favouring the generation of methyl levulinate, levulinic and formic acids. In fact, for contact time as

long as 70 s, the main product resulted to be methyl levulinate, showing 58% of yield. Hence, from these preliminary contact time experiments, it can be noted that, at the rection condition employed, the contact time window at which the furanics production is maximised is extremely short, about 4 s. The need of working in such a narrow range of contact time is a drawback for the intensification prospective of fructose dehydration, since it does not let much variation flexibility to eventually satisfy other process requirements such as catalyst productivity, catalyst stability or mass/heat exchanges. Furthermore, from this preliminary contact time profile it can be observed that the time scale at which the furanics production is maximised in this continuous reactor is much shorter compared to the one required in batch reactors. In fact, in the continuous reactor the maximum furanics yield is obtained in a contact time of around 15 s, compared to the 10 min required by the batch reactor. This is in good accordance with the higher catalyst-to-reactor volume ratio that tubular reactors show in comparison to vessel shape apparatuses. As consequence, in tubular reactors the interaction between the substrate molecules and the catalyst active sites occurs in a more restricted space, and is thus more intense. The more intense interaction between substate molecules and active sites that occur in tubular reactor compared to the batch system might also explain why in this continuous experiment the overall furanics yield obtained, 33%, is lower compared to the one achieved in batch reactor, 52%, despite the same catalyst, same reaction temperature and same substrate feed being used. Indeed, in this tubular reactor the interaction between reactants might be so intimate that as soon as the furanic products are formed they are still in the proximity of the acid functionalities thus, to immediately react again and be converted in consecutive products such as methyl levulinate. Conversely, in vessel systems, substrate molecules and catalyst particles are dispersed in a much wider volume, thus the time gap elapsed between the dehydration reaction and the consecutive ones might be broader. This hypothesis can be supported by the comparison of methyl levulinate yielded by the two systems at the same furanics yield. In the batch reactor, when the furanics yield accounted to 32% (2 min reaction time, Figure 4), the methyl levulinate yield resulted 1%. Whereas, in the PFR at the conditions which yield 33% of furanics (14 seconds contact time, Figure 8), the methyl levulinate yield account to 9%, almost an order of magnitude higher than the one yielded in the batch reactor. Therefore, in PFR, the furanics yield is more limited by the competition of the consecutive reactions which occur faster than in the batch system.

From the preliminary batch study arose the evidence that at increasing water aliquots in the system, all reaction rates decrease. Therefore, the effect of increasing water additions in the feed was studied also in the continuous system with the hope of decelerating all reaction rates and finding a contact time windows in which the reaction of furanics production is less overlapped with the consecutive reaction pathways. Thus, another

contact time profile study was performed in the continuous reactor in the same rection condition of the previous one but with higher amount of water, thus using a 1 wt.% fructose 90:10 wt.% MeOH/H_2O solution feed (Figure 9).

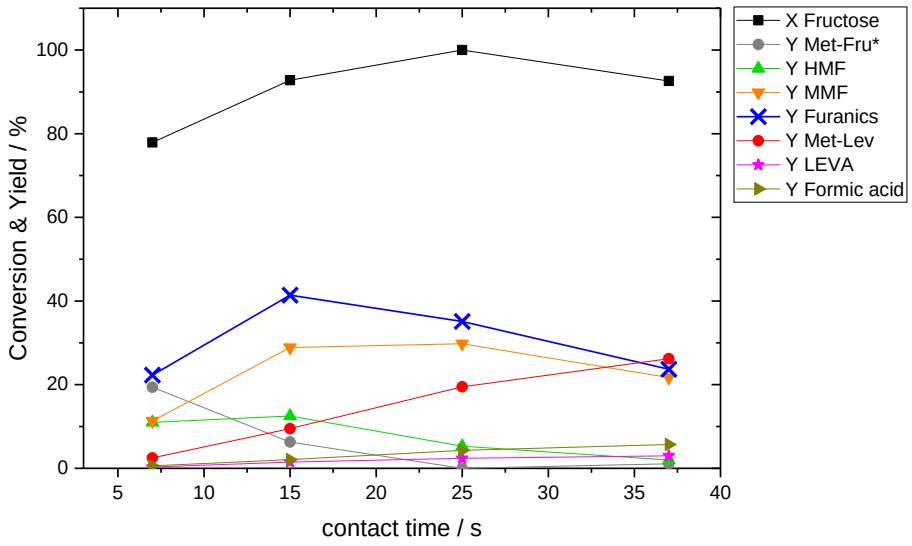

Figure 9 Fructose dehydration performed in plug flow reactor. The continuous reaction was performed by introducing 0.300 g of commercial Amberlyst 15 in a ¼ inch stainless steel tube and flushing through it a 1 wt.% fructose solution in 90:10 wt.% MeOH/H_2O media. The effluent flow was varied between 0.5 and 2 mL min^{-1} accordingly to have the contact times reported in the figure. The reaction was conducted at 180°C and 30 bar by using a back-pressure regulator.

Conducting the continuous fructose dehydration with 10 wt.% (Figure 9) of water presence in the alcoholic feed, compared to the 5 wt.% discussed in Figure 8, it can be noted the benefit of the increasing water aliquots also in continuous reactions. Indeed, it is possible to observe that by operating with 10 wt.% of water presence in the feed, the contact time window in which furanics yield is maximised was enlarged. Furthermore, it can be noted that, by operating with larger amount of water the furanics yield obtained at equal contact time is improved. For example, with 10 wt.% of water presence the highest furanics yield achieved reached 41%, at 15 s of contact time (Figure 9), whereas with 5 wt.% of water the highest furanic yield was only 32% (Figure 8). Again, at 25 s contact time, with 10 wt.% of water present in the feed, furanics compounds reached a value of 35% yield, against the 22% yield obtained in presence of 5 wt.% of water. Therefore, continuous fructose dehydration performed in alcoholic reaction environment not only demonstrate to tolerate amount up to 10 wt.% of water, but that the presence of aqueous aliquots in the feed improve furanics stability and productivity, conversely to what has been reported for other solvents.[93-99] This beneficial effect of water allows also to process much more concentrated fructose streams even in continuous systems, thus opening the opportunity to boost furanics productivities in fructose dehydration continuous processes. Furthermore, the possibility of producing furanics in a continuous alcoholic/aqueous

environment permits to conceptualise the coupling of fructose dehydration with the recently explored continuous glucose isomerisation catalysed by hetero-substituted zeolites, which showed promising performances in MeOH/H_2O media. Having discovered the advantages of working in 90:10 wt.% MeOH/H_2O environment, the amount of water was increased up to 20 wt.% to observe any further improvements. Therefore, a continuous fructose dehydration was conducted in a PFR system with the same reaction conditions of the previous experiments (Figure 8 and 9) but using a 1 wt.% fructose 80:20 wt.% MeOH/H_2O solution feed. (Figure 10).

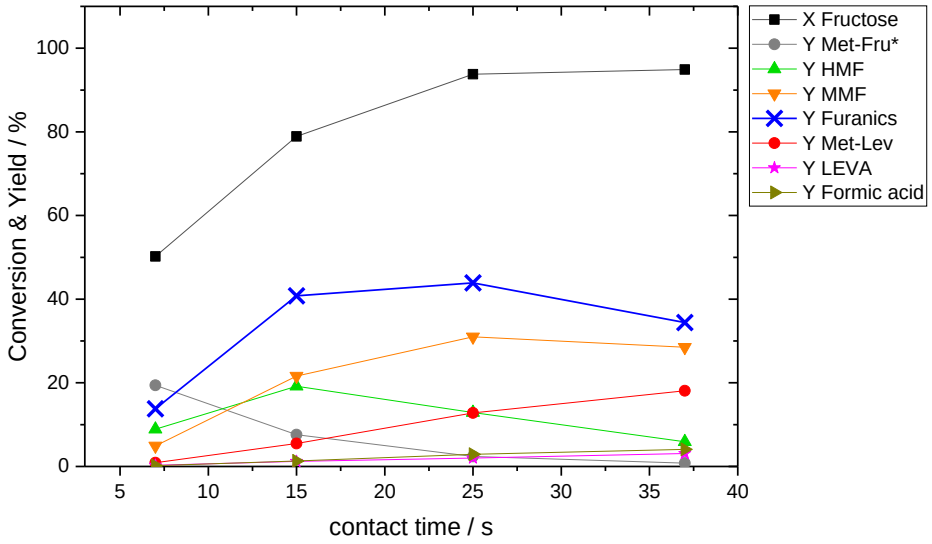

Figure 10 Fructose dehydration performed in plug flow reactor. The continuous reaction was performed by introducing 0.300 g of commercial Amberlyst 15 in a ¼ inch stainless steel tube and flushing through it a 1 wt.% fructose solution in 80:20 wt.% MeOH/H_2O media. The effluent flow was varied between 0.5 and 2 mL min^{-1} accordingly to have the contact times reported in the figure. The reaction was conducted at 180°C and 30 bar by using a back-pressure regulator.

Conducting fructose dehydration in MeOH solution with 20 wt.% of water, compared to 5 wt.% and 10 wt.%, enlarges the contact time window in which substantial furanics production are achieved further again. For example, in this condition, a furanics yield higher than 30% can be obtained in a τ range between 15 - 36 s, against the 15 - 25 s when 10 wt.% of water was used, and against the 14 - 18 s arisen in presence of 5 wt.% of water. It must be also noted that, regardless of the water amount present in the feed, the lower limit of these τ operational windows always resides around 15 s, whereas the upper limit is increased as function of the water amount present in the feed, and thus is the one that permit to operate in a large range of contact time. In fact, passing from 5 wt.% to 20 wt.% of water present in the feed, the upper limit of this contact time range is extended from 18 to 36 seconds. This might indicate that the rate which is most affected by the water additions is the rate of the consecutive reactions which transform furanics into consecutive products, whereas the rate of the dehydration reaction is less affected,

otherwise it must be observed also a shift in the contact time at which furanics start to form. Nevertheless, although in presence of 20 wt.% of water the contact time window in which furanics are stable was enlarged, the maximum of furanics yield obtained was not substantially increased, since the highest value of furanics achieved was 44% yield, against the 41% obtained in presence of 10 wt.% of water. For this reason, higher amount of water in the continuous process feed were not investigated. However, the possibility of working with 20 wt.% of water, compared to the pure MeOH solvent allow 5 times more concentrated sugar streams to be processed,[91] thus opening promising opportunities for intensification studies for continuous fructose dehydration processes.

Despite the improvements observed by increasing amount of water in the feed also in continuous processes, the highest furanics yield obtained in the continuous system, 44%, was substantially lower than the one achieved in batch reactors, 63%, at equal reaction condition (1 wt.% fructose 80:20 wt.% MeOH/H_2O solution feed, 180°C, Amberlyst 15). Therefore, having seen the great performances of furanics production showed by H_2SO_4 in the preliminary catalyst screening (Figure 7) a continuous fructose dehydration was attempted in a PFR system also using this homogeneous catalyst. To construct this continuous system, a proper amount of concentrated H_2SO_4 was added to a 1 wt.% fructose solution in 95:5 wt.% MeOH/H_2O media to have a 4 mM H_2SO_4 solution feed.

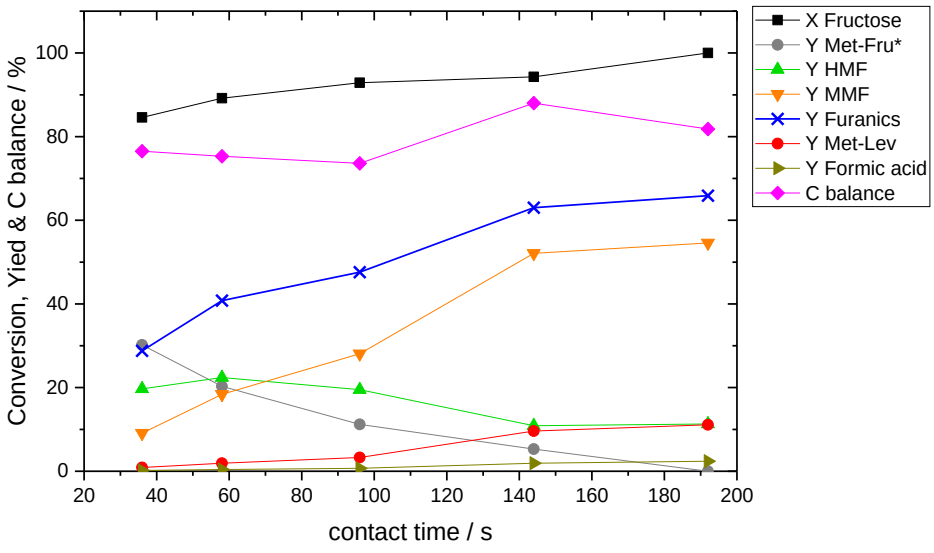

Figure 11 Fructose dehydration performed in plug flow reactor. The continuous reaction was performed by flushing 1 wt.% fructose solution in 95:5 wt.% MeOH/H_2O media and 4 mM H_2SO_4 through a ¼ inch stainless steel tube heated at 180°C and under 30 bar of back pressure regulator. The effluent flow was varied between 0.17 and 0.8 mL min^{-1} accordingly to have the contact times reported in the figure.

This acidic solution was then flushed through a 5 cm long ¼ inch stainless steel tube heated at 180°C. Two cooling ice-water baths were placed before and after the heated zone of the reactor in order to confine this heated zone only to the 5 cm length. In this way, the reactive zone of the system was intended as only the 5 cm heated zone.

As the contact profile of Figure 11 shows, the homogeneous acid H_2SO_4 results in higher furanics yield in the continuous system than Amberlyst 15. In fact, using H_2SO_4 as acid catalyst a 66% yield of furanics can be obtained, against the 33% obtained with Amberlyst 15 (Figure 8). It can be observed that with H_2SO_4, the furanics production obtained as function of the contact time has a much gentler trend then the ones provided by the heterogeneous catalyst Amberlyst 15 (Figure 8, 9 and 10). In this way, it is in fact possible to much better appreciate the evolution of the species involved in the dehydration reaction such as substrate, products and by products. Also in this case, it is possible to observe that at the shortest contact time employed, 36 s, it is prevalently methyl fructoside present as product, with a mild production of furanics, 29%, which are mainly composed of HMF (20%) than its methylated form MMF (9%). It can be also noted that at this short contact time the consecutive rehydration product methyl levulinate was produced in amounts as low as 1%. On the other hand, conducting the fructose dehydration at progressively longer contact times, the substrate conversion increased from 85% to 100%, and the methyl fructoside yield decreased favouring higher production of furanics, 66% at 192 s contact time which, in this case, are prevalently constituted by MMF. Furthermore, it can be also noted the linear increasing of the consecutive rehydration products methyl levulinate and formic acid by the increment of the reaction contact time. Interestingly, comparing the methyl levulinate yield obtained at equal furanic production by the continuous process catalysed by Amberlyst 15 and H_2SO_4, it can be noted that when Amberlyst 15 yielded nearly 30% of furanics the methyl levulinate production accounted to 11% (Figure 8), whereas using H_2SO_4 the consecutive rehydration product yield resulted only 1% (Figure 11). Considering that both reactions were conducted at the same temperature of 180°C and in presence of the same feed water amount, 5 wt.%, this difference might be attributed to the very low concertation of H_2SO_4 (4 mM) used when the continuous reaction was catalysed by this homogeneous acid. Such low acid concentration might help improve furanics selectivity compared to the formation of rehydration consecutive products. This might be also a reasonable explanation why with H_2SO_4 the furanics yield obtained is 22% higher than the one achieved with Amberlyst 15. Therefore, to improve the furanics production yielded by an heterogeneous catalyst it may be attempted to reduce the acid strength of the active materials. For example, it can be explored an acid resin with a lower acid sites density than Amberlyst 15 or attempting to dilute the catalyst Amberlyst 15 with an inert material, such as silica light, before its introduction in the tubular reactor. However, since the final purpose of this work is to study fructose dehydration reaction in

alcoholic/aqueous environment and evaluate the potential of an integrated continuous process for furanics production from glucose, a detailed intensification study of furanics production using exclusively heterogeneous materials goes beyond the aim. Nevertheless, having defined which reaction conditions favour the formation of consecutive rehydration products such as levulinates is of crucial interest as well. Indeed, as illustrated in the introduction of this chapter, levulinates can be transformed in other valuable products different than the one obtained from furanics. Hence, having a continuous process which allow to decide which platform molecules produce just by adapting operational conditions, is a competitive industrial advantage since allows to promptly respond to eventual market product demand variations. Furthermore, in an economic optimisation prospective, separation of furanics from levulinates might be more favourable than the separation from unconverted sugars and their recycling. Therefore, it might be more advantageous obtaining lower yield of furanics but in mixture with levulinates instead of unreacted substrate. Furthermore, it must be noted that assisting the fructose dehydration with H_2SO_4, the average value of carbon balance is constant to 80% regardless to the reaction contact time used and the fructose conversion achieved. It must be also mentioned that using H_2SO_4 in the continuous system, retro aldol fructose products were not detected by GC analysis.

Having observed the great performances of diluted H_2SO_4 in converting fructose to furanics and its easer implementation in a continuous reaction, this homogeneous catalyst has been chosen to preliminary study the integration of continuous glucose isomerisation with the continuous fructose dehydration. Furthermore, it must be recognised that, due to its homogeneous nature as active material, H_2SO_4 is not threatened by deactivation phenomena as a heterogeneous catalyst might be, thus allowing a much easier and quicker evaluation of the integrated process.

5.3.4 Attempting and integrated continuous process for furanics production from fructose.

As already mentioned in the introduction of this chapter, glucose isomerisation is greatly catalysed by hetero-substituted aluminosilicates such as Sn-beta and Hf-beta zeolites. Unfortunately, this kind of materials do not return great furanics production when used as fructose dehydration catalyst, as showed in the previous batch catalyst screening (Figure 7). Therefore, a cascade reaction from glucose to furanics using the same catalyst for the isomerisation and dehydration step can not be developed, even if the two steps are conducted in different reaction condition such as reaction temperature or contact times, as the results in Figure 7 shows. Furthermore, a single catalyst bed constituted by a mixture composed by the isomerisation and dehydration catalysts is hardly applicable. In fact, the catalyst screening performed on batch fructose dehydration (Figure 7), indicate

that in presence of Lewis acids fructose undergoes to substantial degradation in just 10 min of reaction time. Therefore, it might be conceived a two-step continuous process, in which the two reactions, isomerisation and dehydration are conducted individually. Specifically, it might be proposed a two-step PFR process in which the outcoming effluent from the first isomerisation catalyst bed is then processed in a second dehydration catalyst bed. In this way, operating with two separated catalytic zones, the operational conditions of each reaction can be also individually tuned to optimise each reaction step. As discussed in Chapter 1, the separation and recovery of products from a reaction mixture is one of the most expensive and energy demanding unit of a chemical process. Therefore, the best-case scenario for the integrated production of furanics from glucose, is to avoid an intermediate products separation between the two consecutive catalyst beds. In this way, the process design and plant implementation would be simplified, the energy and auxiliary chemicals employment would be minimised, leading to an overall sustainability and profitability enhancement. In this scenario, the outlet effluent of the first isomerisation step is directly processed in the second dehydration process (scheme 4), implying that all the chemical species generated by the isomerisation unit will be subjected to the dehydration catalyst.

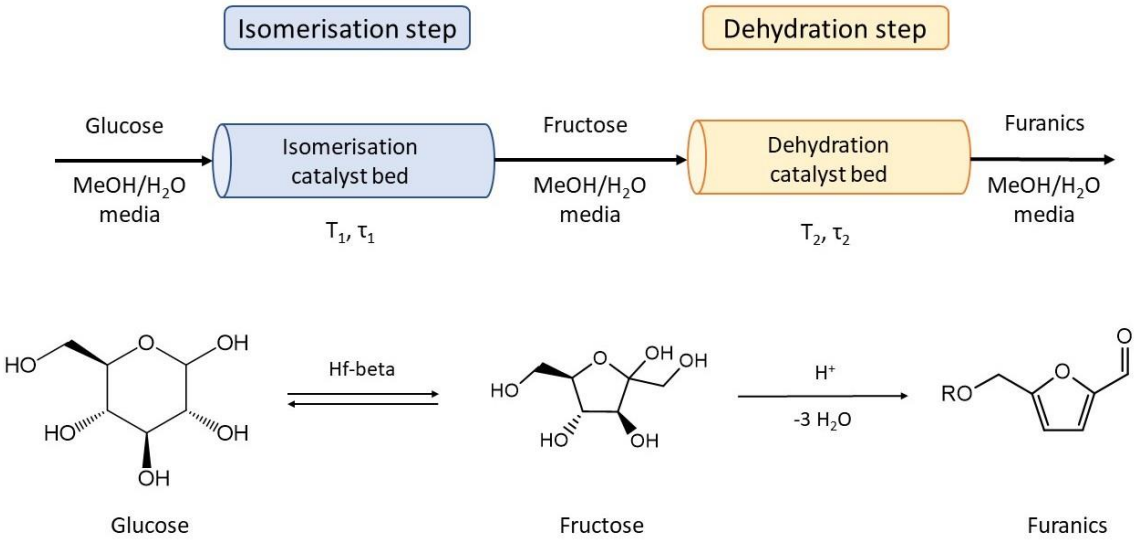

Scheme 4 Schematic representation of the continuous integrated process for furanics production from glucose in MeOH/H_2O media. In the showed approach two different PFR reactor systems are employed in series. Inside each reactor resides the specific catalyst to assist a specific reaction step, glucose isomerisation and fructose dehydration, of the integrated process. In this way each reactor system can be operated at its own temperature (T) and contact time (τ). As showed in the scheme, in between the two catalytic bed is not present any separation unit. Therefore, the effluent of the first isomerisation reaction is directly used as inlet of the dehydration reaction. The chemical representation is placed as an eye guide to show the reaction pathways required to transform glucose into furanics.

Therefore, it must be ascertained that eventual by-products formed during glucose isomerisation, or even unconverted glucose itself, do not interfere with the fructose dehydration which occur in the second unit. In fact, although the great activity, selectivity and stability shown by hetero-substituted zeolites in isomerising glucose,[71-80] the fructose yield they provide is still limited by the thermodynamic equilibrium which characterise glucose isomerisation reaction, yielding a maximum of nearly 50% fructose yield. For this reason, at the end of glucose isomerisation process the methanol/aqueous reaction effluent will be composed, in the best-case scenario, of a 50:50 glucose/fructose mixture. Currently, the industrial separation of glucose from fructose is very energy demanding due to the very similar properties that the two sugars possess. Therefore, constructing an integrated process in which the fructose produced by the isomerisation step is then converted in furanic compounds holds also the advantage that at the end of the integrated process will be obtained a product mixture likely easer to separate than the glucose/fructose mixture. In this way, the unreacted glucose could be easer recovered and recycled for another isomerisation treatment and thus not wasted. However, to allow this, it is of crucial importance understand if the unreacted glucose of the isomerisation step is not degraded under the fructose dehydration condition and does not negatively affect the fructose dehydration reaction. Despite the clear complexity and hardship that is arising in considering all the variables that come to plays when this kind of integrated process is wanted to be achieved, the profit and sustainability benefits that it potentially holds are significant. Therefore, to minimise the variables and phenomena that might affect furanics production in this complex system, a preliminary simplified continuous process was developed. Specifically, to have a dehydration feed of time-invariable composition and to nullify eventual by-products generated by the isomerisation step, a single step continuous dehydration reaction was conducted using a mixture of 1 wt.% 50:50 glucose/fructose in 95:5 wt.% MeOH/H_2O media as feed. Although it adds a level of complexity, 5 wt.% of water was chosen to be added in the methanol feed because, as previously mentioned, is the favoured solvent for the glucose isomerisation step and has provided beneficial effects also on furanics production. Moreover, the presence of water allows to process more concentrated sugar streams, hence an alcoholic/aqueous media will be the favourable solvent also for eventual future intensification studies. Furthermore, to avoid any furanics yield alteration due to catalyst deactivation, an homogeneous catalyst such as H_2SO_4 was used. In fact, as mentioned before, homogeneous catalysts employed in PFR systems do not undergo deactivation phenomena as their heterogeneous analogues. Moreover, H_2SO_4 continuous performances on dehydrating fructose alone have been already studied in the previous paragraphs, thus having a reliable benchmark to which evaluate the effect of introducing eventual unconverted glucose in the dehydration step. Therefore, to understand the behaviour of an ideal

glucose isomerisation effluent in a dehydration process, a continuous dehydration reaction was conducted by acidifying a mixture of 1 wt.% 50:50 glucose/fructose in 95:5 wt.% MeOH/H_2O feed with H_2SO_4 and then flushing it in a heated 5 cm ¼ inch stainless steel tube at different contact times (Figure 12). Since the most valuable products investigated, i.e. furanics, and their by-products, such as methyl levulinate, can be generated only from fructose and not from glucose, the yield of these compounds has been calculated and reported based to the initial fructose amount, 0.5 wt.%, instead on the whole sugar quantity, 1.0 wt.%. In this way it is also possible to directly compare product yields originated from this combined feed experiment (Figure 12) to the product yields resulted from the system in which fructose was dehydrated as sole sugar (Figure 11). Unfortunately, the methylated products of the two substrates, methyl fructoside and methyl glucoside, have the same retention time according to the HPLC method used for saccharides analysis, and thus can not be separated and quantified individually. For this reason, yield of methylated substrates has not been reported in this case due to the misinterpretation that might arise by analysing a not product specific yield trend.

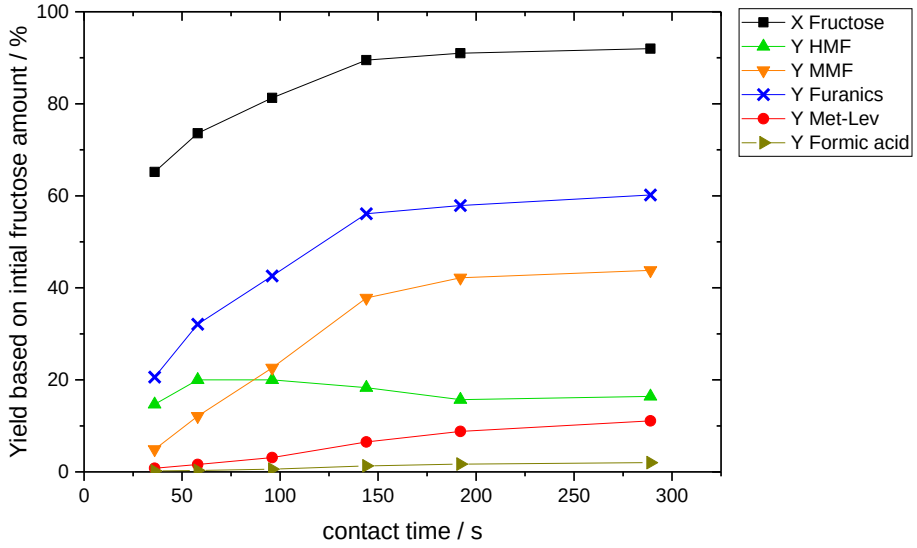

Figure 12 Products yield of the dehydration of 1 wt.% 50:50 glucose/fructose mixture in 95:5 wt.% MeOH/H_2O media performed in a plug flow reactor. The mixture was acidified with H_2SO_4 before starting the reaction thus resulting in a 4 mM H_2SO_4 solution feed. The continuous reaction was performed by flushing the resulting solution through a ¼ inch stainless steel tube heated at 180°C and under 30 bar of back pressure regulator. The effluent flow was varied between 0.1 and 0.8 mL min^{-1} accordingly to have the contact times reported in the figure. Product yields are calculated and reported based on the fructose amount initially present in the feed.

However, from Figure 12 it can be observed that the evolution trend of all other compounds as function of contact time resulted from this experiment is very similar to that obtained when fructose was processed alone (Figure 11). In fact, also in presence of 0.5 wt.% of glucose, it can be observed that fructose is able to fully react if substantially long

contact times are employed. In particular, fructose conversion progressively increased by extending the contact time, starting from a 20% conversion value for 36 s of contact time and reaching 92% conversion if the contact time is prolonged to 289 s. Also the trend of furanics production is very similar to what is obtained when fructose was processed alone (Figure 11). Specifically, in this case, a furanics yield of 21% is obtained for short contact time (36 s) and gradually enhance to 60% if the contact time is extended to 289 s. It must be remembered that maximum furanics yield achieved from the dehydration reaction of fructose alone was 66% (Figure 11). Furthermore, the distribution of the furanics compounds is as well in accordance with previous experiments. In fact, at short contact times the furanic composition is predominantly dominated by HMF, which is consecutively methylated to MMF if higher contact times are employed. Also the generation of consecutive products is similar to those observed when fructose was processed alone, obtaining in both cases 11% yield of methyl levulinate when harsher reaction conditions were used. Therefore, from both a qualitative and quantitative point of view it can be concluded that presence of glucose in the reaction environment does not affect the dehydration of fructose toward furanics.

However, in order to correctly evaluate the possibility of constructing an integrated process from glucose to furanics, it must be also ascertained that the unreacted glucose from the first isomerisation step does not degrade under the reaction condition employed for the dehydration reaction. In fact, some scientific works have reported that glucose processed at reaction condition most likely used during fructose dehydration tents to be converted into unprofitable compounds such as anhydrosugars or disaccharides.[67-69] However, the beneficial effect of using an alcoholic/aqueous solvent observed on furanics stability might improve also glucose stability. Hence, in order to evaluate the reactivity of glucose under the dehydration reaction condition glucose conversion values were reported (Figure 13).

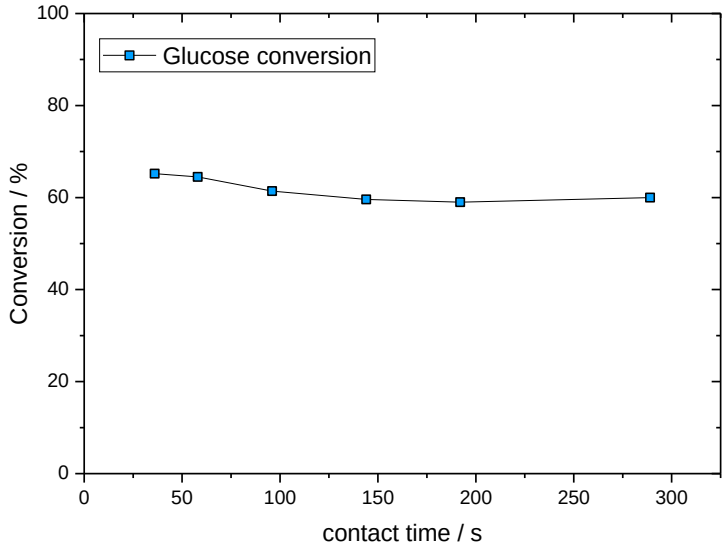

Figure 13 Glucose conversion resulted from the dehydration of 1 wt.% 50:50 glucose/fructose mixture in 95:5 wt.% MeOH/H_2O media performed in a plug flow reactor. The mixture was acidified with H_2SO_4 before starting the reaction thus resulting in a 4 mM H_2SO_4 solution. The continuous reaction was performed by flushing the resulting solution through a ¼ inch stainless steel tube heated at 180°C and under 30 bar of back pressure regulator. The effluent flow was varied between 0.1 and 0.8 mL min^{-1} accordingly to have the contact times reported in the figure.

As can be observed from Figure 13, under the reaction condition employed to dehydrate fructose, around 60% of glucose introduced in the reactor undergoes to some chemical reaction regardless the reaction contact time employed. It must be reported that apart from the compounds discussed in Figure 12, no other chemical species were detected by HPLC and GC analysis during the reaction, except substrate methylation products. As previous introduced, the methylated products of the two sugar substrates, methyl fructoside and methyl glucoside, can not be separated by the HPLC method used to analyse saccharides. However, as demonstrated at the beginning of this chapter (Figure 3), the ELSD response factor of two methylated compounds is very similar, and thus it is possible to determine their quantity as a total amount and use that information to calculate the carbon balance of the whole feed during the dehydration reaction (Figure 14).

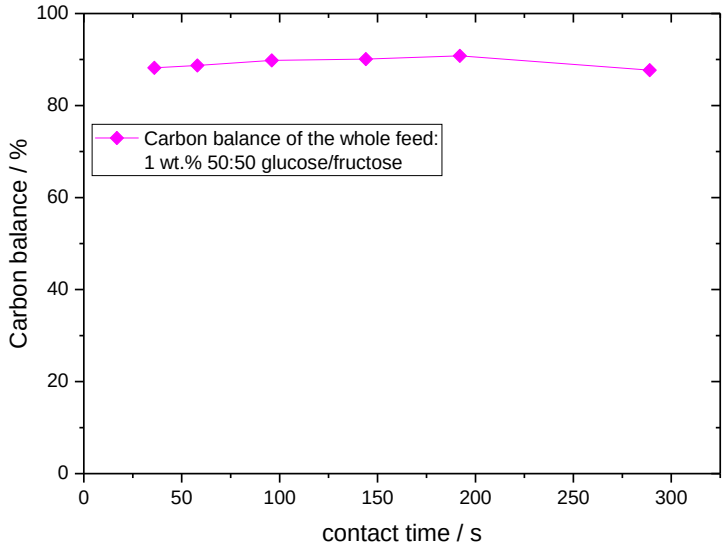

Figure 14 Carbon balance of the combined feed 1 wt.% 50:50 glucose/fructose in 95:5 wt.% MeOH/H_2O media resulted from the dehydration reaction performed in a plug flow reactor. The mixture was acidified with H_2SO_4 before starting the reaction resulting in a 4 mM H_2SO_4 solution. The continuous reaction was performed by flushing the resulting solution through a ¼ inch stainless steel tube heated at 180°C and under 30 bar of back pressure regulator. The effluent flow was varied between 0.1 and 0.8 mL min^{-1} accordingly to have the contact times reported in the figure.

From Figure 14 it can be observed that if the sugar methylated products are included among the products generated by the dehydration reaction, the carbon balance of the combined substrate feed shows a constant 90% value as function of the contact time employed. Therefore, it can be stated that during the dehydration reaction very little amounts of the sugars introduced in the reactor is degraded and thus wasted assuming that methyl glycoside is not an irreversible product. Furthermore, the fact that an almost full carbon balance is achieved when the amount of methylated substrates is considered among the reaction products, points out that also that the 60% of glucose converted (Figure 13) has been predominantly methylated, otherwise a much lower carbon balance would have been observed. This represents an important breakthrough for the development of the integrated production of furanics from glucose because allows to conceive the recycling of the residual glucose and its methylated form after the dehydration step and their utilisation in a further isomerisation treatment, thus to not waste any precious carbon feedstock. However, to ascertain the fact that glucose undergoes to methylation only is required a much more accurate and direct determination of each individual methylated sugar compound. Nonetheless, despite the lack of complete certainty of which products is formed when glucose is treated under fructose dehydration reaction condition, it can be stated that whatever products is formed does not interfere with the fructose dehydration reaction and the furanics production, as demonstrated by

the equal dehydration performances resulted by conducting the fructose dehydration reaction in absence (Figure 11) and in presence (Figure 12) of glucose.

5.4 Conclusion

Among the very large scientific bibliography on furanics production from fructose, only few works have been conducted in an alcoholic environment, which constituted the breakthrough for the development of the continuous dehydration of sorbitol to isosorbide (Chapter 4). For this reason, in this chapter, the opportunity to conduct fructose dehydration in alcoholic media to evaluate any potential improvement for furanics production was investigated. However, conducting fructose dehydration in alcoholic/aqueous reaction media might offers greater advantages rather than in mere alcohol solvent. In fact, if the dehydration reaction is able to tolerate small amount of water, it would be possible to process much more concentrated substrate feed and thus, highly improving process productivity. Moreover, it must be considered that during the dehydration reaction, for each molecule of fructose converted into HMF, three molecule of water are produced. Therefore, for process intensification perspective, when large amount of substrate would be processed and thus high amount of water co-produced, knowing the effect of water on the fructose dehydration reaction is imperative. Furthermore, recent studies on glucose isomerisation to fructose catalysed by metal substituted zeolites have demonstrated that higher catalyst stability and selectivity are achieved if small aliquots of water (5 wt.%) are added in an alcoholic reaction environment. Thus, if fructose dehydration reaction is able to tolerate such small amount of water, the opportunity to couple glucose isomerisation process with the fructose dehydration reaction may arise, allowing to develop an integrated process for furanics production from glucose. Despite these great potential improvements that might spring by conducting fructose dehydration in an alcoholic/aqueous reaction media, this combined solvent, to our knowledge, has never been attempted for furanics production.

Therefore, in this chapter has been explored the opportunity to perform fructose dehydration in an alcoholic/aqueous reaction media. Exploratory batch studies have demonstrated that fructose dehydration catalysed by an heterogeneous catalysts such as Amberlyst 15 is able to tolerate water aliquots since the reaction conducted in a 95:5 wt.% MeOH/H_2O environment at 180°C leads to a successful 63% furanics yield in 10 min of reaction time, compared to the 57% of furanics yield obtained when the reaction is conducted in mere MeOH. This promising result encouraged the study of further water additions to the dehydration environment up to 50 wt.%. The system showed remarkable water tolerance since up to 10 wt.% of water the outcome of the dehydration reaction is not affected, still reporting a 60% of furanics yield. Increased water amounts resulted in a

gradual decreasing of fructose conversion and furanics yield, but without returning any degradation products, as instead reported when water was added to other solvents.[93-99] Time online experiments performed in a 50:50 wt.% MeOH/H_2O confirmed that water, when added in an alcoholic reaction media, only decreases the reaction rate of the dehydration reaction, but it does not favour furanics degradation. In fact, the only by-product detected during these batch experiments was methyl levulinate, the rehydration products of MMF. However, it was observed that the amount of methyl levulinate increases if less water is present in the reaction system, registering the highest yield, 21%, when the reaction was conducted in MeOH alone. Therefore, these experiments demonstrated a strong tolerance to water from furanics and from the fructose dehydration reaction if processed in an alcoholic environment, conversely to what is reported in literature when water is added to other kind of solvents.[93-99]

Subsequently, a batch screening of different acid catalysts was performed to assess how different catalytic features might impact furanics production in this promising alcoholic/aqueous solvent. Weak Brønsted acids, such as aluminium zeolites, have demonstrated lower activity and selectivity in producing furanics than Amberlyst 15, while zeolites that possess only Lewis acid functionalities, such as Hf-beta, did not reported any furanics productivity at all. Conversely, both homogeneous catalysts tested, HCl and H_2SO_4 showed comparable selectivity feature to Amberlyst 15, although H_2SO_4 was more active than Amberlyst 15 and HCl. Therefore, from this batch catalyst screening it was concluded that Brønsted acid sites are mandatory for a successful fructose dehydration to furanics and that sulfonic functionalities boost furanics production.

The promising results obtained on furanics productivity and stability by using an alcoholic/aqueous solvent spurred to investigate the employment of this reaction media also for continuous reactions. Due to its heterogeneous nature, coupled with the great activity and selectivity features showed in batch experiments, Amberlyst 15 was selected to develop the continuous fructose dehydration performed in alcoholic/aqueous environment. Therefore, a PFR system was constructed, and a continuous fructose dehydration assisted by Amberlyst 15 was studied at different reaction contact time employing a 95:5 MeOH/H_2O solvent media. The continuous reactions yielded a volcano plot trend of furanics production in function of contact time, although displaying only a 4 s contact time window in which the furanics production resulted maximised to a 33% of yield. This short operational contact time window represents a drawback for intensification purposes since it does not allow much operational flexibility. Therefore, having previously observed that increasing water additions in the acholic solvents decreases dehydration reaction rates, higher water amount was added to the reaction environment to attempt to enlarge that operational windows and thus increasing furanics production. In fact, by increasing the water amount to 10 wt.%, the operational contact time window in which a

substantial furanics yield was obtained was enlarged. As consequence, also the overall furanics production improved returning a 41% of yield. Additional water amounts to the reaction solvent further enlarged the volcano plot shape trend of furanics production in function of contact time but did not further enhanced furanics yield.
Therefore, also in continuous operation, water additions to the alcoholic reaction solvent demonstrated beneficial effects by increasing the overall furanics yield and allowed to operate in a much broader contact time window in which a substantial furanics production is obtained.

The capability of fructose dehydration to tolerate amount of water in an alcoholic environment also in continuous operation, opened the possibility to couple the process with glucose isomerisation catalysed by metal substituted zeolites, thus to develop an integrated furanics production from glucose. However, prior to develop such a process, a series of assessment experiments must be performed. For example, it must be ascertained that the unreacted glucose fraction from the isomerisation step does not affect the furanics production in the following dehydration step and neither it undergoes degradation reactions under the condition required for the dehydration. Furthermore, it must be verified the behaviour of HMF and MMF in presence of the metal-substituted zeolites used for glucose isomerisation. In fact, if HMF and MMF are not degraded by those catalysts the dehydration effluent might be passed in a further isomerisation step, thus to further convert the unreacted glucose into fructose and fully exploit the glucose amount originally present in the feedstock.

Therefore, to understand the behaviour of an glucose isomerisation effluent in a dehydration process, an ideal 1 wt.% 50:50 glucose/fructose feed was processed in a continuous PFR system and catalysed by H_2SO_4. For this evaluation test was chosen to use H_2SO_4 as catalyst since, in addition of providing the best furanics yields, it does not undergo to any deactivation phenomena due to its homogeneous nature, thus returning invariable performances along the reaction occurring. Interestingly, the dehydration reaction performed with a 50:50 glucose/fructose feed, returned the same dehydration performances resulted when fructose was processed alone, pointing out that the glucose does not affect the fructose dehydration reaction and does not interfere with furanics production. Furthermore, the carbon balance of the whole sugar feed processed resulted 90% for each contact time employed, demonstrating that minimal sugar amounts have been deteriorated during the dehydration process. However, direct quantification and identification of which products is originated from glucose under dehydration conditions has not been possible due to the difficulty of separating the methylated sugar products by chromatographic analysis. Therefore, to evaluate the real potential of an integrated process from glucose to furanics in an alcoholic/aqueous environment a much more in-

depth analysis of which products are originated from glucose when is processed under fructose dehydration condition is required.

However, this work demonstrated that fructose dehydration can tolerate water aliquots up to 50% in the reaction environment if the reaction is processed in an alcoholic reaction media, both in batch and continuous operations, conversely to what has been reported for other solvents.[93-99] The ability of fructose dehydration to tolerate such high amount of water when conducted in an alcoholic environment allows to process much more concentrated fructose streams thus permitting new intensification strategies for furanics production to be designed. Furthermore, the possibility of conducting fructose dehydration in an alcoholic/aqueous environment allows to conceptualise the integration of fructose dehydration with glucose isomerisation, thus opening new opportunities to develop much more efficient technologies to produce important platform molecules, such as furanics, from biomass.

5.5 Reference

1) C. Xu, E. Paone, D. Rodríguez-Padrón, R. Luque, F. Mauriello, *Chem. Soc. Rev*, 2020, **49**, 4273.
2) R. J. Van Putten, J. C. van der Waal, E. de Jong, C. B. Rasrendra, H. J. Heeres, J. G. de Vries. *Chem. Rev.*, 2013, **113**, 1499.
3) K. I. Galkin, V. P. Ananikov, *ChemSusChem*, 2019, **12**, 2976.
4) S. Chen, R. Wojcieszak, F. Dumeignil, E. Marceau, S. Royer, *Chem. Rev.*, 2018, **118**, 11023.
5) A. Gandini, M. N. Belgacem, *Prog. Polym. Sci.*, 1997, **22**, 1203.
6) L. Cottier, G. Descotes, J. Lewkowski, R. Skowronski, *Pol. J. Chem.*, 1994, **68**, 69.
7) C. Thoma, J. Konnerth, W. Sailer-Kronlachner, P. Solt, T. Rosenau, H. W. G. van Herwijnen, *ChemSusChem*, 2020, **13**, 3544.
8) H. Kobayashi, A. Fukuoka, *Green Chem.*, 2013, **15**, 1740.
9) J. Zhang, T. Wang, X. Tang, L. Peng, J. Wei, L. Lin, *BioResources*, 2018, **13**, 7137.
10) A. S. Amarasekara, D. Green, L.D.Williams, *Eur.Polym. J.*, 2009, **45**, 595.
11) Y. Romàn-Leshkov, C. J. Barrett, Z. Y. Liu, J. A. Dumesic, *Nature*, 2007, **447**, 982
12) A. Corma, S. Iborra, A. Velty, *Chem. Rev*., 2007, **107**, 2411.
13) J. J. Bozell, G. R. Petersen, *Green Chem*., 2010, **12**, 539.
14) D. M. Alonso, J. Q. Bond, J. A. Dumesic, *Green Chem.*, 2010, **12**, 1493.
15) J. J. Bozell, L. Moens, D. C. Elliott, Y. Wang, G. G. Neuenscwander, S. W. Fitzpatrick, R. J. Bilski, J. L. Jarnefeld, *Resour., Conserv. Recycl*., 2000, **28**, 227.
16) Y. Guo, K. Li, J. H. Clark, *Green Chem*., 2007, **9**, 839.
17) Y. Gong, L. Lin, J. B. Shi, S. J. Liu, *Molecules*, 2010, **15**, 7946.
18) H. Mehdi, V. Fabos, R. Tuba, A. Bodor, L. T. Mika, I. T. Horvath, *Top. Catal*., 2008, **48**, 49.
19) D. M. Alonso, J. M. R. Gallo, M. A. Mellmer, S. G. Wettsteinab, J. A. Dumesic, *Catal. Sci. Technol.*, 2013, **3**, 927.
20) E. I. Gurbuz, D. M. Alonso, J. Q. Bond, J. A. Dumesic, *ChemSusChem*, 2011, **4**, 357.

21) D. Fegyverneki, L. Orha, G. Lang, I. T. Horvath, Tetrahedron, 2010, **66**, 1078.
22) I. T. Horvath, H. Mehdi, V. Fabos, L. Boda, L. T. Mika, *Green Chem*., 2008, **10**, 238.
23) D. M. Alonso, J. Q. Bond, J. C. Serrano-Ruiz, J. A. Dumesic, *Green Chem*., 2010, **12**, 992.
24) J. Q. Bond, D. M. Alonso, D. Wang, R. M. West, J. A. Dumesic, *Science*, 2010, **327**, 1110.
25) S. G. Wettstein, D. M. Alonso, J. A. Dumesic, *Curr. Opin. Chem. Eng*. 2012, **1**, 218.
26) S. G. Wettstein, D. M. Alonso, Y. Chong, J. A. Dumesic, *Energy Environ. Sci*. 2012, **5**, 8199.
27) G. P. Perez, A. Mukherjee, M. J. Dumont, *Journal of Industrial and Engineering Chemistry*, 2019, **70**, 1.
28) F.W. Lichtenthaler, S. Peters, *C. R. Chimie*, 2004, **7**, 65.
29) B. F. M. Kuster, *Starch-Stärke*, 1990, **42**, 314.
30) N. A. S. Ramli, N. A. S. Amin, *BioEnergy Research*, 2020, **13**, 693.
31) Y. Román-Leshkov, J. N. Chheda, J. A. Dumesic, *Science*, 2006, **312**, 1933.
32) J.N. Chheda, Y. Román-Leshkov, J. A. Dumesic, *Green Chem*. 2007, **9**, 342.
33) D. Mercadier, L. Rigal, A. J. Gaset, *Chem. Tech. Biotechnol*. 1981, **31**, 497.
34) G. A. Halliday, R. J. Young, V. V. Grushin, *Org. Lett.* 2003, **5**, 2003.
35) C. Moreau, R. Durand, S. Razigade, *Appl. Catal. A*, 1996, **145**, 211.
36) C. Aellig, I. Hermans, *ChemSusChem*, 2012, **5**, 1737.
37) P. Rivalier, J. Duhamet, C. Moreau, *Catal. Today*, 1995, **24**, 165.
38) C. Moreau, R. Durand, F. Aliès, *Ind. Crops Prod*. 2000, **11**, 237.
39) M. A. Schwegler, P. Vinke, M. Van der Eijk, H. Van Bekkum, *Appl. Catal. A*, 1992, **80**, 41.
40) R. van Putten, J. C. van der Waal, M. Harmse, H. H. van de Bovenkamp, E. de Jong, H. J. Heeres, *ChemSusChem*, 2016, **9**,1827.
41) L. M. Sanchez, H. J. Thomas, M. J. Climent, G. P. Romanelli, S. Iborra, *Catal. Rev*. 2016, **58**, 497.
42) O. H. Pardo Cuervo, G. P. Romanelli, J. A. Cubillos, H. A. Rojas, J. J. Martínez, J. J. *ChemistrySelect*, 2020, **5**, 4186.
43) A. Takagaki, M. Ohara, S. Nishimura, K. Ebitani*, Chem. Commun.*, 2009, 6276.
44) R. Huang, W. Qi, R. Su, Z. He, *Chem. Commun.*, 2010, **46**, 1115.
45) E. Nikolla, Y. Roman-Leshkov, M. Moliner, M. E. Davis, *ACS Catal.*, 2011, **1**, 408.
46) Y. J. Pagán-Torres, T. Wang, J. M. R. Gallo, B. H. Shanks, J. A. Dumesic, *ACS Catal.*, 2012, **2**, 930.
47) V. Choudhary, S. H. Mushrif, C. Ho, A. Anderko, V. Nikolakis, N. S. Marinkovic, A. I. Frenkel, S. I. Sandler, D. G. Vlachos, *J. Am. Chem. Soc*., 2013, **135**, 3997.
48) M. Moreno-Recio, J. Santamaría-González, P. Maireles-Torres, *Chem. Eng. J.* 2016, **303**, 22.
49) R. Otomo, T. Yokoi, T. Tatsumi, *ChemCatchem*, 2015, **7**, 4180.
50) N. Candu, M. El Fergania, M. Verziua, B. Cojocarua, B. Jurcab, N. Apostolc, C. Teodorescuc, V. I. Parvulescua, S. M. Comana, *Catalysis Today*, 2019, **325**, 109.
51) I. Jiménez-Morales, J. Santamaría-González, A. Jiménez-López, P. Maireles-Torres, *Fuel*, 2014, **118**, 265.
52) L. Zhang, G. Xi, Z. Chen, Z. Qi, X. Wang, *Chem. Eng. J.* 2017, **307**, 877.
53) L. Atanda, S. Mukundan, A. Shrotri, Q. Ma, J. Beltramini, *ChemCatChem*, 2015, **7**, 781.

54) L. Atanda, A. Shrotri, S. Mukundan, Q. Ma, M. Konarova, J. Beltramini, ChemSuschem, 2015, **8**, 2907.
55) X. Qi, M. Watanabe, T. M. Aida, R. L. Smith Jr, *Catal. Commun.*, 2008, **9**, 2244.
56) M. Chidambaram, A. T. Bell, *Green Chem*., 2010, **12**, 1253.
57) L. Hu, Y. Sun, L. Lin, S. Liu, *Biomass Bioenergy*, 2012, **47**, 289.
58) Y. Lu, M. Huo, *RSC Adv.*, 2015, **5**, 30869.
59) C. Fan, H. Guan, H. Zhang, J. Wang, S. Wang, X. Wang, *Biomass Bioenergy*, 2011, **35**, 2659.
60) D. Chen, F. Liang, D. Feng, M. Xian, H. Zhang, H. Liu, F. Du, *Chem. Eng. J.*, 2016, **300**, 177.
61) C. Thoma, J. Konnerth, W. Sailer-Kronlachner, P. Solt, T. Rosenau, H. W. G. van Herwijnen, *ChemSusChem*, 2020, **13**, 3544.
62) L. K. Ren, L. F. Zhu, T. Qi, J. Q. Tang, H. Q. Yang, C. W. Hu, *ACS Catal.*, 2017, **7**, 2199.
63) Y. Román-Leshkov, J. A. Dumesic, *Top Catal*, 2009, **52**, 297.
64) X. Qi, M. Watanabe, T. M. Aida, R. L. Smith Jr, *Ind. Eng. Chem. Res*., 2008, **47**, 9234.
65) X. Hu, C. Li, *GreenChem*., 2011, **13**, 1676.
66) J. Herzfeld, D. Rand, Y. Matsuki, E. Daviso, M. Mak-Jurkauskas, I. Mamajanov, *J. Phys. Chem. B*, 2011, **115**, 5741.
67) H. M. Pilath, M. R. Nimlos, A. Mittal, M. E. Himmel, D. K. Johnson, *J. Agric. Food Chem*., 2010, **58**, 6131.
68) X. Hu, C. Lievens, A. Larcher, C. Li, *Bioresource Technology*, 2011, **102**, 10104.
69) A. A. Marianou, C. M. Michailof, A. Pineda, E. F. Iliopoulou, K. S. Triantafyllidis, A. A. Lappas, *Applied Catalysis A: General*, 2018, **555**, 75.
70) R.Otomo, T. Tatsumi, T. Yokoi*, Catal. Sci. Technol*., 2015, **5**, 4001.
71) J. Dijkmans, D. Gabriels, M. Dusselier, F. de Clippel, P. Vanelderen, K. Houthoofd, A. Malfliet, Y. Pontikes, B. F. Sels, *Green Chem*., 2013, **15**, 2777.
72) M. Moliner, Y. Roman-Leshkov, M. E. Davis, *Proc. Natl. Acad. Sci. U. S. A.*, 2010, **107**, 6164.
73) Y. Roman-Leshkov, M. Moliner, J. A. Labinger, M. E. Davis, *Angew. Chem. Int. Ed.*, 2010, **49**, 8954.
74) Y. Roman-Leshkov, M. E. Davis, *ACS Catal.*, 2011, **1**, 1566.
75) M. Moliner, *Dalt. Trans.*, 2014, **43**, 4197.
76) A. Corma, M. Renz, *Angew. Chem. Int. Ed.*, 2007, **46**, 298.
77) M. Koehle, R. F. Lobo, *Catal. Sci. Technol*., 2016, **6**, 3018.
78) J. D. Lewis, S. Van der Vyver, A. J. Crisci, W. R. Gunther, V. K. Michaelis, R. G. Griffin, Y. Román-Leshkov, *ChemSusChem*, 2014, **7**, 2255.
79) J. Jae, E. Mahmoud, R. F. Lobo, D. G. Vlachos, *ChemCatChem*, 2014, **6**, 508.
80) L. Botti, S. A. Kondrat, R. Navar, D. Padovan, J. S. Martinez-Espin, S. Meier, C. Hammond, *Angew. Chem. Int. Ed*., 2020, **59**, 20017.
81) H. Li, S. Yang, S. Saravanamurugan, A. Riisager, *ACS Catal.*, 2017, **7**, 3010.
82) Z. Zhang, A. A. Donaldson, X. Ma, *Biotechnol. Adv.*, 2012, **30**, 913.
83) M. Dusselier, P. Van Wouwe, A. Dewaele, E. Makshina, B. F. Sels, *Energy Environ. Sci.*, 2013, **6**, 1415.
84) T. Ennaert, J. Van Aelst, J. Dijkmans, R. De Clercq, W. Schutyser, M. Dusse- lier, D. Verboekend, B. F. Sels, *Chem. Soc. Rev.*, 2016, **45**, 584.

85) C. Hammond, *Green Chem*., 2017, **19**, 2711.
86)) I. Sadaba, M. L. Granados, A. Riisager, E. Taarning, *Green Chem*., 2015, **17**, 4133.
87) J. P. Lange, *Angew. Chem. Int. Ed.*, 2015, **54**, 13186.
88) J. P. Lange, *Angew. Chem*., 2015, **127**, 13382.
89) L. S. Scott, *ACS Catal.*, 2018, **8**, 8597.
90) D. Padovan, L. Botti, C. Hammond, *ACS Catal.*, 2018, **8**, 7131.
91) A. M. Peres, E. A. Macedo, *Ind. Eng. Chem. Res.*, 1997, **36**, 2816.
92) M. Bicker, D. Kaiser, L. Ott, H. Vogel, *J. of Supercritical Fluids*, 2005, **36**, 118.
93) J. Zhang, E. Weitz, *ACS Catal.*, 2012, **2**, 1211.
94) D. Garcés, E. Díaz, S. Ordóñez, *Ind. Eng. Chem. Res.*, 2017, **56**, 5221.
95) T. D. Swift, *ACS Catal.* 2014, **4**, 259.
96) B. Karimi, H. M. Mirzaei, H. Behzadnia, H. Vali, *ACS Appl. Mater. Interfaces*, 2015, **7**, 19050.
97) L. Atanda, S. Mukundan, A. Shrotri, Q. Ma, J. Beltramini, *ChemCatChem*, 2015, **7**, 781.
98) K. Shimizu, R. Uozumi, A. Satsuma, *Catalysis Communications*, 2009, **10**, 1849.
99) D. M. Alonso , J. Q. Bond, J. A. Dumesic, Green Chem., 2010, **12**, 1493.
100) C. Moreaua, R. Duranda, S. Razigadea, J. Duhamet, P. Faugeras, P. Rivalier, P. Rosb, G. Avignonc, *Appl. Catal. A Gen*., 1996, **145**, 211.
101) S. Saravanamurugan, A. Riisager, E. Taarning, S. Meier, *ChemCatChem*, 2016, **8**, 3107.
102) S. Saravanamurugan, M. Paniagua, J. A. Melero, A. Riisager, *J. Am. Chem. Soc*., 2013, **135**, 5246.
103) P. E. Shaw, J. H. Tatum, R. E. Berry, Carbohydr. Res., 1967, **5**, 266.
104) K. Loos, R. Zhang, I. Pereira, B. Agostinho, H. Hu, D. Maniar, N. Sbirrazzuoli, A. J. D. Silvestre, N. Guigo, A. F. Sousa, Front. Chem., 2020 **8**, 585.

Chapter 6 - Conclusions and pertaining challenges

As described in the introduction of this thesis (Chapter 1), biomass represents one of the most interesting renewable resources to replace fossil feedstock for the production of chemical commodities. In this regard, heterogeneous catalysts have been widely proposed by the scientific community as potential materials to upgrade biomass-derived compounds into key platform molecules. Although some promising heterogeneously catalysed reactions to upgrade biomass have been developed on laboratory scale, applicability studies for their real industrial implementation are much less common. Therefore, a lack of knowledge of the real potential of these technologies persists among the scientific community. From an industrial standpoint continuous processes hold a series of advantages compared to discontinuous ones, which makes them the preferred solution when a large-scale process needs to be implemented. Therefore, understanding if a chemical reactions can be conducted in continuous mode of operation is crucial to evaluate its industrialisation. In this regard, laboratory continuous systems are precious tools since they allow one to gather the first information on the behaviour of a specific reaction when conducted in continuous modo operandi, pivotal for further scale-up. Moreover, conducting reactions in continuous systems offer the opportunity to perform optimisation studies essential to truly estimate the industrial productivity of these processes. For these reasons, in this thesis, attempts were made to develop continuous processes for heterogeneous catalysed reactions which have shown promising capability to upgrade biomass-derived substrates in laboratory batch experiments. Moreover, a detailed intensification study by optimisation of the developed continuous systems was performed to truly understand their potential industrial applicability. Specifically, due to their commercial interest, this work investigated formic acid decomposition to hydrogen (Chapter 3), sorbitol dehydration to isosorbide (Chapter 4) and fructose dehydration to furanic compounds (Chapter 5).

Chapter 3 explored the opportunity to develop a continuous process to decompose formic acid over a Pd/C catalyst with the aim of producing a continuous flow of hydrogen in portable devices. Preliminary continuous operations were attempted by developing a PFR system in which a formic acid solution was continuously eluted to a Pd/C catalyst bed. Although hydrogen was produced with an excellent selectivity level, continuous productions were impeded by the rapid deactivation of the Pd/C catalyst. Thanks to the intrinsic feature of the PFR, an array of kinetic studies were conducted which, in combination with catalyst characterisation techniques, allowed the causes of such rapid deactivation to be identified. Specifically, it was concluded that during the catalytic decomposition formate anions chelate to the Pd active sites, thus impeding the catalyst

from converting further formic acid molecules. However, water flushing of the catalyst bed resulted in the release of the formate anions from the metal active sites and thus fully restored catalyst activity. The insights gained on the catalyst deactivation and its regeneration allowed the conception and the development of a CSTR process in which formic acid was decomposed for extended periods of time, thus achieving higher hydrogen productivities. Specifically, the CSTR system was shown to be able to convert 27 times more formic acid than the PFR system.

Therefore, this study highlighted the key role that laboratory continuous systems have in the assessment of the industrial applicability of a proposed catalyst. Indeed, in addition to providing excellent level of activity and selectivity, industrial catalysts must show outstanding stability features to provide competitive process productivities. Laboratory continuous systems allow much more direct and accurate catalyst stability evaluations to be obtained compared with batch reactors, in which catalyst stability can be assessed only by means of multiple reusability experiments. Furthermore, conducting the reaction in a laboratory continuous set-up, allowed to perform kinetic studies crucial for the identification of the catalyst deactivation mechanisms, enabling more efficient process to be developed in which such deactivation events can be mitigated. Therefore, screening catalyst performances in conditions much closer to the industrial reality such as in laboratory continuous reactors, is not only pivotal for a reliable evaluation of the catalyst application, but also returned precious insights to achieve enhanced productivities. Furthermore, the batch-to-continuous approach employed in Chapter 3, and especially the diagnostic experiments developed to detect catalyst deactivation, might be used as an intensification study template for other biomass upgrading reactions.

However, although the improved continuous performances accomplished with this study, the formic acid decomposition reaction assisted by Pd/C catalyst looks to be hard to exploit for continuous hydrogen production in portable devices, due to the catalyst deactivation exhibited during long-term operation and to the not compact dimension of a CSTR system. Nevertheless, further investigations and optimisations in larger scale might be performed to evaluate the employment of this system for hydrogen production in medium-scale applications. Moreover, other active catalysts less inclined to be chelated by formate anions than Pd/C could be researched, thus returning more stable continuous performances. Otherwise, other biomass-derived liquid molecules might be screened for hydrogen chemical storage purposes, such as urea.

Chapter 4 instead attempted the development of a liquid-phase continuous process for sorbitol dehydration for the production of isosorbide. Although biomass derivates have the propensity to decompose when processed at high temperatures, only vapour-phase continuous processes were reported among the scientific literature for sorbitol dehydration when this work was commenced. In fact, to tolerate the high temperature required by the

vapour-phase, only very diluted feedstocks were employed, thus poor process productivities were achieved. Therefore, the possibility of conducting continuous sorbitol dehydration in liquid-phase was explored with the aim of processing much more concentrated feedstock, thus enhancing process efficiency. Preliminary batch studies were conducted to identify the best conditions to develop the continuous liquid-phase reactor such as the type of catalyst, reaction solvent, feed concentration and reaction conditions. These investigations pointed out β-zeolites as a suitable catalyst to perform the dehydration reaction due to the good activity and selectivity features provided, coupled with the promising stability showed by the material in previous studies.[1, 2] It was also demonstrated that aqueous reaction environments inhibit the full dehydration of sorbitol to isosorbide, causing the intermediate product 1,4-sorbitan to be predominantly produced. Substitution of the aqueous reaction medium with methanol permitted selective production of isosorbide and remarkably catalyst stability to be achieved. However, the substitution of the vapour-phase with a liquid-phase required a full optimisation study of the process to be reconducted. Specifically, investigation of fluid-dynamic kinetic regime allowed to identify and mitigate catalyst diffusion limitation phenomena. In this way, a catalyst productivity 4.6 times higher than the highest performing vapour-phase continuous reactor was achieved. Therefore, this study demonstrates the large productivity improvements that can be achieved when a catalytic process is designed and optimised for a specific target reaction, considering and tailoring all the elements involved in the chemical process. Particularly, it emerged that, because of the different chemical nature of the compounds involved, the engineering solutions developed over the last century to process crude oil are not suitable to upgrade biomass-derived feedstock. Therefore, if efficient processes and thus competitive products are wanted to be generated from biomass-derived compounds, catalytic processes need to be fully redesigned and optimised. Especially, it follows that in order to correctly evaluate biomass valorisation technologies from an industrial applicability, it is crucial to perform specific intensification studies which allow these processes to express their maximum efficiencies. Otherwise, interesting solutions to upgrade biomass feedstock run the risk of being uncompetitive with the current fossil-based technologies because they have not properly been developed. In fact, despite the enhanced isosorbide productivities achieved within this work, to properly evaluate industrialisation of the continuous liquid-phase sorbitol dehydration, further intensification studies are required. For example, the real isosorbide productivity must be assessed when the process is conducted at maximal sorbitol conversion and at higher temperatures since the highest isosorbide productivity reached in this study was deliberately obtained at sub-maximal conversion values and at mild temperatures. Furthermore, a proper catalyst long-term stability evaluation must be performed due to the promising stability showed by the catalyst over 55 h continuous

reaction. Moreover, it must be considered that the β-zeolite catalyst employed for sorbitol dehydration was a commercial catalyst. Therefore, further investigations on the sorbitol dehydration mechanism might propose the synthesis of reaction-tailored catalysts which might yield higher activity and selectivity features.

In light of the performance enhancement achieved in Chapter 4, thanks to the employment of an alcoholic reaction solvent, a similar reaction medium was investigated within Chapter 5 for the production of furanic compounds from fructose. In particular, the possibility of introducing small water aliquots to the alcoholic solvent were explored, since such an opportunity would allow to conceptualise the integration of the reaction with the recently proposed glucose isomerisation catalysed by metal substituted zeolites. From an economical and sustainability standpoint, integrated processes are one of the most efficient solutions to develop chemical processes since they require fewer intermediate unit operations, such as product separation and recovery, than conventional processes. Therefore, designing an integrated process from glucose to furanics would deeply increase the competitiveness of the whole chain from biomass to key platform molecules, thus increasing the chance of replacing fossil feedstock. Although previous literature works have shown that furanic compounds are subjected to degradation when processed in aqueous environments, Chapter 5 demonstrated that the presence of an alcoholic solvent, such as MeOH, improves furanics tolerance to water. In fact, the same furanic yield (60%) and carbon balance (87%) were achieved when the dehydration reaction was conducted in mere MeOH and in presence of 10 wt.% of water. Specifically, it was shown that, in such a solvent, the addition of water only decreases the rate of the dehydration reaction since the same furanics yield obtained in 10 min in mere MeOH was achieved in 60 min when the reaction was performed in a 50:50 wt.% MeOH/H_2O environment. By means of PFR systems, it was also demonstrated that furanic compounds are also able to tolerate water when processed in an alcoholic solvent in a continuous environment. Furthermore, in such processes, additions of water to the alcoholic solvent provided further benefits since it allowed the maximum furanic yields to be achieved in a broader range of operational parameters, thus permitting to operate in more flexible conditions. Thanks to the improved water tolerance that the alcoholic solvent induces on furanic compounds, it was possible to conceive a continuous integrated process from glucose to furanics. A preliminary feasibility study, performed by dehydrating a 1 wt.% 50:50 glucose/fructose mixture, demonstrated that glucose does not affect the dehydration reaction since a furanics yield equal to the one achieved when fructose was dehydrated as a single sugar substrate was achieved. Furthermore, a total 90% carbon balance resulted for each contact time investigated, demonstrating that glucose does not undergo degradation when processed at the condition employed for fructose dehydration. Although more accurate analyses are required to fully understand which reaction undergoes

glucose under dehydration conditions, indirect evidence indicate that glucose is methylated to methyl glucoside. If this hypothesis is confirmed, it can be conceived that after the dehydration step, methyl glucoside can be reconverted to glucose under mild hydrolysis, thus allowing unconverted glucose to be available and recycled for another isomerisation treatment and not be wasted. In fact, to properly evaluate the possibility of integrating fructose dehydration with glucose isomerisation further investigations are required. For example, it must be assessed that whatever by-products glucose form under dehydration condition is not a dead-end compound but can be instead valorised or recycled. Furthermore, once the possibility of developing such integrated process has been assessed, further intensification studies, for example attempting to process more concentrated feedstock or pursuing the most efficient strategy to integrate the two processes must be performed to achieve maximum furanics productivities. Moreover, a whole feasibility and optimisation study on the recovery of the final product from the reaction mixture must be performed to obtain competitive downstream furanic amounts.
However, the results obtained in Chapter 5 further emphasised that for each biomass upgrading reaction, a specific intensification study is required to be conducted if a clear understanding of its industrial potential wants to be pursued. Indeed, the small amount of water that was shown to be detrimental for sorbitol dehydration described in Chapter 4, resulted in better performance on fructose dehydration. In fact, the ability of fructose dehydration to tolerate water when conducted in an alcoholic environment allows to propose much more efficient solutions for the production of furanic compounds from fructose, such as the processing of more concentrated feedstock or the integration of the dehydration reaction with other key biomass upgrading processes, such as glucose isomerisation. In this way, the importance of conducting specific optimisation studies on biomass upgrade technologies can be stressed, since as Chapter 5 evidences, from these investigations might spring new strategies to process biomass-derived molecules and thus increasing the chance of replacing fossil feedstock with new renewable resources in the production of platform molecules.

Therefore, as a conclusion of this thesis it can be stated that the conduction of intensification studies on a preliminary laboratory scale is a critical procedure in the development of efficient processes for biomass valorisation and thus in the generation of chemical products from renewable sources. In this regard, developing laboratory continuous systems offer the opportunity to conduct reactions in favourable conditions from an industrial perspective, thus permitting better understanding of their potential for industrial implementation. Furthermore, developing laboratory continuous systems permits precious insight to be gained, so as to increase process efficiency and allow the gathering of additional knowledge of critical importance to catalytic phenomena such as catalysts deactivation. Moreover, it can be stressed that, because of the fragile chemical

nature of biomass-derived compounds, each biomass upgrading reaction must be individually investigated and optimised and, as consequence, specific industrial catalytic processes designed. In fact, as demonstrated along this thesis, such an approach might return improved process productivities or provide new strategies to upgrade biomass-derived compounds, thus making the transition from fossil fuels to renewable feedstock in the production chain of chemical commodities more feasible.

However, it must be stressed that to fully evaluate the implementation of biomass-based chemical process, the instable nature of the substrates processed must be considered. Thus, further analyses are required after laboratory intensification studies. For example, process performance assessments and optimisation studies must be conducted on larger scales. In fact, when larger amounts of chemicals are processed, more complex phenomena might arise compared to laboratory smaller scale and thus different engineering solutions might be implemented and optimised accordingly. In this regard, studying the scale-up process in intermediate scale systems, such as in medium-scale pilot plans, allow to gradually increase the complexity of the phenomena to be studied and thus returning more solid and efficient final industrial optimisation. Furthermore, since renewable feedstock will only be adopted if they are the most economically attractive, also comprehensive economic analyses must be performed to identify those operational conditions and process designs that allow to develop the most cost-effective production technology. In fact, although the importance of achieving competitive productivities is discussed in this thesis, there might be operational conditions that return the highest target compound amounts, but do not yield the maximum profit. For this reason, process developments must always be accompanied by accurate economic analyses to find those maximum profit condition that allow the generation of products at competitive market prices, thus making the transition from fossil feedstock to renewable resources in the production of chemical goods economically attractive. Therefore, to properly assess the industrial implementation of the biomass upgrading processes discussed in Chapter 3, 4, and 5, beside to the lab-scale intensification studies conducted in this thesis, larger scale evaluation and technoeconomical analyses should be performed in future.

6.1 References

1) H. Kobayashi, H. Yokoyama, B. Feng, A. Fukuoka, *Green Chem*., 2015, **17**, 2732.
2) R. Otomo, T. Yokoi, T. Tatsumi, *Chemical. Applied Catalysis A: General*, 2015, **505**, 28.